

INIS-MY-009



MY97A0934

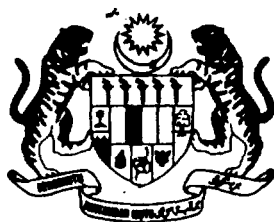
**KONGRES SAINS DAN TEKNOLOGI
MALAYSIA '94
KEMAJUAN DAN PENCAPAIAN PENYELIDIKAN DAN
PEMBANGUNAN**

15 - 18 Ogos 1994
Hotel Ming Court, Kuala Lumpur

Tema
"Teknologi dan Inovasi Menjamin Persaingan Industri"

Anjuran
Kementerian Sains, Teknologi dan Alam Sekitar Malaysia

Dikelolakan oleh
COSTAM
dengan kerjasama
Institusi-Institusi Pengajian Tinggi
Institusi-Institusi Penyelidikan dan Pembangunan
Badan-Badan Ikhtisas Sains dan Teknologi



PROCEEDINGS

Vol. II - New Products & Processes

PROCEEDINGS

***MALAYSIAN SCIENCE AND TECHNOLOGY
CONGRESS '94***

15 - 18 AUGUST 1994, KUALA LUMPUR

Published by

**Confederation of Scientific and Technological
Associations in Malaysia
(COSTAM)**

Kuala Lumpur 1994

***MALAYSIAN SCIENCE AND TECHNOLOGY
CONGRESS '94***

The proceedings of the Congress are published in six volumes:

Vol. I : Information Technology, Robotics & Telecommunications

Vol. II : New Products & Processes

Vol. III : Industrial Technologies & Energy

Vol. IV : Agricultural, Biological & Medical Sciences

Vol. V : Social & Environmental Sciences

Vol VI : Strategic/Basic Research

KONGRES SAINS DAN TEKNOLOGI MALAYSIA '94

Kementerian Sains, Teknologi dan Alam Sekitar menganjur beberapa aktiviti sebagai sebahagian daripada usaha-usahnya untuk menggalakkan pemahaman orang ramai di dalam bidang S & T disamping menolong di dalam perkembangan S & T negara. Aktiviti-aktiviti ini ditujukan kepada semua tahap masyarakat iaitu murid-murid sekolah, profesional-profesional dan juga orang awam. Salah satu daripada aktiviti-aktiviti pada tahap profesional adalah Kongres Sains dan Teknologi yang telah diadakan sejak tahun 1988.

Objektif-objektif Kongres Sains dan Teknologi Malaysia adalah:

- * Untuk memberi maklumat tentang hasil-hasil Penyelidikan dan Pembangunan terbaru daripada penyelidikan yang sedang dijalankan di Malaysia
- * Untuk membiasakan ahli-ahli sains, perancang-perancang dan ahli-ahli tentang Penyelidikan dan Pembangunan yang sedang dijalankan
- * Untuk mewujudkan interaksi yang lebih rapat di antara ahli-ahli sains daripada bidang-bidang berlainan yang berminat di dalam bidang penyelidikan yang serupa
- * Untuk menonjolkan usaha-usaha Penyelidikan dan Pembangunan di Malaysia
- * Untuk menyediakan satu forum bagi ahli-ahli sains untuk bertukar idea-idea saintifik yang baru
- * Untuk memfokus ke atas penggunaan S & T di dalam bidang-bidang keutamaan

***M*ALAYSIAN SCIENCE AND TECHNOLOGY CONGRESS '94**

Organising Committee

Advisors

Mr. V. Danabalan
Tan Sri Datuk Dr. S.H. Ong

Chairman

Dr. M. Mohinder Singh

Secretary

Dr. Soon Ting Kueh

Asst. Organising Secretary

Mr. Loo Keng Kee

Treasurer

Ir. Dr. Ow Chee Sheng

Members

Dr. Ainie Hj. Kuntom (PORIM)
Prof. Dr. Baharuddin b Yatim (UKM)
Dr. Bakri Madon (PORIM)
Mr. Chandrasekaran P. (MOSTE)
Mr. Chin Kee Chin (PEGAMA)
Mr. Chow Choo Kean (ASM)
Mr. Goh Chee Kuan (SIRIM)
Prof Madya Dr Han Chun Kwong (MSORSM)
Dr. K. Inder Singh (IMR)
Prof. Ishak b Ismail (UTM)

Ms. S. Karthyeni (MIMOS)
Dr. Loke Wai Hong (MARDI)
En. Md. Hasan b Hashim (FRIM)
Tuan Hj. Mohd. Reza Hj. Hashim (MSR)
Dr. Mohd. Ismail Noor (NSM)
Dr. Ooi Cheng Keat (PORIM)
Mr. Ramesh Pillai (MINDS)
Prof. R. Ratnalingam (USM)
Dr. Hj. Wan Noordin Wan Daud (RRIM)
Prof. Yap Thoo Chai (MSA)

Secretariat

Ms. Rhenu Kaur
Pn. Laila P. Mohd.
Ms. Helen Lee

ABOUT COSTAM

The Confederation of Scientific and Technological Associations or COSTAM is the national umbrella organisation of professional scientific and technological organisations in Malaysia. It was inaugurated on June 20, 1980 and registered under the Societies Act 1966 on December 8, 1983.

As a confederation of twenty-seven scientific and technological associations in Malaysia, COSTAM has the following objectives:

- *To bring together the resources of member associations for the advancement of science and technology
- *To facilitate the cooperation between and provide a common forum for member associations
- *To promote the effective utilisation of science and technology for human welfare and national development, in a manner consonant with the conservation of nature and natural resources
- *To increase public understanding and appreciation of science and technology for human progress
- *To consolidate, formulate and declare the opinion of scientists and technologists on issues of national importance
- *To encourage and maintain relations between Malaysia and international scientific and technological bodies

The major activities of COSTAM are:

- *Organising scientific and technological conferences, seminars and workshops on issues of national and international interest
- *Promoting public understanding and appreciation of science and technology
- *Publishing jointly with the Ministry of Science, Technology and the Environment, a popular science and technology magazine entitled *Science and Technology Malaysia* or STM
- *Organising the Annual COSTAM Public Lecture which is usually delivered by a prominent person in the government/scientific community

COSTAM represents the scientific and technological community in Malaysia. It is represented in the National Council for Scientific Research and Development (MPKSN). It also holds an annual dialogue with the Minister of Science, Technology and the Environment who is also the Patron of COSTAM.

Dr. Soon Ting Kueh
Hon. Secretary

COSTAM MEMBER ASSOCIATIONS

Agricultural Institute of Malaysia (AIM)
Astronomical Society of Malaysia (ASM)
Environmental Management and Research Association of Malaysia (ENSEARCH)
Geological Society of Malaysia (GSM)
Institut Kimia Malaysia (IKM)
Institut Fizik Malaysia (IFM)
Institute of Foresters Malaysia (IOFM)
Institution of Engineers Malaysia (IEM)
Malaysian Association of Engineers (MAE)
Malaysian Dental Association (MDA)
Malaysian Institute of Food Technology (MIFT)
Malaysian Invention and Design Society (MINDS)
Malaysian Institute of Laboratory Medical Sciences (MILMS)
Malaysian Medical Association (MMA)
Malaysian Plant Protection Society (MPPS)
Malaysian Scientific Association (MSA)
Malaysian Society of Plant Physiology (MSPP)
Malaysian Society of Radiographers (MSR)
Malaysian Society of Soil Science (MSSS)
Management Science/Operational Research Society of Malaysia (MS/ORSM)
Nutrition Society of Malaysia (NSM)
Technological Association of Malaysia (TAM)
Selangor & Federal Territory Gardening Society (SFTGS)
Institute of Quality Control Malaysia (IQCM)
Society of Biochemistry Malaysia (SBM)
Malaysian Oil Scientists and Technologists Association (MOSTA)
The Plastics and Rubber Institute Malaysia (PRIM)

ACKNOWLEDGEMENT

The President and Council Members of COSTAM wish to thank all those who have assisted in the organisation of the Congress. Special thanks are accorded to :

1. Y.B. Datuk Law Hieng Ding
2. Ministry of Science, Technology and the Environment
3. Institutions of Higher Learning
4. Research & Development Institutions
5. Professional Science & Technology Societies
6. Keynote Speakers
7. Authors of Papers
8. Chairmen of Sessions
9. The Organising Committee
10. Lee Foundation
11. Advertisers
12. The Mass Media
13. Ming Court Hotel, Kuala Lumpur
14. The Spastics Centre, Petaling Jaya
15. Participants
16. All those who have helped in one way or another to ensure the success of the Congress.

PROCEEDINGS OF THE MALAYSIAN SCIENCE & TECHNOLOGY CONGRESS '94

VOLUME II - NEW PROCESSES & PRODUCTS

<u>Title</u>	<u>Page</u>
R & D for the Malaysian Manufacturing Sector A. Zaharuddin Idrus	1
Current Trends in Solid State Battery Preparation and Characterization Abdul Kariem Arof , M.J. Maah & E.B. Saniman	9
Potential of Sarawak Clay as Material for LWCA Production Teng Wan Dung, Zuraida Ahmad & Saidin Karim	17
Kesan Penggunaan Abu Kelapa Sawit Sebagai Agen Pengawal Kehilangan Bendalir di dalam Operasi Penyimenan Telaga Petroleum Ahmad Suhaimi, Ariffin Samsuri, Shahrin Sharuddin, Abu Samah & Zainuddin Ahmad	25
The Study of Microstrip Electromagnetic Properties and Method of Measuring ϵ_r Wan Khairuddin Wan Ali	32
Ujian Mampatan Ke atas Paip Komposit Yang Dihasilkan dengan Mengguna Keadah Empar Daud Hj. A. Rahman	42
Penjerapan Ion Logam Pb(II) dan Ni(II) Dengan Menggunakan Serbuk Karbon Teraktif Mikroliang Asiah Hussain & Lai Lee Teng	52
Vibrational Power Flow in Fiber Reinforced Composite Materials Roslan Abd. Rahman & Mohd Salman Leong	62
Improvements on the Design of an Electrostatic Filter Nгах Ramzi b Hamzah, Zainuddin Shaary & Nabil Mahmoud Abdul-Kadir	70
Design of a Zero Dispersion Optical Fibre Abu Samah Mohd Supaat, Norazan Mohd Kassim & G. Kuhaneswaran	75

Effect of Annealing on Evaporated Tin Sulphide Thin Films <i>Samsudi Sakrani & Bakar Ismail</i>	86
Saput Tipis Sn,Se Disediakan dengan Kaedah Penselenidan Tertudung-Tebat <i>Sabar D. Hutagalung, Samsudi Sakrani & Yussof Wahab</i>	91
Performance of Locally Manufactured Hollow-Fiber Membrane for CO ₂ Separation <i>Hamdani Saidi, R.A. Aziz, A. Ariffin & H. Hassan</i>	98
A Compact TE-TE Nitrogen Oscillator-Amplifier Laser System <i>Y.K. Yap, T.Y. Tou & K.S. Low</i>	107
Intermetallics for High Temperature Service <i>A. B. Ismail, A. K. Masrom, Z. A. Ahmad & S. Bhan</i>	114
Locally Produced Blended Cement Suits for Oilwell Cementing Job <i>Shahrin Shahrudin & Ariffin Samsuri</i>	121
Kesan Komposisi Magnesium Ke atas Pemagnetan dan Kerintangan Elektrik Ferit Mg-Zn <i>Ahmad Nazlim Yusoff & Mustaffa Hj Abdullah</i>	129
Catalytic Metathesis of 1-Hexene by Re ₂ O ₇ Impregnated Zeolite Y <i>Zainab Ramli & Halimatun Hamdan</i>	140
Compatibilization of Natural Rubber / Polyvinyl Chloride Blends with Epoxidised Natural Rubber <i>Wan Aizan W. Abdul Rahman, Ibrahim Abdullah & Abu Azam Mohd Yassin</i>	148
Effect of Ultrasonic Agitation on Mechanical and Corrosion Properties of Gold Electrodeposits <i>Noor Hisham Ab Hamid, Tn. Hj Jamil Yusof, Mustaza Hj Ahmadun & Anita Ibrahim</i>	159
Superkonduktor Suhu Tinggi Tl ₂ Ba ₂ CaCu ₂ O _{8-δ} <i>Roslan Abd Shukor</i>	167
Ternary lyotropic Liquid Crystals of Dodecyl Dimethyl Ammonium Bromide <i>Shahidan b Radiman & C. Toprakcioglu</i>	173
Perbandingan Penghasilan Karbon Teraktif Dengan Kaedah Fizikal dan Kaedah Kimia <i>Normah Mulop & Ramlan Abd Aziz</i>	180
Interaksi Mineral-Reagen Dalam Sistem Pengapungan Struverite-Fosfonik <i>Hisham b Jabar & Kamarudin b Hussin</i>	186

Filtration Behaviour of Different Phase Of Slurries Sa'ari Mustapha & Hamdani Saidi	195
Production of Activated Carbon from Palm Kernel Shells by Steam Activation Hoi Why Kong & Puad Elham	204
Process Design and Modelling of Physical Refining: Problems and Opportunities in Physical Refining Deodoriser Column Mustafa Kamal A. Aziz, Abu Azam Mohd Yasin, Harun Sani, Rusli Jaafar & Mohd. Halim Shah Ismail	210
Kajian Kemungkinan Pengubahsuaian Komposisi Gas Petroleum Cecair di Malaysia Zainal Zakaria, Mohd Norani Abd Rahman, Abd Aziz Abd Kadir, G. Raju, Abu Samah Nasir & Mohd Redhuan Ramlee	218
Specific Heat Capacity of Vegetable Oils using the Heat-Flux Differential Scanning Calorimeter Noor Azian Morad, Mohammad Idrees & Siva Kumar Supramaniam	225
Pemprosesan Pasir Hampas dari Kawasan Perlombongan untuk Kegunaan Industri Tempatan Hashim Hussin, Mohd Suhaili Ismail, Khairun Azizi Mohd Azizli & A. K. Masrom	233
Comparative Analysis of Acid Zinc Chloride Electroplating System Noor Hisham Ab. Hamid & Nor Arba'ayah Ramli	243
Study on the Design and Operation of Fine/Speciality Chemical Batch Plant Badrulhisham Abdul Aziz & Khairiyah Mohd. Yusof	252
Dynamic Mechanical Testing of Bitumens Hasanan b Md Nor	261
A New Compression Testing Facility Hamidon Musa, S. Rajesham & Jamaliah Idris	269
The Use of Multiplexer-Demultiplexer Circuit for Centralised Monitoring of Fire Alarm Panel Ahmad Maliki Omar, Mohd Fadzil Saidon & Habibah Hashim	276

R & D FOR THE MALAYSIAN MANUFACTURING SECTOR

Dr. Ahmad Zaharuddin Idrus
Vice Chancellor
Universiti Teknologi Malaysia.

1.0 What is Manufacturing?

Manufacturers must meet the customer's needs for products and components. These products and components have to satisfy certain specifications, namely:

- (a) Consistently of good quality
- (b) Can be produced economically and efficiently
- (c) Can be produced in a flexible manner; e.g. in small batches in response to changing customer requirements
- (d) Can be produced fast in a timely manner.

To understand manufacturing, one has to consider the whole system that transforms customers' orders or perceived needs into components and products. This supply chain [4] is shown in Fig.1. It is neither sufficient to focus on the manufacturing process only, nor is it sufficient to focus on speeding up the actual processes of the various stages. While speeding up individual processes is important, it is erroneously believed by many that this is the benefit that is conferred by modern manufacturing. In reality, the major contributions of modern manufacturing are consistent quality, reduction of non-productive work and time, so as to speed up the whole process and to reduce costs. Such non-productive work includes redesign, design modifications, miscommunication, delays, rework, queueing times and set-up times. Costs are further reduced by targetting non-productive costs like inventory and expensive overheads. What are being sought after are better designs for better products, better manufacturing techniques, and better management and organisation of the whole supply chain. It is recognised that the major inefficiencies in the supply chain occurs at the boundaries between different stages. Efforts are therefore directed towards minimising losses because material waits for substantial periods before it is actually being subjected to value-added work. This requires machines that are flexible and avoid expensive downtime. The situation has become one of managing information, and less of physical control of equipment.

Therefore , manufacturing covers the whole gamut of activities involved in the effective and efficient conversion of client needs (perceived, projected or based on client's orders) to provide quality products . It implies that manufacturing is also about making quality machinery and tools. Quality includes economy, flexibility in meeting frequent changes in customer requirements and timeliness. The activities not only involve technology , but more so its integration, organisation and management. The technologies and integration are shown in Fig. 2.

2.0 Manufacturing Sector in Malaysia and Its Performance

Manufacturing has become very important for Malaysia with the phenomenal growth rate it has experienced in the recent past . Export figures have shown that it has a part to play in creating a balanced economy with agriculture and service sectors being equal partners.

Gross export of Malaysia has expanded [3] by 14.7% per year due to 22.1% export growth of manufactured products. Although the export of palm oil has increased by 9.9% per year, there has been no significant increase in the export of the other raw materials. On the other hand, contribution of the manufactured goods to the total gross export has increased from 58.8% in 1990 to 71% in 1993. That is from 46.832 Billion Ringgit Malaysia in 1990 to 85.360 Billion Ringgit Malaysia in 1993. Household electrical goods and electronic components and parts have continued to be the main contributor to the export of manufactured goods from Malaysia.

Export of transport equipment and parts has increased by 31% per year, increasing its contribution to the total gross export in 1993 to 5%. The increase in the export of transport equipment has been mainly due to the success in widening the market of the national car to United Kingdom , Singapore and New Zealand; and to break into the market of Fiji , Trinidad and Tobago.

Overdependence on just one or two key subsectors would not be healthy for the economy. To reduce such overdependence as well as to offset the effects of declining prospects of export earnings on primary products, it is necessary to adopt a more concerted and coordinated approach to foster the development of the manufacturing sector as well as to stimulate the expansion and deepening of the industrial base to encourage industrial diversification. There has recently been signs of diversification in the downstream activities of the electronics and textile industries.

3.0 Problem of being Competitive

Malaysia had been successful and competitive in the past because it enjoyed relatively low labour cost and it was the leading producer of many raw materials such as rubber, palm oil, cocoa and tin. Within the last five years, countries like Indonesia, Thailand, Phillipines and Vietnam have attracted many foreign investors who have built factories in these countries. These countries have also planted rubber, oil palm and cocoa on a big scale due to the abundance of land. Low cost of labour and raw materials had been transient advantages. Now the cost of labour in Indonesia, Thailand, Phillipines and Vietnam are lower than the cost of labour in Malaysia. The same goes with the cost of raw materials.

One of the key issues facing Malaysia is the continued dominance of the labour intensive electrical, electronics and textile sub-sectors which has so far contributed very substantially towards the revenue of the country and the creation of employment. The made-in-Malaysia products will no longer be cheap. Malaysian manufacturing sector will have to shift to the production of quality and high-tech goods. The bulk of the Malaysian work force will need to be retrained to cater for the manufacturing sector which is based on knowledge and ingenuity. In this way the main contributor to the Malaysian economy can be made more sustaining.

4.0 The Need of the Manufacturing Sector

A sustaining manufacturing sector requires the following inputs:

- (a) Appropriate Research & Development (R&D)
- (b) Skill manpower in critical technologies
- (c) Systematic technology acquisition
- (d) Effective management
- (e) Extensive marketing
- (f) Proper financial incentives.

One of the success story of Taiwan is the fact that it is able to mobilise all these inputs into the manufacturing sector such that a total system is offered to any potential investors dealing with high tech. Taiwan is ready with all the infrastructure as soon as a factory is built.

5.0 R&D Direction

R&D activities in manufacturing in the country are at an extremely low level. Malaysian industry is mainly at a level where almost the whole of the technology is imported, and the activity performed is mainly operation of the technology. This makes it extremely difficult to get industry interested in research, since the major inputs that are required by industry are selection, commissioning and trouble shooting.

There is no tradition of research in this field as in the agriculture industry which has been supporting an industry that requires significant research input (e.g. RRIM , MARDI , PORIM etc.) . It took 10 years for an organisation like Universiti Teknologi Malaysia which concentrated all its educational and research activities in technology to make an impact on the Malaysian manufacturing scene . It will take some time before these manufacturers can see the benefits of local R&D inputs.

Manufacturing is an area which brings about great competitive advantages and one where technology is transportable with lower barriers to entry (for example compared with rubber, petroleum etc.). Hence the bulk of the applied research overseas is conducted mainly in the laboratories of industrial concern (or at other institutes with tight confidentiality requirement). Thus, Malaysian researchers have generally been trained more on the fundamental aspects of the science and technology and less on the applications.

It has always been the policy of Universiti Teknologi Malaysia to focus its activities in manufacturing to bring about high level technical research of direct benefit to industry. However, experience have shown that given the present scenario , the aims of conducting serious research and of providing a service to industry have to be met by a two-pronged approach.

On one hand , the scientists in this field must undertake projects to assist industry in appreciating the benefits of advanced manufacturing technology, and providing consultancy services in introducing, utilising and trouble shooting advanced manufacturing technology. This would include design support, analysis, and evaluation, benchmarking, training etc. in the advanced manufacturing area. It has been noted that a significant proportion of SMI in Malaysia are operating very inefficient manufacturing systems. Introducing automation ,per se , into these systems simply would not do, as it it would only speed up some parts of an inefficient system. Substantial benefit can be obtained by performing Industrial Engineering type of service to these industries, as a precursor to the introduction of advanced manufacturing technology. These activities can be focused on the food, wood, textile and machining sectors as these are facing intense competition and need efficiencies to increase their competitiveness.

On the other hand, serious research into advanced manufacturing can be conducted on the more fundamental aspects. The thrust at this time should be on familiarisation and acquisition of core competence in the enabling technologies. Recognising that advanced manufacturing encompasses a very wide range of enabling disciplines, ranging from the traditional engineering discipline of mechanical, electrical/electronics to IT, physics, chemistry and industrial engineering, it should be possible to address the research and development issues on a very broad front.

6.0 National Programs

The recommendations adopted in the Priority Setting Workshop for the Industrial Panel at Langkawi during the three days from 24 June till 26 June 1994 do reflect the general picture as to the type of R&D inputs which can be of the most benefit to the country. No doubt, some refinements have to be made before full fledged national programs can crystallise from them. All the sub-sector discussions agree on three main broad guidelines. That is, all R&D efforts should enhance Malaysia's international competitiveness in the manufacturing industries. These efforts should contribute to the achievement of a fully industrialised economy through optimal and sustainable development of resource-based industries. These efforts should also help in minimising any adverse environmental impact of the manufacturing industries. These broad guidelines require certain concerted actions. It will be necessary to

1. Establish machinery capability to support and develop the production of locally made machineries components/etc. for industries
2. Be a major player in the production and sale of indigeneous home appliances
3. Become a player with flexibility to move into production of new products as the need arises
4. Develop efficient and environmentally friendly industries or technologies.

They all boil down to the specific issue on how local scientists and engineers can help the manufacturing industries.

7.0 Conclusions

For the manufacturing industries, competing successfully means focussing on customer satisfaction through business strategies that improve the price, time to market, and quality as well as utility of the products or services offered by the company. Achieving competitive advantage requires business processes that deliver products or services at the best mix of cost, time and flexibility to meet market changes. Major successes have been achieved by companies who have challenged their organizations to rethink and redesign how they do businesses. Computer systems that support or enable redesigned business processes are more successful than those that simply automate existing processes.

Many have recognised that "throwing" technology at the problem is not a satisfactory answer. Information technology must be viewed as an enabling tool rather than the driving force for improving processes. With this understanding, a new discipline that combines techniques and tools learned from industrial engineering, quality management, systems analysis and management theory will evolved.

R&D support for Malaysian manufacturing sector requires a two-pronged approach. One offers an immediate short-term assistance. The other looks at the long-term issues. For the short term support, the R&D efforts must respond to the difficulties and the unexpected problems faced by the manufacturing industries by improvising solutions that work immediately. For this it is important to gain the willing cooperation of factory workers and personnels without negative sanctions. For the long term support, the R&D efforts require flexibility and responsiveness through better general problem-solving skills. Experience gained by Universiti Teknologi Malaysia has brought into light the fact that the majority of Malaysian manufacturing establishments (especially SMI's) need to be educated on the need to make production process more efficient. These establishments have the incorrect notion that productivity can only be increased by speeding up the processes. This has resulted in the existence of fast inefficient production lines which gives rise to many negative side effects such as bad power factor compensation and pollution.

8.0 References

- [1] Groover M.P., "Automation, Production Systems and Computer Integrated Manufacturing", Prentice-Hall International Editions, 1987.
- [2] Degramo E.P., Black J.T., Ronald Kohser, "Materials and Processes In Manufacturing", Collier Macmillan, 1988.
- [3] Unit Perancangan Ekonomi, Jabatan Perdana Mentri, "Kajian Separuh Penggal Rancangan Malaysia Keenam 1991-1995", December 1993.
- [4] Noordin Mohd Yusof, Seminar on CMM in Advanced Manufacturing & Control, SIRIM, Paper 3, "Trends in Modern Manufacturing - The UTM Perspective", 9 December 1993.
- [5] Md. Shariff Nabi Baksh, Amir Abdullah, Imran Hj. Idris & Ahmad Yusoff Hassan, APEC-HURDIT Training Project for Industrial Technology, Conference on Innovation of Production Systems for in Manufacturing Industry, "Implication of Diffusion of Microelectronics-Based Factory Automation Technology For Human Resource Development", 28 Feb. - 4 March 1994, Singapore.

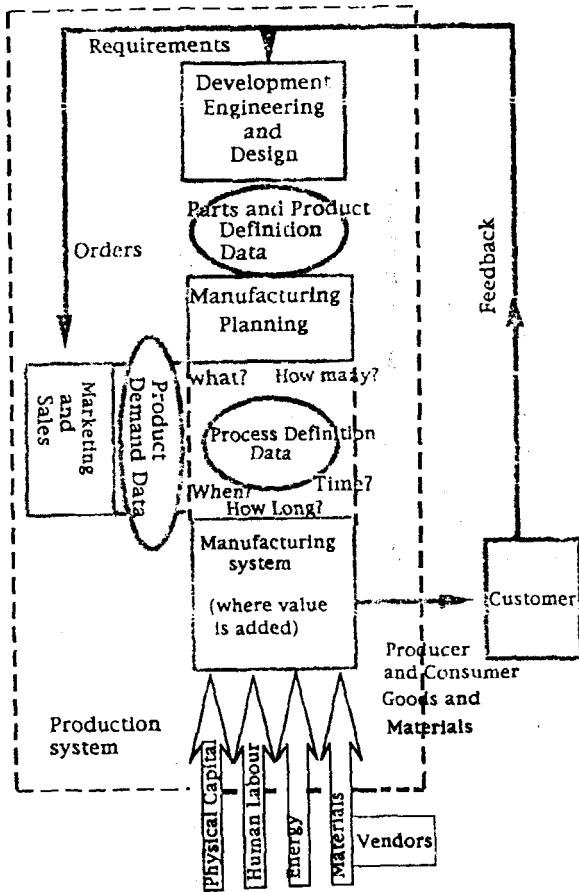


Fig.1 Manufacturing Supply Chain

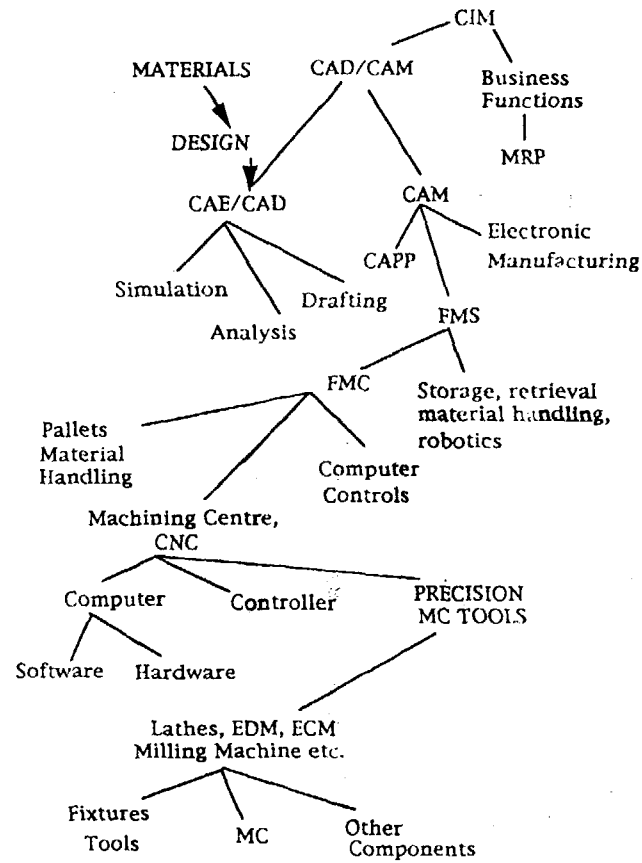


Fig.2 Technologies & Integration for Manufacturing Industries

Year	Total Export (Million RM)	Total Export from Manufacturing Goods (Million RM)	% of Total Export from Manufacturing Goods
1990	79,646	46,832	56.8
1993	120,225	85,360	71.0
1995 (Projected Figure)	148,110	115,677	78.1

Table 1 Total Export from Manufacturing Goods [3]

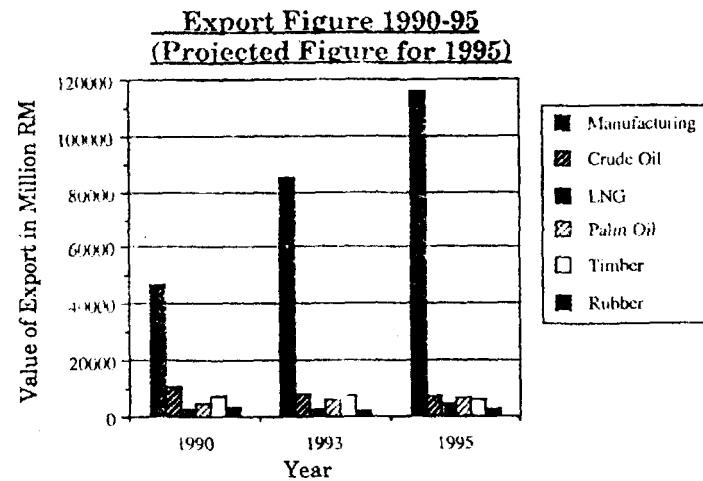


Fig.3 Export Figures (1990-1995) [3]

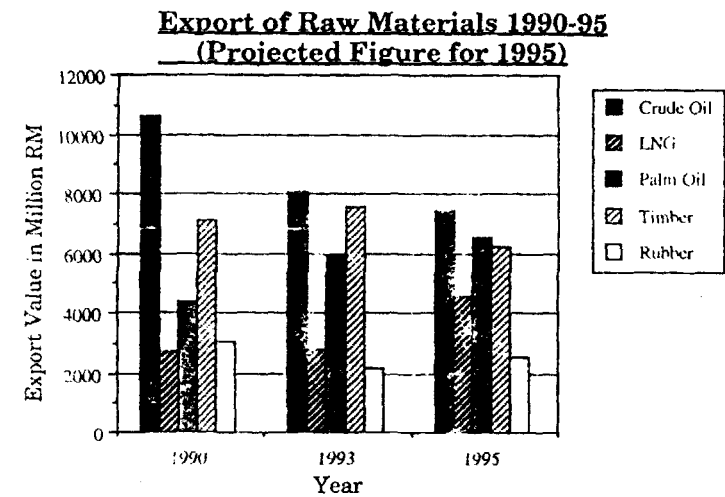


Fig.4 Export of Raw Materials (1990-1995)

CURRENT TRENDS IN THE FABRICATION AND CHARACTERIZATION OF SOLID STATE BATTERIES

A.K. Arof and M.J. Maah
Centre for Foundation Studies in Science,
University of Malaya,
59100 Kuala Lumpur, Malaysia.

and

E.B. Saniman
Materials Science Programme,
Faculty of Physical and Applied Sciences,
National University of Malaysia,
43600 Bangi, Selangor Darul Ehsan, Malaysia.

Abstract

A solid state battery is a battery with electrodes and electrolyte all in the solid state. There are many materials in the solid state which are good ionic conductors. An example of a good ionic conductor is the silver ion conductor which has a room temperature electrical conductivity of 10 mS/cm and negligible electronic conductivity which makes it very suitable for battery applications. In this paper, we present the various silver ion conductors that we have prepared and studied together with performance of the batteries that have been fabricated from these "home-made" materials. The methods used to characterize these materials are also discussed.

Introduction

Research in solid state batteries was initiated in Malaysia during the first International Workshop on Solid State Batteries and Thin Films held at the National University of Malaysia in Bangi from the 16th to 18th January 1989. The convenor of the workshop was Professor S. Radhakrishna who was then on leave from the Indian Institute of Technology at Madras in India. Amongst the invited speakers were Drs B.V.R. Chowdari (Singapore), Roger Linford (United Kingdom), Paul Hagenmuller (France) and M.A. Careem (Sri Lanka). Since then, serious work started at the Centre for Foundation Studies in Science, University of Malaya. On the 17th of October 1992, the research group based at the Centre for Foundation Studies in Science received the Nippon Sheet Glass Foundation Grant in Materials Science for a period of two years. Collaboration with Dr Elias Saniman from the National University of Malaysia started a little earlier that year. Supporting grants came from Associate Professor Dr Mohd. Jamil Maah when this work became the fourth project under his R&D programme and also from the University of Malaya.

A brief historical background on solid state ionics

The terms solid state ionics was first used by Professor Emeritus Dr Takehiko Takahashi in the sixties. However, studies involving the transport of ions have taken place long before the sixties. According to Chandra¹, probably the first report on ionic transport was by Faraday who noted that silver sulphide (Ag_2S) could conduct electricity at elevated temperatures. The first systematic study on ionic transport, however, must be attributed to the works of Tubandt and Lorenz in 1914 when they studied the variation of the electrical conductivity of silver iodide (AgI) with temperature. They observed that at 420 K, the electrical conductivity of AgI abruptly increased by a few orders of magnitude. This observation led to the many structural studies of AgI . According to Chandra¹ and Takahashi², the structure of AgI was visualised first by Strock in 1934. AgI was postulated to have a body centred cubic (bcc) lattice which is composed of the iodide polyhedra. The two silver ions that must accompany these iodide ions are distributed in three dimensions in their own sublattice which contain many defects, much more than the number of silver ions per unit cell. This silver sublattice "melts" at 420 K and the silver ions become "liquid-like". The "liquid-like" silver ions are free to move isotropically in three dimensions from one defect to another and the conductivity increases at 420 K. The conductivity "levels off" as observed by Tubandt and Lorenz at higher temperatures since the silver sublattice is still in the process of melting until the temperature reaches about 823 K which is the melting point of AgI when even the iodide polyhedra melts. Later, more sophisticated experiments showed that there are channel-like structures along which most of the silver ions are detected. These channel-like structures are regarded as preferred pathways for the conduction of silver ions. The conduction of silver ions is therefore anisotropic.

The high electrical conductivity exhibited by AgI is at a temperature above the boiling point of water. This makes the material practically unapplicable. Thus some engineering has to be done on AgI to make it a good electrical conductor at room temperature. The efforts of² Takahashi and Yamamoto in the east and Reuter and Hardell in the west in discovering Ag_3SI which has an electrical conductivity of 10 mS/cm at room temperature, at almost the same time, should be recognised as the starting point for the rapid development of solid state ionics. Since then many materials have been prepared both in the glassy as well as the polycrystalline states. For battery applications, the glassy state is preferred. Among the advantages of preparing materials in the glassy state³ is the higher conductivity it can exhibit over its polycrystalline counterpart.

Materials studied

Some of the glassy materials which have been used in Ag/I_2 batteries are listed in Table 1.

Table 1: Glassy materials that have been fabricated at the Centre for Foundation Studies in Science (January 1991 to June 1994) and some characteristics.

Glasses	Conductivity	Transference Number
60AgI-20Ag ₂ O-2V ₂ O ₅ -18MoO ₃	*10 ⁻³ S cm ⁻¹	0.99
60AgI-20Ag ₂ O-2MoO ₃ -18V ₂ O ₅	*10 ⁻³ S cm ⁻¹	0.99
60AgI-20Ag ₂ O-20MoO ₃	*10 ⁻³ S cm ⁻¹	0.99
60AgI-20Ag ₂ O-20V ₂ O ₅	*10 ⁻⁴ S cm ⁻¹	0.99
70AgI-20Ag ₂ O-10V ₂ O ₅	*10 ⁻⁴ S cm ⁻¹	0.99
66.67AgI-19.04Ag ₂ O-14.29 MoO ₃	10 ⁻³ S cm ⁻¹	0.99
63.75AgI-15.54Ag ₂ O-20.71 MoO ₃	10 ⁻² S cm ⁻¹	0.97
63.75AgI-13.97Ag ₂ O-1.57ZnO-20.71MoO ₃	10 ⁻² S cm ⁻¹	0.97
63.75AgI-15.54Ag ₂ O-2.01ZnO-18.64MoO ₃	10 ⁻² S cm ⁻¹	0.97
63.75AgI-15.54Ag ₂ O-20.71ZnO	10 ⁻³ S cm ⁻¹	0.97

Electrical conductivity values marked with asterisk (*) are obtained from the resistance value of each sample measured with an R-C-L meter at 1 kHz. The electrical conductivity values not marked with asterisk are obtained from the complex impedance plot from 1 kHz to 100 kHz.

Characterization of materials

X-ray Diffraction (XRD):- As we have mentioned earlier, a glassy material is preferred to a polycrystalline for battery applications. This is because a glass has a higher electrical conductivity over its polycrystalline counterpart with the same stoichiometric composition. Conduction in glasses is isotropic whereas in polycrystalline materials, the conductivity is dependent on its various axis. If the XRD pattern consists of peaks which are distinguishable, then the material is polycrystalline. The absence of peaks and the presence of an amorphous hump is indicative of the glassy nature of the material, Fig.1.

Transference number measurements

Having known that the material is a glass, through XRD, it is not conclusive yet to say that the material is a suitable electrolyte for use in solid state batteries without knowing to what extent electrons contribute to the conductivity of the material. In liquid electrolytes, this problem is not seriously encountered⁴ because, however good an ionic conductor a solid can be, there is still some amount of conduction due to electrons. If the electronic conduction is substantial, then internal short-circuiting will occur within the solid state battery which can

lead to battery failure. How good an ionic conductor a glassy material is can be determined by the ionic transference number.

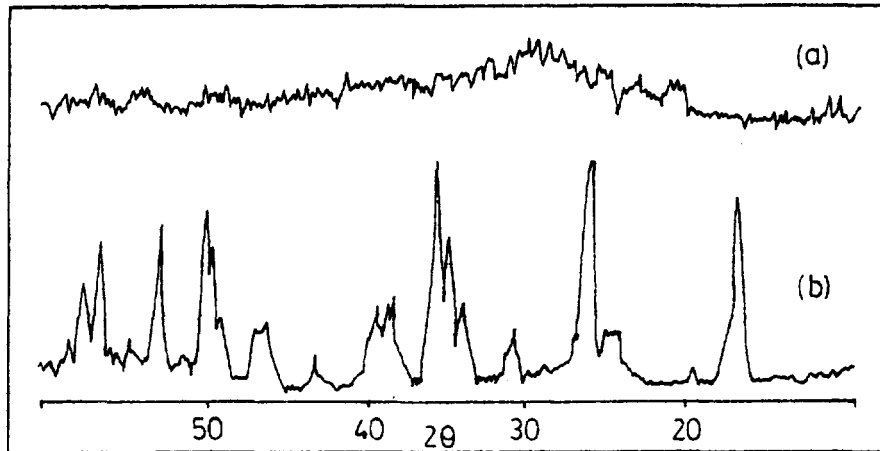


Fig.1 XRD pattern for (a) a glassy and (b) a polycrystalline material.

The ionic transference number, t_i , is defined as the ratio of the conductivity due to itself, σ_i to the total conductivity of the material, σ_T i.e.

$$t_i = \frac{\sigma_i}{\sigma_T} \quad (1)$$

Since $\sigma_T = \sigma_i + \sigma_e$, where σ_e is the conductivity due to the electrons, Eqn (1) can be written as

$$t_i = \frac{\sigma_i}{\sigma_i + \sigma_e} \quad (2)$$

Likewise,

$$t_e = \frac{\sigma_e}{\sigma_i + \sigma_e} \quad (3)$$

One can readily see that

$$t_i = 1 - t_e \quad (4)$$

As with current, conductivity is also proportional to the charge of the conducting species, then

$$t_i = \frac{i_i}{i_T} \quad (5)$$

where i_i is the ionic current and i_T , the total current ($i_i + i_e$). For an electrolyte containing AgI, in which it is well known that the Ag^+ ion in the silver sublattice is the main conducting species, if the electrolyte is sandwiched between silver and carbon electrodes and subjected to an electric field, the Ag^+ ion will migrate to the silver electrode where it will be dissolved. The electrons will travel to the carbon electrode. In time, the total current traversing the electrolyte will decrease and finally saturates to give just the electron current. Subtracting the electron current from the initial total current (i.e. at time zero), one gets the total ionic current. The ratio of the total ionic current to the total current at time zero gives the ionic transference number. If $t_i \rightarrow 1$, the material is an ionic conductor and if $t_e \rightarrow 1$, the material is an electronic conductor. The circuit for measuring the ionic transference number is as shown in Fig.2 and a typical current-time plot is as shown in Fig.3.

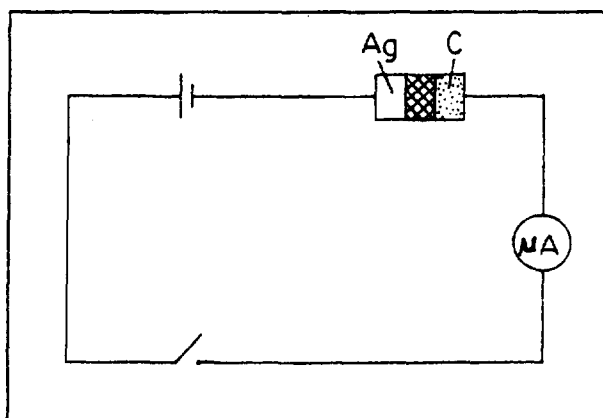


Fig.2 Circuit for transference number measurement.

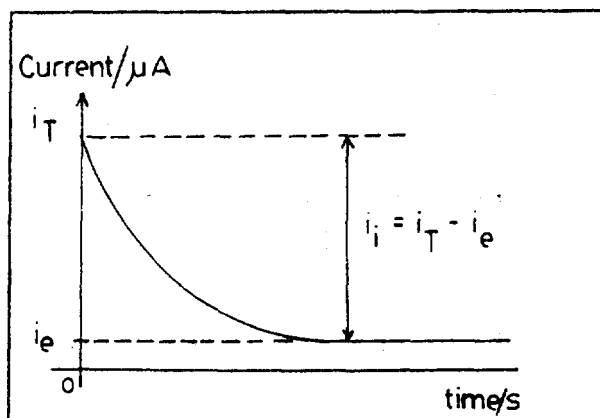


Fig.3 Current-time curve for obtaining transference number.

Impedance spectroscopy

Having known that the glassy material obtained is an electrolyte, it is now necessary to know the conductivity of the material. The conductivity of the material can be obtained from impedance spectroscopy. In impedance spectroscopy, a time varying voltage of the form $V(t) = V_0 \sin(\omega t)$ is applied across the sample and the resultant current usually lags the applied voltage by a phase difference, ϕ and is of the form $i(t) = i_0 \sin(\omega t + \phi)$. If one does not have a bridge that can measure directly the impedance, Z and the phase difference, ϕ then an oscilloscope together with a frequency generator can be used for measuring the impedance spectroscopy following the circuit shown in Fig.4.

The magnitude of the impedance is given by

$$Z = \frac{r(e-s)}{s} \quad (6)$$

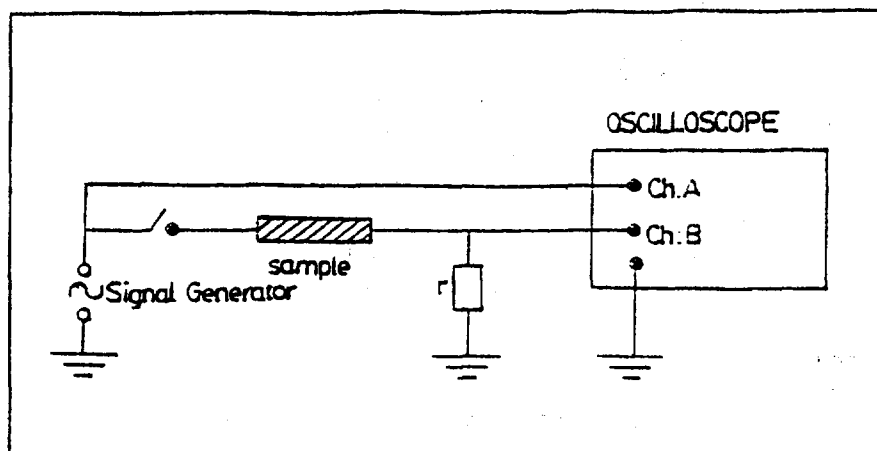


Fig.4 Circuit for impedance analysis using a frequency generator and an oscilloscope.

where r is the standard resistor in the circuit, e and s are both the amplitude of the input and output voltages taken from the oscilloscope trace and the phase difference by $\phi = \arcsin[Y/X]$ where X and Y are the peak to peak input and output amplitudes respectively⁵.

In complex terms,

$$Z(f) = Z_R + jZ_I \quad (7)$$

where the real part of the complex impedance is

$$Z_R = Z \cos(2\pi ft) \quad (8)$$

and the imaginary part is given by

$$Z_I = Z \sin(2\pi ft) \quad (9)$$

Z is given by Eqn(6) and $2\pi ft = \phi$. By varying the frequency f over the range limited by the frequency generator, one can obtain $Z(f)$ values corresponding to a particular phase difference. The method described above can be very tedious to carry out. One might ask "is there a simpler method?" or "why the need to measure over a large frequency range?". The solution to the first question may require a lot of money, for there are instruments that can simply do the job within minutes and they can be very expensive depending on one's budget. The second question requires a more serious answer. One must remember that, the material is a glass and an ionic conductor and when measuring the conductivity, the material is firstly ground and then pelletised. This introduces grain boundary impedance. Also the pellet is then placed in between metallic conductors with leads to the instrument for measuring the impedance response. The metals are electronic conductors and hence gives rise to a double layer which is capacitive and in practice are also resistive. Thus by measuring at

only one frequency, there is a possibility that these impedances are lumped together giving a conductivity that is not true of the bulk. A typical complex impedance plot is as shown in Fig.5.

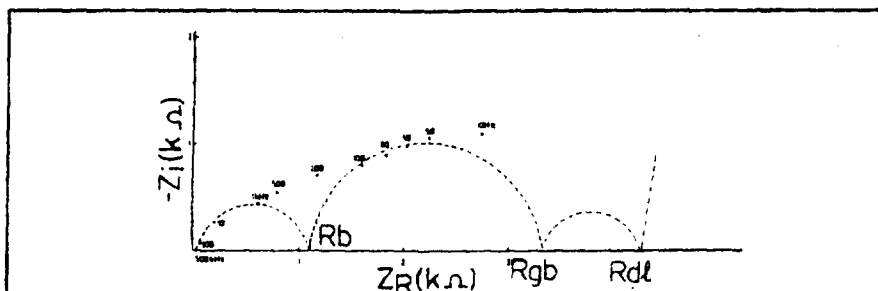


Fig.5 A typical impedance plot. R_b true bulk resistance, R_{gb} grain boundary resistance and R_{dl} is the capacitive reactance.

Knowing the bulk resistance, the conductivity can be measured from the following equation:-

$$\sigma = \frac{L}{R_b A} \quad (10)$$

where L is the thickness of the sample and A its cross-sectional area.

Battery fabrication

Fig.6 shows a schematic representation of a solid state battery. The anode is an ionic conductor and for a silver battery consists of a mixture of silver powder and electrolyte. The cathode is a mixed conductor. For an AgI based silver ion conductor, the cathode consists of iodine, carbon (which is an electronic conductor) and electrolyte (ionic conductor). For an AgI based

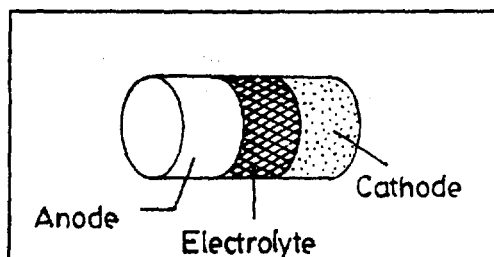


Fig.6 A solid state battery

silver ion battery, the theoretical open circuit voltage (OCV) is 0.687 V. This is because the cell reaction leads to the formation of AgI and the Gibb's free energy of AgI formation is about 66 kJ/mole. Hence the theoretical OCV, E_{th} which is given by the equation

$$E_{th} = \frac{\Delta G}{Z F} \quad (11)$$

is 0.687 V. Here ΔG is the Gibb's free energy of AgI formation, Z is the valency and F is Faraday's number. Fig.7 shows the discharge characteristics for some of the batteries we have fabricated.

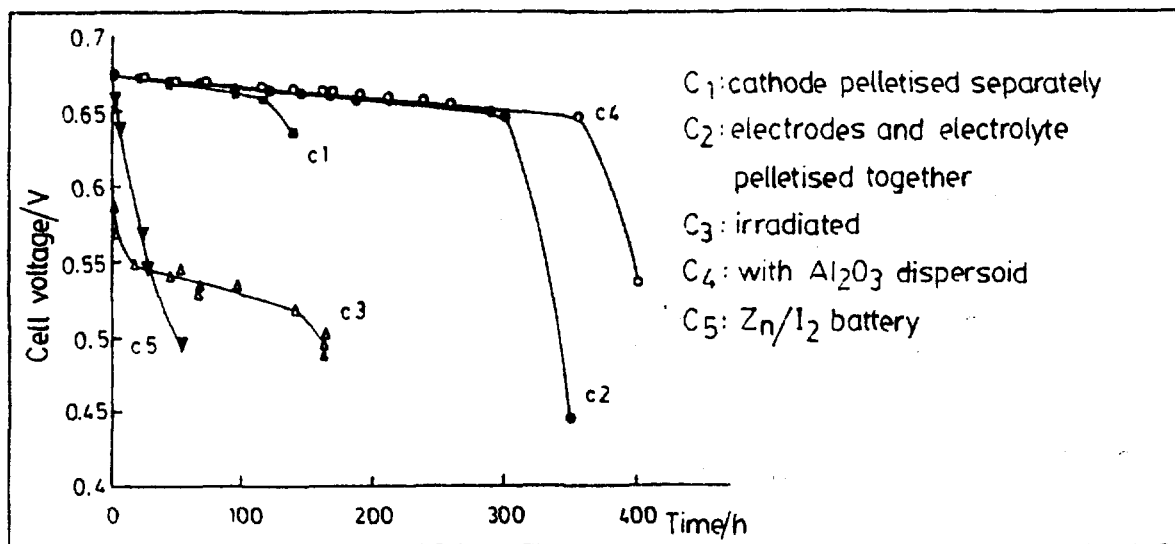


Fig.7 Discharge characteristics of silver molybdate batteries.

Conclusions

The ability of many materials to form glasses and the enormous range of materials that can be used as an electrolyte material has kept the subject matter much alive. Research on silver ion glasses and batteries will continue until these resource materials become exhaustive.

Acknowledgements

A.K. Arof thanks the Nippon Sheet Glass Foundation for Materials Science for awarding a grant which enabled these works to be carried out.

References

- [1] S. Chandra, Superionic Solids: Principles and Applications (North-Holland, 1981).
- [2] T. Takahashi, in "High Conductivity Solid Ionic Conductors: Recent Trends and Applications", ed T. Takahashi, (World Scientific, Singapore, 1989).
- [3] D. Ravaine, J.Non-Cryst. Solids, 38-39 (1983) 353.
- [4] C.C. Liang, Appl. Solid State Sci, 4 (1974) 95.
- [5] T.A. Diallo and A.K. Arof, Jur Sains 1 (1993) 30.

POTENTIAL OF SARAWAK CLAY AS MATERIAL FOR LWCA PRODUCTION

Teng Wan Dung, Zuraida Ahmad, Saidin Karim
Ceramics Technology Group
Materials Technology Centre
Standards and Industrial Research Institute of Malaysia (SIRIM)
Persiaran Dato' Menteri, Section 2, P.O.Box 7035,
40911 Shah Alam, Selangor Darul Ehsan, MALAYSIA.

ABSTRACT

Light-weight clay aggregates (LWCA) are popular in developed countries especially for their applications as light-weight concrete in high-rise structures. This study was undertaken to evaluate the potential of local Sarawak clay as material for LWCA production. Characterization studies revealed that this clay material contains high content of iron and other flux materials. When this raw clay material was subjected to rapid heating, the expansion or bloating of the resulting product occurred. The clay was made into pellets form by mixing with additives and binder. The pellets were subsequently calcined and sintered in a tube furnace to give LWCA. The effects of the sintering temperature and amount of binder on the selected properties of the product such as linear and volume expansions, porosity, bulk density, crushing strength, microstructure and phase transformation were studied.

Key words: Light-weight clay aggregates, rapid heating, bloating, expansions, porosity, bulk density, microstructure, phase transformation

INTRODUCTION

Malaysia has plenty of natural clay resources. Most of the exploited areas are used to producing ceramic products such as bricks, pottery, gift wares, sanitary wares, table wares and various kinds of tiles. In this study, another kind of clay which also known as expandable clay was investigated.

The Sarawak clay was selected for this study as it shows a great potential properties of this expandable clay. When this clay undergoes rapid heating, the clay material will reach a pyroplastic state at elevated temperature and then generates gases that will expand or bloat the resulting product. Due to this pyroplastic properties, sintered clay becomes porous and light-weight substance that will retain its physical strength despite its lighter unit weight when cooled and known as expanded clay.

This expandable clay was processed and fabricated into pellets by using extrusion or pelletization method. The pellets were fed into laboratory tube furnace or industrial rotary kiln furnace for high and rapid firing temperature. The final products by this pyro-processing were called as Light-weight Clay Aggregates (LWCA). The similar kind of product had been marketed under the name LECA (Light Expanded Clay Aggregates) and LIAPOR Light-weight Aggregates in Europe. LWCA are popular in developed countries especially for their applications in high-rise structures, such as

One Shell Plaza Tower at Texas, USA, Australia Square Tower at Sydney, Australia and others. This product has the dual main advantages of low weight and good insulation properties.

In general, "Light-weight Aggregates" refers to aggregates products from clay, shale, slate, fly ash, pumice, vermiculite, perlite, diatomite and blast furnace slag. This study is concerned only with those aggregates that can be incorporated into structural concrete, namely, expandable clay and shale. The LWCA combined with portland or refractory cements, they are formed into light-weight concrete blocks, bricks, beams and slabs of many shapes and sizes. They are also used in the monolithic formation of beams, columns, walls and floors. Besides they are used structural concrete, they are used in hydro-culture, soil conditioner, ornament of the garden, insulation and others.

MATERIALS AND METHODS

Clay Material

The Sarawak clay material obtained from the Kuching-Bau's quarry site was dried in the air. Then, the clay material was crushed down by Jaw crusher and further ground into powder by Fritsch milling machine.

Mineralogical and Chemical Analysis

This sample was dried at 110°C for 24 hours in the oven. The sample was ground in a agate mortar by hand into powder of less than 100µm size. This powder was mounted a aluminum plate and transferred to sample holder in X-Ray Diffractometer for measurement. The X-ray diffraction spectrum of the sample was taken at a scanning rate of 10 degree (2θ) per minute using Cu K-radiation at 35 KV, 15 mA with nickel as filter. The mineralogical compositions of the unfired and fired samples were determined by X-Ray Diffraction powdered method. A portion of the sample was fired in a combustion furnace at 1000°C to determine the Loss of Ignition (LoI). Another portion of the sample was sent to foundry laboratory for chemical composition analysis by X-Ray Fluorescence method(XRF).

Thermal Analysis

About 25 mg of the sample powder was put in platinum crucible where alumina powder was used as the inert reference material. The furnace and differential temperatures were recorded on a three-pen recorder represented temperature, differential thermal analysis(DTA) and Thermogravimetric analysis(TG) curves of the sample. The rate of temperature rise of the furnace was set at 10°C/min to a maximum temperature 1200°C.

Sample Preparation

The Chart 1 shows the procedure of producing LWCA in the laboratory. The expandable body consisted of 98 % Sarawak clay, 1.4 % limestone, 0.4 % dolomite and 0 - 1.0 % binder. The expandable body was manually hand wedged by adding the proper amount of water to give good workability plastic body. The plastic body was put in a mini extruder for extrusion and followed by chopping the extrudate using a string of wire to produce various size of pellets or green aggregates.

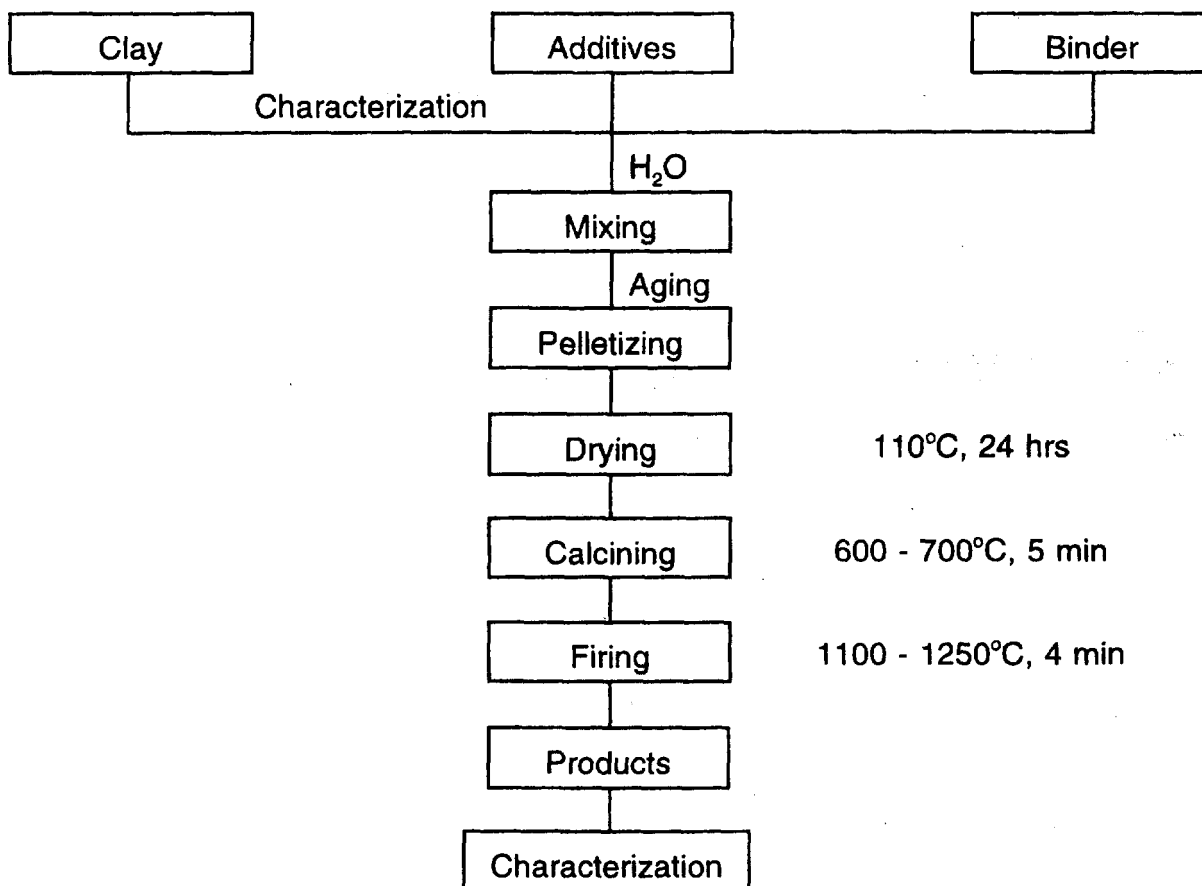


Chart 1 : Flow chart of a laboratory scale for producing LWCA

Heat Treatment

The pellets were dried at 110°C for 24 hours in the oven. The dried pellets were placed on refractory boat and pushed into the calcining zone for 4 minutes and pushed further into the sintering zone for another 4 minutes. The pellets were calcined at 600 - 700°C sintered at elevated temperature. The heat treatment was carried out in a tube of a 1.5 m length and 50 cm diameter furnace. Finally, the expanded pellets were taken 2 minutes to pull out from the firing zone to cooling zone of the furnace. The effect of the binder content was studied at 1200°C sintering temperature and the expanded body that contained 0.8 % binder were used to investigate the effect of sintering temperatures from 1100°C to 1250°C.

Characterization of the Product Properties

The expansion of the pellets was determined by direct measurement after sintering. The expanded aggregates were put in water bath for 2 hours boiling and 22 hours soaking to determine their porosity. The bulk density of the aggregates was obtained by coating with paraffin method. For crushing strength measurement, each aggregate was put on a flat surface of the Universal Testing machine and the load was applied to crush the aggregate. The results of this compaction were taken as a rational since there is not proper standard for this testing in our laboratory.

Selected pellet was cut into two half pieces where the cross section of one half piece of the interior pellet was observed under the Scanning Electron Microscope (SEM) with Wave-length Dispersive X-Ray(WDX) analysis. Another half of the pellet was crushed into powder where phase transformation was determined by X-Ray Diffraction (XRD).

RESULTS AND DISCUSSION

The Characteristic of the Clay Material

XRD studies showed that the clay material contains mainly quartz, albite, illite, and small amount of clinocllore(Fe), microcline and kaolinite. The chemical composition of the clay material in term of oxides and binder are tabulated in Table 1 and 2 respectively.

Clay	SiO ₂	Al ₂ O ₃	TiO ₂	Fe ₂ O ₃	MgO	CaO	Na ₂ O	K ₂ O	LoI
% oxide	65.4	17.0	0.71	6.8	1.30	0.38	0.96	2.05	5.02

Table 1 : The Chemical Composition of the Clay Material analyzed by XRF.

Binder	Reducing Sugar	Total S	Dry matter	Ca	Insoluble w/w
% Substance	20	5.3	68	4.0	2.0

Table 2 : The chemical data of the binder calculated an solid (supplied by LIGNOTECH)

The thermal behaviour of the clay material was plotted as figure 1 below:-

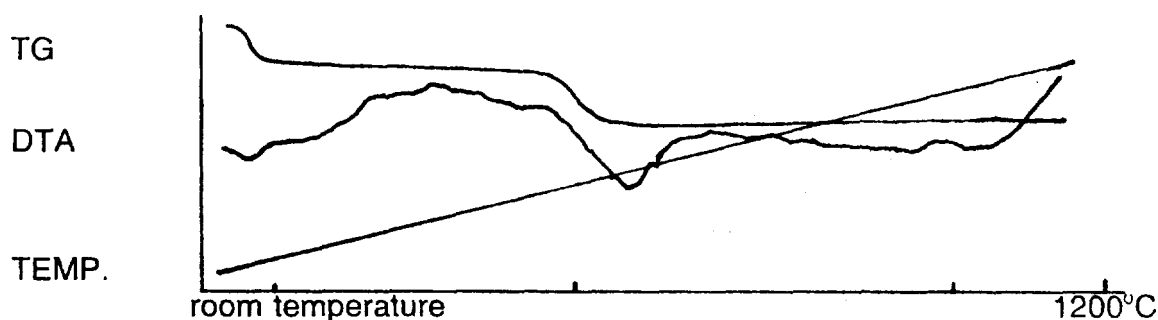


Figure 1 : The DTA/TG curves of the Clay Material

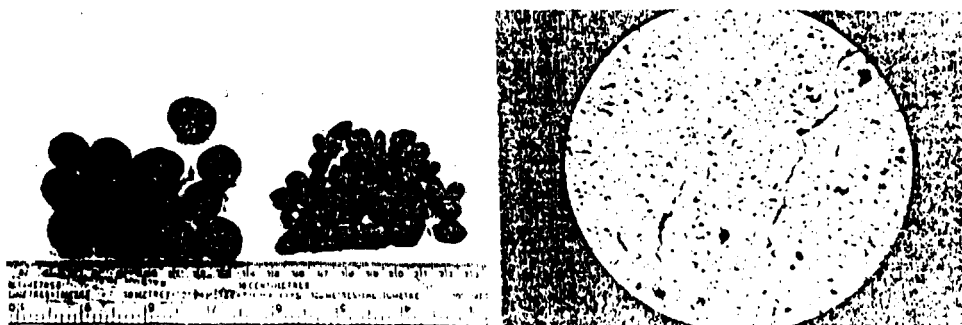


Plate 1 : The photographs of a) unbloated and bloated of aggregates and b) the pores shown by the interior aggregate (20X)

The chemical composition of this clay material is 69.1% SiO_2 , 18.7% $\text{Al}_2\text{O}_3 + \text{TiO}_2$ and 12.1% fluxes (Table 1) falls on Riley's triangular diagram for good bloating materials region. This is the region that clay mineral crystal structures are composed of two tetrahedral layers of (Si, Al) - O and one octahedral layer of (Al, Mg, Fe) - (O, OH), such as mica, illite, albite, anorthite, clinocllore and vermiculite. The XRD studies shown the clay materials contained some of these clay minerals. These multi-layer clay minerals form liquid phase as low as 950°C that could trap those gases evolved resulting the product expanded or bloated. The common expanded gases are CO_2 , CO, O_2 , SO_2 and H_2 . They are formed during the decomposition of organic impurities, sulphur-containing compounds, carbonates, iron oxides at elevated temperatures respectively.

The binder contained sulphur that contributes the expanded gases besides the contribution of high green strength of the aggregates.(Table 2)

DTA curve of the clay shows a wide endothermic peak at 80°C that reflects the strongly moisture - absorption nature of the mixed layer clay and confirmed by TG curve from the view of a sharp drop around 80 - 120°C. The DTA curve shows the exothermic and endothermic peaks at 410°C and 550°C that corresponding to decomposition of carbonaceous materials and commencement of dehydroxylation. This is also indicated by the drop of the TG curve occurred around 500 - 600°C for dehydroxylation of the clay. The small endothermic peak at 573°C indicates the presence of quartz in the clay (Figure 1).

The binder used for this studied assisted the expansion of the aggregates from 19 - 37 % linearly and 69 - 157 % volume expansions and 33 - 62 % porosity without binder to 1 % binder added. In average 0.5 - 0.9 % of binder content induced 30 % linearly and 120 % volume expansions and 60 % porosity. The bulk density and crushing strength of the expanded aggregates were 1.3 - 0.85 gm/ml and 67 - 30Kgf without binder to 1.0 % binder content. In average, 0.5 - 0.8 % of binder content induced 0.95 gm/ml and 53 Kgf bulk density and crushing strength respectively (Figures 2 and 3).

Therefore, 0.8 % binder was selected as a fixed parameter to continue the studies of sintering temperature effect on the properties of the expanded aggregates. A sharp increase of expansions from 1120°C to 1150°C and gently to 1250°C of 35 % and 144% linear and volume expansions respectively. While the porosity increased rapidly from 1170°C to 1200°C of 44 - 61 %. The bulk density of expanded aggregates achieved 0.95 gm/ml commenced from 1150°C and obtained 0.85 gm/ml at 1250°C but the crushing strength decreased from 79 Kgf to 35 Kgf as the sintering temperature increased from 1100°C to 1250°C (Figures 4 and 5).

SEM micrographs showed the expanded aggregates pores increased as the sintering temperature is getting higher. At 1200°C and 1250°C showed that the pores were getting less as the liquid phase increased (Figure 6). It could be deduced that if sintering temperature getting higher, there was possibly that the substance would melt and the expanded aggregates might start to shrink instead of further expand the cavities. It can be observed the loops grew bigger as the sintering temperature increased. The loops caused by the formation of spinel(Fe), hercynite, pyrite or

The properties of expanded aggregates

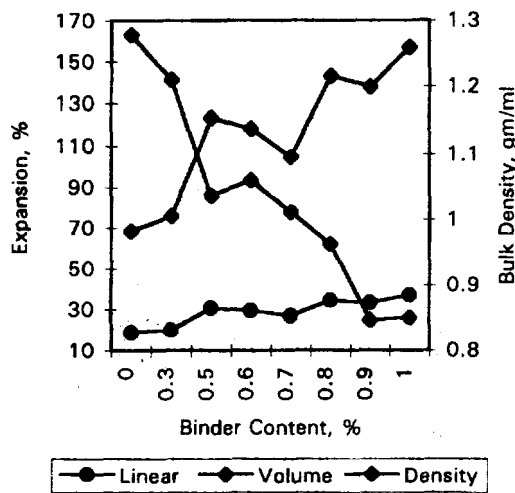


Figure 2 :

The relationships between linear and volume expansions and bulk density of the expanded aggregates fired at 1200°C and binder content.

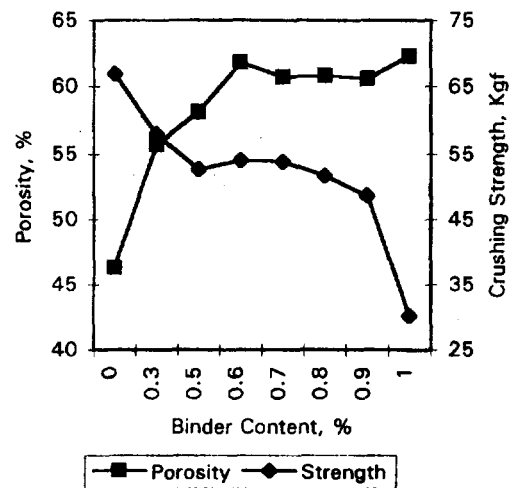


Figure 3 :

The relationships between porosity and comparative crushing strength of the expanded aggregates fired at 1200°C and binder content.

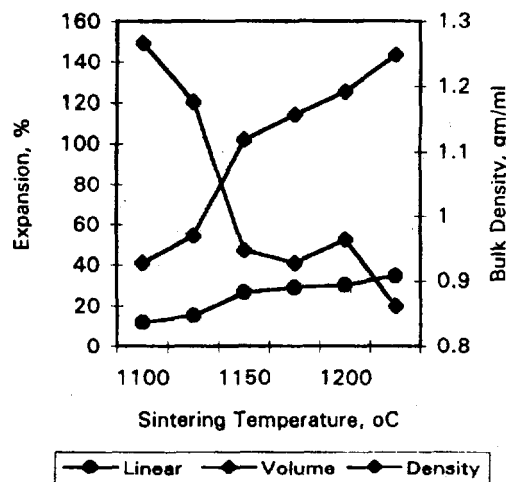


Figure 4:

The relationships between linear and volume expansions and bulk density of expanded aggregates with 0.8% binder and sintering temperature.

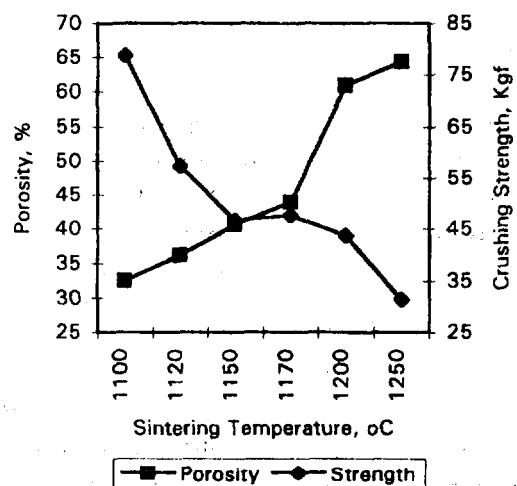


Figure 5:

The relationships between porosity and comparative crushing strength of expanded aggregates with 0.8% binder and sintering temperature.

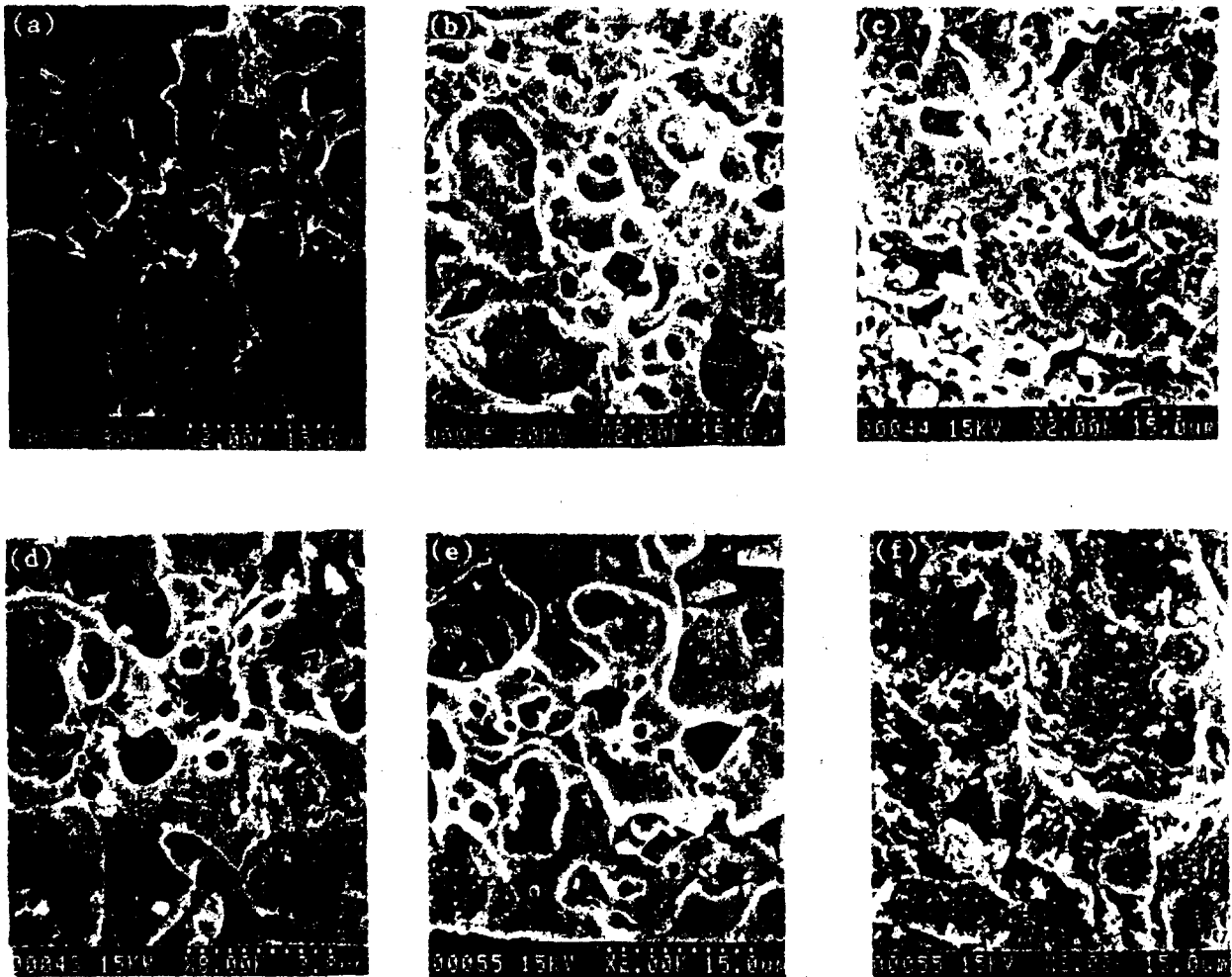


Figure 6 : SEM micrographs showing the pores of the expanded aggregates at sintering temperature of a) 1100 °C, b) 1120 °C, c) 1150 °C, d) 1170 °C, e) 1200 °C and f) 1250 °C.



Figure 7 : SEM micrographs showing the morphology of the expanded aggregates at sintering temperature a) 1150 °C, b) 1200 °C and c) 1250 °C.

increased. The loops caused by the formation of spinel(Fe), hercynite, pyrite or ringwoodite(Fe) as determined by WDX that the loops contained high iron content and confirmed by XRD on phase transformation analysis (Figure 7 and Table 3).

With these LWCA of 0.95 gm/ml, 60% porosity and 44 Kgf at 1200°C sintering temperature, incorporated into concrete to produce light-weight concrete. This light-weight concrete will expect the unit weight drops 20% of the normal concrete where the insulation of the concrete is getting better.

Sintering Temperature, °C	Mineralogical Content
Green	Quartz, Albite, Illite, Clinocllore(Fe), Microcline, Kaolinite, Calcite, Dolomite
1100	Quartz, Spinel(Fe), Hercynite, Pyrite, Tridymite, Albite
1120	Quartz, Spinel(Fe), Hercynite, Pyrite, Tridymite, Albite
1150	Quartz, Spinel(Fe), Hercynite, Pyrite, Tridymite, Albite
1170	Quartz, Spinel(Fe), Hercynite, Pyrite, Ringwoodite(Fe), Mullite
1200	Quartz, Spinel(Fe), Hercynite, Pyrite, Ringwoodite(Fe), Mullite
1250	Quartz, Spinel(Fe), Hercynite, Ringwoodite(Fe), Mullite

Table 3: The mineralogical content of the green body and expanded aggregates at various sintered temperatures.

ACKNOWLEDGEMENTS

We wish to express our appreciation to the IRPA research fund to support the project and Dr. Jang Sung Do of KIST, Korea, Mr. Chang Boon Ping for their technical advice, Mr. Stanley Lau of Li Nguon Quarry for kindly contribution of the clay material.

In addition, the assistance of Ms Lee Lay Kuan for XRF analysis, Mrs. Salbiah Hassan, Mrs. Zalina Saem, Mohd. Syaifurizwan and other whose name may not be printed is acknowledged with gratitude.

REFERENCES

1. Bell, K.E., Brady, J.G. and Zemgals, L.K., "Ceramic Clays and Shales of the Atlantic Provinces" *CANMET REPORT 78-21*
2. Carter, R.A., "Rocky Mountain Light", *Rock Products*, August 1991. pp 50-58
3. Fan, C.M., "A Study on the Characteristics of Bloating Clays and Their Relation to Bloating", *Malaysia Geological Sarveng Annual Report 1986* pp 407 - 420
4. Mc Carl H.N., "Construction Materials", *Industrial Minerals and Rock*. pp 81 - 89
5. Trrell, D.R., "Expanded Products" *Industrial Inorganic Chemistry* pp 399 - 606
6. Wilson, H.S., "Lightweight Aggregates for Structural Concrete" *CANMET REPORT 76-12*

KESAN PENGGUNAAN ABU KELAPA SAWIT SEBAGAI AGEN PENGAWAL KEHILANGAN BENDALIR DI DALAM OPERASI PENYIMENAN TELAGA PETROLEUM

Ahmad Suhaimi, P.M Dr. Ariffin Samsuri, Shahrin Sharuddin,
Abu Samah dan Zainudin Ahmad
Jabatan Kejuruteraan Petroleum
Fak. Kej. Kimia & Kej. Sumber Asli.
Universiti Teknologi Malaysia
Jalan Semarak, 54100 K. Lumpur.

ABSTRAK

Dalam operasi penyimenan telaga petroleum, bahan tambah digunakan untuk mendapatkan sifat-sifat simen yang dikehendaki supaya sesuai dengan keperluan operasi terbabit, antaranya bahan tambah kehilangan bendalir. Setakat ini, semua bahan tambah yang diperlukan masih diimport dari luar negara.

Kajian makmal yang berdasarkan API Spec. 10 telah dilakukan dan perbandingan dibuat terhadap buburan simen yang ditambah dengan agen pengawal kehilangan bendalir yang diimport dengan buburan simen yang dicampur abu kelapa sawit telah menunjukkan abu kelapa sawit boleh digunakan sebagai agen pengawal kehilangan bendalir.

PENGENALAN

Operasi penyimenan merupakan salah satu daripada operasi yang penting bagi melengkapkan sesebuah telaga. Diantara fungsi penting simen adalah untuk melindungi zon-zon pengeluaran hidrokarbon, memperkuat selongsong pada formasi, menghalang letusan zon bertekanan tinggi, melindungi selongsong dari bendalir formasi yang boleh mengarat, menghalang aliran menegak bendalir formasi, mengasingkan zon zon hilangan edaran dan memudahkan operasi kerja semula.

Untuk memastikan operasi penyimenan berjalan dengan lancar maka simen yang digunakan mesti mempunyai ciri ciri yang memenuhi spesifikasi tertentu sesuai dengan keadaan yang dihadapi, terutamanya kedalaman telaga, tekanan, suhu, sifat fizikal dan kimia batuan formasi serta bendalir yang terdapat di dalamnya. Oleh kerana kedalaman purata telaga minyak di Malaysia sekitar 1500m hingga 3000m, maka simen kelas G (menurut pengelasan oleh API) sesuai digunakan. Untuk mendapatkan kesesuaian di antara ciri ciri simen dengan keadaan telaga, maka bahan tambah digunakan yang biasanya terdiri daripada pelanjut, pencepat, perencat, agen kawalan kehilangan bendalir, penyerak dan agen pemberat. Bahan tambah berkenaan diperoleh dari negara luar.

Untuk mengurangkan aliran wang keluar negara dan mengembangkan penggunaan bahan tempatan, suatu kajian di makmal telah dijalankan bagi mengkaji kesesuaian abu kelapa sawit untuk digunakan sebagai bahan tambah pada operasi penyimenan telaga minyak di Malaysia. Secara am, ciri simen yang baik ialah berketertelapan kurang dari 0.1 md dan kekuatan mampatan lebih dari 300 psi.⁽¹⁾ Ketumpatan bagi buburan simen mestilah lebih kurang sama dengan ketumpatan lumpur penggerudian yang digunakan bagi mengawal tekanan hidrostatik formasi. Ketumpatan yang terlalu besar akan mengakibatkan peretakan dan kehilangan edaran manakala ketumpatan yang kecil akan menyebabkan berlakunya letusan liar.

Bahan tambah kehilangan bendalir digunakan dalam operasi penyimenan bagi mengekalkan nisbah air- pepejal dalam buburan simen. Nisbah ini perlu dikekalkan bagi mencegah berlakunya:

1. Pengerasan buburan simen sebelum masanya sehingga menyebabkan penyerasan yang tidak sempurna.
2. Pertukaran reologi buburan simen yang akan turut menurunkan prestasi.
3. Kerosakan formasi zon pengeluaran oleh turasan simen yang membawa zarah zarah kecil sehingga menyumbat ruang pori batuan formasi.

Bahan tambah kehilangan bendalir yang diperolehi dari luar negara terdiri dari "ionic polimer" (Selulos dan Selulos terbitan). Polimer terbitan biasanya terdiri daripada "polystyrenes dan polyacrylates". Penambahan air ke dalam simen telah menyebabkan terbentuknya ikatan elektrostatis dan menyebabkan ujudnya cas pada permukaan antara pepejal dan cecair dan membentuk ion-ion kalsium yang akan bergabung dengan aluminat dan membentuk komponen dikalsium silika dan trikalsium aluminat dikenali sebagai "klinker".

Abu kelapa sawit pula terdiri daripada selulos semula jadi iaitu selulos, alfa selulos, hemi selulos dan lignin. Jadual 1 dengan jelas menunjukkan abu kelapa sawit mempunyai oksida silika yang tinggi. Kandungan silika akan bertindak balas dengan komponen-komponen simen, terutama trikalsium silika dan dikalsium silika.

Ion silika akan bertindak dengan struktur kalsium silikat hidrat bagi membentuk struktur monokalsium yang dinamakan "Zenolit". Ini akan mengelakkan terbentuknya struktur alfa dikalsium silikat hidrat.⁽²⁾ Struktur zenolit merupakan struktur yang stabil walaupun pada suhu perawatan yang tinggi.⁽³⁾ Selain itu, terdapat juga unsur oksida aluminat yang boleh mempercepat masa berlakunya penghidratan simen. Komponen trikalsium aluminat yang terdapat di dalam simen berperanan terhadap tindakbalas penghidratan simen dan ion aluminat yang bertindakbalas dengan komponen trikalsium aluminat akan mempercepat berlakunya proses penghidratan.

BAHAN DAN KAEDAH

Bahan-bahan yang diuji mengikut spesifikasi dan kaedah yang telah ditetapkan oleh American Petroleum Institute (API), sebagaimana yang terkandung didalam API Spec. 10.⁽⁴⁾

Kaedah Penyediaan Bahan Tempatan Yang Akan Diuji.

Langkah-langkah yang dilaksanakan adalah seperti berikut :-

1. Keringkan hampas kelapa sawit dan asingkan daripada bendasing.
 2. Kisar hampas kelapa sawit yang telah kering dengan menggunakan mesin pengisar yang halus.
 3. Ayak bahan yang telah dikisar dengan menggunakan pengayak berukuran 75 mikron (ukuran yang telah ditetapkan oleh API Spec. 10).
 4. Hampas kelapa sawit yang telah dikisar dimasukkan ke dalam kebuk pembakar pada suhu 700 C sehingga berlakunya pembakaran lengkap.
- Ciri-ciri buburan simen yang dikaji adalah kehilangan bendalir buburan simen yang telah dicampur dengan abu kelapa.

Ujian Kehilangan Bendalir Pada Keadaan Reserbor.

Buburan simen yang telah dicampur dengan abu kelapa sawit dimasukkan ke dalam alat "Atmospheric Pressure Consistometer" untuk mengalami proses "preheating" selama 20 minit. Buburan simen kemudiannya dimasukkan ke dalam "Filter Press" bertekanan tinggi dan suhu ditetapkan sepanjang pengujian dilakukan.

Ujian Kehilangan Bendalir Pada Keadaan Permukaan.

Buburan simen yang telah dicampur dengan abu kelapa sawit dimasukkan ke dalam "Atmospheric Pressure Consistometer" selama 20 minit supaya mengalami proses "preheating". Buburan kemudiannya di masukkan ke dalam alat "Filter Press" dan tetapkan tekanan pada 100 psi sepanjang pengujian.

Ujian Kekuatan Mampatan.

Buburan simen dimasukkan ke dalam 1/2 daripada kuantiti acuan bersaiz 2" * 2" * 2". Kacau buburan simen selama 25 saat dengan menggunakan rod pengacau. Penuhkan acuan dengan simen dan kacau simen tersebut selama 25 saat untuk membebaskan gelembung gelembung udara yang terdapat di dalam buburan berkenaan. Masukkan acuan ke dalam " Pressurize Curing Chamber" pada suhu dan tekanan mengikut jadual 5, API Spec. 10. Ujian kekuatan mampatan dijalankan ke atas simen yang telah mengalami proses perawatan selama 8 jam, 1, 3 dan 7 hari dengan menggunakan " Compressive Strength Tester".

KEPUTUSAN

Kesan Abu Kelapa Sawit Terhadap Kadar Kehilangan Bendalir Pada Keadaan Reserbor.

Ujian telah dijalankan pada suhu dan tekanan tinggi iaitu 125 °C dan 1000 psi. Jadual 2 menunjukkan penggunaan abu kelapa sawit sebanyak 1% pada buburan telah mengurangkan kehilangan bendalir sebanyak 7 ml dalam masa 0.25 minit. Peningkatan penggunaan abu kelapa sawit yang seterusnya akan menyebabkan kadar kehilangan bendalir berkurangan. Kadar kehilangan bendalir pada 5% abu kelapa sawit adalah lebih kecil berbanding dengan 1% abu kelapa sawit. Ini menunjukkan bahawa abu kelapa sawit boleh bertindak sebagai agen pengawal kehilangan bendalir. Abu kelapa yang terdiri daripada 70% selulos boleh menyerap air yang terdapat di dalam simen sehingga dapat menghalang perubahan nisbah kandungan cecair dan pepejal di dalam buburan simen.

Perbandingan Kesan Abu Kelapa Sawit Dan Bahan Tambah Piawai (Halad) Terhadap Kehilangan Bendalir Pada Buburan simen.

Gambarajah 1 menunjukkan penggunaan 1% abu kelapa sawit akan mengurangkan kadar kehilangan bendalir sebanyak 29 ml. Penggunaan Halad sebanyak 0.1 % pula akan mengurangkan kehilangan bendalir sebanyak 10 ml. Jelas dilihat bahawa pada peratusan yang kecil ,penggunaan abu kelapa sawit lebih berkesan daripada penggunaan halad. Penggunaan 2% halad menyebabkan kadar kehilangan berkurang sebanyak 223 ml sedangkan penggunaan 5% abu kelapa sawit pula menyebabkan kadar kehilangan bendalir berkurang sebanyak 205 ml. Keputusan ini menunjukkan kesan pengurangan kehilangan bendalir yang dihasilkan dari percampuran abu kelapa sawit ke dalam buburan simen dan halad tidak menunjukkan perbezaan yang ketara.

Kesan Abu Kelapa Sawit Terhadap Kadar Kehilangan Bendalir Pada Keadaan Permukaan.

Gambarajah 2 menunjukkan bahawa kadar kehilangan bendalir berkurangan sebanyak 10 ml apabila 1% abu kelapa sawit digunakan . Penggunaan 5% abu kelapa sawit telah menyebabkan pengurangan kadar kehilangan sebanyak 40 ml, iaitu pengurangan sebanyak 4 kali ganda dari penggunaan 1% abu kelapa sawit. Ini menunjukkan bahawa kesan penggunaan abu kelapa sawit pada buburan simen telah menyebabkan kadar

kehilangan bendalir dapat dikurangkan. Abu kelapa sawit yang terdiri daripada selulos telah memerangkap ion-ion hidrogen dan seterusnya mencegah dari berlakunya perubahan pada nisbah air-pepejal di dalam buburan simen. Keputusan ini juga menunjukkan abu kelapa sawit bertindak dengan lebih berkesan pada keadaan reserbor.

Ujian Kekuatan Mampatan.

Gambarajah 3 menunjukkan hasil ujian kekuatan mampatan pada jangka masa yang tertentu. Keputusan menunjukkan bahawa kekuatan mampatan meningkat dengan jangka masa perawatan, iaitu 8 jam, 1 hari, 3 hari dan 7 hari bila 5% abu kelapa sawit dicampurkan ke dalam simen. Kuartza yang terkandung dalam silika bertindakbalas dengan trikalsium silikat dan dikalsium silikat sehingga membentuk satu struktur baru yang dikenali sebagai Zenolit. Struktur ini merupakan satu struktur yang stabil walaupun pada suhu yang tinggi. Kekuatan mampatan mencapai tahap maksimum pada penggunaan 15% abu kelapa sawit dan penurunan terhadap kekuatan simen berlaku pada 20% dan 25% penggunaan abu kelapa sawit. Penurunan kekuatan ini berlaku akibat kandungan silika yang berlebihan telah menyebabkan terbentuknya struktur alfa dikalsium silikat hidrat yang mana akan mengalami proses pemecahan.

KESIMPULAN.

Dari kajian yang telah dijalankan didapati abu kelapa sawit mampu bertindak untuk mengawal kadar kehilangan bendalir dari buburan simen dan mampu juga meningkatkan kekuatan simen. Bagaimana pun, kajian lanjut untuk menentukan kesan penggunaan abu kelapa sawit terhadap ciri-ciri simen yang lain harus dilakukan dan kesan terhadap bahan tambah lain yang digunakan bersama-sama juga perlu ditentukan bagi mengelakkan kesan negatif terhadap ciri-ciri simen yang berkaitan dan fungsi bahan tambah berkenaan. Di samping itu, kajian ekonomi juga harus dilakukan supaya dapat ditentukan kos pengeluaran serta pengembangan abu kelapa sawit adalah setimpal dengan kelebihan yang diperolehi dan tidak menyebabkan kos keseluruhan operasi penyimenan telaga bertambah.

RUJUKAN

1. Allen T.D., 1978. 'Production Operation'. Vol. 1, Tulsa. Oil & Gas Consultants International, USA.
2. PATCHEN, F.D., "Reaction and Properties of Silica Portland Cement Mixtures at Elevated Temperature". JPT vol. 219, Nov 1960
3. DOWELL Sch lumberger monograf, "Cementing Technology", Chapter 7, pg 9-13
4. API Specification 10, July 1, 1990. Specification For Materials and Testing For Well Cement. American Petroleum Institute, 1220 I street, Northwest, Washington DC, USA.

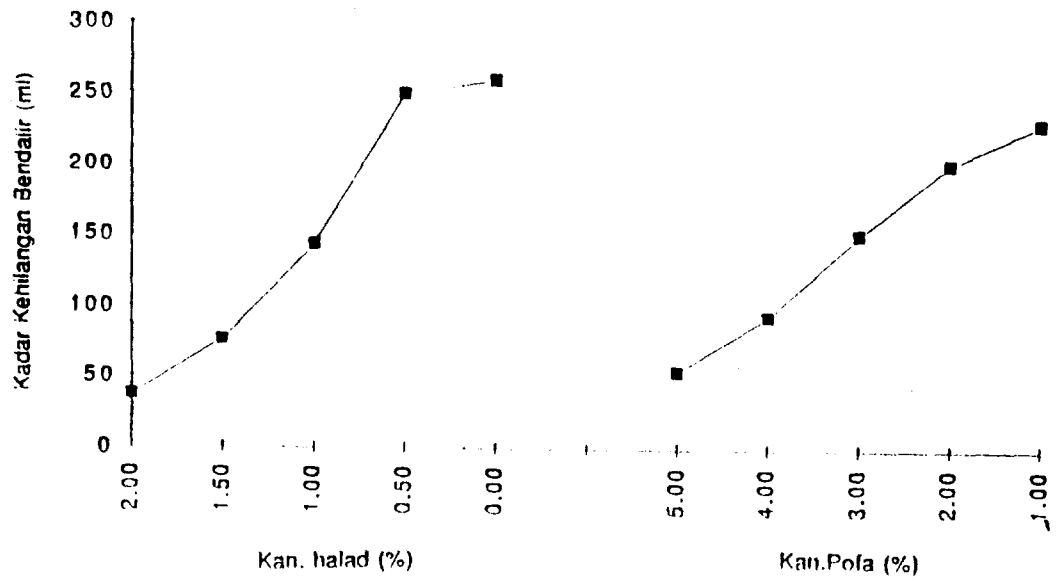
Jadual 1
Mineral Oksida Simen Kelas G,
Abu Kelapa Sawit Dan Halad

Oxide	G Cement (%)	POFA (%)	Halad (ppm)
SiO ₂	62.44	21.75	29,245.2
Al ₂ O ₃	4.77	3.31	bdl
TiO ₃	0.36	0.22	bdl
Fe ₂ O ₃	4.41	4.87	232.8
MgO	3.16	0.95	44.6
CaO	10.89	64.54	1,186.6
Na ₂ O	0.54	0.19	7.9
K ₂ O	9.12	0.10	750.0
Mn ₂ O	0.12	0.08	bdl
P ₂ O	0.17	0.17	40.8
SO ₃	1.93	2.36	bdl
L.O.I *	2.09	1.15	

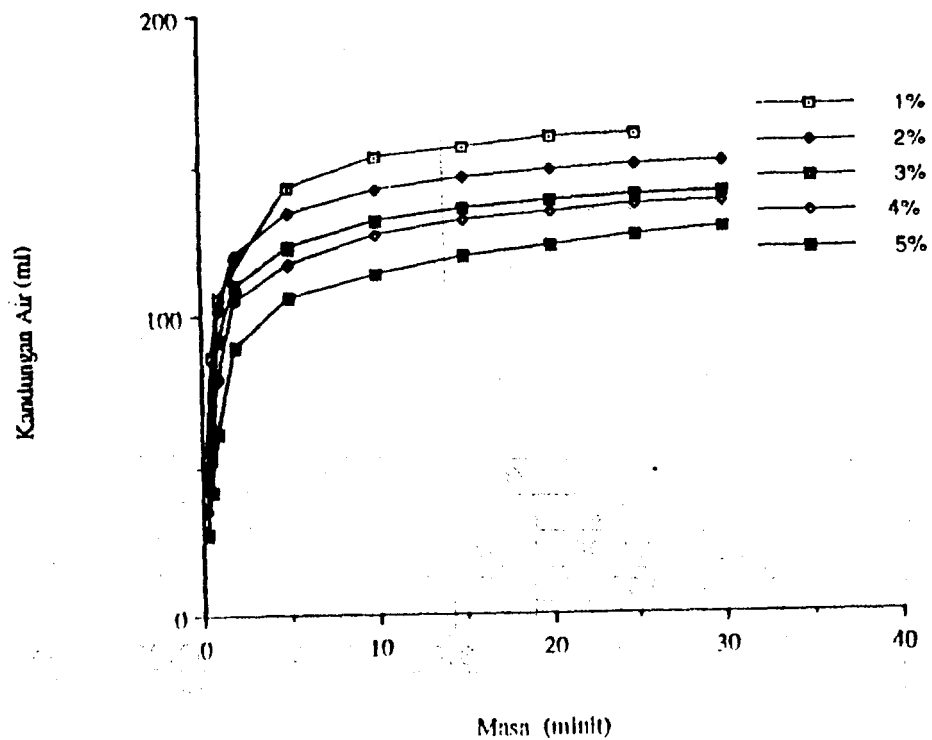
* -Volatiles Other Than SO₃
bdl -Below Detection Limit.
ppm- Part Per Million

JADUAL 2
Kesan Penggunaan Abu Kelapa Sawit Ke Atas Kehilangan Bandalir Pada Keadaan Reserbor

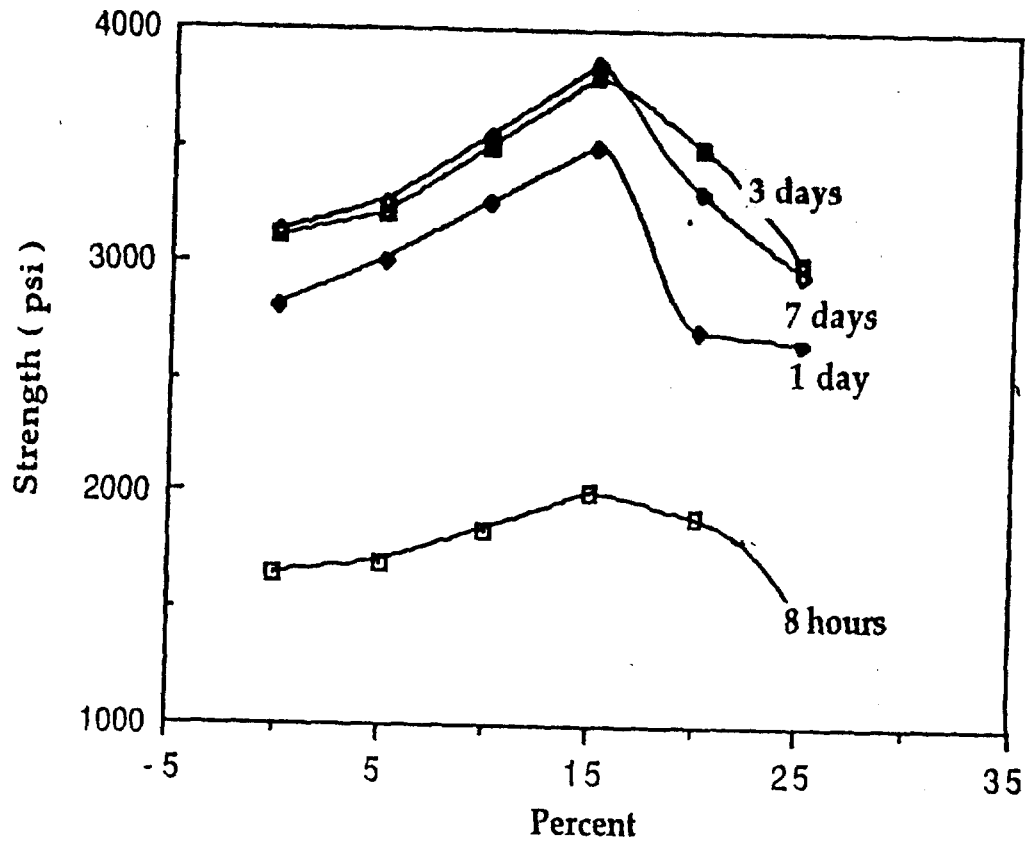
Masa (minit)	Kandungan Pofa					
	1%	2%	3%	4%	5%	0%
0.25	65.00	51.00	45.00	36.00	28.00	70.00
0.50	130.00	102.00	87.00	51.00	33.00	130.00
1.00	187.00	153.00	132.00	70.00	41.00	210.00
2.00	227.00	198.00	143.00	86.00	50.00	253.00
5.00	230.00	201.00	151.00	94.00	54.00	259.00



Gambarajah 1 Perbandingan Diantara Abu kelapa Sawit Dan Halad



Gambarajah 2. Kesan Penggunaan Abu Kelapa Sawit Ke Atas Ujian Kehilangan Bendalir Pada Keadaan Permukaan,



Gambarajah 3. Kesan Penggunaan Abu Kelapa Sawit Ke Atas Ujian Kekuatan.



THE STUDY OF MICROSTRIP ELECTROMAGNETIC PROPERTIES AND METHOD OF MEASURING ϵ_r .

By

Ir. Wan Khairuddin Wan Ali
M.Sc. (Avionic) C.I.T., U.K.
Faculty of Mechanical Engineering
Universiti Teknologi Malaysia.

Abstract.

Equivalent circuits have been derived for microstrip ring resonator using transmission lines theory. From the analysis, two equations were derived. The first equation relates all the parameters of a ring into a single equation. This equation has been used in the design process to determine the ring dimensions. The second equation was used to calculate S_{21} and was given as a function of relative permittivity, ϵ_r , and angular frequency, ω . A procedure has been suggested on how these equations can be used to determine the value of ϵ_r for an unknown substrate. The calculations using the data from experiment were compared with the values given by the manufacturer and was found to be within 8% different.

INTRODUCTION

Figure 1 shows the layout of a symmetrically coupled microstrip ring resonator with a mean radius, r , coupling gap, g , microstrip line width, w and the length of the coupling transmission lines, l .

The resonator essentially consist of a structure in the shape of a ring together with two lengths of transmission lines to provide the required coupling of power. If the effect of the coupling gaps and the transmission lines are neglected, the ring will resonate when its mean circumference is an integer multiple of microstrip wavelength, i.e.,

$$n \cdot \lambda_m = 2 \cdot \pi \cdot r \quad \text{for } n = 1, 2, 3, \dots$$

Where

r = mean radius.

λ_m = microstrip wavelength.

Such a ring resonator has found applications in the measurement of dispersion, phase velocity and effective permittivity, ϵ_{eff} , [1 - 5]. However these applications require a substrate with a known value of relative permittivity, ϵ_r . In many cases, where a new material for the substrate is used, one requires to measure the value of ϵ_r , fast and accurate. A ring resonator can be easily fabricated on the new substrate, thus offering a potentially fast, simple and accurate way of determining ϵ_r .

In this paper, an equivalent circuit model based on transmission line theory, [6], was used. Two equations were derived from analysis and a procedure on how to use these equations to determine ϵ were suggested.

RING RESONATOR DIMENSION

Considering only the ring structure, it will resonate when its mean circumference is an integer multiple of microstrip wavelength, i.e.,

$$l = n \cdot \lambda_m \quad (1)$$

Where

l = The ring mean circumference.

$n = 1, 2, 3, \dots$

If the frequency of the input signal is constrained to a static condition, i.e. $f < 3$ GHz., then the effect of dispersion can be neglected, [3].

This will gives,

$$\epsilon_{eff} = \left[\frac{c}{f \cdot \lambda_g} \right]^2 \quad (2)$$

where,

c = The speed of light in free space.

Substituting (2) into (1) will give,

$$l = \frac{n \cdot c}{f \cdot \sqrt{\epsilon_{eff}}} \quad (3)$$

From Owen [5], for a wide line, $\frac{w}{h} \geq 1$,

$$\epsilon_{eff} = \frac{\epsilon_r + 1}{2} + \frac{\epsilon_r - 1}{2} \cdot \left[1 + 10 \cdot \frac{h}{w} \right]^{-0.555} \quad (4)$$

where,

w = Microstrip line width.

h = The substrate thickness.

Combining equations (3) and (4), gives,

$$\frac{\epsilon_r + 1}{2} + \frac{\epsilon_r - 1}{2} \cdot \left[1 + 10 \cdot \frac{h}{w} \right]^{-0.555} = \left[\frac{n \cdot c}{f \cdot l} \right]^2 \quad (5)$$

Choosing $n = 1$, i.e. for the first resonant frequency and rearranging equation (5), will give,

$$\epsilon_r = \frac{2 \cdot \left[\frac{c}{f_o \cdot l} \right]^2 - 1 + \left[1 + 10 \cdot \frac{h}{w} \right]^{-0.555}}{1 + \left[1 + 10 \cdot \frac{h}{w} \right]^{-0.555}} \quad (6)$$

Where,

f = The first resonant frequency.

It can be seen that equation (6) relates all the parameters of a ring to the first resonant frequency. This equation can be used as a design equation to calculate the require ring dimension.

Figure 2 shows the plots of equation (6) for two rings with $r = 0.015m$ and $r = 0.017m$ and both having $\frac{h}{w} = 0.5$. It shows that, the rings will have the first resonant frequency within the range of 0.5 to 3 GHz if the relative permittivity is between 1.184 and 45.

DERIVATION OF S_{21} .

For a given ring structure as shown in figure 1, Al-Charchafchi, [6] has suggested the equivalent circuit shown in figure 1 to model the ring. This model assumed that the value for ϵ_r is known and the coupling transmission lines having the characteristic impedance equal to the input/output impedances of the measuring equipment, typically 50Ω . Thus the effect of the coupling transmission lines can be ignored. In this paper, ϵ_r is the parameter to be measured and the dimension of the coupling transmission lines were chosen primarily to satisfy the equations used as given below. It is normally not equal to the impedances of the measuring equipment. Thus the effect of the transmission lines are significant and the modified equivalent circuit model for the ring is suggested as shown in figure 1. Figure 1 shows the final simplified equivalent circuit that was derived.

Writing the circuit elements in figure 1 as a function of ϵ_r and angular frequency, ω , will give,

$$Z_{ls}(\epsilon_r, \omega) = jZ_o(\epsilon_r, \omega) \cdot \tan \left[\frac{\beta(\epsilon_r, \omega) \cdot l_s}{2} \right] \quad (7)$$

$$Z_{lp}(\epsilon_r, \omega) = -j \cdot \frac{Z_o(\epsilon_r, \omega)}{\sin(\beta(\epsilon_r, \omega) \cdot l_s)} \quad (8)$$

$$Z_{gp}(\epsilon_r, \omega) = \frac{-j}{\omega \cdot C_{gp}(\epsilon_r)} \quad (9)$$

$$Z_{gs}(\epsilon_r, \omega) = \frac{-j}{\omega \cdot C_{gs}(\epsilon_r)} \quad (10)$$

$$Z_{rp}(\epsilon_r, \omega) = -j \cdot \frac{Z_o(\epsilon_r, \omega)}{\tan\left[\frac{\beta(\epsilon_r, \omega) \cdot l_r}{2}\right]} \quad (11)$$

$$Z_{rs}(\epsilon_r, \omega) = -j \cdot Z_o(\epsilon_r, \omega) \cdot \sin(\beta(\epsilon_r, \omega) \cdot l_r) \quad (12)$$

where,

(Taken from Owen, [5])

$$Z_o(\epsilon_r, \omega) = \frac{119.9}{\sqrt{2 \cdot (\epsilon_r + 1)}} \cdot \left[H - \frac{\epsilon_r - 1}{2 \cdot (\epsilon_r + 1)} \cdot \left(0.4516 + \frac{0.2416}{\epsilon_r} \right) \right] \quad (13)$$

$$H = \ln \left[\frac{4 \cdot h}{w} + \sqrt{\left[\frac{4 \cdot h}{w} \right]^2 + 2} \right] \quad (14)$$

$$\beta(\epsilon_r, \omega) = \frac{\omega \cdot \sqrt{\frac{\epsilon_r + 1}{2} + \frac{\epsilon_r - 1}{2} \cdot \left[1 + 10 \cdot \frac{h}{w} \right]^{-0.555}}}{c} \quad (15)$$

$$l_r = \pi \cdot r \quad (16)$$

l_s = The length of a coupling transmission line.

The coupling gap capacitors, C_{gs} and C_{gp} were found from [7] and [8] with the correction taken from [9] as follows.

$$\left. \begin{aligned} C_{gp} &= 0.5 \cdot C_e(\epsilon_r) \\ C_{gs} &= 0.5 \cdot (C_o(\epsilon_r) + C_{gp}) \end{aligned} \right\} \quad \text{for } 0.5 \leq \frac{w}{h} \leq 2 \quad (17)$$

where,

$$C_o(\epsilon_r) = C_o \cdot 9.6 \cdot \left[\frac{\epsilon_r}{9.6} \right]^{0.8} \quad (18)$$

$$C_e(\epsilon_r) = C_e \cdot 9.6 \cdot \left[\frac{\epsilon_r}{9.6} \right]^{0.9} \quad (19)$$

$$C_o = \left[\frac{g}{w} \right]^{m_o} \exp(k_o) \quad pF \quad (20)$$

$$C_e = 12 \cdot \left[\frac{g}{w} \right]^{m_e} \exp(k_e) \quad pF \quad (21)$$

$$\left. \begin{aligned} m_o &= \frac{w}{h} \cdot \left[0.619 \cdot \log \left[\frac{w}{h} \right] - 0.3853 \right] \\ k_o &= 4.26 - 1.453 \cdot \log \left[\frac{w}{h} \right] \end{aligned} \right\} \quad \text{for } 0.1 \leq \frac{g}{w} \leq 1 \quad (22)$$

$$m_e = 0.8675, \quad k_e = 2.043 \cdot \left[\frac{w}{h} \right]^{0.12} \quad \text{for } 0.1 \leq \frac{g}{w} \leq .3 \quad (23)$$

$$\left. \begin{aligned} m_e &= \frac{1.565}{\left[\frac{w}{h} \right]^{0.16}} - 1 \\ k_e &= 1.97 - \frac{0.03}{\left[\frac{w}{h} \right]} \end{aligned} \right\} \quad \text{for } 0.3 \leq \frac{g}{w} \leq 1 \quad (24)$$

The calculation for the input reflection coefficient with the output matched can be determined from figure 1 as follows.

Simplifying the ring componens using,

$$Z_{rgp}(\epsilon_r, \omega) = \left[\frac{1}{Z_{gp}(\epsilon_r, \omega)} + \frac{1}{Z_{rp}(\epsilon_r, \omega)} + \frac{1}{Z_{rp}(\epsilon_r, \omega)} \right]^{-1} \quad (25)$$

$$Z_{rse}(\epsilon_r, \omega) = \left[\frac{1}{Z_{rs}(\epsilon_r, \omega)} + \frac{1}{Z_{rs}(\epsilon_r, \omega)} \right]^{-1} \quad (26)$$

The S_{11} is given by,

$$S_{11}(\epsilon_r, \omega) = \frac{Z_{in}(\epsilon_r, \omega) - Z_o}{Z_{in}(\epsilon_r, \omega) + Z_o} \quad (27)$$

where,

$$Z_o = \text{Matched impedance} \quad (28)$$

$$Z_{in}(\epsilon_r, \omega) = Z_{1s}(\epsilon_r, \omega) + Z_6(\epsilon_r, \omega) \quad (29)$$

$$Z_6(\epsilon_r, \omega) = \left[\frac{1}{Z_{1p}(\epsilon_r, \omega)} + \frac{1}{Z_{1s}(\epsilon_r, \omega) + Z_5(\epsilon_r, \omega)} \right]^{-1} \quad (30)$$

$$Z_5(\epsilon_r, \omega) = \left[\frac{1}{Z_{gp}(\epsilon_r, \omega)} + \frac{1}{Z_{gs}(\epsilon_r, \omega) + Z_4(\epsilon_r, \omega)} \right]^{-1} \quad (31)$$

$$Z_4(\epsilon_r, \omega) = \left[\frac{1}{Z_{rgp}(\epsilon_r, \omega)} + \frac{1}{Z_{rse}(\epsilon_r, \omega) + Z_3(\epsilon_r, \omega)} \right]^{-1} \quad (32)$$

$$Z_3(\epsilon_r, \omega) = \left[\frac{1}{Z_{rgp}(\epsilon_r, \omega)} + \frac{1}{Z_{gs}(\epsilon_r, \omega) + Z_2(\epsilon_r, \omega)} \right]^{-1} \quad (33)$$

$$Z_2(\epsilon_r, \omega) = \left[\frac{1}{Z_{gp}(\epsilon_r, \omega)} + \frac{1}{Z_{ls}(\epsilon_r, \omega) + Z_1(\epsilon_r, \omega)} \right]^{-1} \quad (34)$$

$$Z_1(\epsilon_r, \omega) = \left[\frac{1}{Z_{lp}(\epsilon_r, \omega)} + \frac{1}{Z_{ls}(\epsilon_r, \omega) + Z_o} \right]^{-1} \quad (35)$$

The forward transmission coefficient with the output matched can be determine by,

$$S_{21}(\epsilon_r, \omega) = S_{21_1}(\epsilon_r, \omega) \cdot S_{21_2}(\epsilon_r, \omega) \cdot S_{21_3}(\epsilon_r, \omega) \cdot S_{21_4}(\epsilon_r, \omega) \quad (36)$$

where,

$$S_{21_1}(\epsilon_r, \omega) = \left[\frac{Z_o}{Z_{ls}(\epsilon_r, \omega) + Z_o} \right] \cdot \left[\frac{Z_1(\epsilon_r, \omega)}{Z_{ls}(\epsilon_r, \omega) + Z_1(\epsilon_r, \omega)} \right] \quad (37)$$

$$S_{21_2}(\epsilon_r, \omega) = \left[\frac{Z_2(\epsilon_r, \omega)}{Z_{gs}(\epsilon_r, \omega) + Z_2(\epsilon_r, \omega)} \right] \cdot \left[\frac{Z_3(\epsilon_r, \omega)}{Z_{rse}(\epsilon_r, \omega) + Z_3(\epsilon_r, \omega)} \right] \quad (38)$$

$$S_{21_3}(\epsilon_r, \omega) = \left[\frac{Z_4(\epsilon_r, \omega)}{Z_{gs}(\epsilon_r, \omega) + Z_4(\epsilon_r, \omega)} \right] \cdot \left[\frac{Z_5(\epsilon_r, \omega)}{Z_{ls}(\epsilon_r, \omega) + Z_5(\epsilon_r, \omega)} \right] \quad (39)$$

$$S_{21_4}(\epsilon_r, \omega) = \left[\frac{Z_6(\epsilon_r, \omega)}{Z_{gs}(\epsilon_r, \omega) + Z_6(\epsilon_r, \omega)} \right] \cdot \left[1 + S_{11}(\epsilon_r, \omega) \right] \quad (40)$$

Equations (7) to (31) can be implemented on a computer and can be used to determine ϵ_r . Figure 2 shows an example of a plot S_{21} against input signal frequencies for a given ring resonator dimensions and fabricated on a substrate with $\epsilon_r = 6.15$. Comparing this result with that obtained experimentally, figure 2, it shows that, within 4% different, both plots are having the same resonant

frequencies. In determining ϵ_r , the reverse process has been used and discussed below.

THEORETICAL AND EXPERIMENTAL RESULT

Equation (6) has been used to determine the required ring dimensions. As shown in figure 2, for a ring with $r = 0.017\text{m}$ and $\frac{h}{w} = 0.5$, it will have the first resonant frequency within the range of 0.5 GHz and 3 GHz when the range of ϵ_r values are between 1.18 and 45. For most cases [10], $r = 0.017\text{m}$ and $\frac{h}{w} = 0.5$ are suitable for determining the unknown ϵ_r . A ring fabricated on RT/duroid 6006 substrate with $r = 0.017\text{m}$ was used to verify the equations. The S_{21} value of the ring was measured using HP 87224 network analyzer and the measured results, shown in figure 2, give the value for the first resonant frequency at 1.305 GHz as well as its harmonics. Using this value for the first resonant frequency together with equation (27), the value of S_{21} against ϵ_r was plotted as shown in figure 2. The plot shows that the ring resonates at the given frequency for two different values of ϵ_r . To avoid ambiguity, both values of ϵ_r were tested for first resonant frequency using equation (27). It was found that $\epsilon_r = 5.7833$ was the only ϵ_r that gave the first resonant frequency at 1.305 GHz. Thus this was the required value for ϵ_r . Two other ring resonator were tested and the result is summarized in the table 1 below.

ϵ_r (Calculated)	ϵ_r (Manufacturer Value)	Ring Radius (m)	Diff. (%)	Manufacturer Substrate Designation
5.7833	6.15	0.017	6	50250M105AGM RT/6006
5.6527	6.15	0.015	8	50250M105AGM RT/6006
2.174	2.2	0.029	1.2	80200M105AQB RT/5880

Table 1. The Summary of The Results.

RESULTS AND DISCUSSION

The ring resonator has been modelled using an equivalent circuit

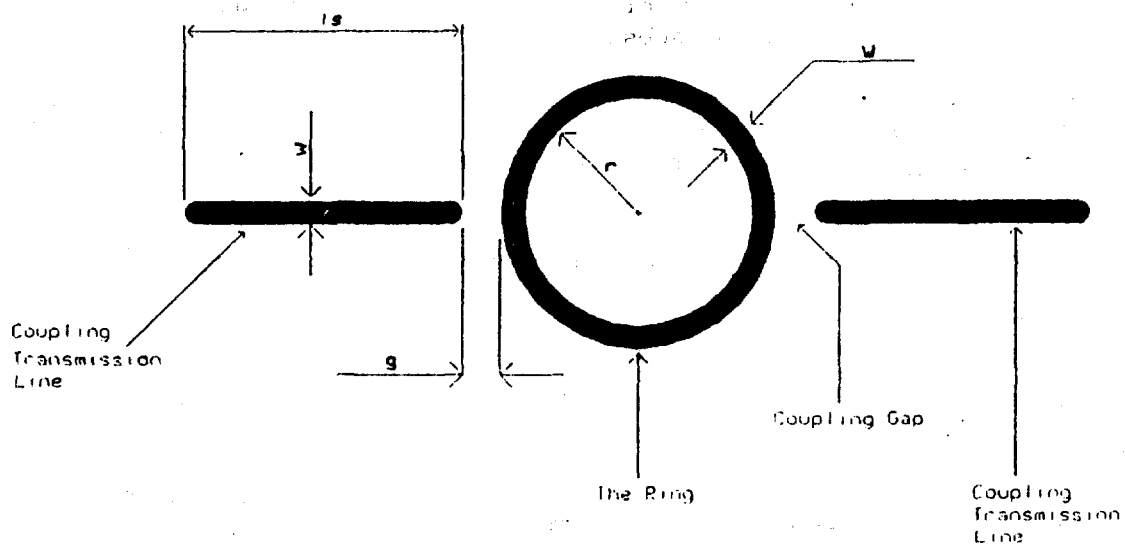
based on transmission line theory. From the derived equation (6) that relates all the parameters of a ring, several rings have been designed and fabricated on substrates with known values of ϵ_r . The equation to calculate S_{21} as a function of angular frequency, ω , and relative permittivity, ϵ_r , was also derived and used together with the experimental results to determine the value of ϵ_r of the substrate used. The experimental result on substrates with known ϵ_r values shows that the worst case was that, the calculated ϵ_r were 8% different.

ACKNOWLEDGMENT

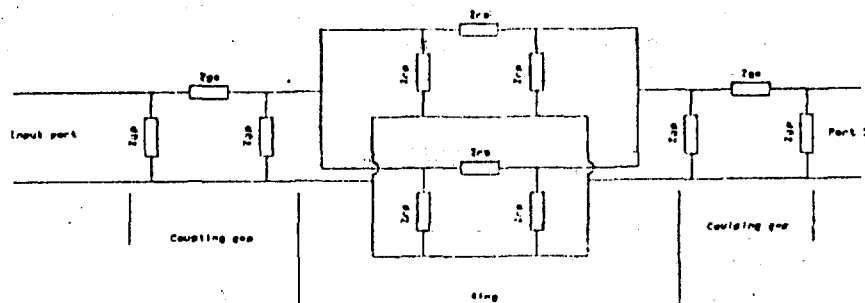
The author would like to thank Mr. Shahrulzaman Hassan, the director of Telecommunication Technology Division, Malaysian Institute of Microelectronic Systems (MIMOS) for allowing him to use the facilities at MIMOS to carry out the experimental measurements.

REFERENCES

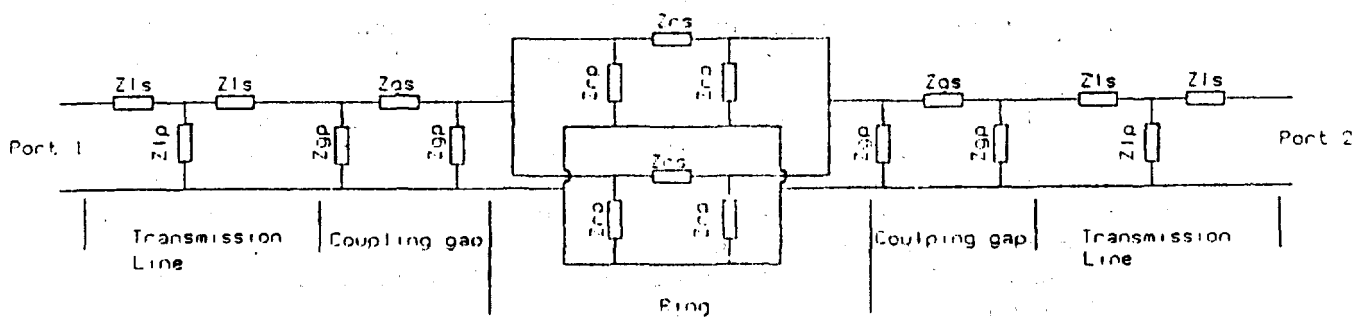
- [1] P. Troughton, "High Q-factor resonator in microstrip", *Electron. Lett.*, Vol. 4, pp. 520-522, 1968.
- [2] P. Troughton, "Measurement Techniques in Microstrip", *Electron. Lett.*, Vol. 5, pp. 25-26, 1969.
- [3] T.C. Edwards, *Foundations for microstrip Circuit Design*, New York, Wiley 1981.
- [4] T.C. Edwards, "Microstrip Measurements", *IEEE MTT-S Int. Microwave Symp., Dig.*, 1982. pp. 338-341.
- [5] R.P. Owens, "Accurate analytical determination of quasi-static microstrip line parameters", *The Radio and Electronic Engineer*, Vol. 46, No. 7, July 1976, pp. 360-364.
- [6] S.H. Al-Charchafchi and C.P. Dawson, "Analysis of asymmetrically coupled microstrip ring resonators", *Int. J. Electron.*, 1990, Vol. 68, (2), pp. 275-282. 82.
- [7] K.C. Gupta, R. Garg and I.J. Bahl, *Microstrip lines and slotlines.*, Dedham, MA: Artech House. 1979.
- [8] R. Garg and I.J. Bahl, "Microstrip discontinuities", *Int. J. Electron.*, Vol. 45, pp. 81-87, July 1978.
- [9] K. Chang, S. Martin, F. Wang and J.L. Klein, "On the study of microstrip ring and varactor-tuned ring circuits", *IEEE Trans., Microwave Theory and Techniques*, Vol. MTT-35, pp.1288-1295, Dec. 1987.
- [10] R. Chatterjee, *Element of microwave engineering*, Ellis Horwood Series, Ellis Horwood Limited, England, 1986.



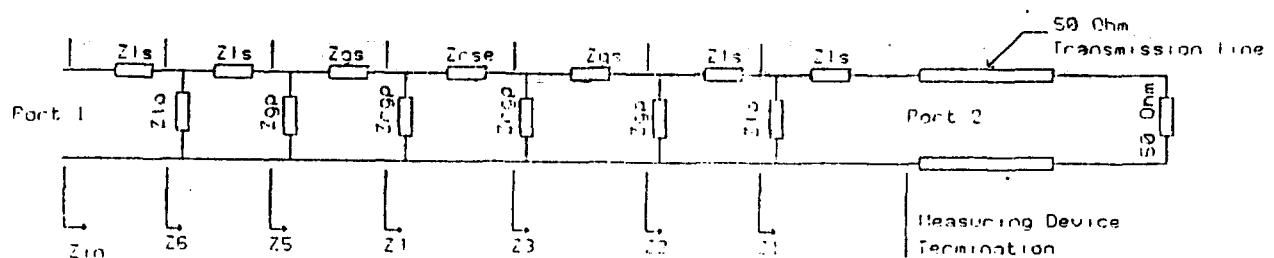
The schematic layout of the ring resonator.



An Equivalent circuit for the ring resonator as suggested in [6].



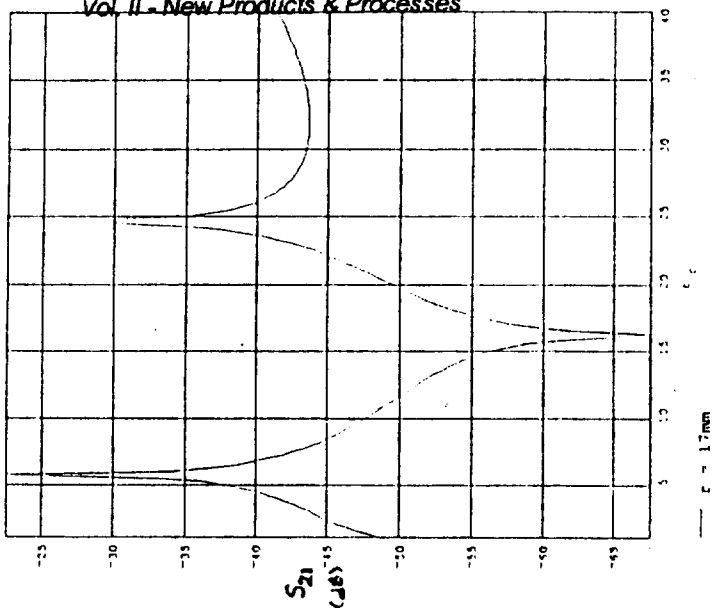
A Modified equivalent circuit for the ring resonator.



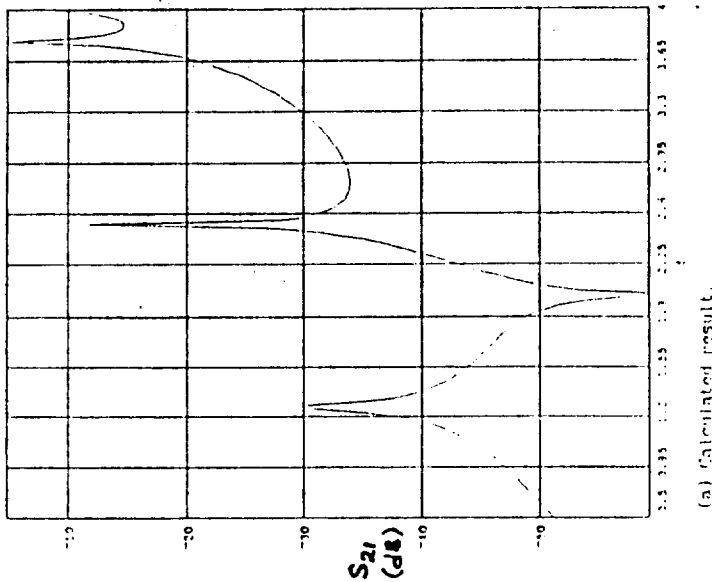
A simplified equivalent circuit for the ring resonator derived from

**POOR QUALITY
ORIGINAL**

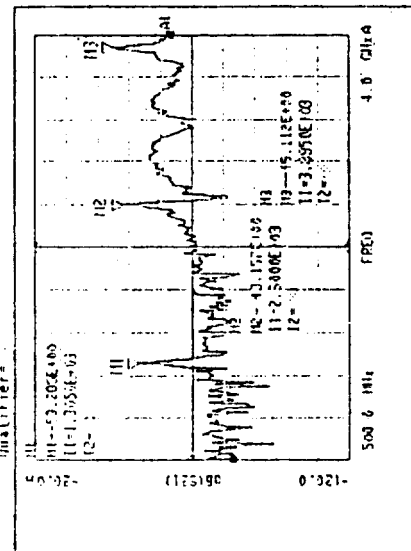
FIGURE 1



The plot of S_{21} against f for a ring with the following parameters : $r = 17.057$ mm, $l_a = 15$ mm, $h = 0.65$ mm, $w = 1.28$ mm, $g = 0.77$ mm.



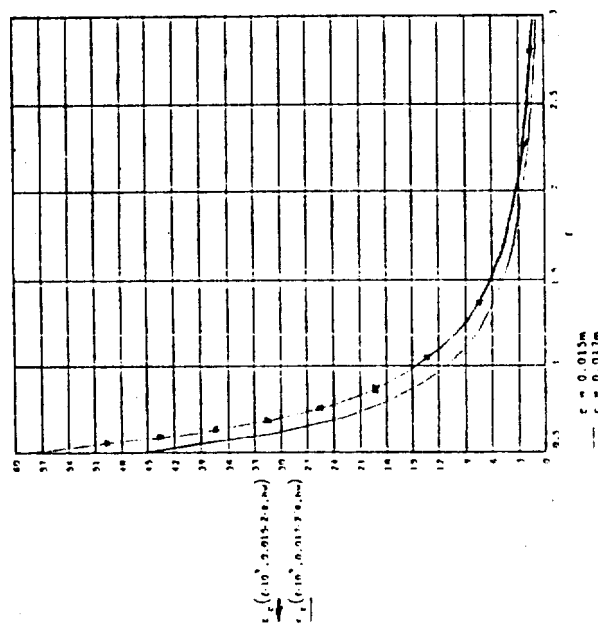
(a) Calculated result.



(b) Experimental result.

The plot for S_{21} (dB) against frequency (f).

FIGURE 2



The plot of r against the first resonant frequencies for the ring with $r = 17$ mm and $r = 15$ mm and both having $h = 0.5$.

UJIAN MAMPATAN KE ATAS PAIP KOMPOSIT YANG DIBUAT DENGAN MENGGUNAKAN KAEDAH EMPAR

. oleh

Prof. Madya Dr. Daud Hj. Abd. Rahman
Jabatan Mekanik dan Rekabentuk
Fakulti Kejuruteraan Jentera
Universiti Teknologi Malaysia
Johor Bahru

ABSTRAK

Kaedah pembuatan paip komposit yang diguna secara meluas adalah bengkalai tangan, belitan filaman dan kaedah empar. Dalam kaedah empar, tikar kaca diletak di dalam acuan silinder geronggang dan kemudiannya acuan tersebut diputar. Damar dituang secara rata ke atas permukaan tikar kaca yang terdedah dengan keadaan acuan masih berputar. Tindakan empar akan menyebabkan damar tersebar dan meresap kedalam tikar kaca. Lapisan kaca yang berada dalam keadaan mampat akan menjamin supaya lompong udara tidak wujud di dalam paip komposit yang terhasil. Kertas kerja ini memaparkan dua aspek kerja yang telah dilaksanakan. Pertama ia membincang rekabentuk dan fabrikasi mesin empar mudah bagi penghasilan paip komposit pendek dan kedua ia membincang mengenai kerja ujikaji yang dijalankan ke atas paip komposit yang terhasil. Tiga contoh paip dibuat dengan menggunakan pelapisan CSM/CSM/CSM, WR/WR/WR dan WR/CSM/WR. Kesemua paip yang diuji dikenakan beban mampat untuk menilai kekuatan paip dalam mampatan dan sifat lain bagi paip tersebut.

Pengenalan

Bahan komposit telah diterima secara meluas sebagai bahan kejuruteraan mudahsuai yang boleh diguna di dalam kebanyakan industri. Sebagai contoh, paip plastik bertetulang kaca (GRP) yang mengabungkan sifat ringan dan kekuatan beserta dengan rintangan kakisan telah diguna di dalam pelbagai loji proses kimia. Selain daripada itu terdapat banyak penggunaan komponen tersebut, bermula daripada pesawat terbang dan pengangkutan udara kepada industri air, sisa terbuang dan keceriaan. Teknik fabrikasi yang tidak melibatkan kos tinggi adalah diperlukan untuk mencepatkan penggunaan bahan komposit pada masa akan datang [1]. Dewasa ini kaedah bengkalai tangan telah diguna dalam penghalan lapisan, pertindanan, *draping* dan sambungan. Arus ini perlu diubah demi untuk memajukan penggunaan bahan komposit dalam industri tempatan.

Kertas kerja ini memperkenalkan satu kaedah pembuatan kos rendah dalam pembikinan paip pendek daripada gentian kaca. Paip yang dihasilkan kemudiannya diuji dalam mampatan bagi menentukan kekuatannya.

Latar belakang teori

Daya empar akan terhasil apabila sesuatu jisim dipusing dengan halaju sudut ω , pada satu pusat pusingan melalui tali panjang r , seperti

digambarkan i dalam Rajah 1. Panjang tali, r , adalah jejari pusingan jisim.

Daya empar, F , yang terhasil diberi oleh persamaan berikut:-

$$F = m\omega^2 r \text{ kN} \quad (1)$$

dengan, m dalam kg
 ω dalam radian per (saat)²
 r dalam meter

Tindakan daya empar F ke atas jisim ditunjukkan di dalam Rajah 1.

Persamaan mudah di atas, merupakan konsep asas berhubung dengan kaedah yang dibincang di dalam kertas-kerja ini. Analisis daya yang lebih terperinci ke atas komponen mesin yang direkabentuk diberi oleh Zalaludin [2].

Rekabentuk Mesin Empar

Lukisan isometrik mesin yang telah di hasilkan sebagai rekabentuk asas adalah seperti didalam Rajah 2. Rajah tersebut menunjukkan bahawa mesin terbahagi kepada tiga komponen penting. Pertama, bahagian silinder acuan. Kedua bahagian kerangka utama dan ketiga, motor eletrik yang diguna sebagai pemacu silinder acuan.

Silinder acuan, yang mempunyai garispusat luar berukuran 258 mm dan tebal dinding 3 mm, disokong pada dua lokasi. Satu berhampiran dengan takal dan satu lagi melalui enam bering yang diikat pada kerangka segienam. Panjang silinder ialah 458 mm. Satu hujung silinder ditutup sementara satu lagi terbuka dan di pasang bibir bulat (berbentuk gelang) pada hujung tersebut. Bibir ini menutupi sebahagian hujung silinder yang terbuka sebanyak lebihkurang 5 mm keliling lubang (lihat rajah). Ini bertujuan untuk memastikan bahan yang dimasukkan kedalam silinder tidak mudah terkeluar apabila silinder berputar. Bahagian kerangka utama yang menyokong silinder dan motor elektrik dibuat daripada besi sesiku berukuran 50 mm x 50 mm x 6 mm. Ukuran maksimum kerangka ialah 750 mm x 415 mm x 600 mm tinggi. Dua pendakap, juga dibuat daripada besi sesiku saiz yang sama seperti di atas, diikat dengan bolt pada kerangka. Ini adalah tempat meletak motor elektrik. Motor elektrik yang diguna adalah jenis DC dan mempunyai kuasa 1 kW.

Rajah 3 pula menunjukkan lukisan untuk alat penuang resin. Alat ini diperlui untuk menuang resin ke dalam silinder acuan semasa silinder berputar. Ini akan memastikan resin dituang dengan sekata ke atas tikar gentian kaca. Alat penuang resin ini terdiri daripada kaki (kerangka utama) dan batang penghulur. Batang penghulur mempunyai pemegang pada satu hujung sementara pada hujung yang lain, bekas resin dikimpalkan kepadanya seperti ditunjukkan di dalam rajah. Ketinggian batang penghulur dari lantai ialah 445 mm. Ketinggian ini adalah hampir sama dengan ketinggian paksi silinder acuan di dalam Rajah 2. Semasa beroperasi, batang penghulur hanya boleh berpusing pada paksinya dan bergerak arah mendatar sahaja. Kedua-dua pergerakan tersebut dapat dilakukan kerana batang penghulur dimasukkan kedalam tiub keluli berukuran 280 mm panjang yang terletak pada bahagian atas rangka utama. Ini juga akan memastikan had kawalan pergerakan batang penghulur dapat dikawal.

Keperluan bahan mentah

Bahan mentah yang diperlukan bagi menghasilkan silinder komposit termasuk tikar gentian kaca, damar poliester, wax, pengeras (hardener), mangkin, *thinner* dan plastik tahan panas. Peralatan lain seperti penimbang, bekas untuk membancuh damar, juga perlu disediakan.

Proses pembuatan paip komposit

Proses membuat paip komposit dengan menggunakan kaedah ini bermula dengan menyediakan bahan mentah yang disenarai di atas. Beberapa keping tikar gentian kaca dipotong dan saiznya disesuaikan untuk menutupi keseluruhan bahagian dalam dinding silinder. Ukuran tikar gentian kaca arah lilitan silinder dilebihkan sedikit supaya kedua-dua hujung terselut berselisih. Ini akan memastikan silinder komposit yang dihasilkan adalah kukuh. Beberapa keping tikar gentian kaca disediakan untuk menyesuaikan dengan ketebalan silinder yang diperlukan (4 keping gentian kaca jenis ringan akan menghasilkan paip lebih kurang 2.5 mm tebal). Campuran damar, pengeras dan mangkin juga hendaklah disediakan terlebih dahulu, mengikut sukatan yang lazim diguna. Gentian kaca dan damar, disediakan mengikut nisbah berat yang disyor oleh piawaian tertentu.

Dua kaedah boleh diguna untuk membuat silinder komposit. Kedua-dua kaedah tersebut telah diterangkan secara mendalam di dalam Rujukan [2]

Kerja Pengujian

Penyediaan contoh

Contoh paip yang akan diuji dibuat dengan menggunakan kaedah yang di terangkan di atas. Tiga daripada beberapa paip yang dihasilkan telah dipilih untuk diuji. Paip tersebut dibuat daripada tiga lapis tikar gentian kaca. Paip 1 dibuat daripada tikar gentian jenis *chopped strand mat* sementara Paip 2 dibuat daripada tikar gentian jenis *woven roving*. Paip 3 mempunyai tikar gentian kaca terdiri daripada dua lapis *woven roving* dan selapis *chopped strand mat* (lapisan tengah).

Seterusnya bahagian paip yang tidak sempurna pada kedua-dua hujung dipotong dan dibuang bagi memastikan paip tersebut mempunyai ketebalan yang hampir seragam pada keseluruhan panjangnya. Ini juga untuk memastikan hujung paip adalah rata dan apabila daya mampatan dikenakan, tekanan ke atas hujung paip adalah seragam. Tolok terikan dipasang arah lilitan dan arah paksi paip bagi kesemua paip pada lokasi $L/4$, $L/2$ dan $3L/4$ (L adalah panjang paip).

Butir-butir lengkap mengenai paip yang diuji diberi di dalam Jadual 1.

Jadual 1: Butir butir paip yang diuji

Rujukan Paip	Jenis Pelapisan	Panjang (mm)	Jejari dlm (mm)	Tebal (mm)	Bilangan Lapisan	Nisbah resin/kaca
Paip 1	CSM/CSM/CSM	412.5	119.5	1.30	3	55 : 45
Paip 1	WR/WR/WR	416.5	120.0	2.30	3	55 : 45
Paip 3	CSM/WR/CSM	396	120.0	1.80	3	55 : 45

Nisbah resin terhadap mangkin ialah 100:1

Mesin Ujian

Ujian mampatan dijalankan dengan mengguna mesin ujian umum Dartec, jenis *Servo Hydraulics*. Keupayaan maksimum mesin ialah 1200 kN. Bebanan adalah dikawal melalui anjakan dan diukur oleh *load transducer*. Semua data masukan dibuat melalui komputer dan sambutan mesin seterusnya dapat diprogram melalui perisian Dartec.

Cara kerja

Bagi memulakan ujikaji, paip diletak atas *platen* bawah dan kemudiannya *platen* atas dirapatkan secara perlahan-lahan sehingga mencecah hujung atas paip. Beban mampatan yang kecil dikenakan ke atas paip supaya sentuhan positif di antara hujung paip dan *platen* diperolehi disamping memastikan paip tidak bergerak apabila LVDT diletak pada titik-titik L/4, L/2 dan 3L/4 disepanjang paip. Rajah 4 menunjukkan, secara skema, bagaimana radas ujikaji disediakan.

Kemudiannya hujung wayer bebas, daripada tolok terikan yang telah dipasang terdahulu disambung kepada Pengellog Data 1 (Data Logger 1) sementara wayer daripada LVDT disambung kepada Pengellog Data 2 (Data Logger 2) (lihat Rajah 4). Semua bacaan kedudukan *platen*, beban dan bacaan kedua-dua pengellog data dilaraskan kepada sifar. Ujikaji bermula dengan menekan kekunci *enter* pada papan kekunci, setelah semua masukan dilakukan dengan sempurna.

Keputusan Ujikaji

Keputusan daripada ujikaji dipaparkan di dalam Rajah 5 dan Rajah 6. Rajah 5 menunjukkan kelakuan Beban lawan Lejang bagi ketiga-tiga paip sementara Rajah 6 menunjukkan kelakuan Anjakan sisi lawan Lejang. Maklumat mengenai kekuatan paip komposit dalam mampatan dapat diperolehi daripada Rajah 5. Gambarfoto 1 menunjukkan jenis kegagalan yang di alami oleh Paip 1.

Perbincangan dan Rumusan

Rekabentuk Mesin

Mesin yang telah direkabentuk, sedikit sebanyak dapat membuka jalan bagi menghasilkan rekabentuk mesin empar yang lebih baik untuk pembuatan paip komposit melalui kaedah empar. Namun demikian, bagi menghasilkan paip atau silinder yang bermutu dengan menggunakan kaedah ini, beberapa perkara perlulah diberi penekanan, khususnya di dalam

perkara berikut:-

- i. Silinder acuan perlu diperbaiki agar ianya benar-benar bulat untuk menghasilkan produk yang lebih sempurna disamping ianya dapat mengurangkan getaran pada kerangka.
- ii. Silinder acuan ditiruskan sedikit supaya mudah mengeluarkan produk.
- iii. Kaedah menuang damar ke atas tikar gentian kaca perlu diperbaiki bagi memastikan taburan damar adalah seragam. Kaedah percikan damar adalah dirasakan sesuai.

Secara amnya, faktor yang mempengaruhi pembikinan silinder komposit ialah halaju silinder, kelikatan damar dan bilangan lapisan tikar gentian kaca. Faktor-faktor tersebut boleh diubah untuk menghasilkan beberapa silinder komposit yang mempunyai sifat yang berbeza. Sekiranya keperluan penggunaan paip atau silinder memerlukan lapisan luar yang mengandungi banyak damar, ini dapat dilakukan dengan meningkatkan pusingan silinder acuan. Dibalikannya sekiranya gentian kaca pada dinding paip (atau silinder) disebelah dalam perlu dilindungi, pusingan silinder acuan perlulah dikurangkan supaya tidak banyak damar meresap kedalam tikar gentian kaca.

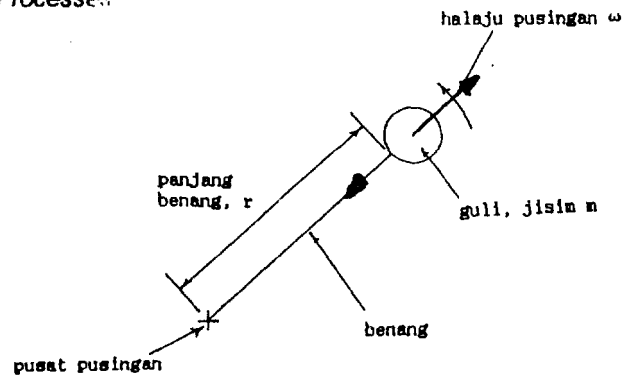
Adalah disyorkan agar kajian lanjut berhubung dengan perubahan halaju silinder, kelikatan damar dan bilangan lapisan gentian kaca diteruskan supaya keputusan yang diperolehi dapat dikumpulkan sebagai data rekabentuk untuk kegunaan di masa akan datang.

Ujian Mampatan

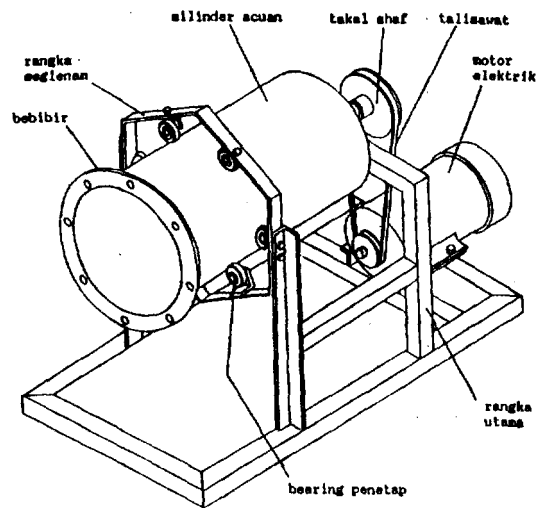
Daripada Rajah 5, beban mampatan maksimum yang ditanggung oleh Paip 1, Paip 2 dan Paip 3 adalah masing-masing 28 kN, 102 kN dan 53.6 kN. Tegasan maksimum yang terhasil ialah masing-masing 57.38 MPa, 117.65 MPa dan 79.06 MPa. Ketiga-tiga paip gagal dalam mampatan dan bukan ledingan. Rajah 6 menguatkan hujah bahawa kegagalan adalah disebabkan mampatan.

Rujukan

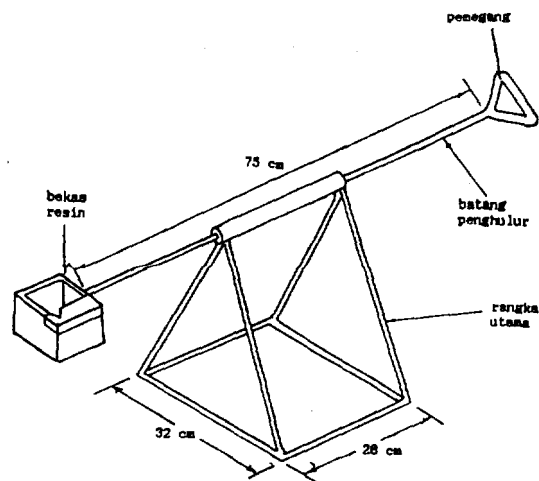
1. Schwartz, M.M.
Composite Materials Handbook.
McGraw-Hill Book Company. 1984.
2. Zalaludin Selamat
Membuat paip rencam dengan menggunakan kaedah daya empar
Tesis Sarjana Muda Kejuruteraan Jentera. UTM. 1990.
3. Daud Hj. Abd. Rahman
Pembikinan paip komposit dengan menggunakan kaedah empar.
Seminar UPP/IRPA Peringkat Fakulti Kejuruteraan Jentera.
23 Julai, 1992. UTM, Skudai.
4. Azraimee Hanif
Menganalisis paip komposit yang dibuat dengan menggunakan kaedah empar.
Tesis Sarjana Muda Kejuruteraan Jentera. UTM. 1993.



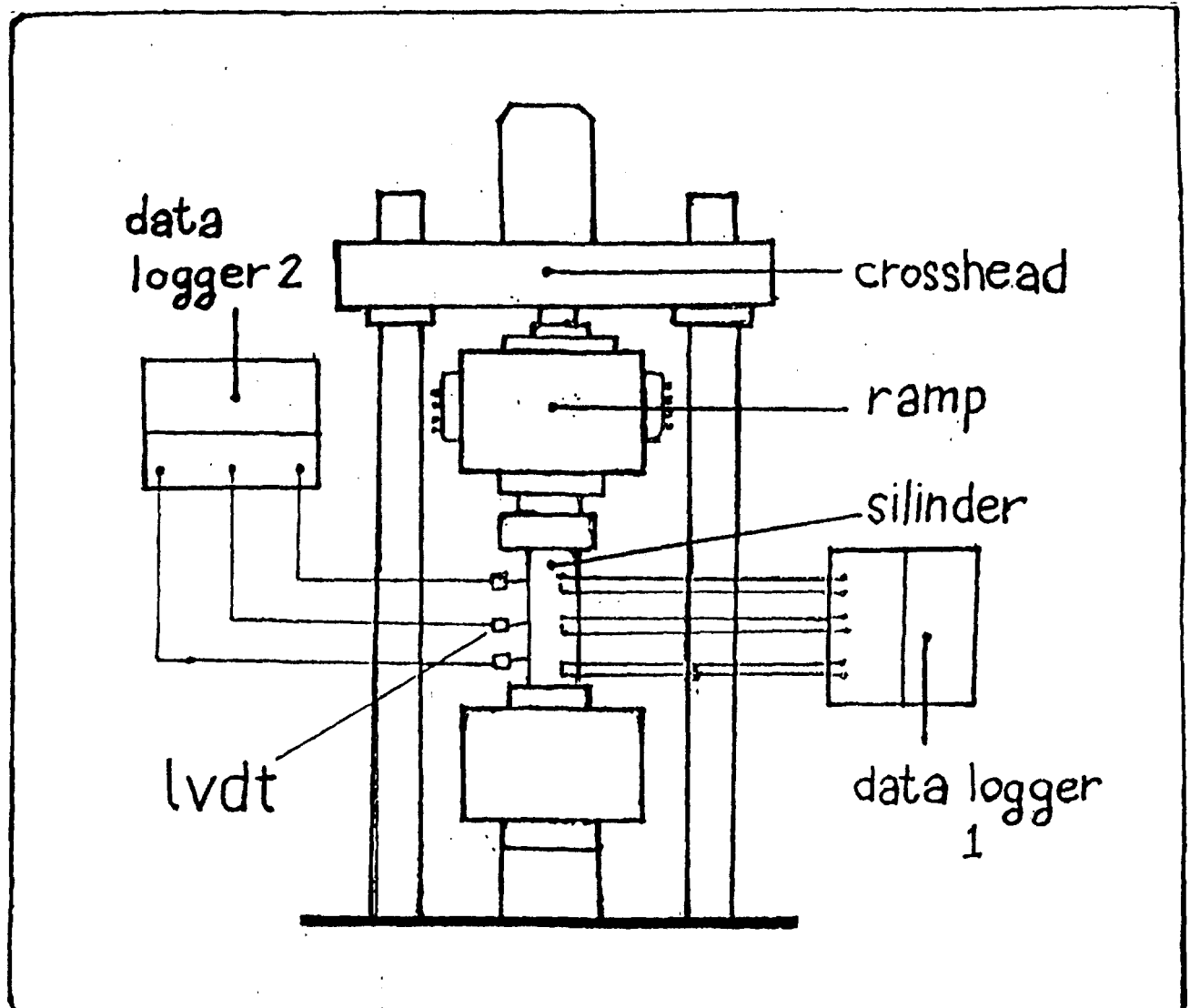
Rajah 1 - Daya Empar



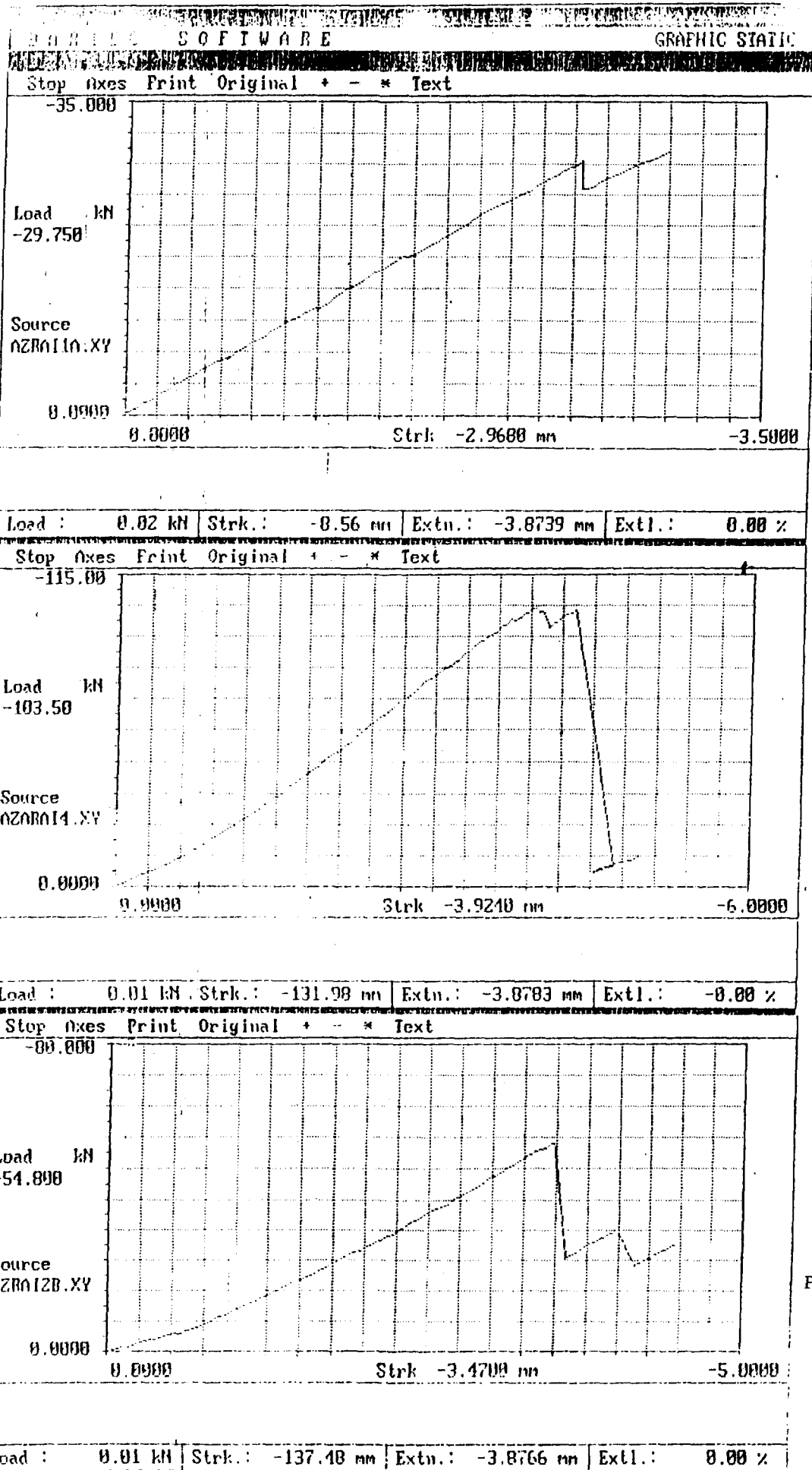
Rajah 2 - Lukisan Isometrik Mesin Empar



Rajah 3 - Alat Penuang Resin



Rajah 4 - Rajah Skema Peralatan Ujikaji

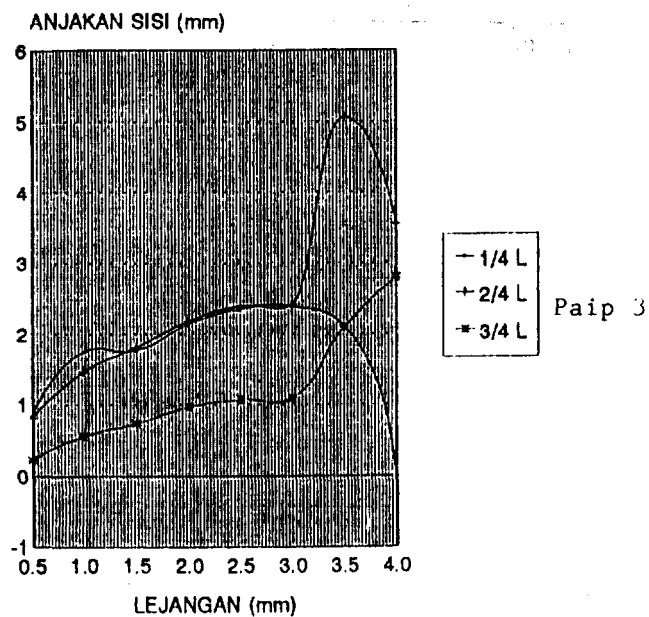
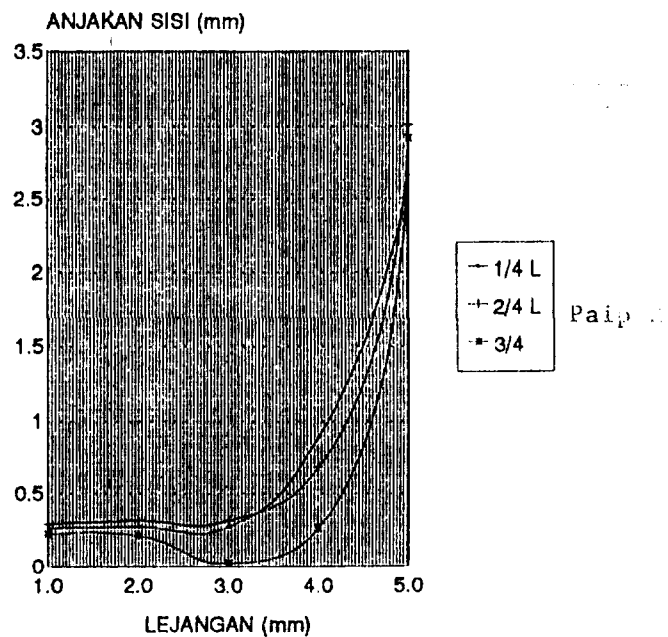
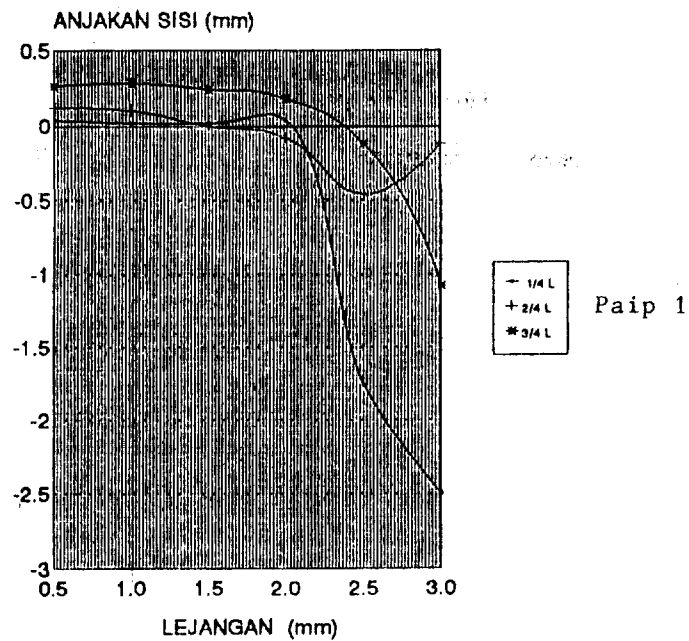


Paip 1

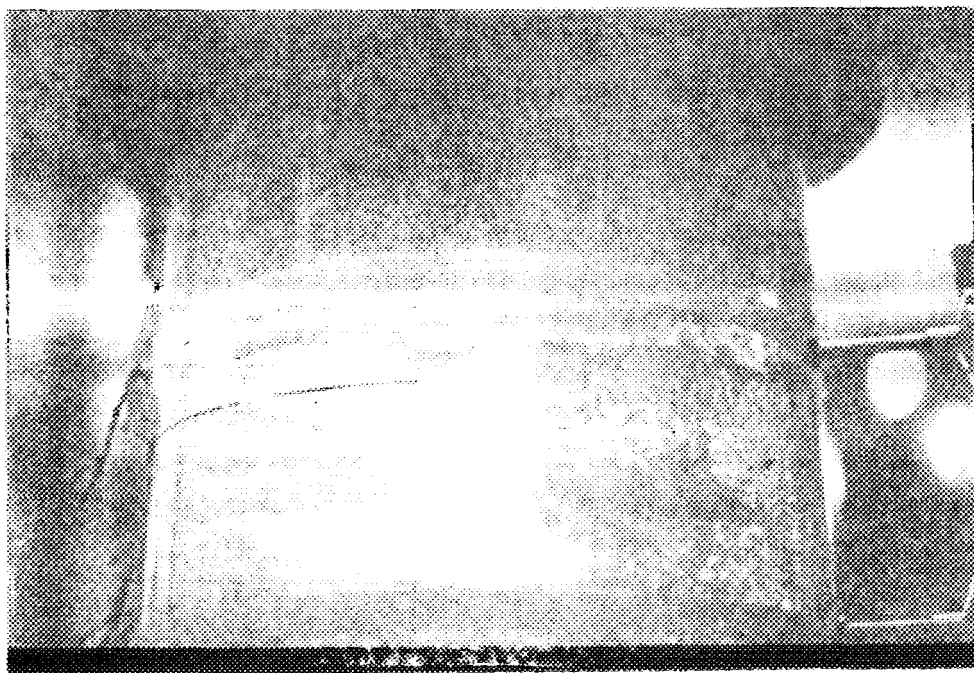
Paip 2

Paip 3

Rajah 5 - Graf Beban Lawan Lejang bagi ketiga-tiga paip



Rajah 6 - Graf Anjakan Sisi Lwn Lejang



Gambarfoto 1 - Paip 1 yang telah gagal

PENJERAPAN ION LOGAM Pb (II) DAN Ni (II) DENGAN MENGGUNAKAN SERBUK KARBON TERAKTIF TEMPURUNG KELAPA SAWIT

Oleh

**Asiah Hussain dan Lai Lee Teng,
Jabatan Kimia, Fakulti Sains,
Universiti Teknologi Malaysia,
Skudai, Johor.**

ABSTRAK

Maklumat literatur menunjukkan penambahan bahan pengaktif tertentu dalam proses penyediaan karbon teraktif dapat meningkatkan kemampuan penjerapan karbon tersebut¹. Satu siri karbon teraktif daripada tempurung kelapa sawit telah disediakan dengan menggunakan kaedah pengaktifan fizik dan kimia. Sifat permukaan dan keliangan karbon teraktif dikaji dengan menggunakan kaedah penjerapan gas nitrogen dan mikroskopi pengimbasan elektron. Kajian pada antara muka pepejal - cecair menunjukkan bahawa karbon teraktif yang dihasilkan melalui pengaktifan fizik dengan menggunakan gas karbon dioksida serta penambahan bahan pengaktif kalium fosfat menunjukkan penjerapan yang paling baik untuk ion-ion logam plumbum dan nikel. Pengaktifan fizik dengan penambahan K_3PO_4 dapat membentuk liang mikro dan liang meso yang lebih halus dan meningkatkan luas permukaan karbon teraktif.

Key words — Karbon teraktif, tempurung kelapa sawit, ion Pb (II) dan Ni (II)

PENGENALAN

Hasil perkembangan aktiviti industri telah menimbulkan berbagai masalah pencemaran alam sekitar. Masalah pencemaran air sungai dan sistem pengaliran yang lain telah menjadi begitu serius terutamanya di kawasan perindustrian. Keadaan ini terjadi akibat daripada pelepasan langsung air buangan industri ke dalam sungai atau sistem pengaliran tersebut. Kandungan air buangan ini antaranya ialah ion-ion logam yang bersifat toksik dan bukan toksik. Dalam kajian ini akan ditumpukan kepada ion logam Pb (II) dan Ni (II). Berbagai-bagai kaedah telah digunakan untuk menyingkirkan ion logam toksik tersebut termasuklah pengendapan kimia, penurasan membran, penukar ion dan karbon teraktif.

Keupayaan penjerapan yang tinggi oleh karbon teraktif menyebabkan ia banyak digunakan dalam kajian merawat air sisa industri. Dalam penyediaan karbon teraktif, pengawalan terhadap sifat taburan liang dan afiniti permukaan merupakan aspek yang penting. Dalam kajian yang lepas

beberapa siri karbon teraktif telah disediakan secara pengaktifan kimia dan fizik tanpa menambahkan bahan pengaktif kimia (mangkin)². Dalam kajian ini karbon teraktif disediakan dengan menambahkan bahan pengaktif kimia kalium fosfat kerana kalium dan beberapa logam alkali yang lain diketahui dapat mempercepatkan proses gasifikasi bahan berkarbon dengan menggunakan karbon dioksida dan stim³. Bahan ini dapat membentuk lapisan fosfat yang bertindak sebagai bahan pengawal pembakaran lampau bagi mengelakkan daripada terjadi pengurangan kandungan karbon⁴.

Kajian ini dilakukan untuk melihat kesan teknik penyediaan karbon teraktif dengan penambahan mangkin kalium fosfat terhadap penyerapan logam Pb (II) dan Ni (II).

EKSPERIMEN

Karbon teraktif disediakan melalui empat kaedah, iaitu :

- (i) Pengaktifan kimia tanpa penambahan kalium fosfat - TS-K
- (ii) Pengaktifan fizik tanpa penambahan kalium fosfat - TS-F-CO₂ dan TS-F-S
- (iii) Pengaktifan kimia dengan penambahan kalium fosfat - TS-K-M
- (iv) Pengaktifan fizik dengan penambahan kalium fosfat - TS-F-CO₂ -M dan TS-F-S-M

Kaedah (i) dan (ii) dilakukan mengikut kaedah yang telah dinyatakan dalam rujukan (2).

Kaedah (III) - Pengaktifan kimia dengan penambahan kalium fosfat (TS-K-M) :

Karbon teraktif TS-K-M disediakan dengan mencampurkan karbon teraktif TS-K, K₃PO₄ dan air mengikut perkadaran berat 1 : 1.5 : 10. Campuran ini dipanaskan sehingga terbentuk serbuk hitam yang kering. Arang yang terhasil kemudian diaktifkan di dalam relau pada suhu 450° C. Seterusnya karbon teraktif dibasuh dengan air suling sehingga pH air basuhan 6 hingga 7.

Kaedah (IV) - Pengaktifan fizik dengan menggunakan mangkin kalium fosfat (TS-F-CO₂ -M dan TS-F-S-M)

Karbon teraktif jenis ini disediakan dengan mencampurkan tempurung kelapa sawit mentah, K₃PO₄ dan air mengikut perkadaran berat 1 : 0.3 : 2. Campuran ini dipanaskan sehingga terbentuk serbuk hitam yang kering. Seterusnya proses pengkarbonan dilakukan pada suhu 450° C selama satu jam. Proses selanjutnya dilakukan pengaktifan dengan menggunakan gas karbon dioksida atau stim seperti kaedah (ii).

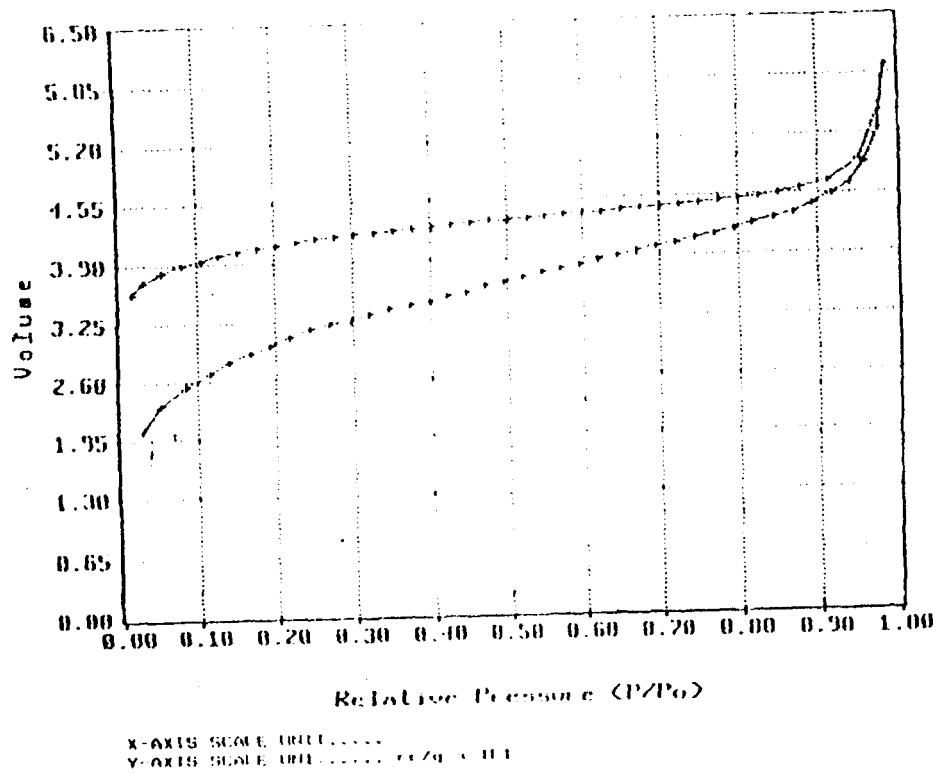
Keliangan, luas permukaan dan isoterma penjerapan ditentukan dengan kaedah penjerapan gas nitrogen pada 77 K dengan menggunakan Autosorb 1. Kepekatan ion logam Pb (II) dan Ni (II) ditentukan dengan menggunakan Spektrofotometri serapan atom (AAS).

Kajian muatan penjerapan logam oleh karbon teraktif dilakukan dengan membandingkan kemampuan penjerapan antara sampel karbon teraktif yang telah disediakan. Logam Pb (II) dan Ni (II) masing-masing mempunyai kepekatan 30 ppm dan 25 ppm dipipet sebanyak 50 mL ke dalam kelalang kun berasingan yang mengandungi 0.3 g sampel karbon teraktif yang berlainan jenis. Campuran digoncang selama satu jam kemudian dituras. Hasil turasan dianalisis dengan menggunakan alatan spektrofotometri serapan atom.

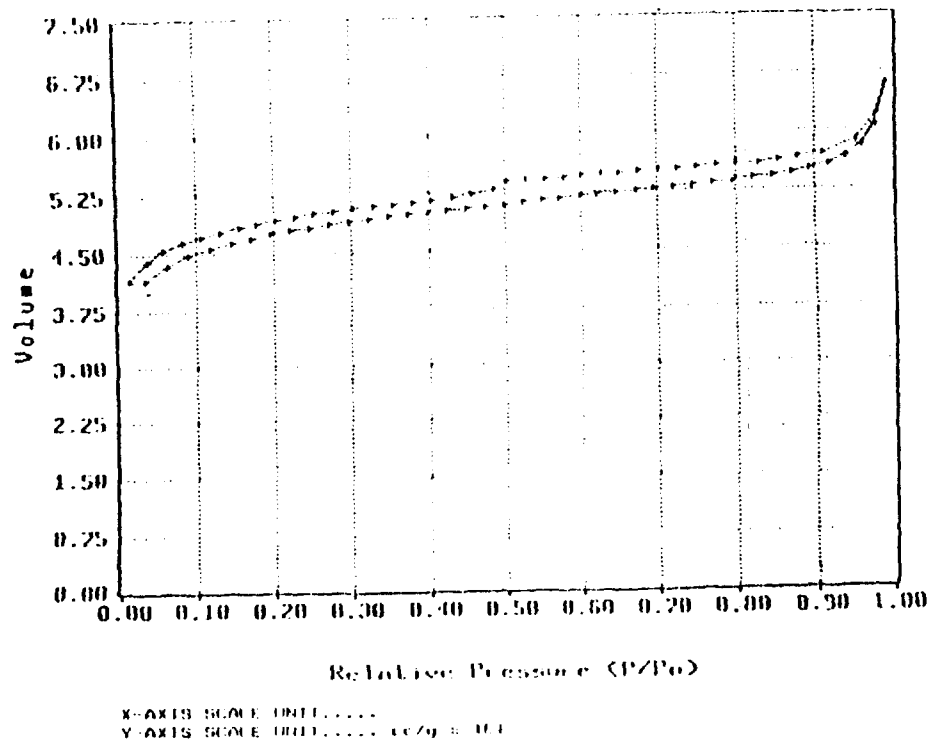
HASIL DAN PERBINCANGAN

Isoterma penjerapan gas nitrogen bagi sampel TS-F-CO₂ dan TS-F-CO₂ -M ditunjukkan dalam Rajah 1 (a) dan 1(b). Bentuk isoterma yang dihasilkan berjenis I (BDDT) yang menunjukkan liang utama yang terdapat di dalam sampel tersebut adalah mikroliang. Isoterma penjerapan TS-F-CO₂ -M didapati tidak berbalik dan mempunyai histeresis bertekanan rendah yang menunjukkan terdapat zat terjerap yang terperangkap di dalam liang semasa terjadinya proses nyahjerapan nitrogen. Apabila dilakukan penambahan K₃PO₄, isoterma penjerapan yang dihasilkan merupakan gabungan jenis I dan IV. Kewujudan gelung histeresis yang hampir tertutup pada tekanan relatif di sekitar 0.45 menunjukkan terjadinya kondensasi kapilari di dalam liang meso. Dengan penambahan mangkin ini telah menyempitkan liang sampel dari 18.90°A kepada 14.90° A. Data yang lengkap ditunjukkan dalam Jadual 1.

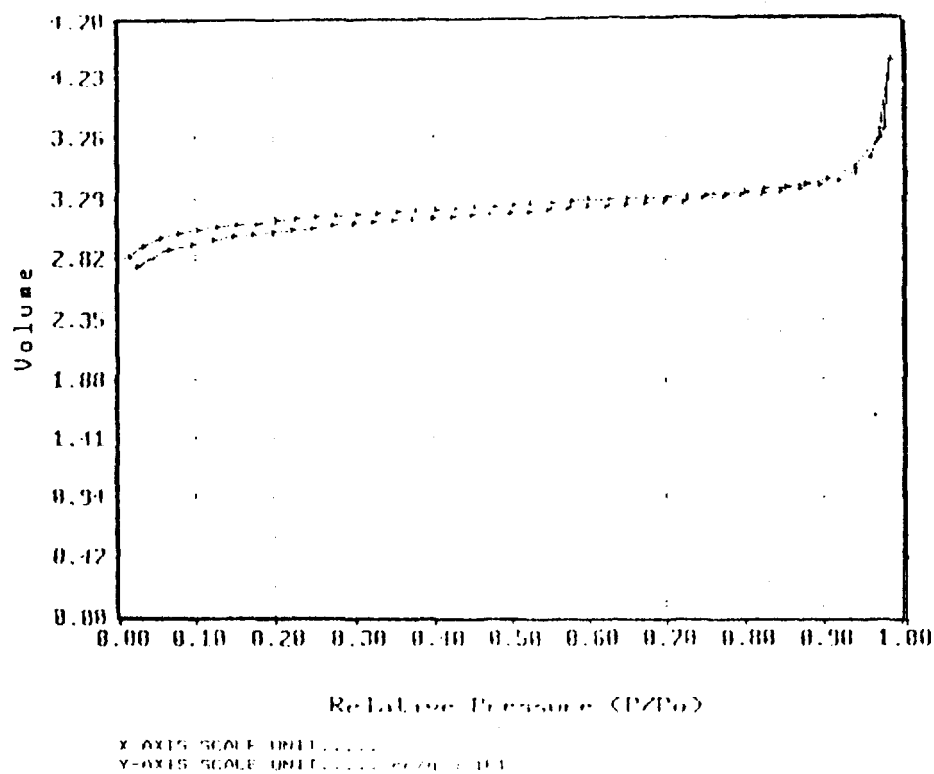
Ciri - ciri yang hampir sama juga ditunjukkan oleh sampel yang disediakan dengan menggunakan bahan pengaktif stim. Isoterma penjerapan bagi sampel TS-F-S dan TS-F-S-M digambarkan dalam Rajah 2(a) dan 2(b). Setelah penambahan mangkin K₃PO₄ sifat keliangan meso juga bertambah dan terjadi penyempitan purata jejari liang dari 15.88°A kepada 15.12°A. Bagi sampel yang disediakan secara kimia, penambahan mangkin akan meningkatkan keliangan meso. Keadaan ini dapat dilihat dengan terjadinya sedikit pelebaran pada gelung histeresisnya. Rajah 3(a) dan 3(b) menunjukkan isoterma penjerapan bagi sampel TS-K dan TS-K-M.



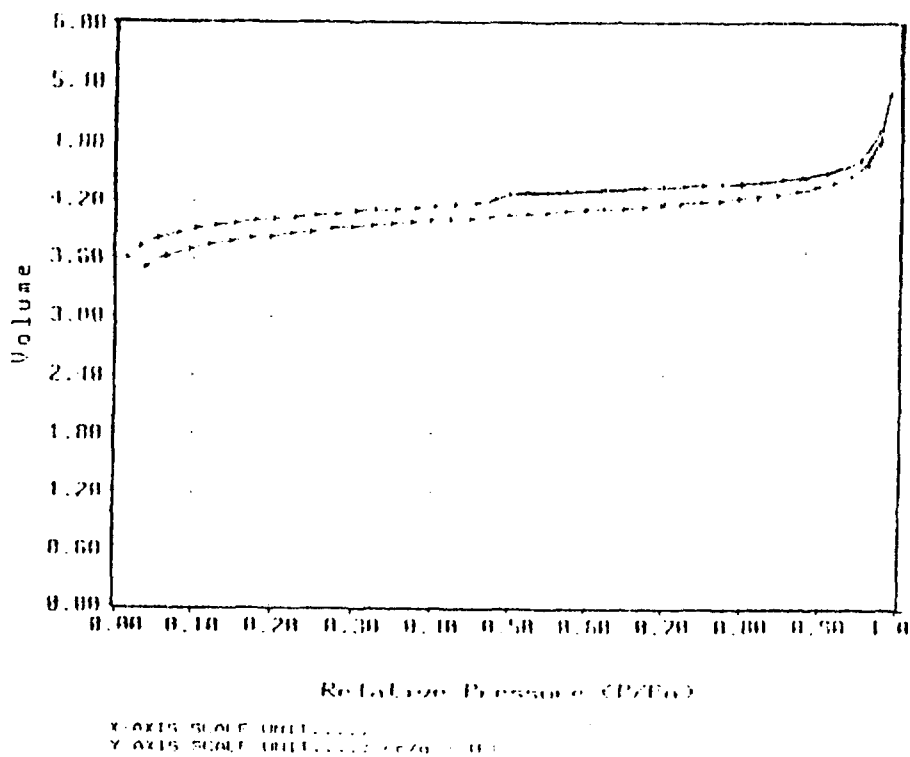
Rajah 1(a) : Isoterma panjerapan gas nitrogen bagi TS-F-CO₂



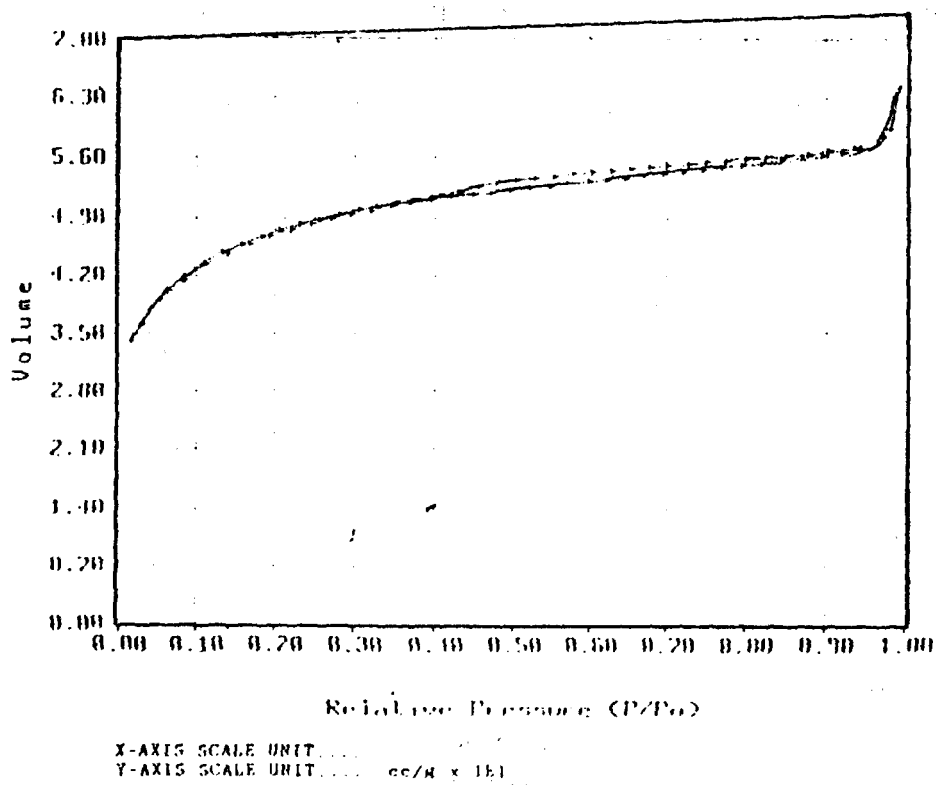
Rajah 1(b) : Isoterma panjerapan gas nitrogen bagi TS-F-CO₂-M



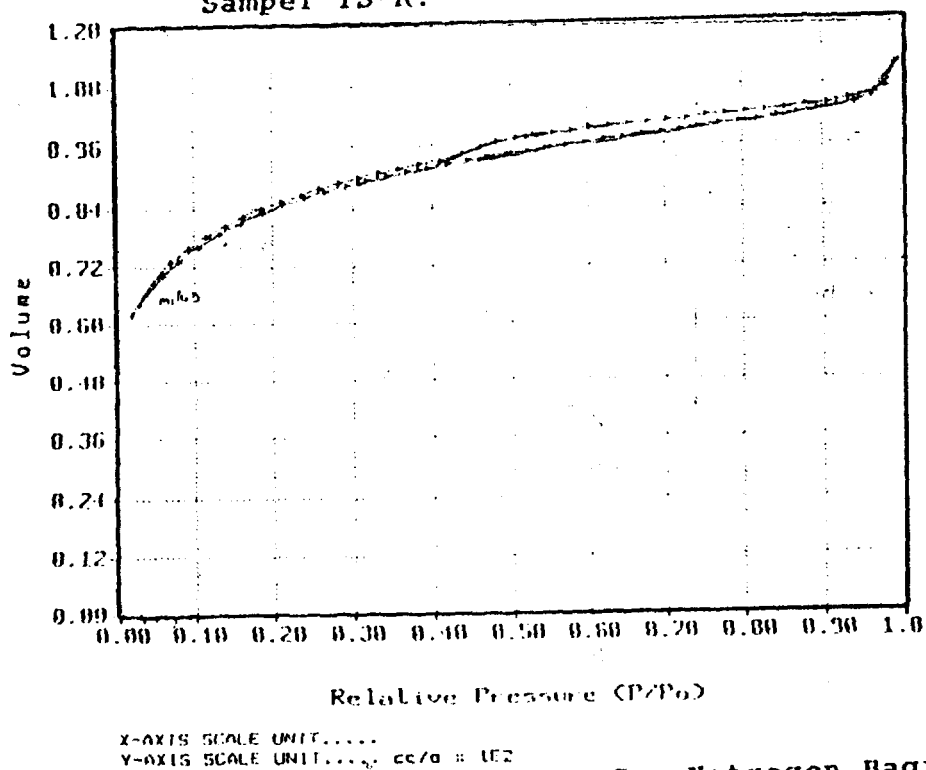
Rajah 2(a) : Isoterma Penjerapan Gas Nitrogen Bagi Sampel TS-F-S.



Rajah 2(b) : Isoterma Penjerapan Gas Nitrogen Bagi Sampel TS-F-S-M.



Rajah 3 (a) : Isoterma Penjerapan Gas Nitrogen bagi Sampel TS-K.



Rajah 3 (b) : Isoterma Penjerapan Gas Nitrogen Bagi Sampel TS-K-M.

Jadual 1 : Sifat Kellangan bagi Karbon Teraktif

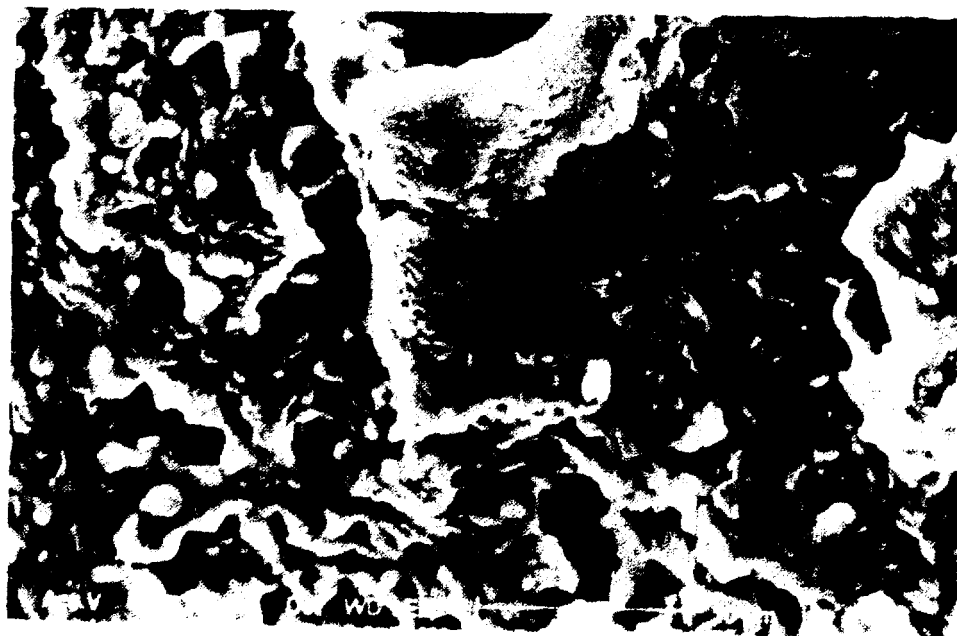
Sampel	Purata Jejari Liang ° A	Jenis Liang	Jenis Isoterma	Jenis Gelung Histeresis
TS-F-CO ₂	18.90	mikro	I	Tekanan Rendah
TS-F-CO ₂	14.90	mikro & meso	I & IV	B & Tekanan Rendah
TS-F-S	15.88	mikro	I	Tekanan Rendah
TS-F-S-M	15.12	mikro & meso	I & IV	B & Tekanan Rendah
TS-K	14.05	mikro & meso	I & IV	B & Tekanan Rendah
TS-K-M	13.45	mikro & meso	I & IV	B & Tekanan Rendah

Rajah 4(a) menunjukkan mikrograf bagi sampel karbon teraktif TS-F-CO₂-M semasa proses pengkarbonan dilakukan. Didapati morfologi permukaannya tidak teratur dan belum terjadi pembentukan liang yang jelas. Setelah dilakukan proses pengaktifan dengan mengalirkan gas karbon dioksida pada suhu 700°C, didapati morfologi permukaannya lebih sekata dan terjadi pembentukan liang yang baik dan jelas seperti ditunjukkan pada Rajah 4(b).

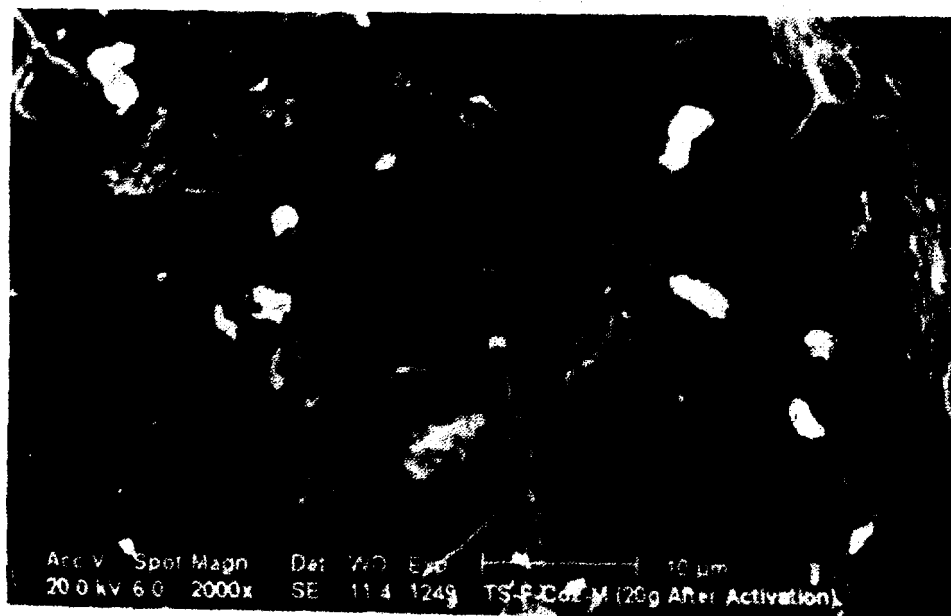
Jadual 2 : Muatan Penjerapan Logam Oleh Karbon Teraktif

Kepekatan larutan asal : Pb = 30 ppm ; Ni = 25 ppm

Sampel Karbon Teraktif	Kuantiti Logam Terjerap			
	Pb		Ni	
	%	g/kg	%	g/kg
TS-F-CO ₂ -M	98.30	4.915	96.99	4.041
TS-F-S-M	95.40	4.770	87.97	3.749
TS-F-CO ₂	35.88	1.794	18.05	0.753
TS-F-S	30.95	1.548	13.91	0.580
TS-K-M	25.85	1.293	15.79	0.658
TS-M	13.75	0.688	13.53	0.564

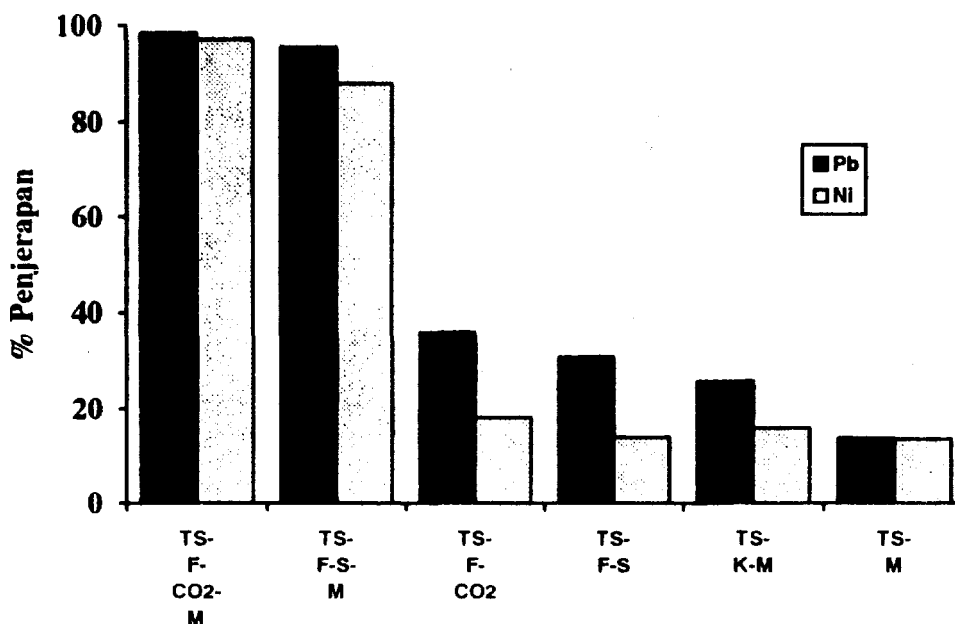


Rajah 4 (a) : Mikrograf bagi sampel TS-F-CO₂-M yang belum diaktifkan



Rajah 4 (b) : Mikrograf bagi sampel TS-F-CO₂-M setelah diaktifkan

Jadual 2 dan Rajah 5 menunjukkan data peratus penjerapan dan jisim logam yang dijerap oleh satu kilogram karbon teraktif. Hasil menunjukkan semua sampel karbon teraktif yang disediakan mempunyai keupayaan penjerapan yang lebih tinggi terhadap Pb (II) berbanding dengan Ni (II).



Rajah 5 : Peratus penjerapan ion Pb(II) dan Ni(II) terhadap jenis karbon teraktif

Berdasarkan keputusan yang diperolehi, keupayaan penjerapan logam oleh karbon teraktif adalah mengikut tertib seperti berikut : TS-F-CO₂-M > TS-F-S-M > TS-F-CO₂ > TS-F-S > TS-K-M > TS-K. Teknik penyediaan karbon teraktif melalui proses fizik dengan penambahan mangkin kalium fosfat dan diaktifkan dengan gas karbon dioksida atau stim dipilih sebagai kaedah yang paling sesuai untuk menyediakan karbon teraktif bagi penjerapan ion logam Pb dan Ni. Pengaktifan dengan gas karbon dioksida menghasilkan karbon teraktif yang menunjukkan kemampuan penjerapan yang paling tinggi terhadap ion logam Pb (II) dan Ni (II) dalam larutan akueus.

Kajian ini juga dapat menunjukkan bahawa penjerapan ion logam Pb(II) dan Ni (II) sangat bergantung kepada cara pengaktifan yang dilakukan dan juga ukuran purata jejari liang karbon teraktif. Bagi sampel TS-F-CO₂ penjerapan ion Pb dan Ni jauh lebih rendah, hal ini mungkin disebabkan oleh terjadinya penyempitan leher mikrolang yang mengakibatkan ion ini tidak dapat menjerap masuk dengan baik ke dalam liang tersebut (gelung histeresis bertekanan rendah). Penambahan K₃PO₄ dapat membentuk lapisan fosfat bagi terjadinya pembakaran setempat dan

menghakis leher liang yang sempit yang dapat memberi laluan baru bagi ion Pb dan Ni menjerap ke dalam liang tersebut. Model penjerapan ion logam Pb dan Ni pada permukaan karbon teraktif yang dicadangkan dapat dilihat pada Rajah 6. Walaupun purata jejari liang sampel tanpa mangkin lebih lebar dan dianggap ion logam lebih mudah menjerap ke dalam liangnya tetapi keadaan disebaliknya mungkin terjadi. Keadaan ini mungkin disebabkan ion-ion logam itu bebas bergerak dan sukar untuk mencapai keseimbangan. Setelah penambahan mangkin dan terjadi penyempitan liang maka ion logam itu akan berada lebih dekat dengan dinding liang sehingga daya tarikan antara dinding liang dan ion logam akan lebih kuat yang dapat mendorong lagi penjerapan dan keseimbangan terjadi dengan lebih mudah. Fenomena penjerapan ion logam pada permukaan karbon teraktif mungkin melibatkan beberapa mekanisme, iaitu : mekanisme penjerapan fizik , penjerapan kimia, pertukaran ion-ion logam dengan ion hidrogen H^+ dan juga melalui pembentukan kompleks di antara ion logam dengan kumpulan berfungsi yang masih tertinggal pada permukaan karbon teraktif.

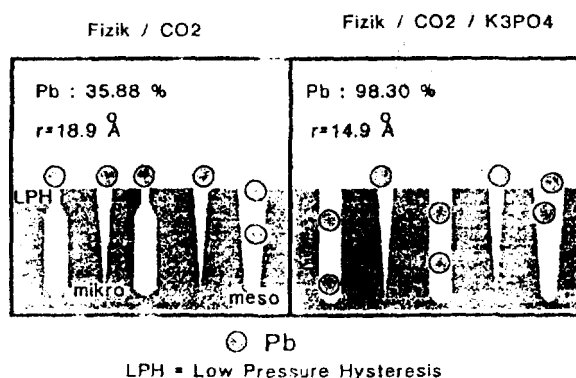
KESIMPULAN

Hasil daripada kajian ini telah dapat mencirikan beberapa jenis karbon teraktif berdasarkan teknik penyediaannya. Tempurung kelapa sawit yang disediakan melalui kaedah pengaktifan fizik - CO_2 dengan penambahan mangkin kalium fosfat menunjukkan prestasi penjerapan yang paling baik terhadap ion logam Pb (II) dan ion Ni (II). Kecenderungan penjerapan ion logam Pb (II) lebih tinggi jika dibandingkan dengan Ni (II).

RUJUKAN

1. F.Caturla, M.Molina-Sabio, and F.Rodriguez-Reinoso, *Carbon*, 1991, **29**,7, 999 .
2. Asiah Hussain dan Ui Sui Yin, *Proceedings Malaysian Science and Technology Congress '93*, 1993, Kuala Lumpur, 1993, **1**, 188.
3. J.Laine and A.Calafat, *Carbon*, 1991, **29**, 7, 949.
4. J.J.Freeman and F.G.R.Gimblett, *Carbon*, 1988, **26**, 501

Pengaktifan



Rajah 6 : Model Penjerapan ion Pb

VIBRATIONAL POWER FLOW IN FIBRE-REINFORCED COMPOSITE MATERIALS

Roslan Abd. Rahman, Mohd. Salman Leong.
Fakulti Kejuruteraan Jentera
UTM, Karung Berkunci 791,
Skudai, 80990 Johor Bharu

ABSTRACT

Vibrational power input due to flexural force excitation on fibre-reinforced composite beam was studied experimentally. The material parameters and geometrical dimensions controlling the power input were investigated for unidirectional off-axis type of ply. The variables of the laminate examined include fibre orientation angle, beam width and thickness, and influence of finite beam length. It was shown that the fibre orientation angle is insensitive to the vibrational power input to the structure.

Key Words : Vibrational Power Flow, Composite.

1. INTRODUCTION

Machines, inevitably, generate unwanted vibration which are then transmitted to connected structures. Excessive vibration in structural element need to be controlled and minimised to avoid possible damage to structures. Previous studies have been undertaken on steel, aluminium and concrete structures to control the vibration transmission resulting from forces, moments and torque excitations^(1,2,3,4). The method commonly used in the vibration control studies is the vibrational power flow technique. Review of this technique is well documented by White.⁽⁵⁾

In this work, the power flow concept is applied to substructure of fibre-reinforced composite materials. Experimental results on the variation in power input upon material properties and geometrical dimensions are presented. Consideration is given here for flexural type of wave motion in beam structures.

2. VIBRATIONAL POWER INPUT TO A STRUCTURE

Vibrational Power Input to a structure subjected by harmonic force, F , is given by the relationship,

$$P = 1/2 |F|^2 \operatorname{Re}(M), \quad 2.1$$

where $M = \text{Velocity/Force} = \text{Mobility}$. If the structure is excited by random force of spectral density G_{FF} , giving rise to a velocity at that point of spectral density G_{VV} , the Power/Hz is then obtained as :

$$P/\text{Hz} = G_{FF} \operatorname{Re}(M) = G_{VV} \operatorname{Re}(Z), \quad 2.2$$

where Z is the impedance.

The time averaged power input to an infinite beam structure by a point harmonic force, as given in Eq.(2.1), is written as,

$$P = |F|^2 / \left[8 \omega^{1/2} B_{11}^{1/4} (\rho A)^{3/4} \right] \quad 2.3$$

where ω is the frequency, B_{11} is the flexural rigidity, ρ is the density and A is the beam cross-sectional area. The above theoretical formulation need to be verified by carrying the experimental study on "infinite beam" structure of fiber-reinforced composite material..

3. SPECIMEN PREPARATION

Plate samples of unidirectional fibre-reinforced composites were manufactured by hand lay-up method. Glass fibre unidirectional woven roving mat was laid in one direction and resin was spread on. The laying

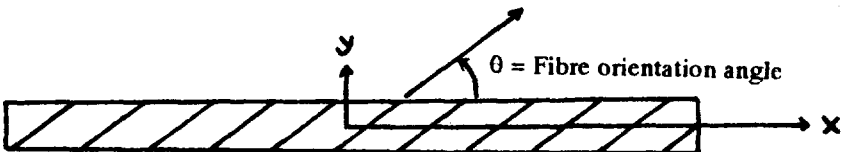
on of the next layer was repeated until the laminate was built up to the desired thickness. The laminate was then pressed by a heavy roller to ensure flatness and free from air cavities.

The glass fibre used was ERW-430-551C E-Glass unidirectional woven roving (649.11 gm/m²). The resin system was 268 BQT polyester resin. One to two spoonful of catalyst (MPKT 1.2-1.5 kg) was used and curing was done at room temperature for 24 hrs. The fiber volume was in the range 43-46 % as measured by density determinations.

Three plates of varying thickness were manufactured. Each plate was then cut to beam size having fiber orientations of 0°, 30°, 45°, 60°, and 90° with respect to the beam axis. The nominal dimensions of these beams is tabulated in Table 1.0. The maximum length of the plate allowed was 1.0 m due to the limitation of the mat width available, which was 1.05 m. The, beam specimen, A and B, were then cut from two plates due to inability to cut the whole desired angle in a single plate as indicated in Table 1.0.

TABLE 1.0 Dimensions and physical constant of the beam specimens

Plate No.	Beam Specimen No.	Fibre Orientation Angle	Dimension in mm	Mass (gm)	Density (kg/m ³)
1	UD0A	0°	981 x 24.845 x 5.843	249.22	1754.92
	UD30A	30°	981 x 24.867 x 5.827	249.37	1754.31
	UD0B	0°	920 x 14.996 x 5.772	143.44	1801.28
	UD30B	30°	920 x 15.06 x 5.932	145.81	1774.08
	UD45B	45°	920 x 15.0 x 5.868	143.96	1777.76
2	UD60A	60°	981 x 24.737 x 5.886	253.54	1775.05
	UD90A	90°	981 x 24.98 x 5.838	255.25	1784.18
	UD60B	60°	920 x 14.936 x 5.832	144.45	1802.51
	UD90B	90°	920 x 14.98 x 5.844	144.31	1791.78
3	UD0C	0°	700.5 x 21.56 x 5.867	157.25	1774.67
	UD30C	30°	701 x 21.43 x 5.913	157.36	1771.52
	UD45C	45°	710 x 21.33 x 5.83	157.36	1805.2
	UD60C	60°	710 x 21.34 x 5.853	157.33	1784.69
	UD90C	90°	699 x 21.68 x 5.853	157.30	1773.43



The diagram shows a rectangular beam with diagonal hatching representing fibers. A coordinate system is centered on the beam with the x-axis along the beam's length and the y-axis perpendicular to it. An angle θ is shown between the x-axis and the fiber direction, labeled as $\theta = \text{Fibre orientation angle}$.

(Fibre : E-Glass Unidirectional woven roving ERW-430-551C (Japan), Resin :Polyester BQT 924, Catalyst : MEKP, Fibre Volume Fraction : 0.43 - 0.46)

4. MEASUREMENT SET-UP AND INSTRUMENTATION

Schematic diagram of the test arrangement and instrumentation layout is shown in Fig.1. The test specimen was suspended to move freely in the vertical direction. The force excitation from the shaker to the system was provided at the end of the beam. At the other end of the beam, a rubber sponge was used as the anechoic termination. This material was chosen instead of normally used sand as rubber sponge is much lighter. The tapering angle of the rubber sponge that allows gradual attenuation of wave propagation was experimentally selected by varying its depth and length. It was noted experimentally that the condition of attachment or tightness between the top and bottom rubber sponge affect considerably the

peak mobility amplitude of the test structures at low frequencies. To ensure constant boundary condition for all test specimens, gravity tightness was thus chosen.

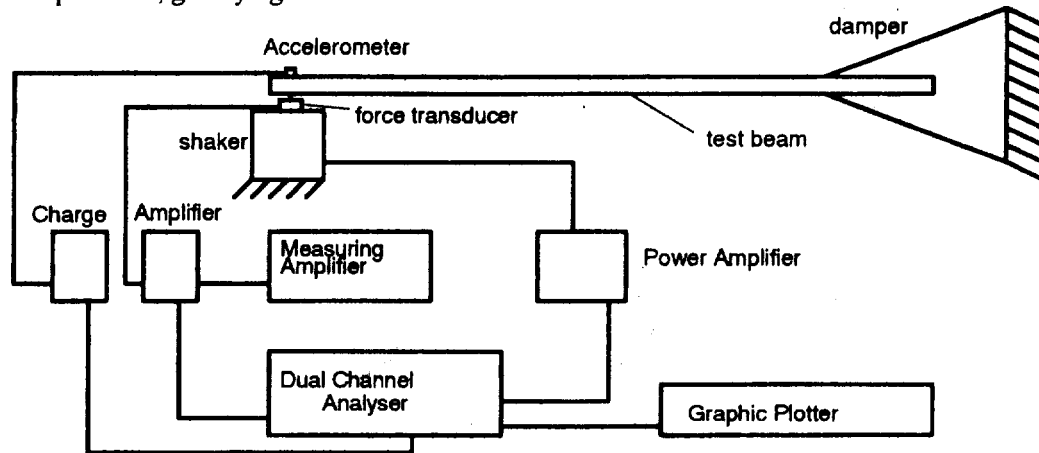


FIGURE 1. Schematic diagram showing experimental set-up and instrumentation.

Figure 1 shows the block diagram of the instrumentation used in the tests. A miniature accelerometer (Bruel & Kjaer (B&K) 4374, weight 0.65 gm.) was mounted with bees wax to the excitation end of the beam. A dual channel signal analyser (B&K Type 2034) provided random signal driving a small permanent magnet vibration shaker (B&K Type 4810, force rating up to 112 N). A force transducer (B&K Type 8200) attached between the shaker and the test beam, measured the force applied. The frequency response between the force signal and the velocity signal were measured by the analyser, and measured data plotted using a graphic plotter (Hewlett-Packard HP 7550A).

Calibration tests of the transducers and the whole measurement chain were carried out before the measurements. The force transducer sensitivity and analyzer were calibrated following the provided manual. The calibration of the miniature accelerometer was done by mounting the transducer and a reference calibrated accelerometer on opposite side of a short rectangular hollow beam. The axis of these accelerometers was inline with the axis of force excitation provided by the shaker on which the beam was attached to. Ideally, the frequency response function between the two accelerometers is equal to unity, as well as 180° out of phase. The sensitivity of the miniature accelerometer was calibrated, and the result was shown in Fig. 2. A magnitude error of 1% and a maximum phase error of 0.6 % between the two transducers were estimated in the frequency range of 0 to 6.4 kHz.

5. VERIFICATION OF MEASUREMENT METHODOLOGY

Noise generator of the analyzer provides random white noise to the shaker via the power amplifier (B&K Type 2706). The frequency responses between the force and acceleration signals were measured by the analyzer. Typically, 100-200 ensemble averages of the frequency response function are collected by the analyzer. Results are then presented in the modulus form of point mobility which corresponds to the direct averaged vibrational power input to the structure.

A verification of the measurement set-up and methodology was made on steel beam (984 mm x 24.94 mm x 5.84 mm). Figure 3(a) shows the measured mobility of the "infinite beam" presented in modulus form. Comparison with theoretical result computed from Eq. (2.3), confirmed good correlation of averaged behaviour, thereby verifying the methodology. The results were also similar to reported work by others on steel beam^{2,3}. The magnitude of the resonances and anti-resonances occurred to close proximity with each other at the higher frequencies. Wide separation of peaks occurred at low frequencies and narrow at higher frequencies. Equation (2.1) shows that power input was proportional to the real component of mobility. Figure 3(b) shows the real component of mobility for the steel structure. It was observed that most power flow occurred in single direction, from the source to the receiver for the measured frequency range (0 - 6.4

kHz). This therefore correlated with the theoretical expression, and hence verified the measurement methodology.

Test on 0° unidirectional fibre-reinforced composite beam (UD0A) having the same dimension as steel was also plotted in Fig. 3(a). It was observed that the power input into the composite structure was much higher to steel. Composite structures are however significantly lighter and thus have high mobility. A plot of power input to composite having same weight as steel, is also shown in Fig. 3(a). It was observed that composite accepts lower vibrational power input compared to steel.

6. RESULTS

Measurement results on the variation of vibrational power input to fibre-reinforced composite beam due to variation in the material properties and geometrical dimension are presented below.

6.1 Effect of fiber orientation angle

The variation in the moduli of point mobilities associated with force excitation upon the fibre orientation angle for sample A and B are shown in Fig.4 and Fig.5 respectively, for the frequency range of 0 to 5 kHz. The peaks correspond approximately to the resonant frequencies of the system and represent maximum power input to the structures. Both groups of specimen gave similar pattern of results. The averaged behaviour of point mobility at various fibre orientation angle were almost the same. This correlated well with analytical predictions as computed from Eq. (2.3). These results have a significant practical implication which suggest that there is no need for fibre orientation control in manufacture of engineering structures for a minimal power input in machine foundation.

The graphs also showed wide and broad peak separations at low frequency, and was thought to be attributed to standing waves caused by reflection of incident waves at beam end. At high frequencies, the peaks were closer spaced, and with variations in amplitude due to the inability of the rubber sponge to attenuate the wave motion.

6.2 Effect of geometrical dimension

The vibrational power input of Eq.(2.3) may be written as,

$$P = |F|^2 / [8 \omega^{1/2} B_{11}^{1/4} (\rho b h)^{3/4}] \quad 6.1$$

where h and b are the beam thickness and width respectively. Flexural rigidity, B_{11} , is defined as,

$$B_{11} = b/D_{11}'$$

where D_{11}' is the inverse flexural stiffness, defined as

$$D_{ij}' = 1/3 (Q_{ij}')^k (h_k^3 - h_{k-1}^3) \quad 6.2$$

in which $(Q_{ij}')^k$ is the transformed reduced stiffness of the k^{th} lamina. The vibrational power input may then be written as,

$$P = |F|^2 (D_{11}')^{1/4} / [8 \omega^{1/2} b \rho^{3/4} h^{3/4}] \quad 6.3$$

a) Effect of beam width

Equation (6.3) shows that the power input is inversely proportional to beam width, with all other terms constant. Thus an increase in beam width results in reduction in power input. UD0A of sample A and UD0B of sample B, both having approximately same thickness, were tested to verify the above theoretical expression. Both of these samples were cut from the same plate; thus averagely having the same physical properties such as density and fibre volumetric fraction.

Figure 6 shows the modulus form of mobility for the two samples. The averaged behaviour is almost the same especially at high frequency. At low frequency, sample UD0B, having smaller width than UD0A, gave comparatively higher peaks which correlated with Eq. (6.3).

b) Effect of beam thickness

Equations (6.2) and (6.3) indicate that the power input had a complicated function to beam thickness. This relation can however be obtained by testing beam that have different thickness but same other

dimensions. Fig. 7 shows the numerical result as computed from Eqs. 6.2 and 6.3 which suggests that minimum power input associated with flexural force and moment excitations to the structure may be achieved by using thicker laminates.

6.3 Effect of finite beam

Practical structures are often of finite length and thus, tests on the effect of finite beam upon power input were undertaken on beam specimen C. Random force signal was applied at the mid-span of each beam via mini-shaker and the response measurement being measured by the miniature accelerometer positioned as close to the excitation point as possible. The force applied was kept to a constant value for all beam samples by adjusting the gain of the power amplifier and noted by the measuring amplifier. The schematic diagram of the measurement setup is illustrated in Fig.(8).

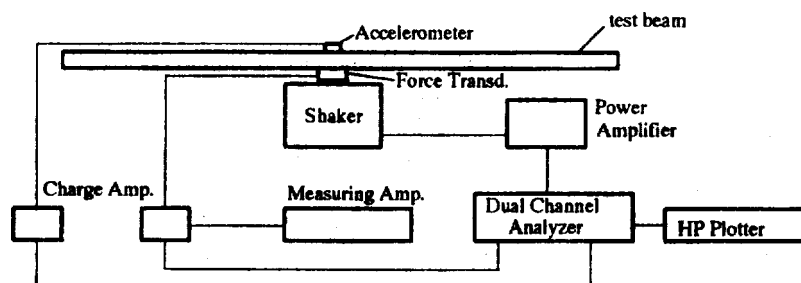


FIGURE 8. Schematic diagram of experimental set-up and instrumentation for finite-beam test.

Fig.(9) shows the result of mobility modulus in the frequency range of 0 to 2 kHz for several orientation of fibre angle. It is clearly observed that the effect of finite beam resulted in emergence of high peaks of resonance frequencies. This is due to the reflection of wave motion at beam ends which then create standing wave. There is a shift of natural frequency peaks towards low frequency as the fiber orientation angle increased. The shift in frequency of about 100 to 500 Hz between 0° and 90° fibre orientation angle was observed. The 0° orientation has the highest peaks amplitude indicating low damping compared to other orientation angle. The high frequency range result of 2 kHz to 8 kHz shown in Fig (10) shows same pattern as at low frequency range. At this frequency range, the shift in natural frequency is however much higher, i.e. about 1000 to 1500 Hz. The 0° orientation again shows low damping property and 45° orientation shows highest damping at high frequency.

The practical implication of the above results is that if one install a machine having discrete working frequency, such as motor, the suitable fibre orientation angle for the foundation structure may be chosen which will give minimum vibrational power input to the structure.

7. CONCLUSION

The vibrational power input to fibre-reinforced composite beams subjected to flexural force excitation was studied, and influences of fibre orientation angle, beam width and thickness, and finite beam length were examined experimentally. This study therefore confirmed the following :

- 1). The variation of fibre orientation angle with point mobility showed that there were minimal differences in the average behaviour of mobility. This suggest that there is no constraint imposed on fibre orientation angle of laminated structure for vibration control.
- 2). The vibrational power input may be minimised geometrically by having thicker laminates. This however increases the weight of the structure. The variation in width has minimal effect on the vibrational power input.
- 3). The effect of finite beam creates high frequency peaks which shifted towards lower frequencies as the fibre orientation angle increases. This has practical significance to machine having discrete working frequency in which suitable fibre orientation angle may be chosen to gave minimal power input.

REFERENCES

1. Goyder, H.D. and White, R.G., "Vibrational power flow from machines into built-up structures. Part I: Introduction and approximation analyses of beam and plate-like foundations", *Journal of Sound and Vibration*, Vol.68, No.1, pp.59-75. 1980.
2. Pinnington, R.J., "Power flow through machine isolators to resonant and non-resonant beams", *Journal of Sound and Vibration*, Vol.75, No.2, pp.179-197. 1981.
3. Petersson, B. and Plunt, J., "On effective mobilities in the prediction of structure-borne sound transmission between a source structure and a receiving structure. Part I: Theoretical background and basic experimental studies", *Journal of Sound and Vibration*, Vol.82, No.4, pp.517-529. 1982.
4. White, M.F. and Liasjo, K.H., 1982, "Measurement of mobility and damping of floors", *Journal of Sound and Vibration*, Vol.81, No.4, pp.535-547. 1982.
5. White, R.G., "Vibration control of machinery installations and structures : Some design procedures and experimental diagnostic techniques", *Vibration and Noise Conference, Melbourne*, Sept. 1990. pp.1-9.

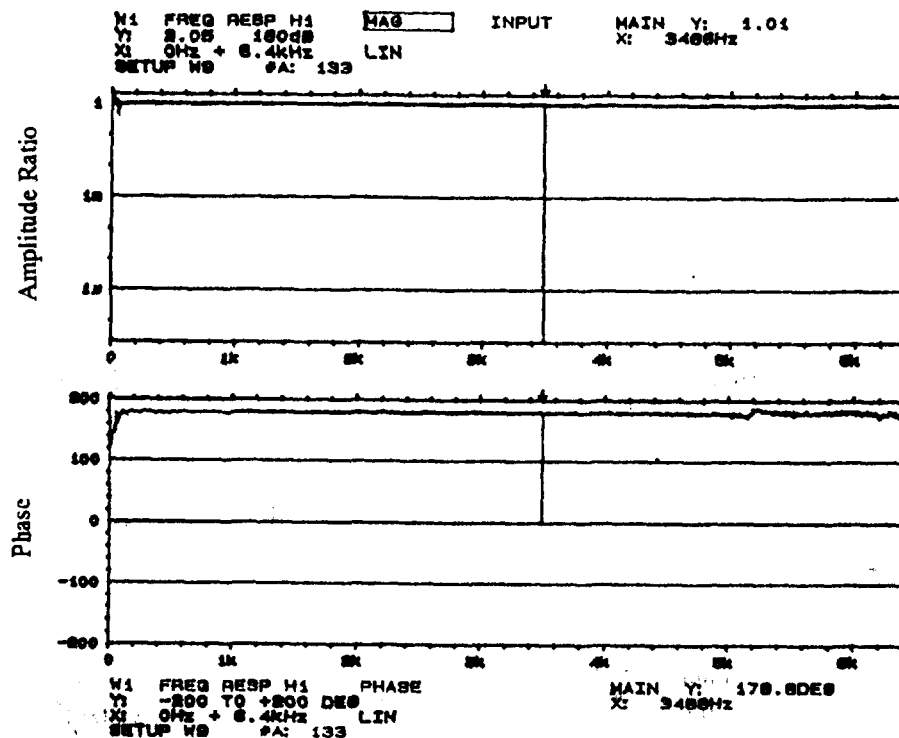


FIGURE 2. Amplitude ratio and phase between two accelerometers

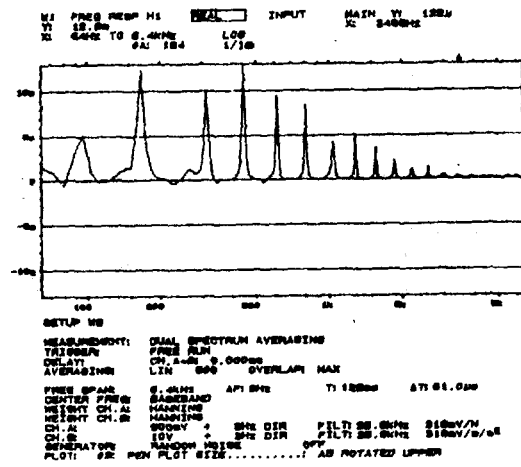
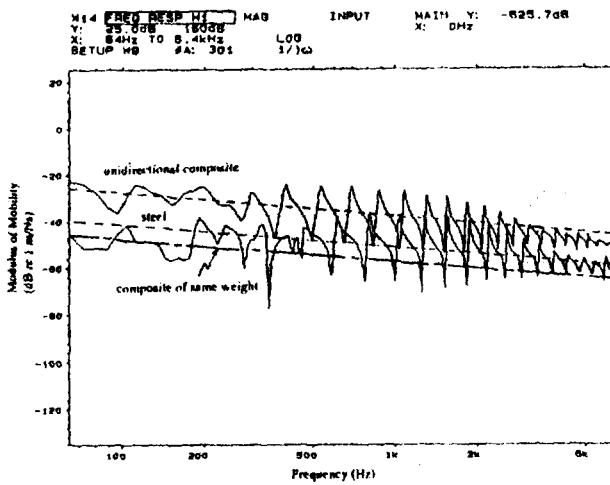


FIGURE 3. Modulus and real component of mobility for steel and 0° unidirectional composite structures subjected by constant point force. “- - -”, Theoretical averaged behaviour.

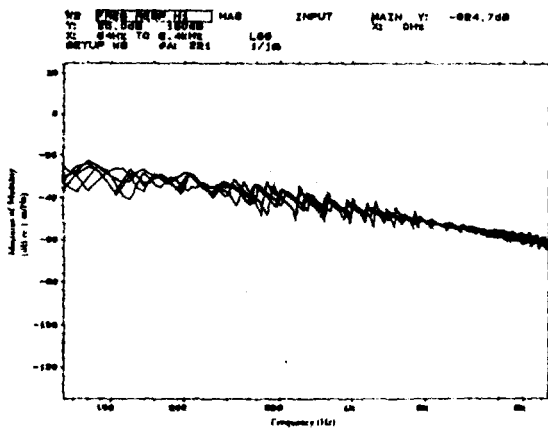


FIGURE 4. Measured values of mobility modulus of beams UD0A, UD30A, UD60A, and UD90A.

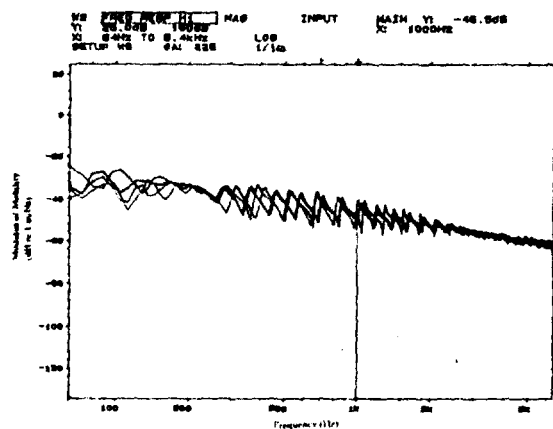


FIGURE 5. Measured values of mobility modulus of beams UD0B,UD30B,UD45B,UD60B, and UD90B.

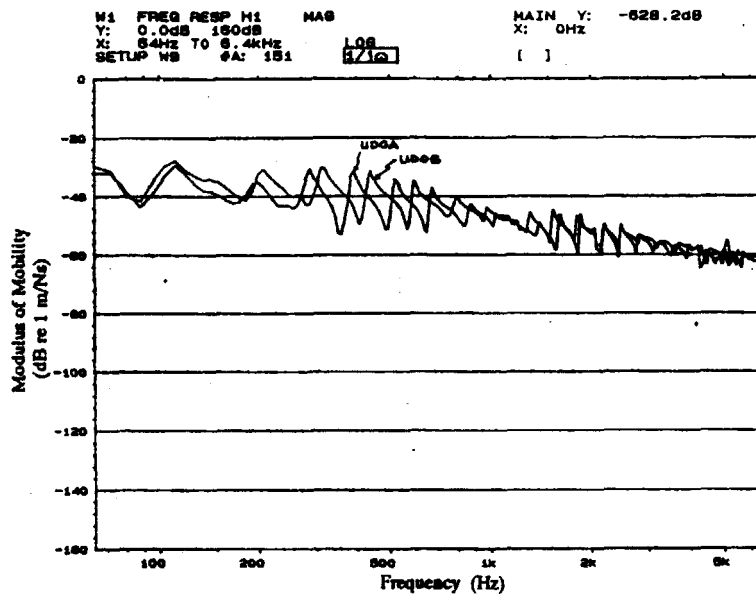


FIGURE 6. Measured values of mobility for beam UD0A, and UD0B having different width.

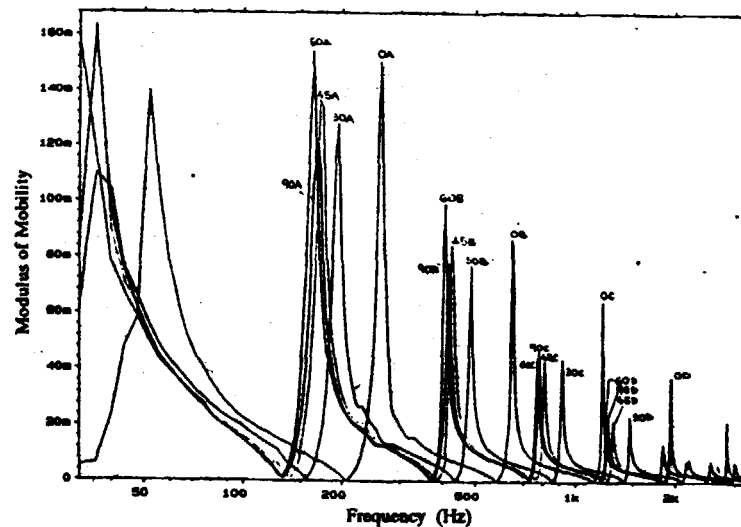


FIGURE 9 Measured values of mobility of modulus for beams UD0C, UD30C, UD45C, UD60C, and UD90C in the frequency range of 0 to 2 kHz.

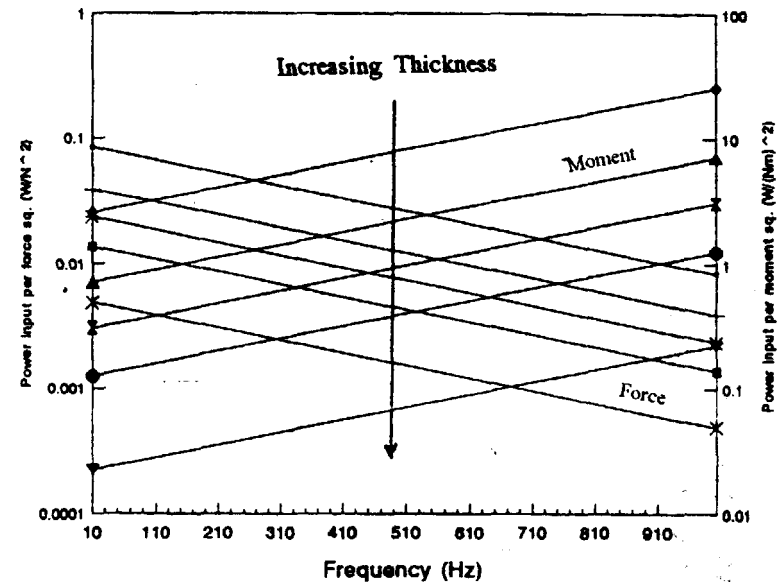


FIGURE 7 Numerical plot of power input per unit force square for laminated beam having variable thickness.

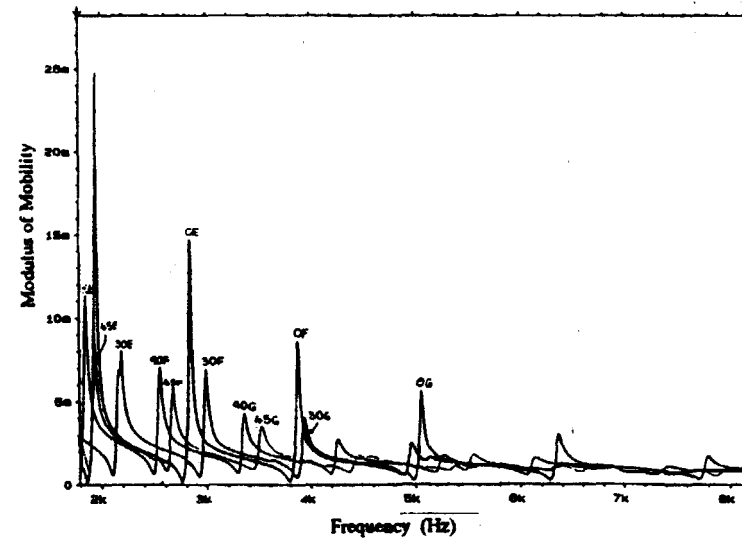


FIGURE 10 Measured values of mobility of modulus for beams UD0C, UD30C, UD45C, UD60C, and UD90C in the frequency range of 2 to 8 kHz.

IMPROVEMENTS ON THE DESIGN OF AN ELECTROSTATIC FILTER

Ngah Ramzi bin Hamzah, Zainuddin Shaary & Nabil Mahmoud Abdul-Kadir
Department of Electrical Engineering
Institut Teknologi MARA
40450 Shah Alam, Malaysia

ABSTRACT

This paper describes improvements on the filter design and power supply unit based on previous works of the authors. A new configuration are proposed for the filter and power supply to overcome previous adversities. The filter was designed to cater for the usually cylindrical form in existence with typical exhaust pipes. The technique can be used simultaneously as a silencer thus increasing the overall function that could be obtained. Laboratory tests carried out has indicated satisfactory results leading to promising future on the technique.

Keywords : *Electrostatic Precipitators, Air Filters, Automobile Exhaust Systems, Air Conditioning in Automobile, Air Pollution.*

1. INTRODUCTION

In the previous work[1], one of the mentioned applications of the electrostatic filter is in an automobile's exhaust system. As the dust is removed, the pollution from the exhaust is considerably reduced; enhancing the engine's performance. Further works as reported in reference[2] has been concerned with the objective of producing a compact design for increased viability on the applications as previously described. This is due to the fact that any technique that needs to be applied into an automobile environment has limited space as the major constraint. The technique if successful could then be easily adaptable to other areas of applications such as air-conditioning ducts, ventilation systems and etc.

In this work a new configuration are proposed for improvements on the filter and power supply design so as to overcome previous adversities. The filter was designed to cater for the usually cylindrical form in existence with typical exhaust pipes. Further aims, includes; reduction of air-pollution from an automobile's exhaust system thus improving the engine's efficiency. The technique can be used simultaneously as a silencer thus increasing the overall function that could be obtained. The DC power supply was designed so as to have both positive and negative high-voltage from a single AC source.

Laboratory tests that was carried out has indicated promising results leading to future technique that can be adopted. To increase the range of applications, attempts were made to carry out water treatment using the same technique and has indicated feasibility through continuous future development.

2. DESIGN CONSIDERATION

In the course of the work two possible configurations (i.e cylindrical and rectangular forms) are studied as will be described. The system makes use of multi-layer electrodes.

In its basic form the filter is an air-capacitor, that has electrodes separated by an air medium of which the electric field breakdown is about 30 kV/cm; a considerable factor in design.

The range of dust particles used in the tests ranges from 340 to 500 μm although the dust particles from the exhaust engines especially carbon ranges approximately 0.01 to 0.1 μm . The reason is that employed dust particles is much heavier and easily available. If the latter is employed, the weight collected would be almost the same but with a larger volume.

3. THE ELECTRODE MATERIAL

Through several experiments, aluminium was found to be the best material for the electrodes. When tested for a separation distance of 1 cm and at 10 kV, aluminium with a thickness of 1.5 mm will yield the best results with a collection efficiency of 38% compared to copper, galvanised iron and iron which yield 26%, 14% and 16% respectively; subjected to the same condition. The time taken to fully attract the dust was discovered to be the fastest for the case of aluminium when compared with the others. Several separation distances were also tested using the aluminium electrodes. By increasing the separation gap in steps of 0.5 cm; the efficiency reduces from 10% to 4%.

4. METHOD OF FIELD ENHANCEMENT

The field enhancement of the filter has the following standard relationships:

$$E = \frac{V}{d} \quad V/cm \quad (1)$$

where;

E = the electric field of the medium within the electrodes;

V = the applied potential difference between the electrodes;

d = the separation distance of the electrodes.

It can be seen that the magnitude of the field can be raised by increasing the applied voltage. The present supply voltage although designed for a maximum 12.5 kV_{dc} but for safety reasons, it is operated only up to 10 kV_{dc}.

An alternative method of enhancing the field is to modify the surface of the electrodes. The electrode surface onto which the dust is to be attracted is made rough by lightly punching it with sharp cold chisel within a limiting constraint. The surface must be such that; when the potential is applied with the other surface being grounded, the field between the electrodes will be slightly non-uniform but not to the extent of producing unstable conditions[3]. If the surface is punched until a grotesque appearance, the field would be totally non-uniform which in turn will render poor collection efficiency. With

rough surfaces, the collection efficiency is improved by 25%. One should note that the effective separation distance of gap due to the surface irregularity shall not create a field exceeding 30 kV/cm.

5. EXPERIMENT SET-UP

A duct is constructed for simulating the exhaust system (see Fig. 1). The length of the duct is 2.5 m and the cross-section diameter is 15 cm. The filter system is positioned at one end of the duct and close to that location an inverted paper cone with its vertex fixed to the duct. A portion of the vertex is cut-off to provide a small orifice for the insertion of dust during the tests. Throughout the experiments, the same amount is poured so as to maintain the accuracy. At the other end of the duct, a blower can be placed when testing the effect of velocity is performed. The blower speed is varied by adjusting its input voltage supply.

6. POWER SUPPLY

The applied voltage to the electrodes are from a standard simple rectifier circuit with minor modifications. There are two branches emerging from the high-voltage AC source, one for obtaining positive supply and the other for negative supply (see Fig.2). This is due to the fact that both supplies are needed for the electrode configuration. Each branch consists of stacked capacitors made in parallel with a stack of high value resistance. The capacitors are made up of ceramic capacitors stacked in parallel and series. The rectifier's efficiency at 10 kV is about 60% and with a time constant of about 0.5 sec.

7. FILTER DESIGN

In continuation to the earlier work[1], two new types of filter configuration, the rectangular and cylindrical, have been studied in view of application in an automobile's exhaust system. The dimension of both designs are shown in Fig.3.

Several supply configurations were then tested. By comparison, the cylindrical type proved to be the best as its collection efficiency is 7 to 8% better. As anticipated, the field is more uniform in the quasi-uniform configuration. The field distribution in the rectangular configuration,

especially at the corners, is difficult to be determined. This irregularity leads to poor collection efficiency. As such, the cylindrical configuration is chosen for the succeeding work. Furthermore, it is mechanically convenient in application.

The tests above were conducted on a 5 layer electrode configuration with the supply arrangement as "+ve gnd +ve" alternately between the electrodes. Also, a "+ve +ve gnd" arrangement had been tested but has resulted in inferior collection efficiency to the former. The former has been shown to be 10% better.

A third supply arrangement "-ve gnd +ve" yields an improvement of 60% compared to the "+ve gnd +ve". It is believed that the particles are randomly charged and floating in the medium and each charge is attracted to the oppositely charged electrode. The supply arrangement mentioned above and the corresponding collection results are as shown in Fig.4-1 and Fig.4 respectively.

8. EFFECT OF AIR VELOCITY

There is an drastic change in collection efficiency when there is an air velocity involvement. The effect of velocities on the collection efficiency are as shown in Fig.5. From the figure, for example, at 10 kV, the efficiency drops from 90% at zero velocity to 40% at approximately 0.5 m/s. At the same applied voltage and the highest tested velocity 5 m/s, the efficiency drops to only 6%.

9. CONCLUSION

From Fig.5 it can be seen that at 18 km/h (5 m/s), the collection efficiency is at 6%. In its present form the filter could not be employed in any system. The major setback is the limitation of the applicable voltage of the power supply (at the moment only up to 10 kV). At the above-mentioned velocity, to achieve an ideal efficiency, the applied voltage should theoretically be 18 kV. The present design of power supply is not capable of producing this magnitude. One of the reasons is the use of ceramic capacitors. They are primarily used because of their fast risetime but it is known that they have significant loss in capacitance as the applied voltage across them is increased. Furthermore, they are not able to store efficiently at high voltages which has a direct

influence on the efficiency of the output voltage and energy[4]. Currently another method of supplying the applied voltage is being developed for improvements.

The actual exhaust gas velocity at respective speed of the automobile is highly needed so as to determine the actual working condition. In this way, the applied voltage can be predicted and consequently the power supply with the required capacity can be designed.

The cylindrical filter configuration was designed in view of employing it as a silencer where holes are to be made on the grounded electrodes to muffle the exhaust noise.

10. ACKNOWLEDGEMENT

The authors wish to express their deepest gratitude to Mustafar Kamal Hamzah from Electrical Department, Institut Teknologi Mara for his editorial and constructive comments; invaluable to the preparation of this paper.

REFERENCES

- [1] N.R. Hamzah, N.M. Abdul-Kadir, *Design and implementation of Automobile Electrostatic Filter*, COSTAM 1993.
- [2] Zamri Che Ani and Wan Mohd Asri Mustapha, *High Voltage Filter*, Adv.Dip.(MARA) Thesis 1994
- [3] Kuffel, E., Zaengl, W.S., *High Voltage Engineering Fundamental*, Pergamon Press 1984.
- [4] Ogura, T. et al, *Output performance of the coaxial-type Marx generator consisting of BaTiO₃ series ceramic capacitors*, Rev. Sci. Instrum. **52(2)** Feb. 1981, American Inst. of Physics.

FIG. 1 THE DUCT SET-UP FOR EXHAUST SYSTEM SIMULA

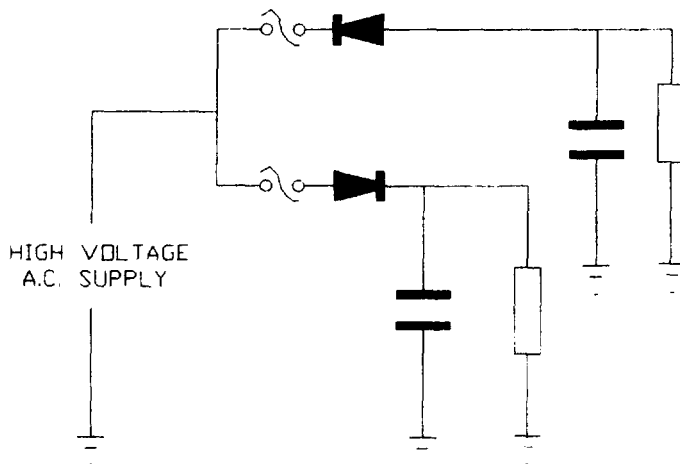
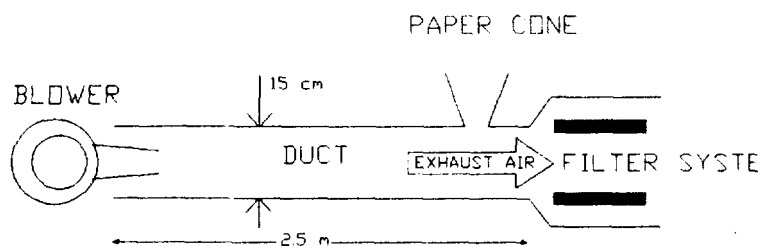
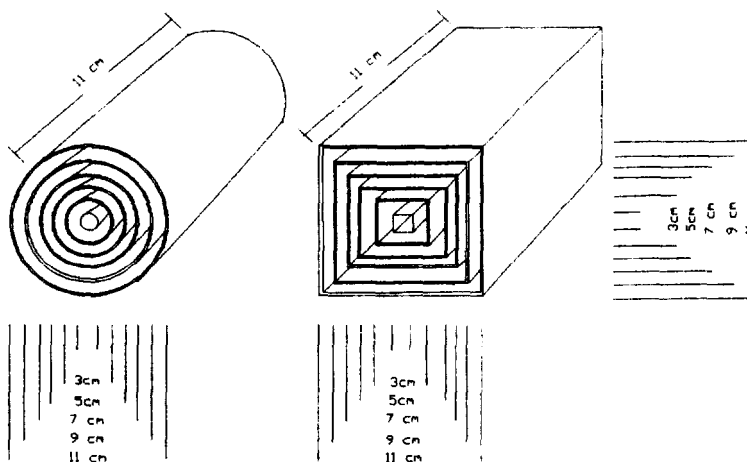


FIG. 2 THE POWER SUPPLY SCHEMATIC

FIG. 3 DIMENSION OF THE NEW FILTER CONFIGURATIONS



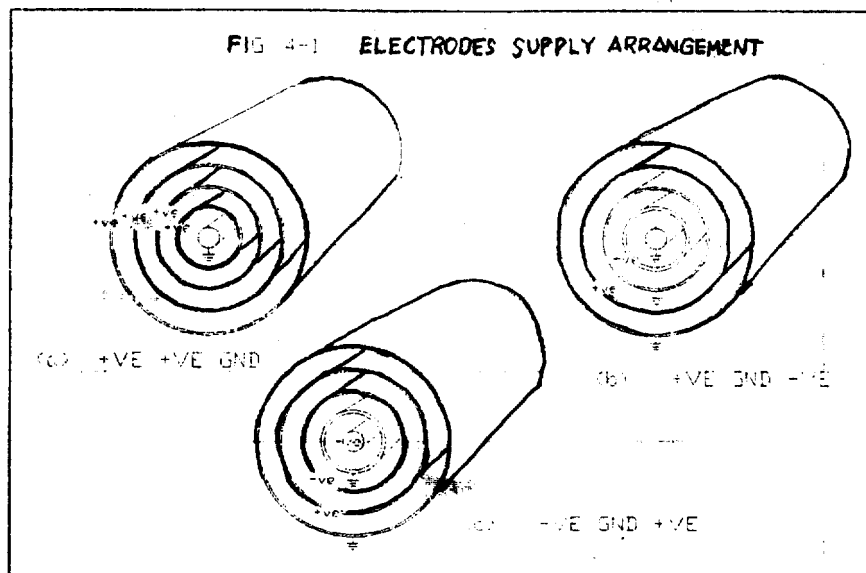


FIG.4 MASS VS SUPPLY ARRANGEMENT

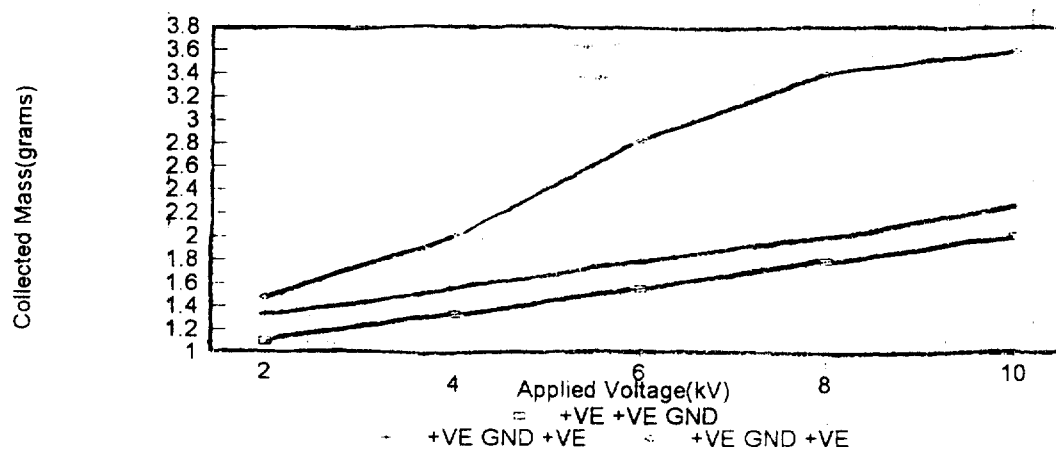
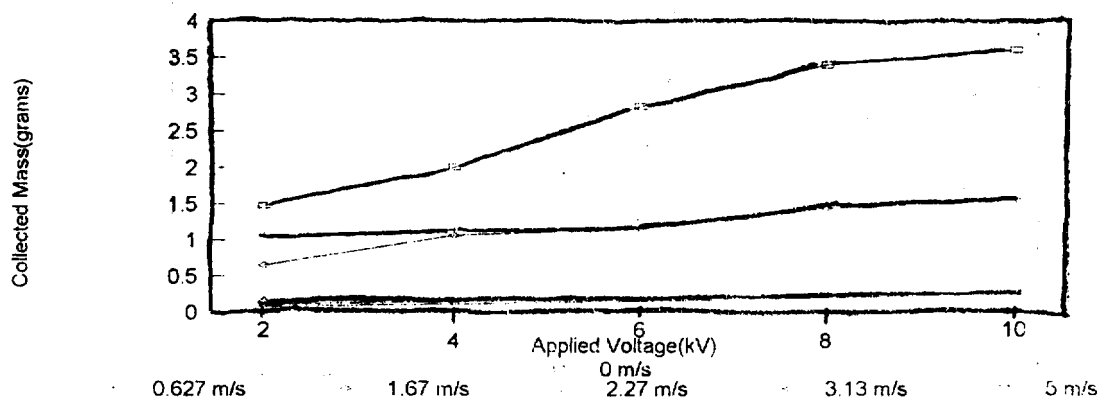


FIG.5 MASS VS APPLIED VOLTAGE



**POOR QUALITY
ORIGINAL**

DESIGN OF A ZERO DISPERSION OPTICAL FIBER

A.S. Supaat, N.M. Kassim, G. Kuhaneswaran
Telematic Optic Panels (TOPs), Jabatan Elektrik Perhubungan,
Universiti Teknologi Malaysia.

ABSTRACT

Pulse dispersion in an optical fiber is a result of several interacting mechanism. They can be divided into intramodal dispersion (consists of material and waveguide dispersion) and intermodal dispersion. In single mode fibers intramodal dispersion is the main source of dispersion as only one mode propagates along the fiber. By carefully designing the fiber, the effects of material and waveguide dispersion can be made to be self canceling to produce a zero dispersion optical fiber. This produces a fiber with a very small pulse broadening and a large bandwidth. This paper will explain the theoretical background of dispersion and the method employed to develop zero dispersion fibers. The results obtained and a discussion is also presented.

I. INTRODUCTION

One of the important characteristic of the fiber is bandwidth. Bandwidth, however, is limited by signal dispersion occurring within the fiber. Signal dispersion determines the data rate that can be used on the fiber. Dispersion is the effect of pulse spreading with time in the optical fiber. It is a function of the refractive index of the fiber material and wavelength or mode of light traveling within the fiber. There are two types of dispersion namely intermodal and intramodal dispersion. Intramodal dispersion can further be divided into material and waveguide dispersion. Intermodal dispersion is present only in multimode fibers and is due to propagation delay differences of the various modes in the fiber. Intramodal dispersion results from the finite spectral width of the optical source. The propagation delay of the various spectral components of the transmitted signal cause the broadening of each mode and hence dispersion. Intramodal dispersion plays a significant role in the single mode fiber where is only one mode propagating.

In order to overcome dispersion problems, zero dispersion fibers were developed. This is the focus of this paper. Intramodal dispersion is eliminated by having its two main components, material and waveguide dispersion, cancel each other by varying the fiber parameters. Zero dispersion can be achieved at any desired operating wavelength using this technique. The two most favoured operating wavelengths are 1300 nm and 1550 nm. 1300 nm is favoured because zero material dispersion occurs at this point and 1550 nm because of the low losses at this wavelength.

II. THEORETICAL BACKGROUND

Intermodal dispersion is prominent in multimode fibers and not in single mode fibers. It is due to the differential time delay between modes at a single frequency. Intramodal dispersion, also known as chromatic dispersion, is due to the variation of group velocity of a particular mode with wavelength. It can further be divided into material and waveguide dispersion. In practical optical fibers, both intermodal and intramodal dispersion exists. In single mode fibers, when operating under zero dispersion conditions, the two orthogonally polarized modes of the HE_{11} mode will travel down a birefringent fiber with a slightly different group velocity, thus making intermodal dispersion important again [1].

Intramodal dispersion results from the finite spectral width of the optical source. The propagation delay of the different spectral components of the transmitted signal causes the broadening at each mode and thus intramodal dispersion. The delay differences are caused by the dispersive of the waveguide material and also guidance effects within the fiber structure. They are namely material and waveguide dispersion.

Material dispersion is due to the different group velocities of the various spectral components launched into the fiber from the optical source. This happens when the phase velocity of a plane wave propagating in the dielectric medium varies nonlinearly with wavelength. A material is said to exhibit material dispersion when the second differential of the refractive index with respect to wavelength is not equal to zero.

The waveguiding of the fiber causes waveguide dispersion which is due to the variation in group velocity with wavelength for a particular mode. From ray theory, this dispersion is caused by the angle between the ray and the fiber axis varying with wavelength which subsequently leads to a variation in the transmission times for the ray. In multimode fibers, the majority of the modes propagate far from cutoff thus making it almost free from waveguide dispersion. The very small amount that exists is negligible compared with material dispersion. However in single mode fiber waveguide dispersion may be significant.

III. Overall Fiber Dispersion

In single mode fibers, pulse dispersion is due entirely to intramodal dispersion. The bandwidth in single mode fibers is limited by the finite spectral width of the source. Dispersion in a single mode fiber may be represented mathematically as shown below [7].

$$\text{Dispersion} = Y_1 + Y_2 + Y_3 \quad (1)$$

where

$$Y_1 = w \cdot \frac{dN_2}{dw} \cdot \left(1 + \frac{\Delta(dV)}{dV} \right)$$

$$Y_2 = \frac{\Delta N_2^2}{n_2} \cdot V \cdot \frac{d^2(bV)}{dV^2}$$

$$Y_3 = wN_2 \cdot \frac{d\Delta}{dw} \cdot \frac{d^2(bV^2)}{dV^2}$$

The first parameter (Y_1) is the material dispersion parameter, the second parameter (Y_2) is the waveguide dispersion parameter and the third (Y_3) is the profile dispersion parameter.

Profile dispersion in single mode fiber is very small (less than 0.5 ps/nm.km) especially at longer wavelength and often is neglected in single mode dispersion calculations [2]. In standard single mode fiber, total dispersion tends to be dominated by material dispersion of fused silica. However material dispersion tends to zero at a wavelength of about 1270 nm. This point is called the Zero Material Dispersion (ZMD) point.

The total fiber dispersion may be minimized by trading off material and waveguide dispersion while limiting profile dispersion. Profile dispersion is limited by restricting the variation in refractive index with wavelength. For wavelengths longer than the ZMD point material dispersion has a positive sign whereas waveguide dispersion has a

negative sign. Using this feature, zero dispersion fibers are designed by having the material dispersion cancel out waveguide dispersion so that the total first order dispersion is equal to zero [3,4,5]. This technique can be used to design zero dispersion fibers which operate in the 1300 nm to 2000 nm wavelength range [2]. This canceling is done by carefully controlling the fiber core diameter, V value and the refractive index difference.

IV. METHODOLOGY

(A) Approach Used

By using the properties of material and waveguide dispersion, Dispersion Shifted fiber are created. This is the method employed in the design. The ZMD point occurs at about 1270 nm for pure silica [2]. The ZMD point may be shifted to any wavelength between 1200 nm and 1400 nm by suitable doping of the core. Waveguide dispersion is influenced by the V value. Therefore waveguide dispersion may be altered by changing the V value of the fiber. The V value may be altered by altering the fiber parameters or operating wavelength.

Dispersion shifted single mode fibers are designed by using a combination of three methods namely [2]:

- Lowering the V value of the fiber.
- Increasing the refractive index difference of the fiber.
- By suitable doping of the core material.

Dispersion shifting employs the minimizing of first order dispersion. Although zero first order dispersion can be achieved with careful design, it should be noted that there are other higher order chromatic effects which impose limitations on the possible bandwidth that may be achieved with these single mode fibers.

(B) Design Specifications

As mentioned earlier total dispersion in a fiber may be represented as:-

$$\text{Dispersion} = Y_1 + Y_2 + Y_3$$

As $\Delta \ll 1$, the term containing Δ in Y_1 may be neglected. The same applies for the differential component in Y_3 which has a very small value. Therefore the three parameters above become:-

$$Y_1 = w \cdot \frac{dN_2}{dw}$$

$$Y_2 = \frac{\Delta N_2^2}{n_2} \cdot V \cdot \frac{d^2(bV)}{dV^2}$$

$$Y_3 = 0$$

The design a zero dispersion step index single mode fiber, the material and waveguide dispersion must be made to cancel out. Therefore,

$$Y_1 + Y_2 = 0$$

This is done by varying the V value, refractive index difference and core radius. These three parameters are related together by

$$V = n_2 ka(2\Delta)^{1/2} \quad ; \quad k = 2\pi/\lambda$$

The second differential term in the waveguide dispersion parameter can be obtained by using an approximate equation. The empirical approximation is as below [6]:-

$$\begin{aligned} V \cdot \frac{d^2(dV)}{dV^2} &\approx 0.0080 + 0.549 (2.834 - V)^2 \quad (2) \\ &\approx 0.080 + 0.549 (2.834 - 2.405 \cdot \frac{\lambda_c}{\lambda})^2 \end{aligned}$$

This approximation has an error smaller than 4% for the V value range of $1.2 < V < 3.0$.

The values for N_2 (Group Index) and n_2 (Cladding Refractive Index) for pure silica was obtained from the graphs [7]. There was no approximate equation which could be used to calculate these values. Two sets of values were chosen to be used namely the group index, N_2 , and core refractive index, n_2 , values at wavelengths of 1300 nm and 1550 nm. These wavelengths were chosen to design zero dispersion fibers that operate at these wavelengths. The values used are as shown below:-

Wavelength	N_2	n_2
-----	---	---
1300 nm	1.462	1.4477
1550 nm	1.463	1.444

Material dispersion is calculated using the equation below:

$$\begin{aligned} Y_1 &= w \cdot \frac{dN_2}{dw} \\ &= N_2 - n_2 \quad (3) \end{aligned}$$

Therefore,

$$\begin{aligned} \text{Wavelength} &= 1300 \text{ nm}, Y_1 = 0.0143 \\ \text{Wavelength} &= 1550 \text{ nm}, Y_1 = 0.019 \end{aligned}$$

For suitable power confinement of the fundamental mode, the V value was maintained in the range of 1.5 to 2.405. This method of designing a zero dispersion fiber may be used to design fibers which operate in the wavelength range of 1300 nm to 2000 nm [2].

The same procedure as above was repeated for a fiber with a different type of core material. The core material used in this case was Quenched Silicon Oxide (SiO_2). The physical data for this material was obtained from reference [3] and is presented below.

Wavelength	n_2	N_2	Y_1
-----	---	---	---
1310 nm	1.4392	1.4405	0.0013
1550 nm	1.4420	1.4514	0.0094

V. RESULTS

In order to obtain a solution to the problem of a fiber that fulfills zero dispersion conditions, there are many answers. For example, the V value may have any value between 1.5 and 2.4 and each V value would have a unique solution and fiber parameters.

From the calculations, it was found that two parameters play an important role in reducing the dispersion in a fiber. The mentioned parameters are the fiber V value and refractive index difference (Δ) for a given material. These designs were for two operating wavelengths, 1300 nm and 1550 nm. The results obtained are graphically presented as shown in figure 1 to 4. This data is also presented in tabular form as in Table 1 to 4. Dispersion graphs for two the extreme designs, namely with V value of 1.5 and 2.4, are also presented as in Figure 5 to 8.

VI. DISCUSSION

The graphs of Figure 1 to 4 show the various designs of a zero dispersion fiber using a core material of pure silica and quenched silicon oxide, designed to operate at a wavelength of 1300 nm and 1550 nm. From the graphs, it can be noted that, as the V value specified increases so does the refractive index difference in order to satisfy zero dispersion conditions. The core diameter instead, decreases as the V value increases. Therefore by carefully choosing a V value or refractive index difference a fiber that has the wanted core diameter can be produced.

The shifting of the zero dispersion point to a desired wavelength causes fiber parameters to change. The amount of material dispersion at different wavelengths is different. Corresponding changes also occur to the core refractive index value and the refractive index difference at different wavelengths. As the material dispersion increases so will the refractive index difference along with a corresponding reduction in the core diameter for a given V value to maintain zero dispersion conditions. This observation can be clearly seen from the equations for zero dispersion calculations. The opposite happens to the V value if the refractive index difference is kept constant. As material dispersion increases, the V value reduces to maintain zero dispersion conditions. The above can be seen more clearly from the mathematics below:-

Material Dispersion = Waveguide Dispersion

$$w \cdot \frac{dN_2}{dw} = \frac{\Delta N_2^3}{n_2} [0.80 + 0.549 (2.834 - V)^2]$$

From the equation operating wavelength influences the value of the material dispersion and the core refractive index value. The operating wavelength also directly affects the calculation of the core radius as shown below:-

$$a = \frac{V \cdot \lambda}{(2\Delta)^{1/2} n_2 2\pi} \quad ; \quad \lambda = \text{wavelength}$$

From the graphs in Figure 1 to 4, it can be noted that the V value ranges from 1.5 to 2.4. This follows the theoretical background as this range is needed to ensure the necessary power confinement. The core diameter size ranges from 2.2 μm to 3.3 μm for the quenched silicon oxide designs operating at 1550 nm. For the 1300 nm designs, the pure silica core diameter ranges from 2.1 - 3.2 μm whereas the Quenched Silicon Oxide diameter ranges from 7.0 to 10.5 μm . Commercially available fibers have core diameters sizes that range from 5 μm to 10 μm , typically about 8.5 μm [2]. There are a

number of reasons for this difference in the pure silica and quenched silicon oxide designs operating at 1550 nm.

First, the type of core material used here is pure silica whereas commercially available fibers have silica doped cores. The fiber core is doped to reduce attenuation as well to alter the ZMD point. The ZMD point can be shifted anywhere between 1200 nm and 1400 nm by using suitable dopants such as GeO_2 . This doping influences the material dispersion of a fiber at every wavelength and thus the zero dispersion calculations. Lower material dispersion at a certain wavelength means that the refractive index difference will also be lower at the point for a specified V value. This would allow the fiber to have a bigger core diameter such as the case of the commercially available fiber.

The observation also shows that pure silica is not a suitable material for making optical fibers. The small diameters make it difficult to couple the light from lasers to the fiber. The same goes to the second type of material, quenched silicon oxide. It is not suitable for making fibers that operate at 1550 nm but it is well suited to making fibers that operate at 1310 nm.

The second reason for the difference, is that the zero dispersion calculations in this project take into account only material and waveguide dispersion. This approach only minimizes the first order dispersion in a fiber. There are other dispersion parameters in a fiber that influence the dispersion such as differential material dispersion and cross product dispersion which were not taken into account. A more accurate design could be obtained by taking into account these dispersion parameters. This factor also accounts for the differences in the calculated values and commercially available fibers. It is possible that a better design that meets commercial requirements may be obtained by more accurate calculations.

A third reason would be that in the industry, a tradeoff between core diameter size and dispersion is used for certain cases. Fiber with larger core diameters are used for easy coupling while allowing a very small amount of dispersion to exist. However, the problems mentioned above can be overcome by careful choice of material as in the case of the quenched silicon oxide fibers designed to operate at 1310 nm.

Four dispersion graphs were plotted as in Figure 5 and 6 for pure silica and Figure 7 and 8 for quenched silicon oxide. The plots were for the extreme V values of 1.5 and 2.4. From the four graphs it can be observed that the fiber dispersions at a given wavelength, throughout the wavelength range of 1000 nm to 2000 nm, is lower for the designs with V value of 1.5. Thus it is advantageous to have a fiber with a V value approaching 1.5. Also at this V value the designs also have larger core diameters compared to at 2.4.

A second observation is that the quenched silicon oxide designs for both 1300 nm and 1550 nm have dispersion throughout the wavelength range compared to pure silica. The quenched silicon oxide design for 1310 nm has the lowest dispersion among the four graphs. The quenched silicon oxide designs also have larger core diameters compared to the pure silica designs. The refractive index difference is also smaller for the quenched silicon oxide designs at each V value and wavelength specified compared to the pure silica designs. From this we can say that Quenched Silicon Oxide is a better material to make optical fiber compared to pure silica.

The results obtained for quenched silicon oxide zero dispersion fiber operating at 1550 nm was compared to that obtained by C.T. Chang in Figure 9 [3]. The results in Figure 4 generally follows for the V value range 1.5 to 2.4 with a very small variation. This could be due to the differences in the values of the core refractive index and group index as well as the number of decimal points taken in the calculations. The results in Figure 4 confines that V value in the range of 1.5 to 2.4 to meet the power confinement requirements.

As for the cladding diameter of the Zero Dispersion fibers, it is usually ten times the core diameters to avoid losses from the evanescent field.

VII. CONCLUSION

From the results obtained, it is found that zero dispersion fibers can be designed using the method of material and waveguide cancellation for operation at any wavelength from 1300 nm to 2000 nm.

The various designs obtained for zero dispersion fibers that operate at a wavelength of 1300 nm and 1550 nm illustrate the point above. It is favorable to have zero dispersion fibers with a V value approaching 1.5. This is because at this V value the overall dispersion along the entire wavelength range of 1000 nm to 2000 nm is the lowest.

There are four main parameters in designing zero dispersion optical fibers namely the V value, refractive index difference, material dispersion and operating wavelength. The choice of material also plays an important role in successfully designing a zero dispersion fiber.

1.5	0.92	3.2
1.6	1.06	3.1
1.7	1.23	3.1
1.8	1.45	3.0
1.9	1.73	2.9
2.0	2.10	2.8
2.1	2.58	2.6
2.2	3.22	2.5
2.3	4.09	2.3
2.4	5.28	2.1

Table 1 : Various Zero Dispersion silica Fiber Designs. (Operating Wavelength 1300 nm)

V value	Refractive Index diff (%)	Core Diameter (μm)
1.5	1.21	3.3
1.6	1.40	3.3
1.7	1.63	3.2
1.8	1.92	3.1
1.9	2.29	3.0
2.0	2.78	2.9
2.1	3.41	2.7
2.2	4.26	2.6
2.3	5.42	2.4
2.4	6.99	2.2

Table 2 : Various Zero Dispersion Silica Fiber Designs. (Operating Wavelength 1550 nm)

V value	Refractive Index diff (%)	Core Diameter (μm)
1.5	0.09	10.5
1.6	0.10	10.4
1.7	0.11	10.3
1.8	0.14	10.0
1.9	0.16	9.7
2.0	0.20	9.3
2.1	0.24	8.8
2.2	0.30	8.2
2.3	0.38	7.6
2.4	0.49	7.0

Table 3 : Various Zero Dispersion Quenched SiO_2 Designs. (Operating Wavelength 1310 nm)

V value	Refractive Index diff (%)	Core Diameter (μm)
1.5	0.61	4.7
1.6	0.70	4.6
1.7	0.82	4.5
1.8	0.96	4.4
1.9	1.15	4.3
2.0	1.39	4.1
2.1	1.71	3.9
2.2	2.14	3.6
2.3	2.72	3.4
2.4	3.51	3.1

Table 4 : Various Zero Dispersion Quenched SiO_2 Designs. (Operating Wavelength 1550 nm)

Fig. 1 : Refractive index & Core Diameter vs V value
 (Pure silica at 1300 nm)

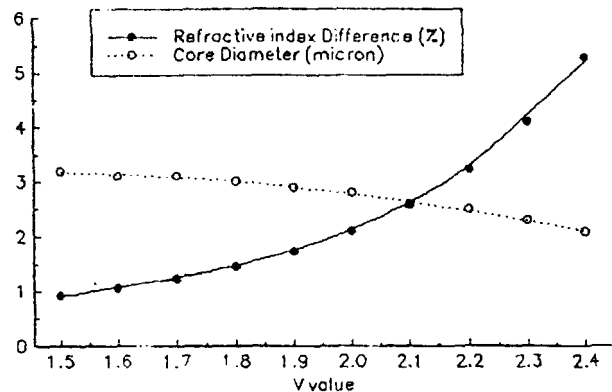


Fig. 3 : Refractive index & Core Diameter vs V value
 (Quenched Silicon Oxide at 1310 nm)

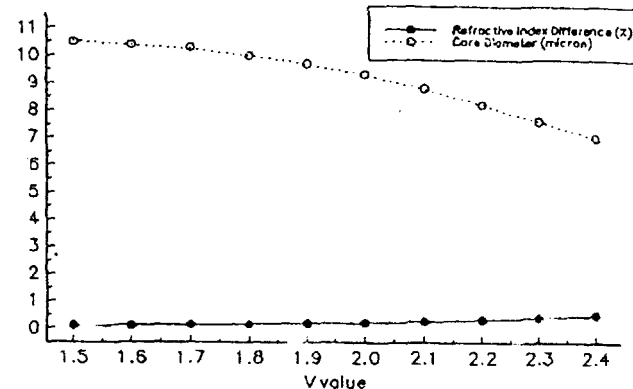


Fig. 2 : Refractive index & Core Diameter vs V value
 (Pure Silica at 1550 nm)

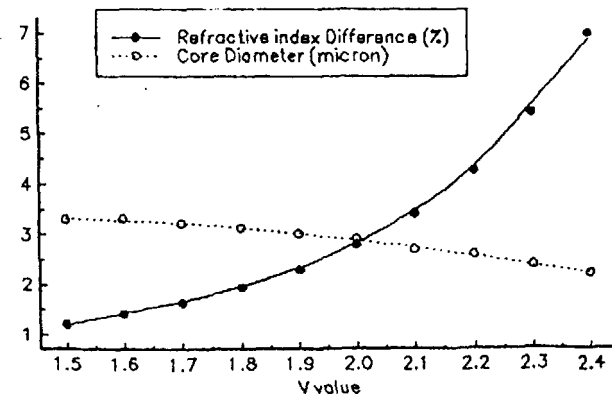


Fig. 4 : Refractive index & Core Diameter vs V value
 (Quenched Silicon Oxide at 1550 nm)

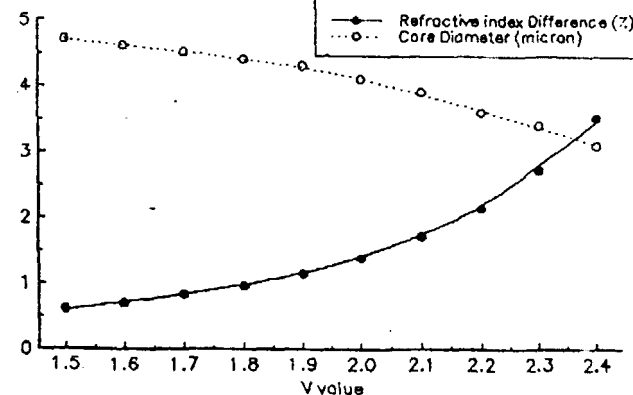


Fig. 5 : Dispersion Graph for Pure Silica Fiber
(Operating Wavelength : 1300 nm)

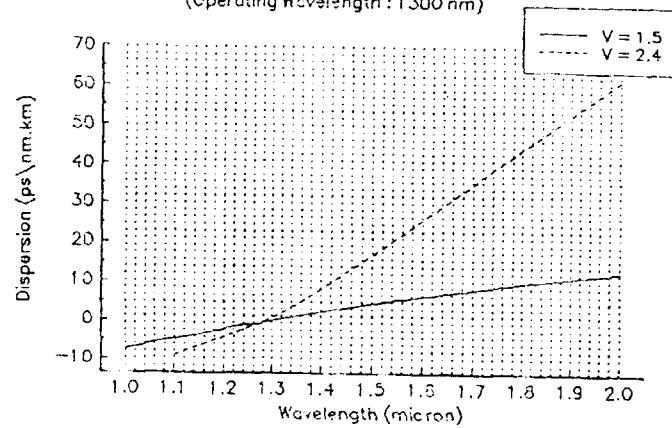


Fig. 7 : Dispersion Graph for Quenched Silica Oxide Fiber
(Operating Wavelength : 1310 nm)

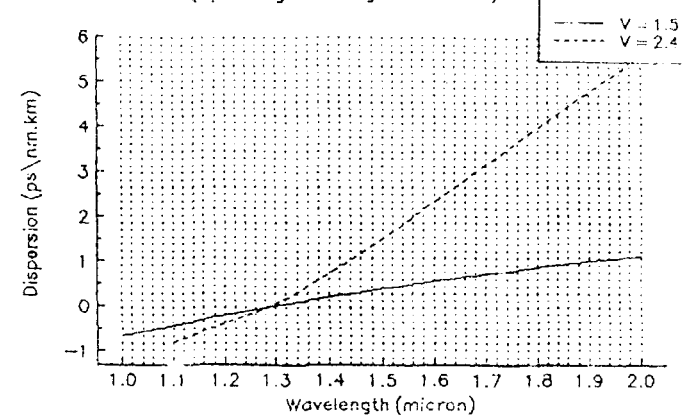


Fig. 6 : Dispersion Graph for Pure Silica Fiber
(Operating Wavelength : 1550 nm)

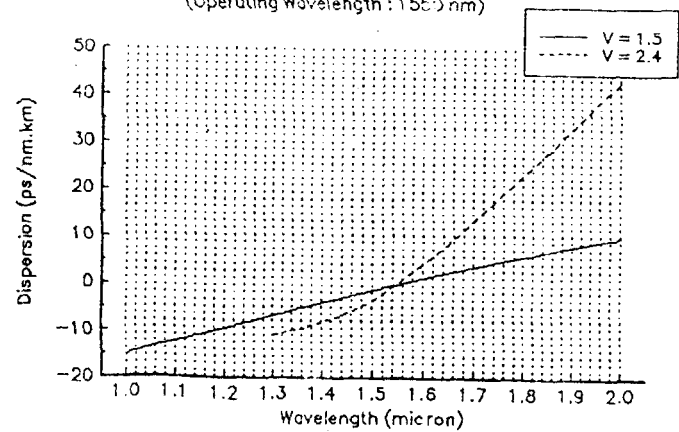
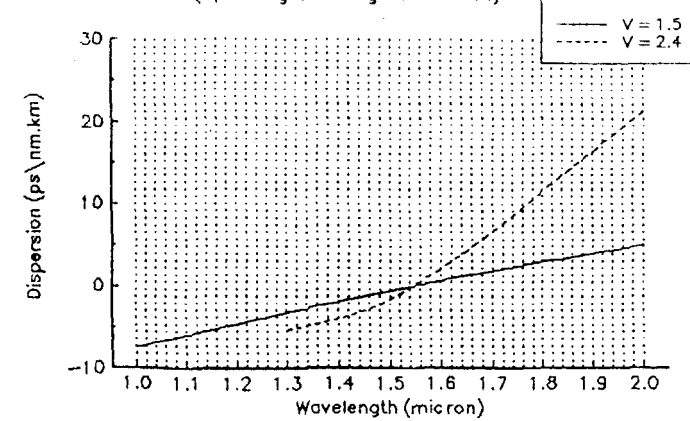
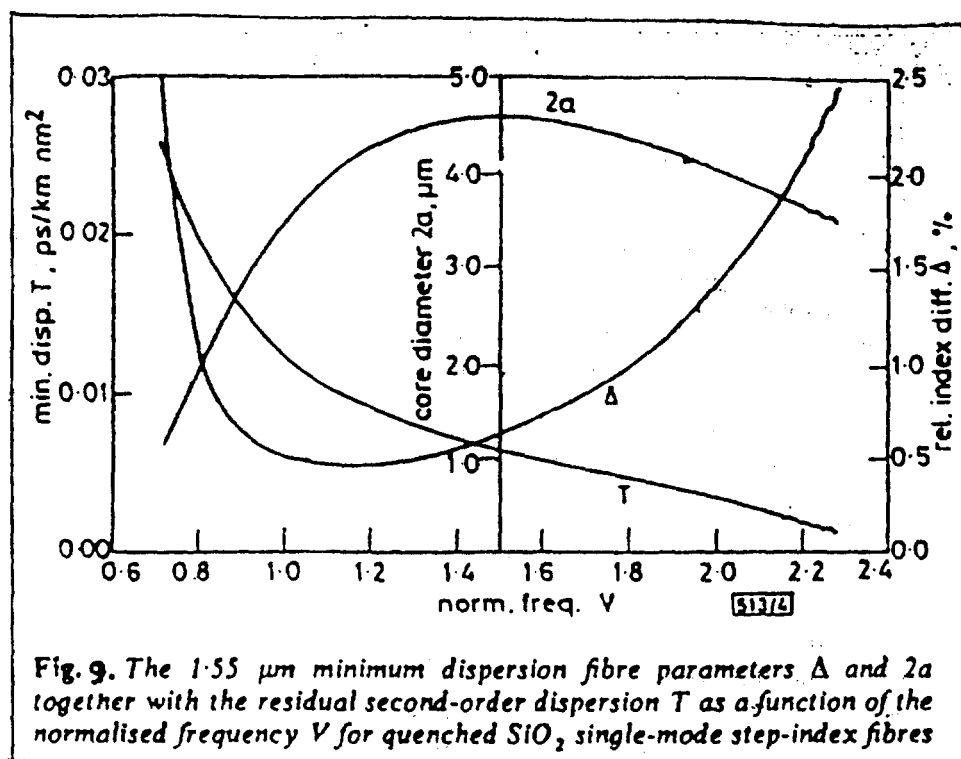


Fig. 8 : Dispersion Graph for Quenched Silica Oxide Fiber
(Operating Wavelength : 1550 nm)





References

- [1] Yeh, Chai (1990). Handbook of Fiber Optics: Theory and Applications. San Diego, California, Academic Press Inc.
- [2] Senior, John M. (1985). Optical Fiber Communications: Principles and Practices. (2nd Edition) Hemel Hempsted : Prentice Hall International (UK).
- [3] Chang, C.T. Minimum Dispersion at 1.55 μm for Single Mode Step Index Fibers. Electronic Letters, 8th. November, Vol. 15, No.23, Pg. 765.
- [4] Cohen L.G., Lin Chinlon, French W.G. Tailoring Zero Chromatic Dispersion into the 1.5 - 1.6 μm Low Loss Spectral Region of Single ModeFibers. Electronic Letters, 7th June 1979, Vol. 15, No. 12, Pg. 334.
- [5] Jeunhomme, Luc B. Dispersion Minimisation in Single Mode Fibers Between 1.3 and 1.7 μm . Electronic Letters, 19th. July 1979, Vol. 15, No. 15, Pg. 478-479.
- [6] Jeunhomme, Luc B. (1983). Single Mode Fiber Optics: Principles and Applications. New York: Marcel Dekker Inc.
- [7] University of Glasgow. Department of Electronic and Electrical Engineering. Design of a Zero Dispersion Optical Fiber. (Unpublished).



EFFECTS OF ANNEALING ON EVAPORATED SnS THIN FILMS

Samsudi Sakrani and Bakar Ismail
Thin Film Laboratory, Physics Department
Universiti Teknologi Malaysia
Karung Berkunci 791, 80990
Johor Bahru, Malaysia

ABSTRACT

The effects of annealing of evaporated tin sulphide thin films (SnS) are described. The films were initially deposited onto glass substrate, followed by annealing in an encapsulated carbon block under the running argon gas at 310°C. Short time annealing of the films results in a slight change of the compositions to a mix SnS/SnS₂ compound, and the tendency of increasing SnS₂ formation was observed on the films annealed for longer periods up to 20 hours. X-ray results showed the transformation of SnS peaks ((040) and (080)) to predominantly SnS₂ peaks ((001), (100), (101) and (110)). The associated absorption coefficients measured on the films were found to be greater than 10⁵ cm⁻¹, with indication of higher photon energy leading to the formation of SnS₂ compound.

INTRODUCTION

SnS is a semiconducting material with an optical band gap in the ranges 1.10 - 1.26 eV^{1,2} and hence has the potential to become a versatile solar energy material. There were also reports on the use of SnS in the holographic-recording system³ and optoelectronic devices.⁴ Recent interest in SnS thin film was due to the high in conversion efficiency of about 25% obtainable from it in photovoltaic devices and also its availability, low cost, less toxicity and stability.⁵ Tetragonally-structured SnS₂ is one of the sulphur-rich derivative of rhombohedrally-structured SnS. The n-type nature in the former and p-type conduction exhibited by the latter is an interesting feature for the tin-base semiconducting material technology in very near future.⁶⁻⁸

Much attention has been given on the bulk and single crystal properties of SnS and SnS₂ so far. It is hence of prime importance in the interest of semiconductor material technology to understand the basic thin film properties to promote versatile electronic/optoelectronic devices. The studies of SnS thin films have been made by Grozdanov et al.⁹ whom they investigated the effects of annealing on the chemically prepared films. Annealing for 24 hours in air at 280°C results in change of type of conductivity from p-type (SnS) to n-type (SnS₂). Evaporated SnS thin films are normally non-stoichiometric, i.e. excess of either Sn or S atoms which leads to the formation of higher derivatives of SnS₂, Sn₂S₃ and S₃S₄ and are temperature dependent. Deraman et al.^{10,11} have successfully deposited SnS thin films at substrate temperature of 300°C, and the measured optical band gap was found to be 1.07 eV.

EXPERIMENTAL

Thermally evaporated SnS thin films were prepared from its granules (6N) onto cleaned glass substrate at room temperature and at a pressure about 10^{-5} mbar. Two set of film thicknesses were fixed at 71 nm and 400 nm using quartz crystal monitor and ellipsometer during and after the evaporation, respectively. These were later confirmed and further justified using a computer programme. The films were placed in a carbon block (35 mm x 35 mm x 6 mm) which was mounted at the centre of electrically-heated cylindrical tabular glass. Annealing process was carried out at pressure 10^{-1} mbar under the running argon gas at 310°C for 2, 6, 12 and 20 hours. The 400 nm films were studied using a Philips PW 3710 X-ray diffractometer in order to observe the compositional changes occurring in the as prepared and annealed samples. The optical absorption measurements were carried out on transparent samples of 71 nm thick, using a UV Hitachi Spectrophotometer within the visible wavelength regions, and the absorption coefficients were obtained using an expression given in equation (1).

RESULTS AND DISCUSSION

Figure 1 shows the X-ray diffraction spectrum of as deposited film (a) and annealed films (b to d). It is clear that SnS composition becomes the predominant film in the former case except the existence of (003) SnS₂ peaks which are also detected in the latter case. Such a behaviour is expected from the analysis of thicker films greater than 70 nm, probably by the slow diffusion of sulphur atoms into the Sn atoms. Deraman et al.¹⁰ found weak Sn₂S₃/ Sn₃S₄ peaks with stronger SnS peaks observed on 50 nm films. After 2 hours of annealing at 310°C a detectable chemical change takes place; part of SnS disproportionates to SnS₂, resulting in a weak (001) peak. See Figure 1(b). The samples annealed for 6 hours give a clear (001) peak and an additional (100) peak on the X-ray diffractogram (Figure 1(c)), showing an increase of the SnS₂/SnS ratio. Similar trend is observed on the samples annealed for 12 hours (not shown in Figure 1). Further annealing for 20 hours results in considerable amount of SnS₂ composition, with more pronounce detectable peaks of (001), (100), (101), (102) and (110) and the disappearance of SnS composition. See Figure 1(d). A longer period of annealing (attempted for 30 hours) caused a considerable reduction of these peak intensities, probably the loss of Sn and S atoms by prolong heating. The existence of most of the SnS₂ peaks obtained in this experiment predicts that, during annealing preferred orientation of the crystal along the axes (a-, b- and c-axis) takes place. This result is different from those obtained earlier¹⁰ on chemically prepared SnS films where the dominant crystal orientation occurred along the c-axis only. X-ray analysis of the annealed films is shown in Table 1.

The optical absorption, α varies with photon energy according to the curves shown in Figure 2. For the as prepared films α increases in the range $0.8 - 8.0 \times 10^5 \text{ cm}^{-1}$ with an increase of photon energy. Similar curves are observed for the annealed films but the trend shifts to the right with slight reduction in the range of α ($0.3 - 3.8 \times 10^5 \text{ cm}^{-1}$ annealed for 20 hrs.) due to compositional changes occurring in the films. These higher values of α are expected to meet the prerequisite requirements for solar cell material

which ensures effective light absorption into the film, and the results are in a good agreement with those reported earlier.^{6,7}

α is related to the intensities of light incident, I and light absorbed, I_0 ($> I$) to the film of thickness, t given by

$$I = I_0 \exp(-\alpha t) \quad \text{or} \quad \alpha = \frac{1}{t} \ln\left(\frac{I_0}{I}\right) \quad (1)$$

where T is the transmittance of the absorbed light (%) on the transmittance-wavelength plot. Accordingly, for the as prepared films with known α and T in the range 0.5 - 47.8% the calculated film thicknesses or so-called absorption thickness limits, t_1 vary from 7100 to 7380 nm. This means that, any SnS thin film deposited at thicknesses less than 7380 nm has the absorption amount fairly enough for solar energy conversion. t_1 for the annealed films are tabulated in Table 1 as follows.

TABLE 1. Results of the calculated absorption thickness limits, t_1 and X-ray analysis

Measurement	Annealed samples		
	2 hrs	6 hrs	20 hrs
Absorption thickness limit (nm)	7083-7270	7025-7180	7000-7100
X-ray analysis (SnS ₂ peak)	SnS/SnS ₂ (003), (001)	SnS ₂ /SnS (003), (001) (100)	Mostly SnS ₂ (003), (001), (100) (101), (102), (110)

CONCLUSIONS

The effects of annealing on evaporated SnS thin films is based on the X-ray analysis and optical absorption measurements. It was found that, in the former case, annealing for 20 hours caused the transformation of orthorhombically-structured SnS into tetragonally-structured SnS₂, compared to a SnS/SnS₂ mixture for shorter period of annealing (less than 6 hours), with the expectation of crystal orientation occurring along all the three axes. In the latter case, annealing caused the photon energy to increase its magnitude in order to enable light absorption into the films, but the absorption coefficient remain unchanged. In other word, extra energy is needed for light absorption into SnS₂ films if compared to the SnS films. These properties, together with the wider absorption thickness

limits and ease of fabrication make SnS and SnS₂ thin films the possible choices for solar cell material in the near future.

ACKNOWLEDGEMENTS

This project is part of the IRPA research programme. Thanks are due to Unit Penyelidikan dan Perundingan, Universiti Teknologi Malaysia for providing the facilities and support, all the colleagues in the Physics Department and thin film research group for valuable discussion and encouragement. Finally, to Prof. T. Nagatomo of Shibaura Institute of Technology, Tokyo Japan for the comments and correction.

REFERENCES

1. Elkorashy A.M., Optical Constants of Tin Sulphide Single Crystals Measured by The Interference Method, *Phys. Stat. Sol. (b)*, **159**, 903-915 (1990).
2. Parenteau M. and Carlone C., Influence of Temperature and Pressure on The Electronic Transitions in SnS and SnSe Semiconductors, *Phys. Rev. B*, **41**, 5227-5234 (1990).
3. Valiukonis, D.A., Guseinova G., Krivaite G. and Sileika A., Optical Spectra and Energy Band Structure of Laser-type A^{IV}-B^{VI} Compounds, *Phys. Stat. Sol.(b)*, **135**, 299-307 (1986).
4. Nikolic P.M. and Todoric D.M., Photo-acoustic and Thermo-acoustic Properties of Single-crystal SnS Compared with its Near-infrared Optical and Transport Measurements, *J. Phy. C: Solid State Phys.*, **20**, 39-46 (1987).
5. Gupta V.P., Agarwal P., Gupta A. and Srivastava V.K., Electronic Properties of Tin Dichalcogenides (SnS₂ and SnSe₂), *Phys. Chem. Solids*, **43**, 291-295 ((1982).
6. Shibata T., Miura T., Kishi T. and Nagai T., Systhesis of Single Crystal SnS₂ by Vapour Transport Method at Low Temperature Using Reverse Temperature Gradient, *J. Crystal Growth*, **106**, 593-604 (1990).
7. Abbas A.K., Majeid K.J. and Jassim H.A., Optical Properties of Chemically Deposited Tin Disulphide Coatings, *Sol. Stat. Comm.*, **57**, 805-808 (1986).
8. Shibata T., Muranushi Y., Miura T. and Kishi T., Chemical and Structural Characterization of SnS₂ single Crystals Grown by Low-temperature Chemical Vapour Transport, *J. Materials Sci.*, **26**, 5107-5112 (1991).
9. Grozdanov I., Ristov M., Sinadinovski Gj. and Mitreski M., Effects of Annealing on The Composition and Properties of SnS Thin Films, *FIZIKA*, **21** suppl., 320-323 (1989).
10. Deraman K., Sakrani S. and Ismail B., Evaporated SnS Semiconducting Thin Films, *Paper Presented at The International Seminar on Thin Film Physics and Applications*, Shanghai China, 15-17 May 1994.
11. Deraman K., Sakrani S. and Ismail B., Electrical Conductivity Measurements on Evaporated Tin Sulphide Thin Films. *Paper Presented at The International Workshop on Electronic Properties on Metal/non-metal Systems*, Sheffield Hallam University, UK., 29 Aug. - 3 Sept. 1993.

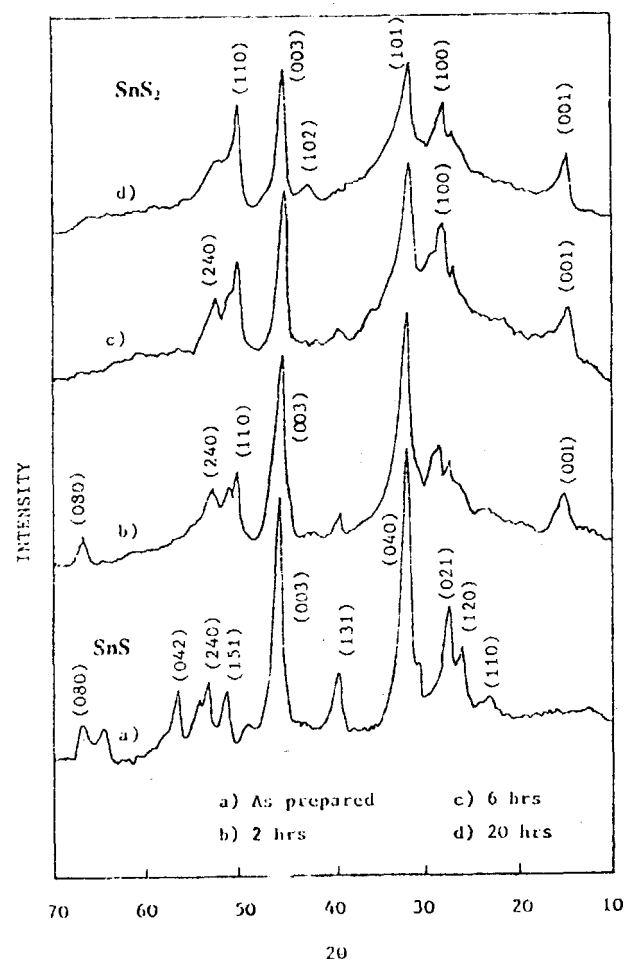


FIGURE 1. X-ray diffraction spectra of SnS thin films: a) SnS as prepared, and annealed for b) 2 hrs., c) 6 hrs. and d) 20 hrs.

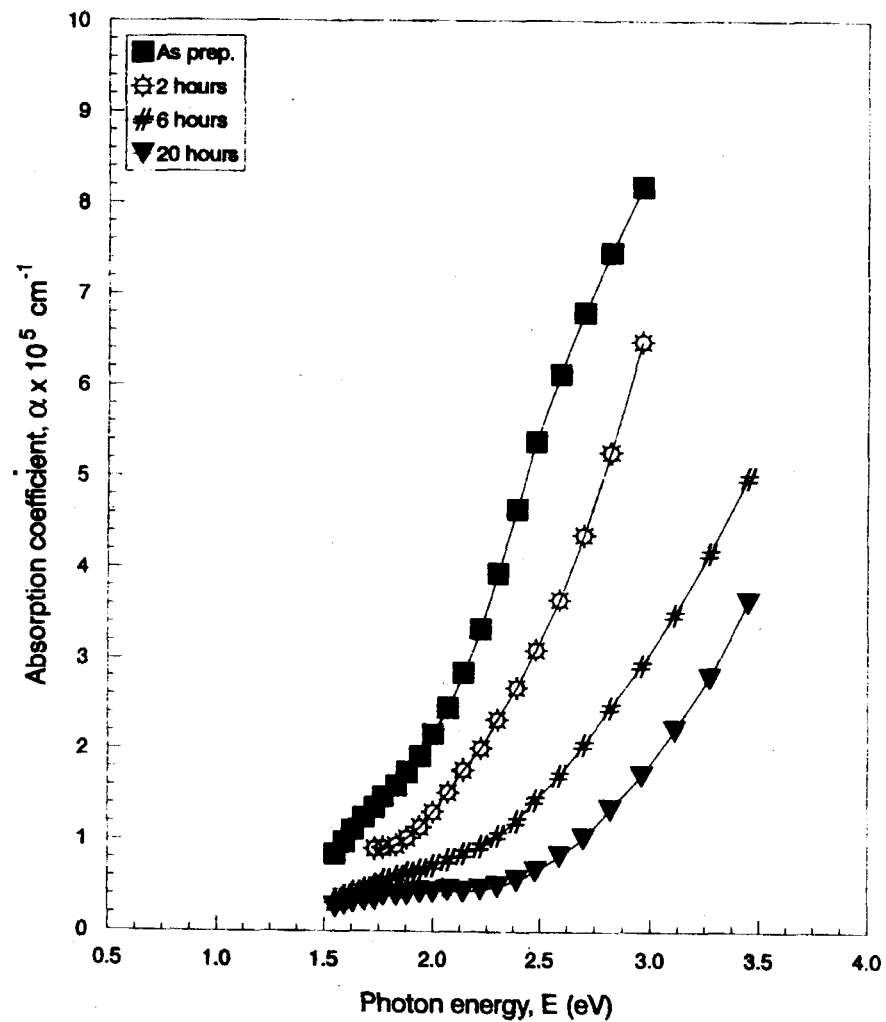


FIGURE 2. Absorption coefficient, α of the as prepared and annealed SnS thin films



MY9700936

SAPUT TIPIS SnSe DISEDIAKAN DENGAN KAEDAH PENSELENIDAN TERTUDUNG-TEBAT

Sabar D. Hutagalung*, Samsudi Sakrani dan Yussof Wahab

Makmal Saput Tipis, Jabatan Fizik

Universiti Teknologi Malaysia

Karung Berkunci 791, 80990

Johor Bahru, Malaysia

ABSTRAK

Saput tipis timah selenida telah disediakan secara penselenidan tertudung-tebat. Lapisan Sn dan Se telah disejatkan secara vakum dan disepuh lindap dalam blok karbon pada suhu 100 - 500°C selama 3 jam. Keputusan analisis sinar-X dan mikrograf SEM menunjukkan bahawa SnSe mula terbentuk pada 150°C dengan saiz hablur 30.0 nm dan menjadi optimum pada 200°C (saiz hablur 25.5 nm). Kerintangan saput didapati bertambah mengikut suhu sepuh lindap, iaitu 0.56 Ω cm (100°C), 42.34 Ω cm (200°C), dan 54.28 Ω cm (300°C). Perubahan nilai ini disebabkan oleh pembentukan sebatian SnSe.

ABSTRACT

Tin selenide thin films were prepared by encapsulated selenization. A stacked layer of evaporated Sn and Se films were annealed in a carbon block at temperatures 100 - 500°C for 3 hours. X-ray analysis and SEM micrograph results showed that SnSe was initially formed at 150°C with crystal size 30.0 nm and reached optimum formation at 200°C (crystal size 25.5 nm). The resistivity of the films were found to increase with the annealed temperatures, i.e. 0.56 Ω cm (100°C), 42.34 Ω cm (200°C), and 54.28 Ω cm (300°C). These higher resistivity were due to the formation of SnSe compound.

PENGENALAN

Timah selenida (SnSe) adalah bahan semikonduktor daripada kumpulan IV-VI dalam jadual berkala. Bahan ini mempunyai ciri-ciri semikonduktor berikut: kekonduksian jenis-p, ketumpatan lohong dalam julat 10^{17} - 10^{18} cm⁻³, kerintangan antara 10^{-2} - 10^2 Ω cm, dan tenaga jurang jalur yang rendah, iaitu antara 0.8 - 1.3 eV. Justeru itu potensinya sebagai peranti elektronik¹⁻⁵ dan sistem sel suria⁶⁻⁸ amat menggalakkan. hablur sebatian SnSe mempunyai struktur orthorombik⁶, memiliki lapan atom per unit sel dan parameter kekisinya pada suhu bilik adalah $a = 4.448$ Å, $b = 11.496$ Å dan $c = 4.158$ Å.⁹

Berbagai kaedah telah dilakukan untuk menyediakan saput tipis SnSe; antaranya pemendapan vakum¹⁰ iaitu dengan mencampurkan bahan pukal timah dan selenium dengan nisbah tertentu dan dimendapkan secara penyejatan vakum; pemendapan

Kertas kerja dibentangkan pada Kongres Sains & Teknologi Malaysia '94 di Ming Court Hotel, Kuala Lumpur, 15-18 Ogos 1994.

**Alamat tetap: Jurusan Fisika, Universitas Sumatera Utara, Medan 20155, Indonesia.*

elektrik¹¹ iaitu pemendapan secara elektrokodot dimana saput SnSe diperolehi pada katod melalui proses elektrolisis larutan asid SnCl_2 dan SeO_2 atau H_2SeO_3 dan larutan N-dimethylformamida; pemendapan kimia¹² iaitu dengan mencampurkan serbuk selenium dan larutan natrium sulfat untuk mendapatkan larutan natrium selenosulfat dan akhirnya saput SnSe pada substrat yang letakkan secara menegak dalam larutan; pemendapan epitaksi dinding panas¹³ dimana pemendapan SnSe berlaku pada tekanan wap bahan pada substrat yang terkandung dalam satu bekas panas; penyejatan kilat¹⁴ dimana SnSe disediakan secara stoikiometri dan dipanaskan pada suhu 1150 K dan tekanan 10^{-5} mbar selama 50 jam dan kemudian dimendapkan secara penyejatan kilat ke atas substrat mika dan kaca pada suhu yang berbeza; penyejatan rintangan⁸ iaitu saput SnSe dimendapkan pada suhu 373 K ke atas substrat kaca; dan kaedah tindak balas bahan pepejal^{15,19} bagi memendapkan lapisan Sn dan Se dengan menggunakan filamen berbilang keatas substrat kaca pada suhu bilik dan tekanan 10^{-5} mbar.

Kaedah penselenidan tertudung-tebat telah dilakukan untuk menyediakan saput CuInSe_2 ¹⁶ dengan Cu, In dan Se dimendapkan keatas substrat kaca pada suhu bilik secara penyejatan vakum atau percikan. Lapisan Cu/In/Se kemudiannya disepuh lindap di dalam blok karbon dan gas nitrogen. Suhu dikawal pada julat 200°C - 400°C dengan perubahan masa antara 1 - 6 jam. Kaedah ini didapati menghasilkan sebatian yang dikehendaki tanpa berlaku perubahan komposisi dan oleh itu sesuai untuk penyediaan sebatian binari seperti Sn dan Se. Kertas kerja ini melaporkan kaedah baru penyediaan saput tipis SnSe yang dinamakan penselenidan tertudung-tebat. Ujikaji pembelauan sinar-X, mikroskop imbasan elektron dan pengukuran kerintangan dengan penduga empat titik turut serta dilaporkan.

EKSPERIMEN

Lapisan Sn dan Se dimendapkan dengan penyejatan vakum ke atas substrat kaca pada suhu bilik. Peralatan vakum yang digunakan adalah penyejat vakum Edwards, model E306 pada tekanan kurang daripada 10^{-4} mbar. Substrat diletakkan pada jarak lebih kurang 6.5 cm di atas sumber penyejatan (perahu molybdenum) yang mengandungi bahan pukal Sn atau Se yang akan dimendapkan. Kepingan silikon diletakkan berhampiran substrat kaca untuk pengukuran ketebalan menggunakan ellipsometer. Kadar pemendapan ditetapkan pada 0.1 % per saat. Ketebalan saput semasa penyejatan dikawal oleh monitor hablur kuartza. Nisbah ketebalan lapisan Sn : Se adalah 1 : 2 iaitu 110 nm : 220 nm (untuk ujikaji mikroskop imbas elektron) dan 200 nm : 400 nm (untuk ujikaji pembelauan sinar-X dan pengukuran kerintangan). Saput Sn/Se yang diperolehi disepuh lindap pada suhu 100°C , 150°C , 200°C , 250°C , 300°C , 400°C dan 500°C masing-masing selama 3 jam dalam blok karbon dan persekitaran gas argon pada tekanan 10^{-2} mbar. Penyejukan semula dilakukan secara perlahan-lahan pada suhu bilik.

Saput tipis SnSe yang diperolehi diuji dengan pembelauan sinar-X dan mikroskop imbasan elektron (SEM) untuk mengetahui sifat-sifat strukturnya. Corak pembelauan sinar-X dirakamkan pada perakam carta dengan sumber sinaran $\text{CuK}\alpha$ dan penapis nikel. Kerintangan saput diukur dengan menggunakan penduga empat titik¹⁷.

HASIL DAN PERBINCANGAN

Corak pembelauan sinar-X keatas sampel yang disediakan pada suhu bilik dan sampel yang telah disepuh lindap pada suhu 100°C sampai 500°C ditunjukkan dalam Rajah 1. Pembelauan sinar-X terhadap sampel yang disediakan pada suhu bilik menunjukkan sifat permukaan saput tipis Sn/Se yang mengandungi struktur hablur. Kesan bahan pukal Sn dan Se dapat diperhatikan daripada puncak-puncak spektrum; ini menunjukkan Sn dan Se masih merupakan lapisan yang berasingan. Pada suhu 100°C, keamatan puncak-puncak belauan semakin jelas tetapi belum menunjukkan pembentukan sebatian SnSe. Pada suhu 150°C pula sebatian SnSe mula terbentuk dengan puncak-puncak belauan yang baharu selain daripada Sn dan Se. Pembentukan sebatian SnSe menjadi lengkap pada 200°C tanpa adanya puncak-puncak lain seperti sebelumnya. Puncak-puncak SnSe yang dikenal pasti adalah (111), (031), (041), (012), (131), (141) dan (132), lihat Rajah 2. Pada suhu 250 - 500°C, didapati corak belauan semakin berkurangan dan hanya puncak (031) yang bersesuaian dengan nilai pemisah $d = 0.2871$ nm sahaja yang jelas kelihatan sebagai SnSe, manakala beberapa puncak lain dikenal pasti sebagai sebatian timah diselenida (SnSe_2). Hasil yang sama dilaporkan oleh Siddiqui et. al.³

Pengiraan saiz butiran dengan kaedah persamaan Scherrer diperolehi nilai purata saiz butiran saput tipis SnSe sebesar 18.4 nm (100°C), 30.0 nm (150°C), 25.5 nm (200°C), 22.3 nm (300°C) dan 19.5 nm (400°C). Struktur mikrograf hablur SnSe menunjukkan bahawa pembentukan hablur bermula pada suhu 150°C dan menjadi lengkap pada suhu 200°C, lihat Rajah 3.

Daripada hasil pengukuran kerintangan dengan menggunakan peralatan penduga empat titik diperolehi bahawa kerintangan saput yang disepuh lindap pada suhu 100°C, 200°C dan 300°C diukur pada suhu bilik masing-masing adalah 0.56 Ω cm, 42.34 Ω cm dan 54.28 Ω cm. Nilai kerintangan yang kecil pada suhu 100°C menunjukkan bahawa kesan bahan pukal logam Sn masih dominan dan nilainya menjadi bertambah besar apabila sebatian semikonduktor SnSe terbentuk pada 200°C dan 300°C.

Kerintangan bahan pukal semikonduktor SnSe hablur tunggal dilaporkan oleh Yu et. al.⁴ sebesar 0.04 Ω cm diukur dengan kaedah Van der Pauw, manakala Bhatt et.al.¹⁸ mendapatkan nilai sebesar 0.07 Ω cm diukur dengan kaedah penduga empat titik. Pramanik dan Bhattacharya¹² melaporkan bahawa kerintangan saput tipis SnSe yang disediakan secara penyejatan kimia adalah dalam julat 10 Ω cm diukur dengan penduga empat titik pada suhu bilik, manakala Siddiqui dan Desai¹⁹ memperolehi bahawa kerintangan saput tipis SnSe yang disediakan secara tindak balas bahan pepejal keatas substrat kaca bersuhu 30°C, 100°C dan 150°C masing-masing adalah 1.970 Ω cm, 0.395 Ω cm dan 0.074 Ω cm yang diukur dengan kaedah Van der Pauw. Jadi, kerintangan SnSe yang diperolehi dalam ujikaji ini masih agak besar jika dibandingkan dengan nilai yang diperolehi oleh penyelidik lain.

KESIMPULAN

Saput tipis timah selenida (SnSe) telah berjaya disediakan secara penselenidan tertudung-tebat. Kaedah ini merupakan suatu kaedah yang mudah dan murah, dimana nisbah masing-masing lapisan Sn dan Se dapat dikawal dengan mudah semasa pemendapan, sedangkan pembentukan hablur sebatian SnSe dilakukan dengan sepuh lindap pada suhu optimum 200°C selama 3 jam.

Saput tipis SnSe yang diperolehi dengan penyejatan vakum adalah hablur secara semulajadi, bagaimanapun kehabluran ini merupakan paduan bahan pukal Sn dan Se. Pembentukan hablur sebatian saput tipis SnSe bermula pada suhu sepuh lindap 150° C dan menjadi optimum pada suhu 200°C. Pada suhu di atas suhu optimum ini, hanya puncak (031) yang dapat dilihat dengan jelas. Nilai purata saiz butiran pada suhu optimum ini adalah 22.5 nm, manakala nilai purata terbesar adalah 30 nm pada suhu 150°C. Kerintangan saput yang diperolehi adalah dalam julat 10^{-1} - 10^2 Ω cm.

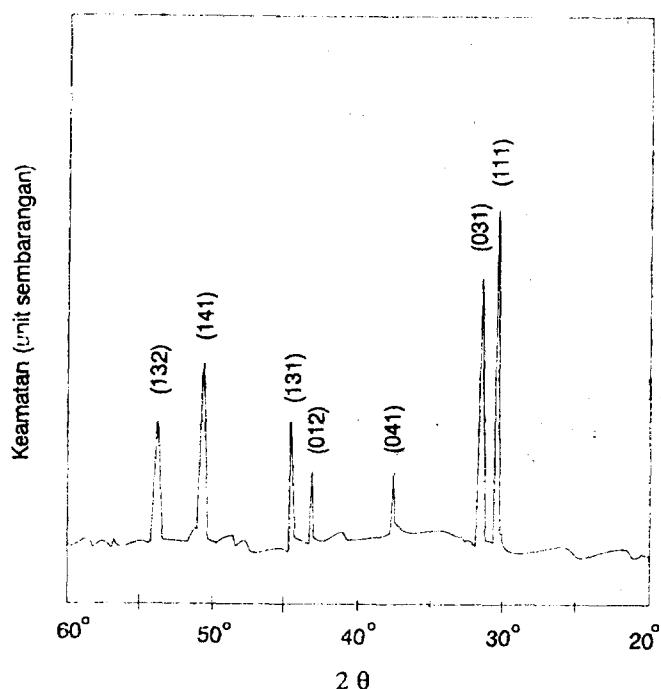
PENGHARGAAN

Sabar D. Hutagalung ingin merakamkan penghargaan kepada Universiti Teknologi Malaysia yang memberikan biasiswazah pengajian doktor falsafah di Jabatan Fizik, dan kepada Universitas Sumatera Utara (Medan - Indonesia) yang memberikan izin cuti belajar kepadanya. Juga kepada Unit Tenaga Nuklear, Puspati, Bangi kerana bantuan analisis sampel menggunakan XRD dan SEM.

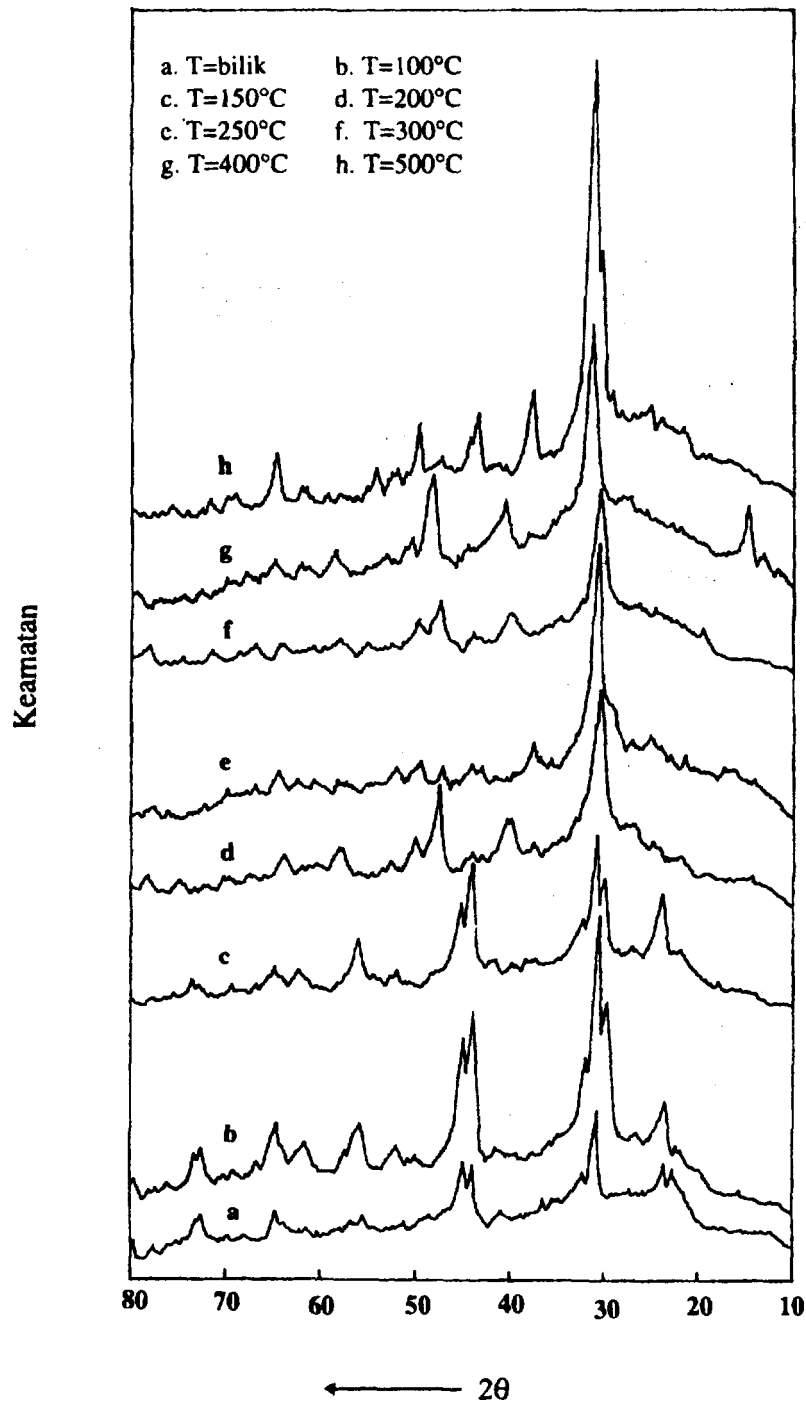
RUJUKAN

1. Albers W. and Verberk J., The SnSe-SnSe₂ Eutectic: a p-n Multilayer Structure, *J. Mater. Science*, **5**, 24 -28 (1970).
2. Bhatt V. P., Gireesan K. and Desai C. F., Preparation and Characterization of SnSe-SnSe₂ Heterojunctions, *Indian J. Pure Appl. Phys.*, **29** Iss: 1, 27-30 (1991).
3. Siddiqui S.S., Desai C.F. and Pandya G.R., Electrical Properties of Thin films of SnSe-SnSe₂ Eutectic Alloy, *Cryst. Res. Technol.*, **28** Iss: 6, K59 - K63 (1993).
4. Yu J.G., Yue A.S. and Stafsudd Jr. O.M., Growth and Electronics Properties of the SnSe Semiconductor, *J. Crystal Growth*, **54**, 248 - 252 (1981).
5. Dongwoochu R.M., Walser R.W.B. and Courtney T.H., Polarity-dependent Memory Switching in Devices with SnSe and SnSe₂ Crystals, *Appl. Phys. Letters*, **24** Iss: 10, 479-481 (1974).
6. Abrikosov N.Kh., Baukina V.F., Poretskaya L.V., Shelinova L.E. and Skudnova E.V., Semiconducting II-VI, IV-VI, and V-VI Compounds, *Plenum Press, NY*, 65 - 151 (1969).
7. Bennouna A., Tersier P.Y., Priol M., Quan D.T. and Robin S., Far Ultraviolet Photoelectric Study of Thin SnSe Evaporated Films, *Phys. Status Solidi (B)*, **117**, 51-56 (1983).

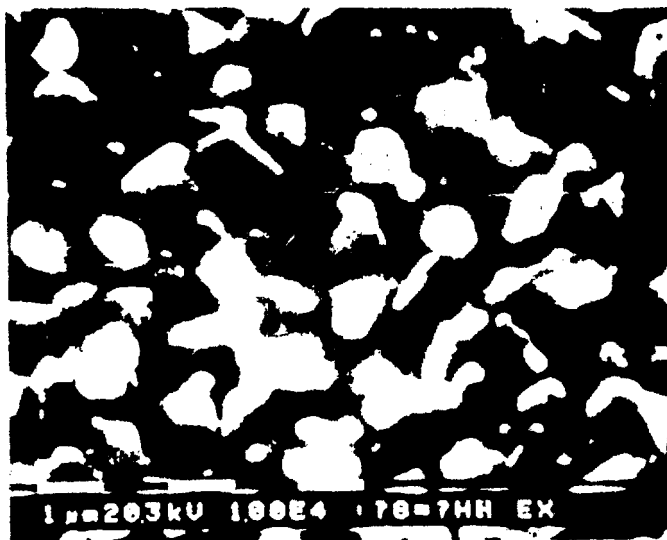
8. Bhatt V.P., Gireesan K. and Desai C.F., Photoconductivity of SnSe Thin Films, *J. Mater. Sci. Letters*, **11** Iss: 7, 380-381 (1992).
9. Wiedemeir H. and Csillag F.J., The Thermal Expansion and High Temperature Transformation of SnS and SnSe, *Zeit. Kristallographie*, **149**, 17-29 (1979).
10. Terada T., Vacuum Deposition of Tin-selenium Films, *J. Phys. D: Appl. Phys.*, **4**, 1991-1997 (1974).
11. Engelkan R.D., Berry A.K., van Doren T.P., Boone J.L. and Shahnazary A., Electrodeposition and Analysis of Tin Selenide Films, *J. Electrochem. Soc.*, **133**, 581-585 (1986).
12. Pramanik P. and Bhattacharya S., A Chemical Method for the Deposition of Tin(II) Selenide Thin Films, *J. Mater. Sci. Letters*, **7**, 1305-1306 (1988).
13. Singh J.P. and Bedi R.K., Tin Selenide Films Grown by Hot Wall Epitaxy, *J. Appl. Phys.*, **68** Iss: 6, 2776-2779 (1990).
14. Singh J.P. and Bedi R.K., Electrical Properties of Flash-evaporated Tin Selenide Films, *Thin Solid Films*, **199** Iss: 1, 9-12 (1991).
15. Quan D.T., SnSe Thin Films Synthesized by Solid State Reaction, *Thin Solid Films*, **149** Iss: 2, 197-203 (1987).
16. Tanda M., Yamanaka S., Nakada N., Konagai M. and Takahashi K., Preparation of CuInSe₂ Films by Encapsulated Selenization and its Characterization by Raman Scattering Spectroscopy, *Annual Research Report, Semiconductor Science Laboratory, Tokyo Inst. of Technology, Tokyo*, 82-85 (1990).
17. Sakrani S., Wahab Y. dan Hutagalung S.D., Ralat Dalam Pengukuran Kerintangan Saput Tipis Dengan Menggunakan Penduga Empat Titik, *Mal. J. St. Sc. & Tech.*, **1**, 6-12 (1994).
18. Bhatt V.P., Gireesan K. and Pandya G.R., Growth and Characterization of SnSe and SnSe₂ Single Crystal, *J. Cryst. Growth*, **36**, 649-659 (1989).
19. Siddiqui S.S. and Desai C.F., Electrooptic Properties of SnSe Thin Films Synthesized by Solid State Reaction, *Cryst. Res. Technol.*, **28** Iss: 8, 1169 - 1173 (1993).



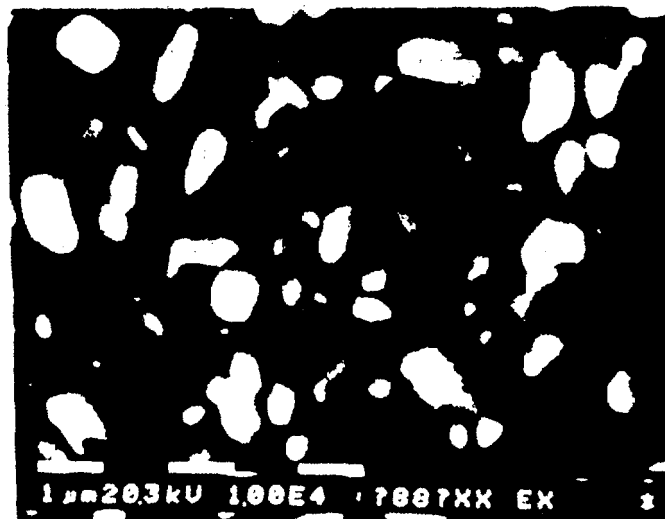
RAJAH 2. Corak Pembelauan sinar-X sampel yang disepuh lindap pada 200°C selama 3 jam



RAJAH 1. Corak pembelauan sinar-X keatas sampel yang disediakan pada suhu bilik dan yang disepuh lindap pada suhu 100 - 500°C selama 3 jam.



(a)



(b)

RAJAH 3. Mikrograf mikroskop imbas elektron bagi saput tipis SnSe yang disepuh lindap pada suhu (a) 150C dan (b) 200C selama 3 jam

PERFORMANCE OF LOCALLY MANUFACTURED HOLLOW-FIBER MEMBRANE FOR CO₂ SEPARATION

**H.SAIDI, R.A.AZIZ, A.ARIFFIN, H.HASSAN,
MEMBRANE RESEARCH UNIT,
FAK.KEJ. KIMIA & KEJ.SUMBER ASLI,
UNIVERSITI TEKNOLOGI MALAYSIA
KUALA LUMPUR**

ABSTRACT

Hollow fiber membrane is the latest and advanced gas separation technology currently employed in the gas industries. Malaysia which is rich in natural resources has huge natural gas reserves amounting to more than 5 Trillion Standard Cubic Feet (5 TSCF). Membrane Research Unit has produced a hollow-fiber module by using a locally made spinneret which is capable of producing hollow fiber membranes using a wet-spinning method. This module contains hollow fiber membranes with surface area of 72.22cm². The module is utilised in the existing membrane gas separation pilot plant (MGSP) for performance test. The performance of this module was based on its permeation rate and selectivity for each pure gases tested namely N₂, CO₂ and O₂. Based on the result obtained the module has the capability to separate CO₂ from natural gas, helium recovery in Enhanced Oil Recovery (EOR), nitrogen and oxygen recovery in the production of urea.

INTRODUCTION

In order to apply membranes on a commercial scale, large membrane areas are normally required. The smallest unit into which the membrane area is packed is called a module. The module is the central part of a membrane installation ⁽¹⁾. The simplest design is one in which a single module is used. Figure 1 below gives a schematic diagram of such a single module system.

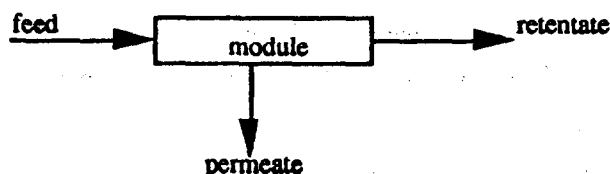


Figure 1 : Schematic drawing of a module

A feed inlet stream enters the module at a certain composition and a certain flow rate. Because the membrane has the ability to transport one component faster than the other, both the feed composition and the flow rate in the feed stream the module will change as a function of distance. The feed inlet stream is separated into two streams, i.e. a permeate stream and a retentate stream. The permeate stream is the fraction of the feed stream which passes through the membrane whereas the retentate stream is the fraction retained.

Different module configuration designs are possible and which are based on two types of membrane geometry : (i) flat; and (ii) tubular. Plate-and-frame and spiral-wound modules involve flat membranes whereas tubular, capillary and hollow fiber modules are based on tubular membrane configurations. The difference between the latter types of module arises mainly from the dimensions of the tubes employed, as is shown in Table 1⁽¹⁾.

configuration	diameter(mm)
tubular	>10.0
capillary	0.5 - 10.0
hollow fiber	<0.5

Table 1 : Approximate dimensions of tubular membranes

If tubular/hollow fiber membranes are packed close together in a parallel fashion than the membrane area per volume is only a function of the dimensions of the tube.

The membranes are self-supporting . Two types of flow arrangement can be distinguished ⁽¹⁾:

- (i) The feed solution passes through the bore of the capillary (lumen) whereas the permeate is collected on the outside of the capillaries ("inside-out")
- (ii) The feed solution enters the module on the shell side of the capillaries (external) and the permeate passes into the fiber bore ("outside-in").

The choice between the two concepts is mainly based on the application where parameters such as pressure, pressure drop, type of membrane available, etc. are important. Depending on the concept chosen, asymmetric capillaries are used with their skin on the inside or on the outside.

Hollow fiber module

The hollow fiber module is the configuration with the highest packing density, which can attain values of 30,000 m²/m³ ⁽¹⁾. The hollow fiber module is used when the feed stream is relatively clean, as in gas separation and pervaporation. Hollow fiber module have also been used in the case of sea water desalination, another relatively clean feed stream. The module construction is given in Figure 2. In gas separation the module will be of the "outside-in" type to avoid high pressure losses inside the fiber.

The choice of the module is mainly determined by economic considerations. This does not mean that the cheapest configuration is always the best choice because the type of application is also very important. In fact the functionality of a module is determined by the type of application.

METHODOLOGY

The hollow fiber membranes were produced by a locally made spinnerette using a wet spinning method^[1]. The hollow fiber module consists of a large number of membranes assembled together in a module as shown schematically in Figure 3. The free ends of the fibers are potted with an epoxy resins.

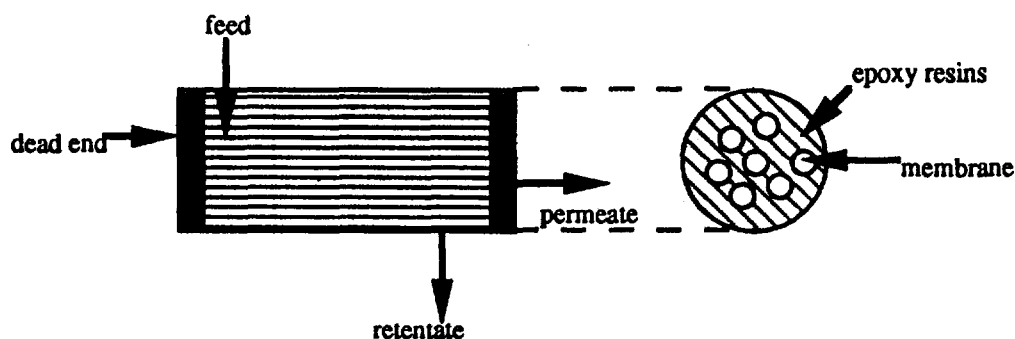


Figure 3 : Schematic drawing of a hollow fiber module , "outside-in" type

These modules were tested using the Membrane Gas Separation Pilot Plant using three pure gases namely; N₂, CO₂ and O₂. The effect of pressure on permeability was analyzed. The permeability and selectivity of the modules was calculated for different gases.

RESULTS AND DISCUSSION

The permeabilities of gases (N_2 , O_2 , CO_2) are shown in Table 1,2,3 respectively. The data was plotted and shown in Graph 1,2,3 for the dependent of permeability on pressure. Typically for all the three gases, it show a similar trend where its permeation rate increased with feed pressure. The ideal selectivity of O_2 and CO_2 to N_2 are given in Table 4 as a function of feed pressure. The permeability and selectivity for a commercial membrane module for N_2 , O_2 , CO_2 are shown in Table 5 ⁽³⁾. The results show that the performance of the locally made hollow fiber membrane module. Its performance was based on the permeation rate and the selectivity.

CONCLUSIONS

The locally made hollow fiber membrane module produce shows a good quality in terms of its permeation rate and selectivity. Based on the above results, this module is recommended in the removal of CO_2 from natural gas, air separation etc.

REFERENCES

1. Mulder, Marcel. (1991). Basic principles of membrane technology. Dordrecht - Netherlands : Kluwer Academic Publisher.
2. Design and Manufacture of Hollow Fiber Membranes for Gas Separation, H.Saidi, R.Abd. Aziz, H.Hassan, A.Ariffin, Seminar Penyelidikan dan Perundingan, Unit Penyelidikan dan Perundingan Universiti Teknologi Malaysia, Hotel Selesa, Pasir Gudang, Johor Bahru, 28 & 29 Ogos, 1993.
3. Arisaka et al., U.S Patent 4,127,625 Nov. 28, 1978.

Table 1 : Permeability of Hollow-Fiber Membrane Module for N₂

Pressure (psi)	Permeation rate (cm ³ /cm ³ .sec.cmHg)
5	0.0000056084
10	0.0000068866
15	0.0000080318
20	0.000008472
25	0.000008081
30	0.0000088081
35	0.0000086552
40	0.0000093756
45	0.0000100204
50	0.0000098111

Table 2 : Permeability of Hollow-Fiber Membrane Module for CO₂

Pressure (psi)	Permeation rate (cm ³ /cm ³ .sec.cmHg)
5	0.000005561
10	0.0000069772
15	0.0000068579
20	0.0000072784
25	0.0000077907
30	0.0000077226
35	0.0000086292
40	0.0000087573
45	0.0000087311
50	0.0000091055

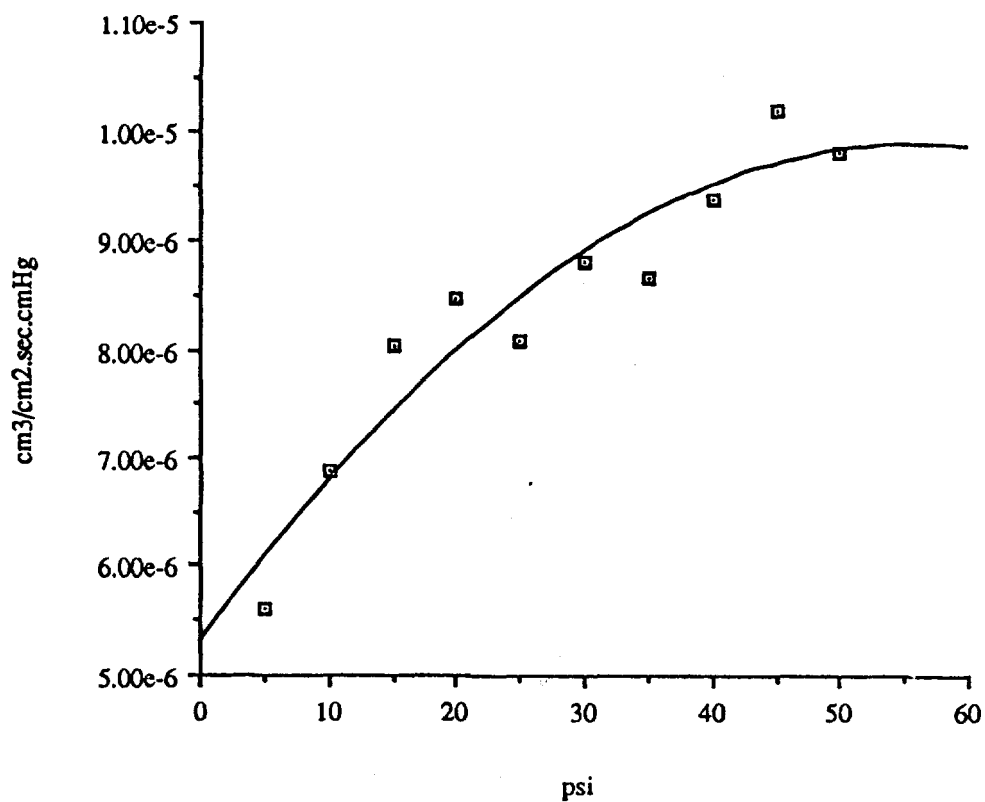
Table 3 : Permeability of Hollow-Fiber Membrane Module for O₂

Pressure (psi)	Permeation rate (cm ³ /cm ³ .sec.cmHg)
5	0.0000072781
10	0.0000074089
15	0.0000074715
20	0.0000073795
25	0.0000081148
30	0.0000072347
35	0.0000068746
40	0.0000083528
45	0.0000086696
50	0.0000092841

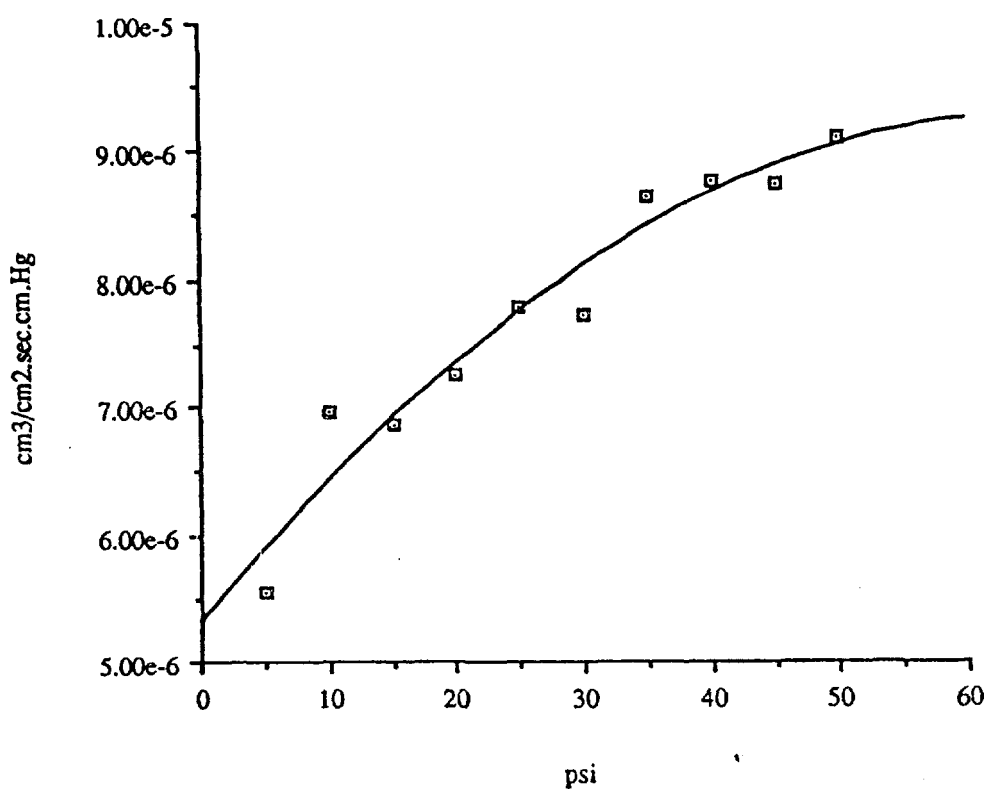
Table 4 : Selectivity for O₂/N₂ and CO₂/N₂

Pressure (psi)	Selectivity	
	O ₂ /N ₂	CO ₂ /N ₂
5	1.290	0.990
10	1.080	1.010
15	0.930	0.850
20	0.870	0.860
25	1.000	0.960
30	0.820	0.880
35	0.790	0.990
40	0.890	0.930
45	0.870	0.870
50	0.950	0.930

Graph 1 : Permeation rate vs pressure for N2



Graph 2 : Permeation rate for CO2



Graph 3 : Permeation rate vs pressure for O₂

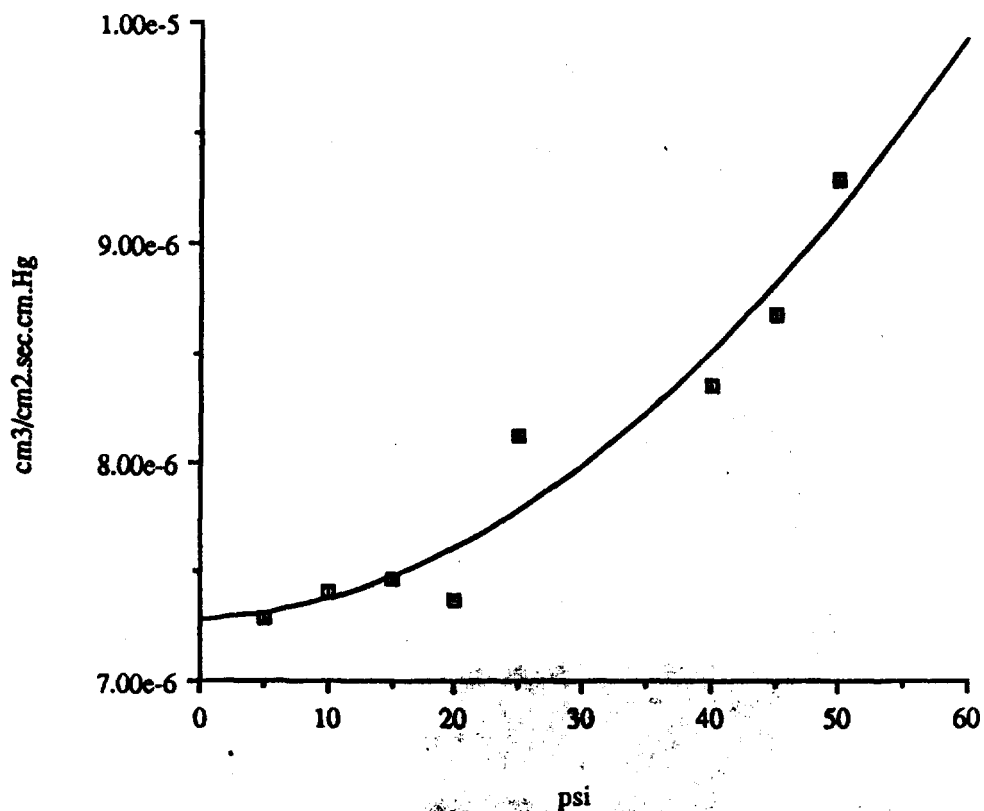


Table 5 : Permeation rate and selectivity(of each gas to N₂)for a commercially hollow fiber membrane module⁽³⁾.

Gas	Permeation rate cm ³ /cm ² .s.cmHg	Selectivity
H ₂	1.01 x 10 ⁻²	2.86
He	7.11 x 10 ⁻³	2.01
O ₂	3.17 x 10 ⁻³	0.899
Ar	2.73 x 10 ⁻³	0.776
CO ₂	2.62 x 10 ⁻³	0.743
CH ₄	3.64 x 10 ⁻³	1.03
C ₃ H ₆	2.61 x 10 ⁻³	0.739

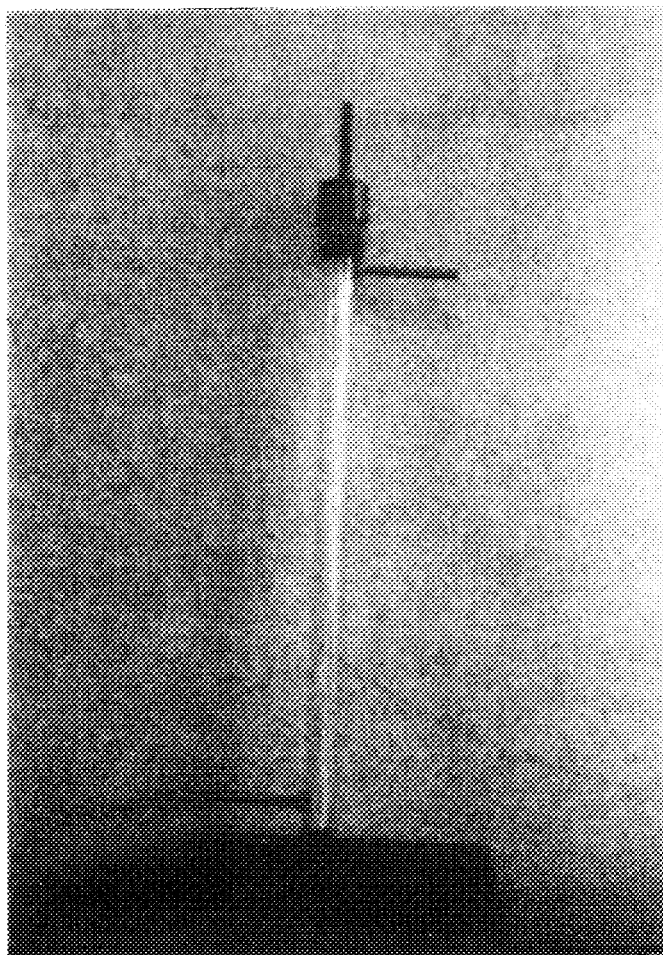


Plate 1 : Hollow Fiber Membrane Module

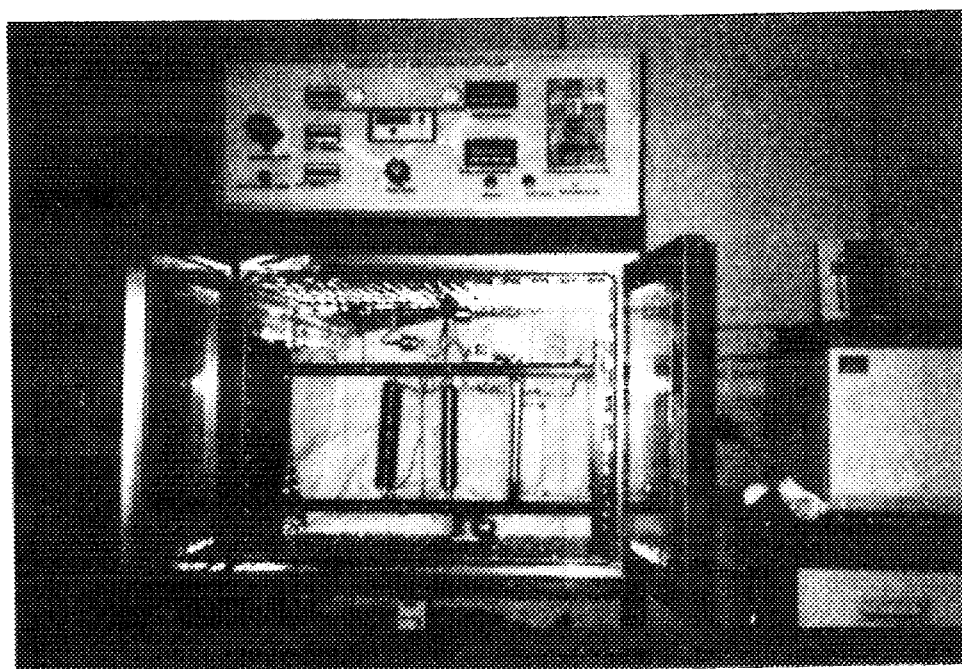


Plate 2 : Membrane Gas Separation Pilot Plant for Separation Process



A COMPACT TE-TE NITROGEN OSCILLATOR-AMPLIFIER LASER SYSTEM

Y. K. Yap, T. Y. Tou, and K. S. Low
Lasers and Optoelectronics Laboratory
Institute of Advanced Studies
University of Malaya
59100 Kuala Lumpur

ABSTRACT

High power Ultraviolet (UV) lasers with good beam quality are required in many scientific as well as industrial applications. The usual method to generate such laser output is using oscillator-amplifier laser system with multiple amplifiers. This paper discusses the design and operation of a compact TE-TE nitrogen oscillator-amplifier laser system. This system comprises of three electrodes with the center one being a wire mesh, and is housed inside a single laser chamber. Two sequential gaseous discharges are created between these electrodes, with the first one acting as the active medium for the oscillator and the other for the amplifier. An amplified laser pulse of 6ns FWHM with a peak power of about 280 kW is obtained. The beam divergences of this laser pulses are 1.0 mrad and 2.5 mrad respectively in the horizontal and vertical directions.

KEY WORDS:- Nitrogen lasers, oscillator-amplifier, wire mesh electrode, pulsed amplification.

INTRODUCTION

A nitrogen (N_2) laser provides useful and convenient source of coherent ultraviolet (UV) radiation at 337.1 nm for dye laser pumping and fluorescence studies¹. Transversely Excited Atmospheric pressure (TEA) nitrogen lasers produce subnanosecond pulses without complex modelocking schemes. On the other hand, low pressure Transverse Excited (TE) nitrogen lasers produce laser pulses of a few nanoseconds. Due to the very short population inversion time and the high gain of these lasers, usually a proper optical cavity may not be necessary. Oscillation takes place with multiple transverse modes having various propagation directions. Thus, the output beam quality is always poor in spatial coherence and has very high divergence when compared with other pulse lasers such as the Ruby, Nd-YAG and CO_2 lasers. Such poor beam quality is inadequate for many applications such as in nonlinear optics and in high resolution spectroscopy.

Various methods of beam spatial quality control can be employed to reduce the beam divergence but introduce significant output energy reduction. In order to suppress these losses, these lasers may be operated with larger dimensions or at higher pumping powers. However, this will increase the divergence further. Pulsed amplification has been the most popular method to partially overcome this short coming².

In an oscillator-amplifier system, the pulse width, beam qualities are primarily determined by the oscillator, whereas pulse energy and power are determined by the amplifier. Thus, by operating a small scale oscillator and coupling with a relatively larger dimension amplifier, the same order of magnitude in energy output as the amplifier can be obtained in a beam of smaller beam divergence and narrower linewidth³. Optimum amplification is obtained when the peak of the oscillator optical pulse enters the amplifier just before the peak of the Amplified Spontaneous Emission (ASE) of the amplifier. Examples of single- and multi-pass oscillator- amplifier configurations are illustrated² in figure 1.

The early development of TE-TE N_2 oscillator-amplifier lasers^{4,5} usually utilized two or more individual laser systems. These arrangements for oscillator-amplifier, besides taking up space, also pose complications in optical alignment as well as temporal synchronization. As a result, it may be cumbersome to carry out applications using such N_2 oscillator- amplifier lasers. In this paper, a single chamber TE-TE N_2 oscillator-amplifier system will be discussed. Figure 2(a) shows the equivalent circuit for the laser system. Two discharges between the three electrodes are utilized as the active media for the oscillator and the amplifier. A capacitive voltage divider⁶ is applied across the two discharge gaps to control the formation time of the discharges. Instead of a C-C (Capacitor to Capacitor) circuit⁶, the storage capacitor bank is of the LC inversion type for lower operation voltages.

DESIGN AND OPERATION

The cross section of our single laser chamber for double laser discharges is shown in figure 2(b). The laser chamber consists of a rigid rectangular PVC frame work, which is sealed with rubber gaskets, by two brass plates on the top and the bottom. Two optical apertures are provided at the back and the front walls of the chamber which are non-parallel such that their quartz windows are inclined at an angle of 5° to the normal of the optical axes. These inclinations are meant to eliminate⁴ undesired optical feedback of the ASE. These two apertures are sufficiently large to accommodate both the laser outputs from the upper (amplifier) and the lower (oscillator) channels. The top and bottom electrodes, of rounded brass bars of 50 cm long, become the cathode and anode of the laser system respectively. These electrodes are rounded to form a curvature of about 2 cm radius. Instead of a solid electrode⁶, a wire mesh is used as the center electrode, to improve the compactness of the design. The upper and lower laser channels have different gap separations of about 2.0 cm and 1.3 cm respectively.

A total of twenty six capacitors (C_B) are arranged in two rows on both sides of the anode. The wire mesh electrode is then fastened on top of these capacitors with screws. In order to flatten the wire mesh, it is connected to and stretched by 13 feedthroughs at the laser chamber. These feedthroughs also enable the measurement of the voltages across the laser channels. Another two rows of capacitors (C_T) are arranged on both sides of the cathode.

The LC inversion energy storage circuit consists of two capacitor banks C_1 and C_2 connected between three aluminium plates, as shown in the figure 2(b). The top and the bottom aluminium plates are directly connected to the brass plates of the laser chamber. The center aluminium plate, acting as the charge collector, is connected to the high voltage charger. The spark gap is mounted between the top and the center aluminium plates. The two capacitor banks C_1 and C_2 are mounted as close as possible to the laser chamber so that the laser performance may be improved.

Two different types of UV-preionisations are employed in this laser chamber. The first one is the self-synchronized UV- preionisation produced by two arrays of spark sources, which are formed between the upper two rows of capacitors (C_T) and the wire mesh electrode. The other one is the corona preionisation which is produced by two insulated corona wires on both sides of the anode. The wire mesh allows the UV radiations from both preionisers to illuminate both discharge media simultaneously. The upper discharge medium is thus preionised by both preionisers as well as the gas discharge of the lower channel.

The laser is usually operated at a N_2 pressure of 130 mbar with a charging voltage -20 kV; the capacitances used are: $C_1 = 15.6$ nF; $C_2 = 50$ nF; and $C_A = C_B = 18.2$ nF. When the switching spark gap is closed, the voltage (V_1) of C_1 will reverse its polarity. The potential difference (V_2) between the two solid electrodes will then increase until the lower laser channel (oscillator) breaks down ahead of the upper laser channel (amplifier).

RESULTS AND DISCUSSION

The experimental setup for pulse amplification is shown schematically in figure 3. A pair of rectangular slits are placed on both ends of the chamber, to suppress the undesirable oscillation modes, as shown in the figure. The temporal synchronization between the oscillator laser pulse and the peak of the amplifier gain is guided by the time delay between the optical pulses of the oscillator and the amplifier. This is done by adjusting the optical delay path and fine tuned by the positions of mirrors M_4 and M_5 , until a maximum laser output from the amplifier is obtained.

The experimental and theoretical⁷ relationship for I/O energy densities at 130 mbar of operating pressure is shown in figure 4. The maximum amplified output energy through this channel is 1.7 mJ, with FWHM of 6 ns (= 280 kW). The final output beam profile is then determined by scanning its cross section with a fast photodiode, which is covered by a pinhole of 0.2 mm in diameter. The profile scanning is carried out in directions parallel and perpendicular to the electrode flat surface, located at half the electrode distance or width respectively. A laser beam divergence of 1.0 mrad in the horizontal and 2.5 mrad in the vertical direction were deduced from the final output. The corresponding beam divergences for the ASE output are 7.0 and 8.0 mrad respectively.

CONCLUSION

The design, operation and performance of a single chamber TE-TE N_2 oscillator-amplifier laser were presented. An amplified laser output power of 280 kW was obtained. The amplified laser beam divergence has greatly reduced from 7 and 8 mrad to 1 and 2.5 mrad, respectively, in the horizontal and vertical directions.

FIGURE CAPTIONS

FIGURE 1. Examples of conventional single- and multi-pass oscillator-amplifier configurations².

FIGURE 2(a). Equivalent circuit for the single chamber TE-TE N₂ oscillator-amplifier laser system. C₁, C₂, C_T, C_B = capacitors, SG = spark gap, R = charging resistor, CP = corona preioniser, SP = spark preioniser, T = top electrode, B = bottom electrode and W = wire mesh electrode.

FIGURE 2(b). Cross section of the laser chamber. C₁, C₂, C_T, C_B = capacitor, SG = spark gap, CF = conducting feedthrough, PVC = PVC frame, SC = screw, CP = corona preioniser, SP = spark preioniser, T = top electrode, B = bottom electrode and W = wire mesh electrode.

FIGURE 3. Experimental setup for pulse amplification in the single chamber TE-TE N₂ oscillator-amplifier laser system. P = power meter, M1 to M5 = total reflector and F = neutral density filter.

FIGURE 4. Amplifier output versus oscillator input at N₂ pressure of 130 mbar.

REFERENCES :-

- ¹J.Hecht, Laser Focus World, 87, May 1993.
- ²J.F.Reintjes, Laser Handbook, edited by M.Bass and M.L.Stitch (North-Holland, 1985), vol.5, Chapter 1.
- ³W.Koechner, " Solid state laser engineering, " Springer Series in Optical Sciences, 2nd.ed., (Springer, Berlin 1988), Vol.1, Chapter 1-4.
- ⁴K.Kagawa, M.Tani, N.Shibata, R.Ueno, and M.Veda, J.Phys.E 15, 1192 (1982).
- ⁵K.Kagawa, I.Wamamoto, and M.Veda, J.Phys.E 21, 608 (1988).
- ⁶T.J.McKee, S.D.Hastie, and R.W.Weeks, J.Appl.Phys. 56, 2170 (1984).
- ⁷L.M.Frantz, and J.S.Nodvik, J.Appl.Phys. 34, 2346 (1963).

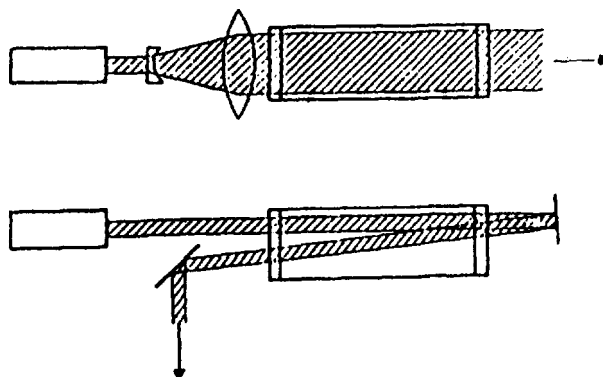


Fig. 1

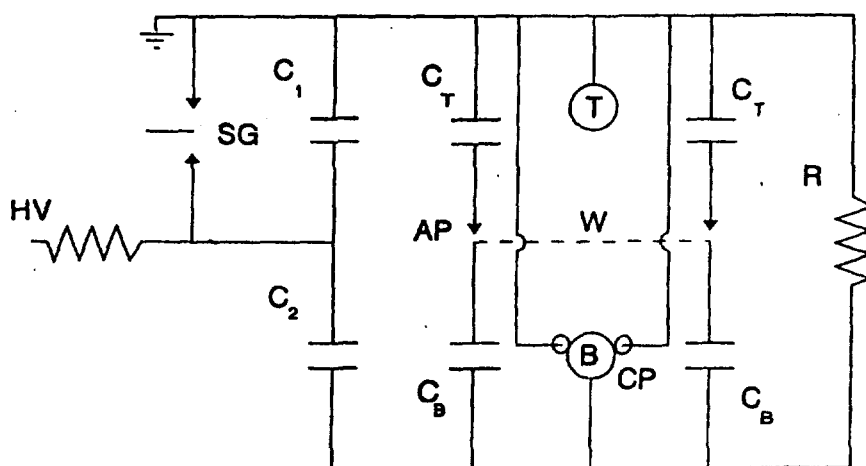


Fig. 2 (a)

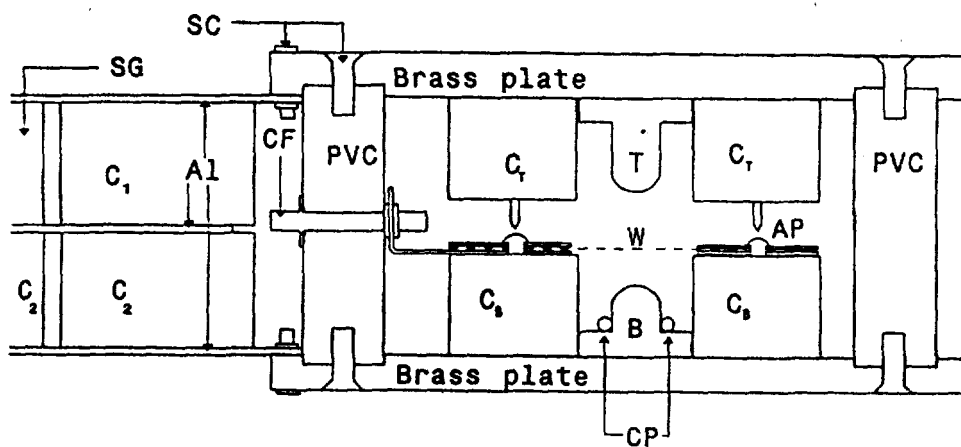


Fig. 2 (b)

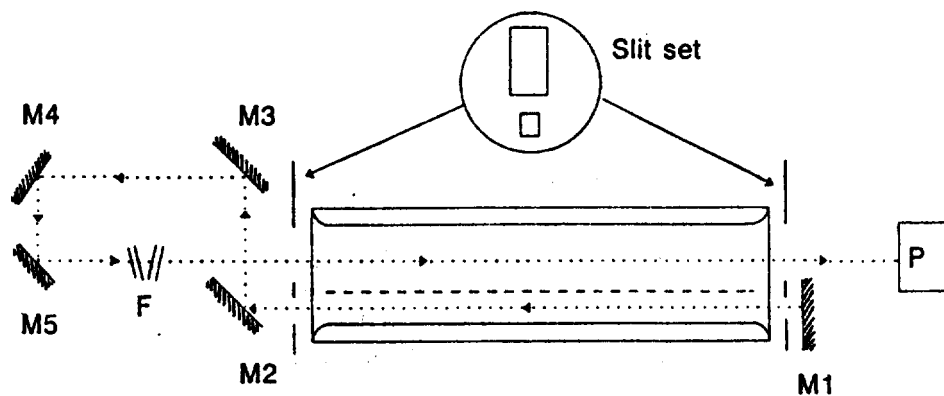


Fig.3

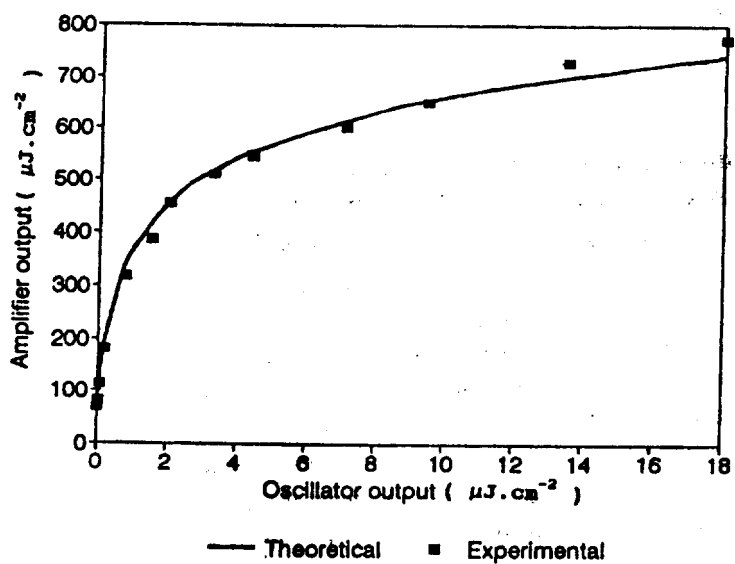


Fig.4

INTERMETALLICS FOR HIGH TEMPERATURE SERVICE

A.B. Ismail, A.K. Masrom, Z.A. Ahmad and S. Bhan
School of Materials and Mineral Resources Engineering
Universiti Sains Malaysia, Perak Branch Campus
31750 Tronoh, Perak

SUMMARY

Recent developments in structural intermetallics viz. nickel aluminides and titanium aluminides as new materials for high temperature service for high performance aeroengines are reviewed. Our own work on synthesis and characterization of these intermetallics is presented.

INTRODUCTION

Increasing demand for better performance materials from aeronautical industry has been the main driving force for development of advanced materials for high temperature service in the manufacture of safety - critical components.

Ni-base superalloys:

The nominal compositions of the Ni-based superalloys for turbine blades and vanes in aeroengines developed in the last 50 years is given in the Table 1. The tight adhering Cr_2O_3 surface oxide film formed during exposure at elevated temperature provides excellent oxidation resistance to these alloys. The fine dispersion of $\text{Ni}_3(\text{Al,Ti})$ precipitate called γ' and the low mismatch between γ matrix and γ' hinders grain coarsening retaining creep strength during high temperature service.

Even with complex multialloying and adopting casting route to avoid hot forging problem associated with some of the wrought alloys, operating temperature for existing Ni-base superalloys cannot be exceeded above $\sim 1250\text{K}$ for prolonged exposure in service.

Titanium alloys:

Titanium alloys are widely used for airframe and aeroengines due to relatively high melting point and low density. The alloys are classified in relation to their microstructure as α , near α , $\alpha + \beta$ or β alloys Table 2 lists the nominal composition of the alloys commonly used. Recent reviews on titanium alloys are available [2-6]. In spite of the efforts of the last forty years, the maximum temperature capability of the conventional titanium alloys has not gone up more than 875 K.

Intermetallics:

In view of the operating temperature limitation for conventional Ni-based superalloys and titanium alloys, interest has focused on intermetallics and structural ceramics. Intermetallics retain their ordered structure up to the melting point. There are about 300

binary intermetallic compounds with melting points higher than 1500°C. However for aerospace applications and in rotating parts, important parameters are high specific strength and high specific stiffness and therefore density enters the consideration. Fig. 1 (from Ref. 7) shows the relationship between melting temperature and specific gravity of the high T_m compounds with B2 (CsCl) or L1₀ (CuAu) type of crystal structures. Some intermetallics in Fig. 1 are designated with BCC (A2 type) structure perhaps due to difficulty in observing superlattice reflections and the structures may actually be CsCl (B2 type). Although AlRu, IrNb, RuSc and RuTa have high T_m and high toughness but could be considered for future specialized application only due to their high cost. The best combination of relatively high T_m and low density is obtainable in the intermetallics NiAl and TiAl. These two intermetallics have excellent properties, useful for high temperature service but have poor ductility leading to fabrication problems. Powder metallurgy route is preferable over casting as it results in homogeneous and fine grained microstructure.

We have followed the elemental powder metallurgy route for processing these intermetallics. The essential steps involved in the EPM method are shown in Figure 2. Elemental powders of Ni or Ti and Al with or without addition of organic additives and powders of other alloying elements are ball-milled for optimum time as the agglomerate particle size first increases and then decreases followed by increase again with ball-milling. Since Al is more ductile than Ti or Ni, Al grains get heavily deformed and elongated. In case of TiAl, the intermetallic is found to form partly after 50 hours of ball-milling (Fig. 3) while in case of NiAl, there is no formation of NiAl intermetallic with ball-milling leading only to line broadening with decrease in peak intensities. The decrease in intensity of reflection is much more in Al than in Ni (Fig. 4) as Al gets deformed more easily than Ni.

After ball-milling, the powder mixture is compacted and reaction sintered at 700 °C for one hour under argon atmosphere. The liquid phase sintering reaction is very fast compared to solid state sintering. In fact in case of NiAl, the exothermic reaction is vigorous and can partly melt the pellet unless ball-milling has been done for sufficient time or some reaction diluent is added to control the reaction. We have observed that shape of the pellet is retained if ball-milling is carried out for 40 - 50 hours (ball to powder weight ratio 10:1) and liquid phase sintering is done at 690 or 700 °C. Homogenization of the reaction sintered pellets at 1000 °C takes about 4 hours.

The intermetallics have poor ductibility at low temperatures and addition of small amount of boron results in fine grained structure with improvement in ductility [8]. We have found that there is an optimum amount of boron addition that refines the grain structure. Fig. 5 shows the effect of boron addition to NiAl intermetallic whereas 0.1 wt % B is found optimum. Larger addition of boron results in coarse structure [9].

It is observed that boron addition results in grain refinement of intermetallics with B2 structure much more than the intermetallics with L1₀ structure. Similar results are observed by Fleischer [7] in the four intermetallics with high melting points and which

are tough at room temperature (Fig. 6). Composition variation within the homogeneity range of the intermetallics also effects specific stress and strain under compression.

CONCLUSIONS

A wide variety of new materials is being developed for high temperature use and the intermetallics both in monolithic and composite forms are attracting increasing attention. However a lot of work is required not only in upgrading the processing but also in investigating fatigue and stability problems.

ACKNOWLEDGEMENT:

Authors acknowledge the research grant provided by the Universiti Sains Malaysia that has resulted in this acticle. Authors would also like to thank Mr. Chan Yen Kok and Mr. Chee Chee Meng for their help in the research project. Authors are also grateful to the Dean of the School of Materials and Mineral Resoucers Engineering, Universiti Sains Malaysia for his encouragement in the research work.

REFERENCES

1. B. Wilshire, Proc. Int. Conference on Recent Advances in Materials and Mineral Resources edited by Azmi Rahmat *et. al.*, Univ. Sains Malaysia Publication 1994, P.1.
2. P.J. Bania, 'Beta Titanium Alloys in the 90's', Ed. D. Eylon, R.R. Boyer and D.A. Koss, TMS Pub., 1984, 3.
3. P.A. Blenkinsopp, "Titanium Science and Technology", Oberursel, Germany, 1985, 2322.
4. P.A. Blenkinsopp, 'Advanced Materials - New Processes and Reliability' Ed. T. Kishi, N. Takeda and S. Kagawa, SAMPE, Tokyo, 1993, 1861.
5. P.J. Bania, 'Advanced Materials - New Processes and Reliability, Ed. T. Kishi, N-Takeda and S. Kagawa, SAMPE, Tokyo, 1993, 1.
6. T. Nishimura, 'Advanced Materials - New Processes and Reliability, ' Ed. T. Kishi, N.Takeda and S.Kagawa, SAMPE, Tokyo, 1993, 1596.
7. R.L. Fleischer, Platinum Metals Rev. 36(3), 1992, 138.
8. K. Akoi and I. Izumi, Nippon Kimzoku Gakkaishi 93, 1979, 1190.
9. A.B. Ismail, A.K. Masrom, Z.A. Ahmad and S. Bhan. Proc. Int. Comf. on Recent Advances in Materials and Mineral Resources.Ed. Azmi Rahmat *et. al.*, USM Publication 1994, 21.

Table 1: Compositions (nominal) of Ni-base superalloys for turbine blades and vanes in aeroengines (Ref. 1)

Alloy	Elements (wt%)									
	C	Cr	Co	Mo	V	Al	Ti	W	others	wrought/ cast
Nimonic 80A	0.07	19.5	-	-	-	1.4	2.4	-	-	wrought
Nimonic 90	0.08	19.5	17	-	-	1.4	2.4	-	-	wrought
Nimonic 105	0.13	15.0	20	5.0	-	1.3	4.7	-	-	wrought
Nimonic 115	0.15	14.5	13	3.3	-	5.0	3.8	-	-	wrought
IN-100	0.18	10.0	15	3.0	2.0	5.5	4.7	-	-	cast
MarM-002*	0.15	9.0	10	-	-	5.5	1.5	10.0	2.5Ta, 1.5Hf	cast

(Rest is nickel in composition).

* Maximum operating temperature 1250K for MarM-002

Table 2: Compositions (nominal) for conventional Ti-alloys for airframe and aeroengine applications (Ref. 1)

Alloy	Elements (wt%)							
	Al	V	Sn	Mo	Zr	Si	Nb	others
Ti-6-4	6.0	4.0	-	-	-	-	-	-
Ti-6-2-4-2	6.0	-	2.0	2.0	4.0	-	-	-
IMI315	2.0	-	-	-	-	-	-	2.0Mn
IMI550	4.0	-	2.0	4.0	-	0.5	-	-
IMI679	2.25	-	11.0	1.0	5.0	0.25	-	-
IMI685	6.0	-	-	0.5	5.0	0.25	-	-
IMI829	5.5	-	3.5	0.25	3.0	0.3	1.0	-
IMI834	5.8	-	4.0	0.5	3.5	0.35	0.7	0.06C

(Rest is titanium in composition)

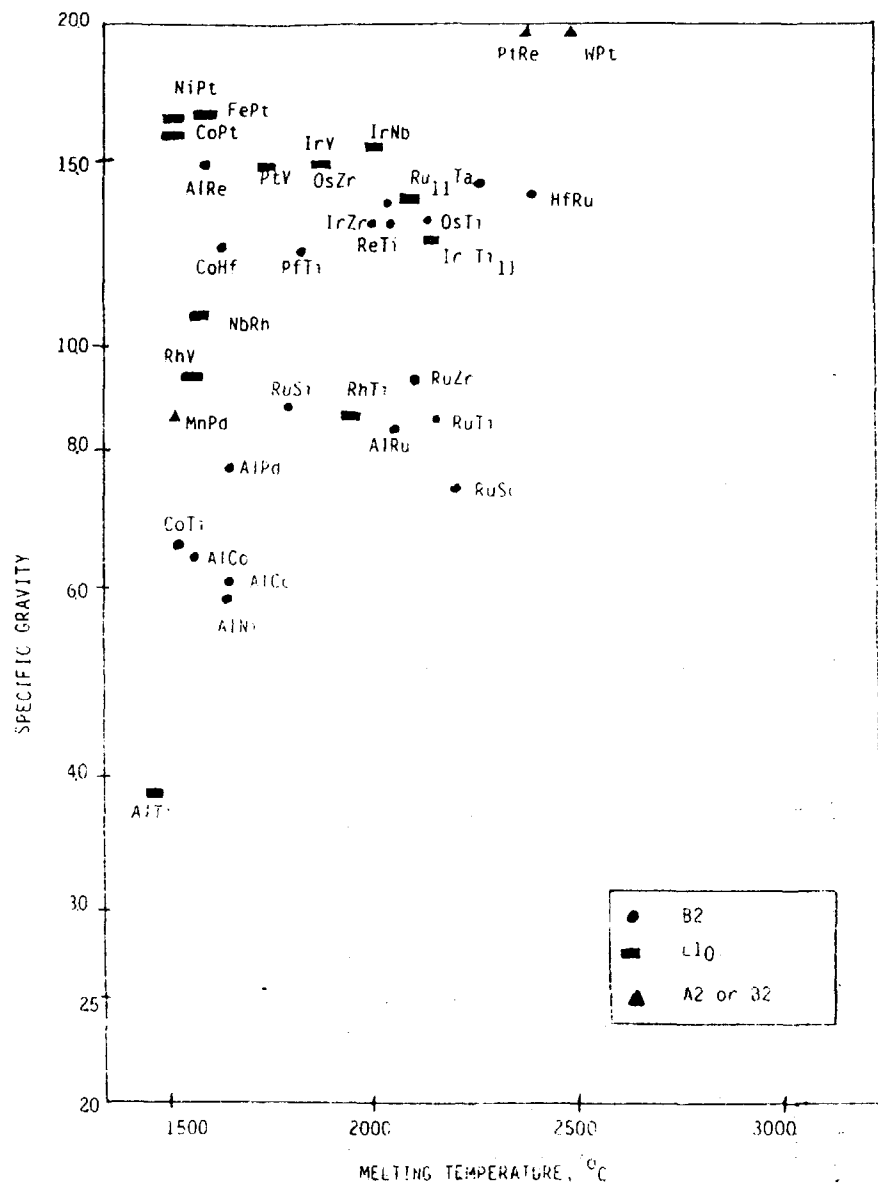


Fig. 1 Plot of the specific gravities as a function of the melting temperatures for selected intermetallics (After Ref. 7)

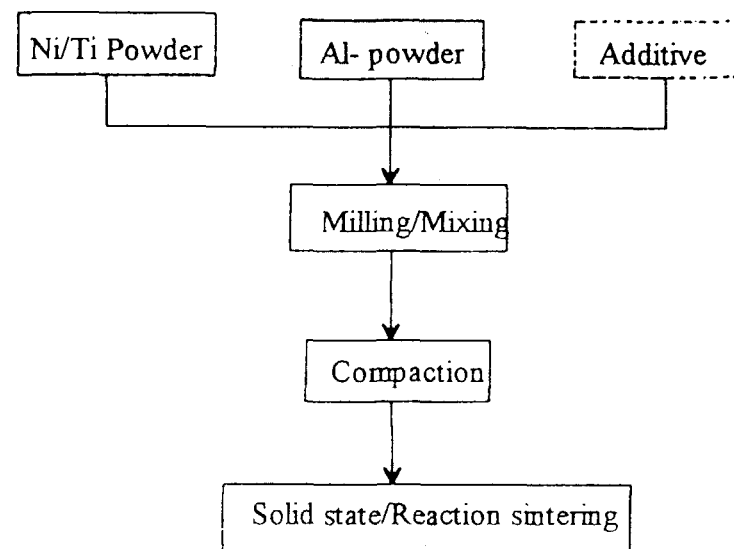


Figure 2 : Schematic flow diagram for EPM processing

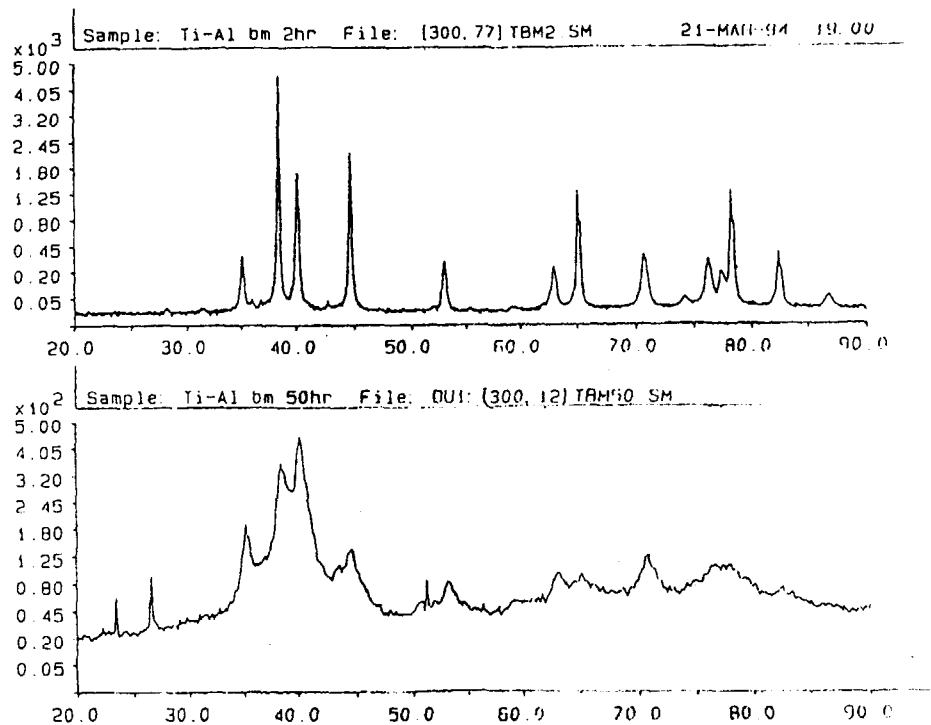


Figure 3 : A partly formed of intermetallic TiAl after 50 hours ball milling.

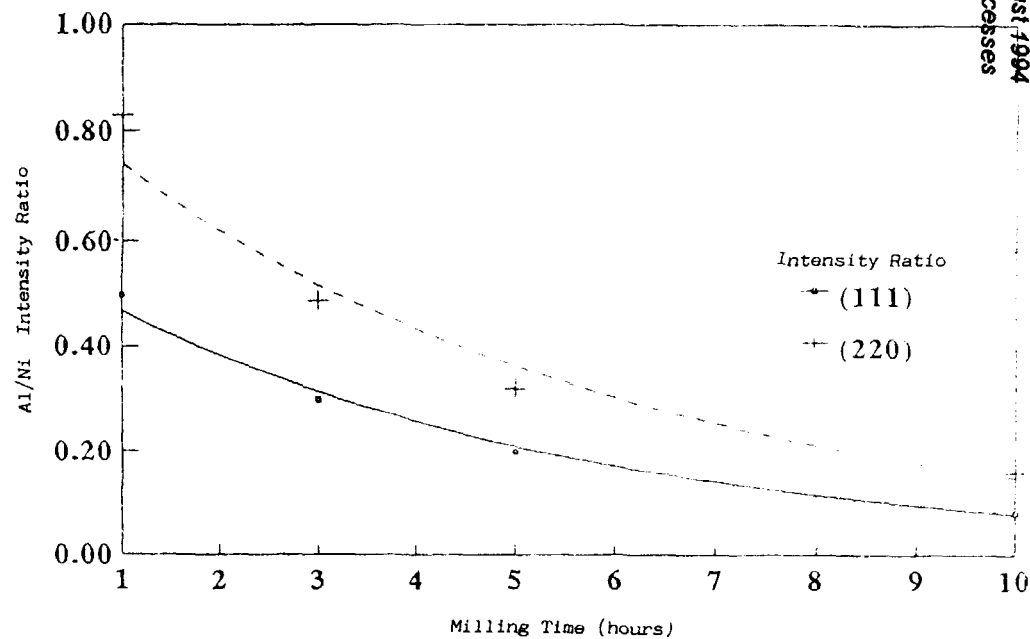
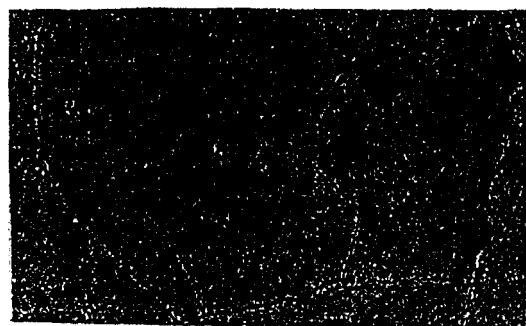


Fig. 4: Changes of peak intensity ratios with milling time for Al(111)/Ni(111) and Al(220)/Ni(220).



(a) Addition of 0.05% B



(b) Addition of 0.1% B

Figure 5 : A microstructure that shows the grain refinement due to the addition of boron to NiAl alloys.

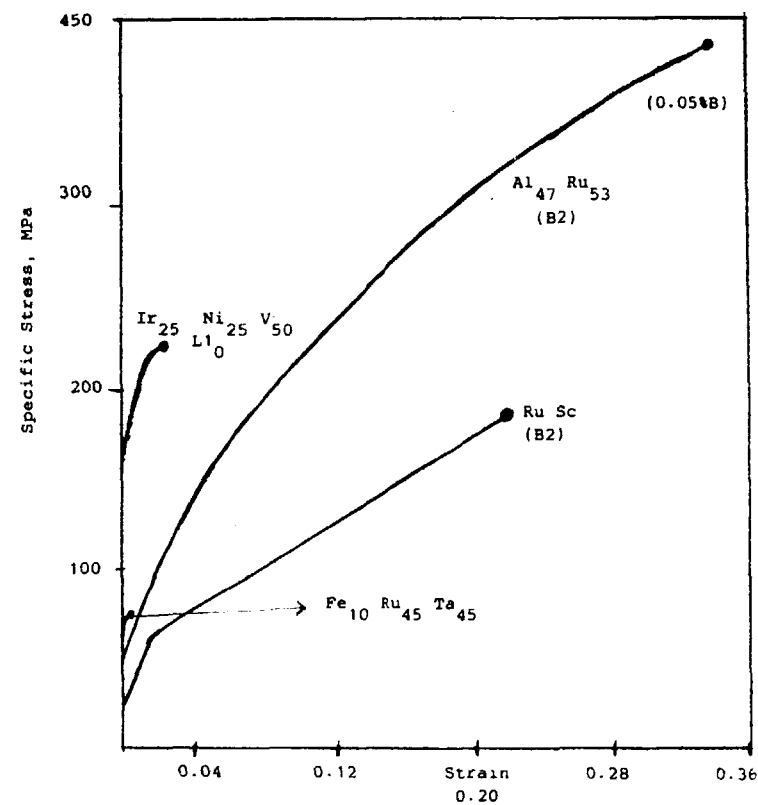


Fig. 6: Compressive specific stress - strain behaviour at room temperature of four tough intermetallics. (After Ref. 7).

LOCALLY PRODUCED BLENDED CEMENT SUITS FOR OILWELL CEMENTING JOB

Shahrin Shahrudin, Ariffin Samsuri
Petroleum Engineering Department
Faculty of Chemical and Natural Resources Engineering
Universiti Teknologi Malaysia
Jalan Semarak, 54100 Kuala Lumpur

ABSTRACT

With the same chemical compound as the imported class G cement used for the oil and gas wells cementing jobs; further suitability studies on the physical properties of pulverize fly ash cement were carried out to determine its real potential. Compressive strength, free water, thickening time and fluid loss tests were carried out according to API Specification 10. Samples were prepared with oil well additives and were conducted at simulated reservoir condition at 8000 feet. Comparison results with class G cement proved that blended cement suits to be used for oil well cementing job.

INTRODUCTION

In cementing an oil/gas well, the cement is placed from several hundred to several thousand feet below the surface of the earth and there are many factors over which the well cementer has no control i.e. temperature and pressure.¹ The cement is pumped through the casing and then back up through the small annular space between the walls of the hole and the casing. Therefore, the slurry mixed must remain as a fluid and pumpable until it is in its final resting place regardless of the temperatures and pressures to which it is subjected or to the time required.

At the setting depth, the cement slurry should set hard quickly and develop sufficient strength to withstand the tensile and compressive stresses in the well and should also form a permanent and enduring bond between the formation and the casing.² The set cement has to seal off the undesirable water and to protect the casing from external corrosion and provides the strength and the reinforcement to the casing.

In order to achieved these requirements, additives were used with the cement to produce a satisfactory slurry performance for a given well condition.

The purpose of this paper is to present the laboratory data on the comparison studies done on blended and G cement when they were mixed with different percentage of additives.

LABORATORY WORK

Locally produced pfa cement and imported class G cements were mixed with retarder and fluid loss additive and their physical properties which includes the , thickening time, fluid loss. free water and compressive strength were tested by closely followed the API Specification 10.³

THICKENING TIME TEST

In the thickening time test, prepared slurry is immediately poured into the consistometer container and while the slurry being stirred, the temperature and pressure is increased according to schedule no. 5, Specification Test For Classes G and H. Stiring is then continued until the slurry reaches a consistency of 100 Bc.³

FLUID LOSS TEST

Prepared slurry is immediately placed in the preheating atmospheric pressure consistometer and stirred for 20 minutes. The slurry is then poured into the preheated high pressure filter press and maintained at the final temperature of the schedule for the duration of the test.

FREE WATER TEST

Slurry is prepared according to section 5, and immediately place in the atmospheric pressure consistometer and stirred for 20 minutes. The slurry is then remixed for an additional 35 seconds and followed by pouring it into a 250 ml graduated cylinder. The mouth of the cylinder is sealed and then is place on a vibration free surface and allowed to stand undisturbed for 2 hours. The volume of water removed from the top of the slurry is recorded as the amount of free water content.

COMPRESSIVE STRENGTH TEST

The prepared slurry is immediately poured in the prepared molds in a layer equal to 1/2 of the mold depth and puddled for 25 times per specimen with puddling rod. After puddling the layer, the remaining slurry is stirred to eliminate segregation and the molds are filled to overflowing and puddle as before. The prepared molds are then placed in the high pressure and high temperature curing chamber and cured according to schedule 5g, Well Simulation Test Schedules for Curing Compressive Strength Specimens for a

period of 8 hours, 24 hours, 3 days and 7 days and the removed and crushed with the compressive strength machine.³

RESULTS AND DISCUSSIONS

THICKENING TIME ANALYSIS

Table 1 shows the results of the thickening time for both cements when mixed with different percentage of retarder and fluid loss additive and tested at 8000 feet and 52 degree celcius. It can be seen that there is an increased in pumping time as the amount of additive is added to the cement and class G cement proved to has better pumping time in all tests run as compared to pfa cement. In this situation the pozzolanic reactivity has caused the pfa cement to set a little faster but this cement is still can be used because of its compatibility with additives. Although the pumping time for pfa is less but the time clocked is reliable and can be considered suitable for well cementing job if five hours or less operating time is required. The difference in time setting of these cements can be seen in Figure 2 and 3.

FLUID LOSS ANALYSIS

Results of fluid loss when cement were mixed with different percentage of additives are shown in Table 2. The amount of fluid loss starts to decrease as the amount of mixing additive is increased and the trend is the same for both types of cement. However, the pfa cement gives better results in the amount of water loss to the formation. Besides the additives played their role in preventing fluid loss, the finely fly ash played its part in occupying micro pores and the pozzolanic reactivity provided by the ash has help in reducing the permeability of the cement and thus reduced the amount of water, as can be clearly seen in Figure 1.

FREE WATER ANALYSIS

The results of free water test between pfa and class G cement when added with different percentage of both additives are shown in Table 3. Generally, with the mixing proportion of additives, pfa cement proves to have less free water produced compared to the class G cement until when the mixing of fluid loss additive comes to 1.5 % and 2 %, whereby there is no free water for both cement. At these level, both cement were not set. The fly ash content in pfa cement delayed the reaction of cement with water by filling the pores between the cement grains and thus traps some of the water and further more some of the water is consume by the fly ash to disintegrate and react with calcium hydroxide and produced cementitious material and make the cement to set with less free water.

COMPRESSIVE STRENGTH ANALYSIS

Results of compressive strength cured at different period for each type of cement plus retarder and fluid loss additive are shown in Table 4 . With retarder, both types of cement does not set at 8 hours curing period and data were only obtained after 24 hours of curing period. However, with fluid loss additive only class G cement does not set at 8 hours curing period. In all tests run, the pfa cement gives a better strength development results as compared to class G cement. Besides the delaying effect of cement to set cause by the additives, the slow pozzolanic activities which took place between the calcium hydroxide that is the product of cement hydration has helped in developing the extra gel of tricalcium silicate hydrate which occupied the pores and contribute to the strength development of the cement. The profile of these development is shown in Figure 4 and 5.

CONCLUSION

Pfa cement proved to be better than class G cement in terms of fluid loss, free water and compressive strength but not in the thickening time aspect. The results also proved that pfa cement is compatible to be used with the existing oilwell cement additives. In general, pfa cement is suitable for a cementing job if five hours or less working time is required.

REFERENCE

1. R. Floyd Farris, A Practical Evaluation of Cement For Oil wells, Drilling and Production Technology, Volume 18, pg283-292.
2. John Bensted, Cement With a Specific Application - Oilwell Cements, World Cement March 1987, pg 72-79.
- 3 . API Specification 10, July 1, 1990. Specification For Material and Testing For Well Cements. American Petroleum Institute, 1220 L Street, Northwest, Washington DC, USA.

TABLE 1
Thickening Time of Cement Sample According to
Schedule No. 5 API Specification 10.

SAMPLE	THICKENING TIME					
	40 BC (MINIT)		70 BC (MINIT)		100 BC (MINIT)	
	G	PFA	G	PFA	G	PFA
G/M + 1.0 %R	430	275	NS	293	NS	308
G/M + 0.7 %R	362	181	371	196	384	220
G/M + 0.5 %R	272	162	287	183	297	204
G/M + 0.2 %R	143	96	161	127	170	152
G/M + 2.0 %FL	243	174	260	183	275	198
G/M + 1.5 %FL	215	160	230	177	248	194
G/M + 1.0 %FL	162	154	173	168	196	180
G/M + 0.5 %FL	112	89	142	114	169	144

TABLE 2
Fluid Loss of Sample Tested With 1000 psi Differential
Pressure at 52 deg. C With Different Percentages of
of Additives.

SAMPLE	GCEMENT (ml)/30 min.	PFA CEMENT (ml)/30 min.
G/M 0.2%R + 2%HL	76	72
G/M 0.5%R + 2%HL	81	76
G/M 0.7%R + 2%HL	89	81
G/M 1.0%R + 2%HL	98	87
G/M 0.2%R + 1.5%HL	164	120
G/M 0.5%R + 1.5%HL	172	136
G/M 0.7%R + 1.5%HL	181	157
G/M 1.0%R + 1.5%HL	200	171
G/M 0.2%R + 1% HL	344	312
G/M 0.5% R + 1% HL	352	325
G/M 0.7%R + 1% HL	367	338
G/M 1.0%R + 1% HL	282	356
G/M 0.2%R + 0.5%HL	636	610
G/M 0.5%R + 0.5%HL	642	619
G/M 0.7%R + 0.5%HL	668	631
G/M 1.0%R + 0.5%HL	686	648

TABLE 3

Free Water of Samples When Mixed With Different Percentage of Additives.

Sample	G CEMENT (ml)	Pfa CEMENT (ml)
G/M 0.2%R + 0.5%FL	1.3	1
G/M 0.5%R + 0.5%FL	0.85	0.8
G/M 0.7%R + 0.5%FL	0.7	0.6
G/M 1.0%R + 0.5%FL	0.35	0.2
G/M 0.2%R + 1.0%FL	0.25	0.2
G/M 0.5%R + 1.0%FL	0	0
G/M 0.7%R + 1.0%FL	0	0
G/M 1.0%R + 1.0%FL	0	0
G/M 0.2%R + 1.5%FL	0	0
G/M 0.5%R + 1.5%FL	0	0
G/M 0.7%R + 1.5%FL	0	0
G/M 1.0%R + 1.5%FL	0	0
G/M 0.2%R + 2.0%FL	0	0
G/M 0.5%R + 2.0%FL	0	0
G/M 0.7%R + 2.0%FL	0	0
G/M 1.0%R + 2.0%FL	0	0

TABLE 4

Compressive Strength of Samples When Mixed With Different Percentage of Additives and Tested at Simulated Reservoir Condition.

SAMPLE	COMPRESSIVE STRENGTH			
	G / PFA 8 HOURS (psi)	G/PFA 1 DAY (psi)	G/PFA 3 DAYS (psi)	G/PFA 7 DAYS (psi)
G/M + 0.2 %R	1750/1820	2500/2650	3100/3300	3200/3450
G/M + 0.5 %R	1550/1660	2320/2510	2950/3190	3150/3310
G/M + 0.7 %R	1010/1250	1850/2150	2450/2920	2980/3120
G/M + 1.0 %R	NS	980/1170	1260/1490	1410/1700
G/M + 0.5 %FL	1800/1920	2610/2800	3450/3780	3340/3610
G/M + 1.0 %FL	1720/1810	2500/2650	3290/3450	3160/3300
G/M + 1.5 %FL	1540/1660	2210/2360	3120/3280	3010/3180
G/M + 2.0 %FL	1310/1410	2020/2180	3050/3190	2910/3090

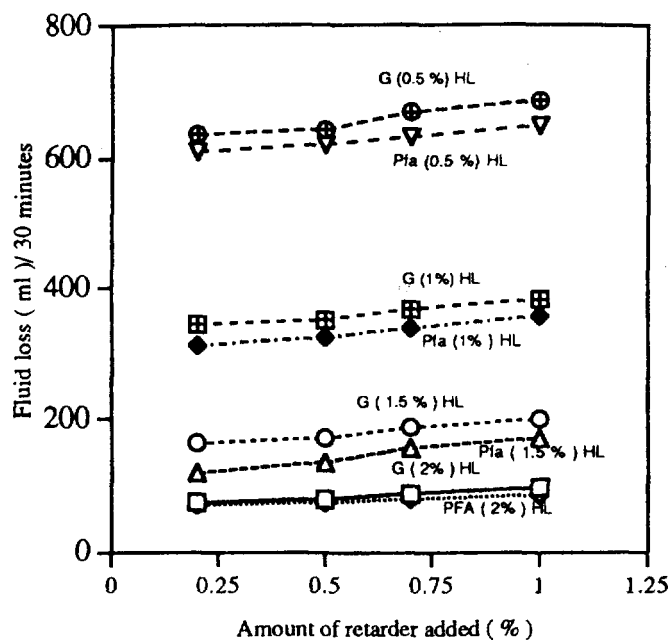


FIGURE 1. Fluid Loss Profile Tested With 1000 psi Differential Pressure at 52 deg. C With Different Percentage of Additive.

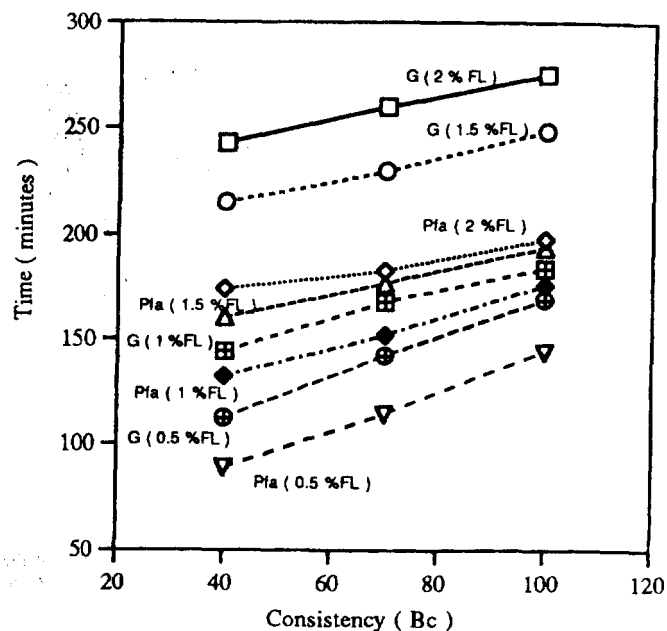


FIGURE 3. Thickening Time Profile When Cement Is Added With Different Percentage Of Fluid Loss Additive

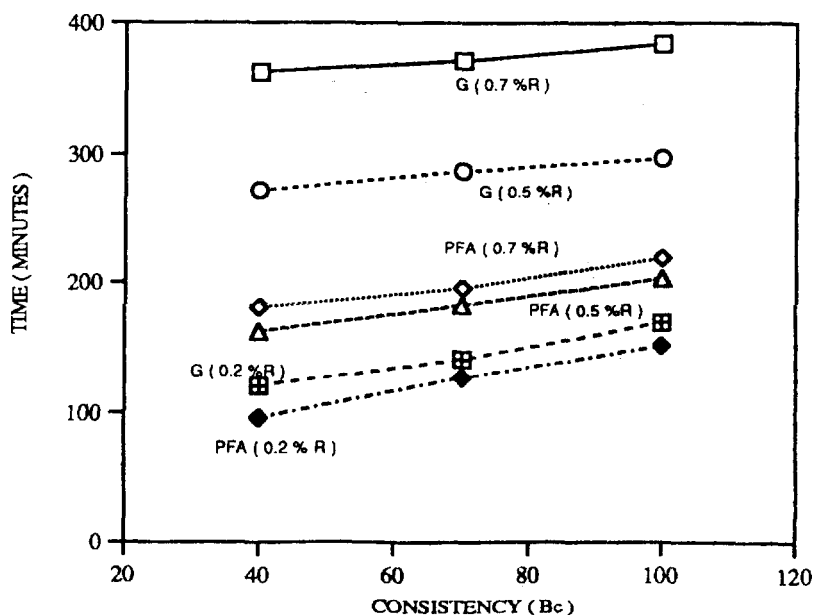


FIGURE 2. Thickening Time Profile When Cement Is Added With Different Percentage of Retarder.

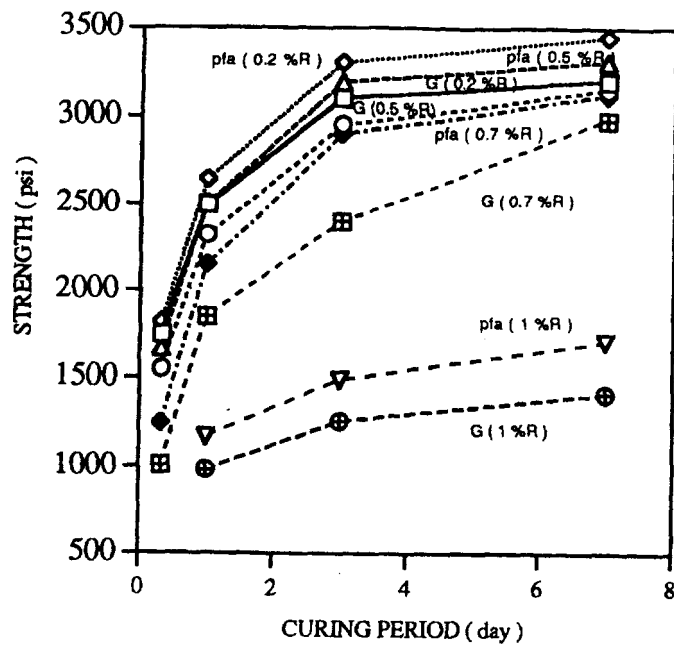


FIGURE 4. Strength Profile Of Sample When Added With Different Percentage Of Retarder At Simulated Reservoir Condition.

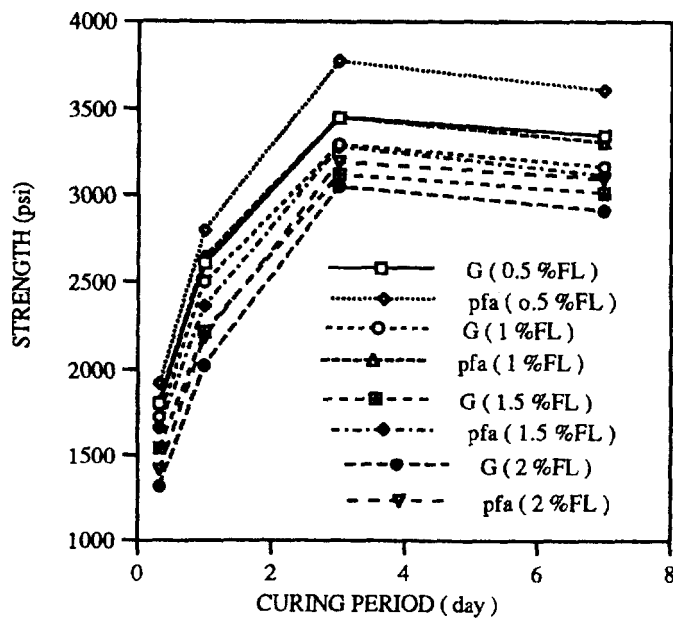


FIGURE 5. Strength Profile Of Sample When Added With Different Percentage Of Fluid Loss Additive And Tested At Simulated Reservoir Condition.

KESAN KOMPOSISI MAGNESIUM KE ATAS PEMAGNETAN DAN KERINTANGAN ELEKTRIK FERIT Mg-Zn

AHMAD NAZLIM YUSOFF DAN MUSTAFFA HJ. ABDULLAH

Jabatan Fizik
Universiti Kebangsaan Malaysia, 43600 Bangi
Selangor Darul Ehsan

ABSTRAK

Ferit $\text{Mg}_x\text{Zn}_{1-x}\text{Fe}_2\text{O}_4$ ($x = 0.4, 0.5, 0.6$ dan 0.7) disediakan dengan kaedah seramik piawai. Pembelauan sinar-X (XRD) mengesahkan sampel yang dihasilkan itu berstruktur spinel fasa tunggal dengan pemalar kekisi (a) dan ketumpatan sinar-X (ρ_{XRD}) yang mengurang dengan x . Suhu Neel (T_N) ditentukan daripada perubahan pemagnetan dengan suhu dan nilainya didapati meningkat dengan x . Suatu penurunan kerintangan dicerap pada lengkung kerintangan sebagai fungsi suhu untuk semua sampel. Anomali yang berlaku pada T_{ot} ini dibincangkan sebagai berpunca daripada sumbangan kekonduksian pada tapak tetrahedron (A). Momen magnet per molekul (n_B) pada 300 K bernilai maksimum manakala kerintangan arus terus (ρ) dan T_{ot} bernilai minimum bagi sampel dengan $x = 0.6$, yang mempunyai ketumpatan ujikaji (ρ_{uji}) tertinggi. Keputusan ini menunjukkan saling tindak tukar-ganti yang meningkat menghasilkan sampel yang lebih tumpat, seterusnya ρ lebih kecil. Saling tindak yang lebih kuat juga menyebabkan pengelibatan kekonduksian daripada ion-ion $\text{Fe}^{2+}/\text{Fe}^{3+}$ pada tapak A berlaku pada T_{ot} yang lebih rendah. Saling tindak tukar-ganti yang meningkat di antara ion-ion dalam fasa ferimagnet menerangkan tenaga pengaktifan fasa ferimagnet yang lebih rendah daripada tenaga pengaktifan fasa paramagnet. Mikrograf SEM menunjukkan keliangan bahan mengurang untuk bahan yang mempunyai pemagnetan yang tinggi.

ABSTRACT

$\text{Mg}_x\text{Zn}_{1-x}\text{Fe}_2\text{O}_4$ ferrites ($x = 0.4, 0.5, 0.6$ and 0.7) were prepared by conventional ceramic method. X-ray diffraction (XRD) confirmed the formation of a single phase spinel structure with lattice parameter (a) and X-rays density (ρ_{XRD}) decreased with the increase of x . Neel temperature (T_N) was determined from the variation of magnetization with temperature and was found to be increasing with x . A drop in the resistivity was observed in the resistivity versus temperature curve for all samples. This anomaly at T_{ot} is interpreted as due to a contribution of conductivity from the tetrahedral (A) sites. Magnetic moment per molecule (n_B) at 300 K is maximum while

d.c resistivity (ρ) and T_{Ot} are minimum for the sample with $x = 0.6$, which corresponds to the highest experimental density (ρ_{uji}). The results indicate that a stronger exchange interaction producing a sample with a higher density, thus ρ would be smaller. A stronger interaction is possibly the reason that the conductivity contributed by the Fe^{2+}/Fe^{3+} ions at the A sites started at a lower T_{Ot} . The existence of exchange interaction between the ions in the ferrimagnetic state explains the result that the activation energy in the ferrimagnetic state is lower than that in the paramagnetic state. SEM micrographs indicate that the porosity decreases for materials with higher magnetization.

PENDAHULUAN

Keputusan kajian sifat elektrik ferit $Mg_xZn_{0.3}Fe_{2.7-x}O_{4+\delta}$ ¹ dan sifat magnet $Cu_{1-x}Zn_xFe_2O_4$ ² dan $Cu_xZn_{1-x}Fe_2O_4$ ³ menunjukkan bahawa jenis dan nisbah di antara kation-kation yang terlibat serta taburannya di antara tapak-tapak tetrahedron (A) dan oktahedron (B) memainkan peranan yang penting dalam mencirikan sifat fizikal bahan ferit berstruktur spinel kubus misalnya; pemalar kekisi dan ketumpatan ^{1,4}, kerintangan elektrik ¹, momen magnet per molekul ³ dan suhu Neel ². Sifat-sifat tersebut juga menunjukkan kebergantungan terhadap suhu ⁴. Ferit polihabur berketumpatan tinggi mempunyai keliangan yang sedikit pada butiran dan sempadan butiran. Susunan atom atau molekul dalam struktur habur menjadi lebih padat dan rapat. Saling tindak magnet akan meningkat dan seterusnya meningkatkan nilai momen magnet per molekul bagi sampel. Ini berlaku pada ferit $Co_{1-x}Zn_xFe_2O_4$ ⁵. Akan tetapi kerintangan elektrik dijangka berkurang dengan pertambahan ketumpatan disebabkan saling tindak tukar-ganti atau proses lompatan elektron di antara ion-ion Fe^{2+} dan Fe^{3+} dapat berlaku dengan lebih mudah.

Dalam kajian ini beberapa sifat magnet, sifat elektrik dan sifat struktur ferit $Mg_xZn_{1-x}Fe_2O_4$ dengan nilai nominal $x = 0.4, 0.5, 0.6$ dan 0.7 diselidiki untuk mendapatkan perkaitan di antara sifat-sifat fizikal tersebut dan mengkaji kesan yang wujud apabila komposisi dan suhu diubah. Ini dilihat dari segi saling tindak tukar-ganti A-B dan mekanisme lompatan elektron yang berpunca daripada saling tindak di antara ion-ion magnet Fe^{2+} dan Fe^{3+} .

BAHAN DAN KAEDAH KAJIAN

Sistem ferit $Mg_xZn_{1-x}Fe_2O_4$ dengan nilai nominal $x = 0.4, 0.5, 0.6$ dan 0.7 disediakan dengan kaedah piawai seramik menggunakan serbuk oksida MgO , ZnO dan Fe_2O_3 berketulenan tinggi (5N). Campuran dalam kuantiti yang dikehendaki dikisar selama 2 jam sebelum diprasinter pada suhu $1000\text{ }^{\circ}\text{C}$ selama 6 jam. Sampel ferit yang separa terbentuk itu dibiarkan menyejuk secara perlahan-lahan ke suhu bilik dan dikisar secukupnya sekali lagi. Pelet bersaiz 2 mm tebal dan berdiameter 13 mm disediakan pada tekanan 50 MPa. Pelet dan sebahagian daripada serbuk kemudiannya disinter di dalam

relau selama 15 jam pada suhu 1150 °C sebelum dibiarkan menyejuk secara perlahan-lahan ke suhu bilik. Untuk mengesahkan sampel yang terbentuk berstruktur spinel fasa tunggal, difraktogram untuk kesemua sampel diperolehi daripada teknik pembelauan sinar-X (XRD) menggunakan difraktometer model Siemens-D5000 dengan sinar $\text{CuK}\alpha_1$ berkeamatan tinggi ($\lambda = 1.541 \text{ \AA}$). Sampel berbentuk serbuk digunakan untuk tujuan ini. Sudut pembelauan 2θ diambil dari 2° hingga 60°. Parameter-parameter yang didapati adalah pemalar kekisi (a) dan ketumpatan sinar-X (ρ_{XRD}). Ketumpatan ujikaji (ρ_{uji}) ditentukan secara berasingan dalam udara. Kajian morfologi ke atas sampel pelet dilakukan menggunakan mikroskop imbasan elektron (SEM) model Phillips XL-30 pada pembesaran 5000x. Sampel terlebih dahulu disalut dengan lapisan emas setebal 22 Å yang bertindak sebagai lapisan pengalir.

Kerintangan elektrik arus terus (ρ) diukur menggunakan kaedah penduga dua titik dengan kedua-dua permukaan sampel disalut dengan cat perak sebagai lapisan pengalir. Pengukuran dilakukan pada suhu bilik (300 K) dan seterusnya sehingga 673 K dengan kenaikan suhu sebanyak 2 K untuk setiap pengukuran. Sampel dibiarkan stabil selama 1 minit pada suatu suhu tertentu sebelum pengukuran dibuat. Data kerintangan sampel untuk proses penyejukan diambil dari suhu 673 K hingga 300 K semasa suhu diturunkan secara perlahan-lahan.

Pengukuran magnet dilakukan menggunakan magnetometer sampel bergetar (VSM) model LDJ-9600. Nilai pemagnetan terhadap medan magnet dan gelung histeris pada suhu bilik dengan medan maksimum 10 kOe diukur untuk kesemua sampel. Nilai pemagnetan pada suhu-suhu yang lebih tinggi diukur untuk menentukan suhu Neel (T_N) bagi setiap sampel.

KEPUTUSAN DAN PERBINCANGAN

Jadual I memberikan data-data yang diperolehi daripada pengukuran magnet, elektrik dan sifat struktur sampel. Difraktogram XRD mengesahkan kesemua sampel berstruktur spinel fasa tunggal dengan puncak-puncak keamatan terbelau daripada satah (111), (220), (311), (222), (400), (422) dan (511). Berat molekul (M), pemalar kekisi (a) dan ketumpatan sinar-X (ρ_{XRD}) didapati mengurang dengan nilai x (Rajah 1). Ini boleh diterangkan sebagai kesan daripada berat atom, jejari ion dan ketumpatan atom magnesium yang lebih kecil daripada berat atom, jejari ion dan ketumpatan atom zink menyebabkan a dan ρ_{XRD} mengurang tetapi dalam kadar yang sedikit dengan penggantian Zn^{2+} oleh Mg^{2+} .

Taburan ion bagi sistem yang dikaji dijangkakan sebagai $[\text{Zn}^{2+}_{1-x}\text{Mg}^{2+}_x\text{Fe}^{3+}_{x-\delta}\gamma\text{Fe}^{2+}_\gamma]^A[\text{Mg}^{2+}_{x-\delta}\text{Fe}^{3+}_{2-\gamma-(x-\delta)}\text{Fe}^{2+}_\gamma]^B\text{O}^{2-}_4$ dengan superskrip A dan B masing-masing mewakili tapak tetrahedron dan oktahedron. Ion Fe^{2+} adalah minoriti dan wujud dalam tindakbalas semasa proses pensinteran sampel. Akan tetapi kewujudannya pada tapak B

akan menyesarkan ion Mg^{2+} dengan kuantiti yang sama ke tapak A. Proses sesaran ion Mg^{2+} ke tapak A dilaporkan berlaku juga dalam MgFe_2O_4 ⁶ dengan 10% daripada ion Mg^{2+} didapati berada pada tapak A. Dalam sistem ini, hanya ion-ion Fe^{2+} dan Fe^{3+} sahaja yang mempunyai momen kerana ion-ion Mg^{2+} dan Zn^{2+} masing-masing tiada mempunyai momen magnet.

Rajah 2 menunjukkan perubahan pemagnetan spontan sampel terhadap suhu. Pemagnetan spontan untuk setiap sampel diterbitkan daripada lengkung pemagnetan isoterma. Didapati untuk kesemua sampel, pemagnetan spontan berkurang dengan peningkatan suhu. Ini disebabkan oleh momen-momen yang pada mulanya tersusun dalam medan magnet menerima tenaga termal yang mencukupi dan mula berkeadaan rawak apabila suhu semakin meningkat. Darjah kerawakan menjadi semakin ketara apabila suhu Neel (T_N) dihampiri menyebabkan pemagnetan spontan keseluruhan mengurangkan dan menjadi sifar pada T_N . Daripada kaedah ini dapat ditentukan T_N bagi setiap sampel. Didapati T_N meningkat dengan pertambahan kandungan magnesium dan mencapai nilai maksimum untuk $x = 0.7$ (Rajah 3(a)). Ini dapat diterangkan dengan merujuk kepada taburan kation; iaitu dengan bertambahnya nilai x , maka lebih banyak ion Fe^{3+} dan seterusnya ion Fe^{2+} berada pada tapak A sehingga menyebabkan saling tindak A-B semakin bertambah. Diketahui T_N sangat sensitif kepada perubahan komposisi dan taburan kation terutamanya kepada kepekatan ion Fe^{2+} pada tapak A ⁷, maka tenaga termal yang diperlukan untuk melenyapkan penyusunan momen-momen meningkat dengan bertambahnya kepekatan Mg^{2+} pada tapak B sehingga nilai T_N pun meningkat.

Rajah 3(b) dan 3(c) menunjukkan perubahan nilai pemagnetan spontan (M_s), momen magnet per molekul (n_B), kebolehtelapan awal (μ_i) dan daya koersif (H_c) terhadap kandungan magnesium. Didapati n_B dan M_s meningkat dengan kandungan magnesium dan masing-masing mencapai nilai maksimum pada $x = 0.6$ dan $x = 0.7$. Walaupun M_s bagi $x = 0.7$ adalah tinggi sedikit daripada $x = 0.6$, disebabkan sampel $x = 0.7$ mempunyai bilangan molekul yang lebih banyak dalam 1 gram sampel maka nilai n_B nya didapati kurang sedikit daripada nilai n_B untuk $x = 0.6$. Ini disokong oleh nilai berat molekul $x = 0.7$ (212.32) yang lebih kecil daripada berat molekul $x = 0.6$ (216.43). Nilai n_B maksimum untuk $x = 0.6$ adalah wajar dan bersetuju dengan keputusan yang didapati untuk sistem $\text{Cu}_x\text{Zn}_{1-x}\text{Fe}_2\text{O}_4$ ³. Diketahui, untuk ferit campuran yang mengandungi zink dengan formula $\text{Me}_x\text{Zn}_{1-x}\text{Fe}_2\text{O}_4$ (Me = logam dwivalensi), penambahan atom zink akan meningkatkan nilai n_B sampel sehingga mencapai nilai maksimum pada kandungan zink 40 % ⁸. Dijangkakan dengan penambahan Mg^{2+} seterusnya akan mengurangkan nilai n_B . Ini boleh diterangkan sebagai kewujudan momen-momen antiselari di antara Fe^{3+} pada tapak A dan B. Ini diperkukuhkan lagi dengan andaian Neel yang mengatakan bahawa momen pada tapak A akan tersusun secara antiselari dengan momen pada tapak B maka dengan bertambahnya kandungan Mg^{2+} akan mengakibatkan momen pada tapak B terlalu lemah untuk berinteraksi dengan momen pada tapak A seterusnya mengurangkan nilai n_B keseluruhan. Nilai H_c turun naik di sekitar 1.0 - 3.5 Oe menunjukkan ferit $\text{Mg}_x\text{Zn}_{1-x}\text{Fe}_2\text{O}_4$ bersifat lembut dengan luas gelung histeresis yang kecil menunjukkan kehilangan tenaga yang kecil. Kebolehtelapan awal (μ_i) pada 300 K bertambah dengan kandungan

magnesium. Ini menunjukkan saling tindak A-B yang meningkat dengan peningkatan kandungan magnesium.

Sampel dengan ketumpatan ujikaji (ρ_{uji}) yang maksimum memberikan nilai n_B yang tertinggi, iaitu pada $x = 0.6$. Sampel yang lebih tumpat mempunyai susunan butiran yang padat dan keliangan yang kurang, seterusnya meningkatkan saling tindak magnet di antara momen-momen pada tapak A dan B menyebabkan n_B meningkat. Sungguhpun ρ_{uji} untuk $x = 0.4$ sama dengan $x = 0.7$ akan tetapi M_s dan n_B untuk $x = 0.4$ adalah jauh lebih rendah. Ini disebabkan untuk $x = 0.4$, kepekatan Fe^{3+} yang lebih rendah pada tapak A mengurangkan saling tindak A-B, jadi nilai M_s dan n_B pun mengurang.

Rajah 3(d) juga menunjukkan perubahan kerintangan $Mg_xZn_{1-x}Fe_2O_4$ pada 300 K yang tidak linear dengan komposisi. Kerintangan meningkat daripada $x = 0.4$ hingga $x = 0.5$ sebelum jatuh sedikit pada $x = 0.6$ dan meningkat semula untuk $x = 0.7$. Kekonduksian bahan ferit dibincangkan sebagai berlakunya mekanisma lompatan elektron setempat di antara Fe^{2+} dan Fe^{3+} dan dominan pada tapak oktahedron. Mg^{2+} yang menggantikan Zn^{2+} memasuki tapak oktahedron lalu menyesarkan Fe^{3+} ke tapak A menyebabkan kurangnya saling tindak tukar-ganti di antara Fe^{2+} dan Fe^{3+} pada tapak oktahedron. Mg^{2+} yang mempunyai petala yang lengkap terisi bertindak sebagai pusat serakan⁹ dan menghalang pergerakan elektron seterusnya meningkatkan nilai kerintangan sampel. Nilai kerintangan jatuh sedikit untuk $x = 0.6$ disebabkan ketumpatannya yang agak tinggi berbanding dengan $x = 0.5$ membenarkan pergerakan cas yang lebih mudah di dalam bahan yang berkenaan. Saling tindak yang lebih kuat di antara ion-ion magnet Fe^{2+} dan Fe^{3+} juga menyebabkan proses lompatan lebih mudah berlaku.

Plot $\ln \rho$ melawan $10^3/T$ (Rajah 4) bagi proses pemanasan untuk kesemua sampel menunjukkan kerintangan yang berkurang dengan peningkatan suhu. Rajah 5 menunjukkan satu kitar pengukuran (pemanasan dan penyejukan) untuk sampel ferit $Mg_{0.7}Zn_{0.3}Fe_2O_4$ dan $Mg_{0.4}Zn_{0.6}Fe_2O_4$. Anomali pada $T = T_{Ot}$ dapat dicerap untuk semua pengukuran dan didapati berkurang untuk pengukuran semasa penyejukan semula. Kewujudan anomali dibincangkan sebagai meningkatnya proses lompatan elektron di antara Fe^{2+} dan Fe^{3+} pada T_{Ot} . Ini boleh terjadi sekiranya kepekatan Fe^{2+} pada tapak oktahedron meningkat. Akan tetapi Fe^{2+} yang cenderung untuk memasuki tapak tetrahedron semasa pensinteran menyebabkan hanya sedikit yang wujud pada tapak oktahedron. Ini sebaliknya menghasilkan mekanisma lompatan elektron pada tapak tetrahedron dan menyebabkan kerintangan jatuh pada T_{Ot} . Pada suhu tinggi Fe^{2+} meresap masuk ke tapak oktahedron menggantikan Fe^{3+} ke tapak tetrahedron untuk mencapai taburan kation yang seimbang. Apabila penyejukan semula dilakukan, disebabkan kuantiti Fe^{2+} pada tapak tetrahedron mengurang maka sumbangan kekonduksian pada tapak tetrahedron berkurang menyebabkan anomali berkurang. Ini menunjukkan nisbah Fe^{2+}/Fe^{3+} yang tidak malar dengan suhu.

Nilai T_{Ot} setiap sampel diambil pada titik apabila nilai kerintangan mulai jatuh secara mendadak. Lengkung T_{Ot} melawan kandungan magnesium (Rajah 3(a))

menunjukkan minimum pada $x = 0.6$ dan maksimum pada $x = 0.5$. Nilai T_{Ot} difikirkan sebagai bersandar kepada kadar kandungan ion-ion Fe^{2+}/Fe^{3+} dan saling tindak di antara ion-ion tersebut. Memandangkan ketumpatan Fe^{2+}/Fe^{3+} lebih tinggi pada komposisi $x = 0.6$, maka tenaga terma yang lebih rendah diperlukan untuk mengaktifkan proses lompatan elektron dan sebaliknya. Nilai T_{Ot} bagi $x = 0.5$ adalah lebih tinggi memandangkan darjah saling tindak di antara ion-ion magnetnya kurang sedikit berbanding dengan sampel $x = 0.6$. Jadual I menunjukkan tenaga pengaktifan fasa ferimagnet (E_f) yang lebih rendah daripada tenaga pengaktifan fasa paramagnet (E_p). Ini menerangkan saling tindak tukar-ganti lebih mudah berlaku dalam fasa ferimagnet. E_f dan E_p diukur di kawasan garislurus pada lengkung kerintangan. T_N daripada pemagnetan digunakan sebagai rujukan. T_N tidak dapat ditentukan daripada lengkung kerintangan. Ini diandaikan sebagai berpunca daripada gangguan anomali pada T_{Ot} dan kepekatan ion Fe^{2+} yang agak tinggi pada tapak oktahedron. Perkaitan di antara kepekatan ion Fe^{2+} yang tinggi pada tapak oktahedron dan anomali yang lenyap pada T_N dibincangkan berdasarkan saling tindak supertukar-ganti di antara ion-ion Fe^{2+} dan Fe^{3+} yang diganggu oleh kepekatan Fe^{2+} yang tinggi. Tukar-ganti elektron di antara Fe^{2+} dan Fe^{3+} berlaku melalui saling tindak supertukar-ganti dengan oksigen sebagai ion perantaraan. Rantau genting dikenalpasti sebagai rantau saling tindak jarak dekat di antara ion-ion magnet; maka saling tindak adalah lemah apabila kepekatan Fe^{2+} rendah menyebabkan tenaga pengaktifan lebih tinggi seterusnya menghasilkan anomali. Sebaliknya jika bahan ferit mengandungi kepekatan Fe^{2+} yang tinggi, saling tindak supertukar-ganti masih lagi kuat walaupun pada rantau genting menyebabkan tiada perubahan tenaga pengaktifan seterusnya tiada anomali dapat dicerap. Satu lagi kemungkinan adalah terbentuknya magnetit (Fe_3O_4) ¹⁰ dalam matriks bahan ferit tersebut dengan bertambahnya kepekatan Fe^{2+} . Ini akan menyebabkan perubahan tenaga pengaktifan dan seterusnya anomali tidak dapat dikesan sehinggalah pada suhu Neel bagi magnetit.

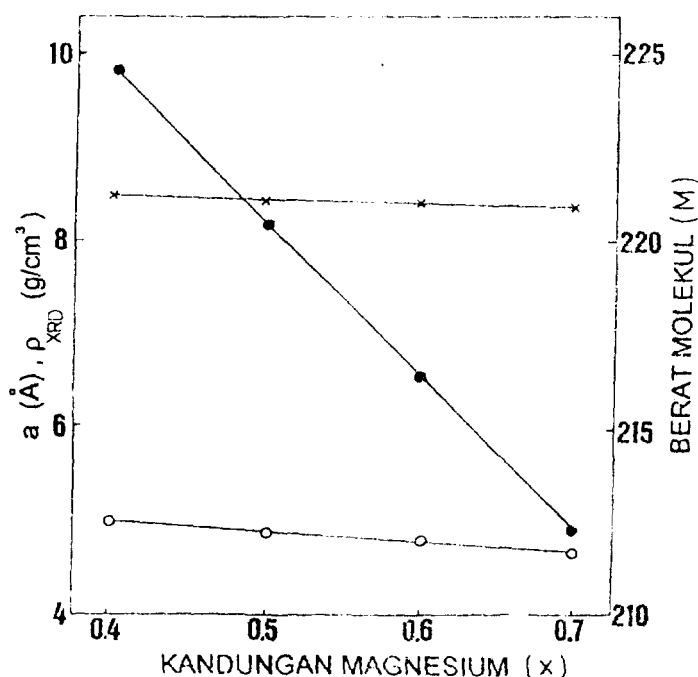
Gambarfoto SEM pada pembesaran 5000x untuk kesemua sampel (Rajah 6) menunjukkan kesan penambahan kandungan magnesium ke atas morfologi sampel. Jadual I memberikan nilai peratus keliangan sampel yang dikira berdasarkan Keliangan (%) = $[(\rho_{XRD} - \rho_{uji}) / \rho_{XRD}] \times 100\%$ dengan ρ_{XRD} dianggap sebagai ketumpatan sampel tanpa keliangan. Didapati sampel $x = 0.6$ mempunyai saiz butiran yang besar dan keliangan yang berkurangan dengan susunan butiran yang padat dan rapat. Keputusan ini menunjukkan saling tindak magnet yang kuat menghasilkan bahan magnet yang lebih tumpat dan keras.

PENGHARGAAN

Pengarang ingin mengucapkan ribuan terima kasih kepada En. Zahari bin Hussin dari Jabatan Geologi UKM dan En. Hing Hian Lian dari Unit Mikroskop Elektron UKM, di atas kerjasama mereka menjalankan pembelauan sinar-X dan imbasan elektron ke atas sampel. Projek ini di bawah pembiayaan Penyelidikan dan Pembangunan, IRPA 4-07-03-034, Kementerian Sains Teknologi dan Alam Sekitar, Malaysia.

RUJUKAN

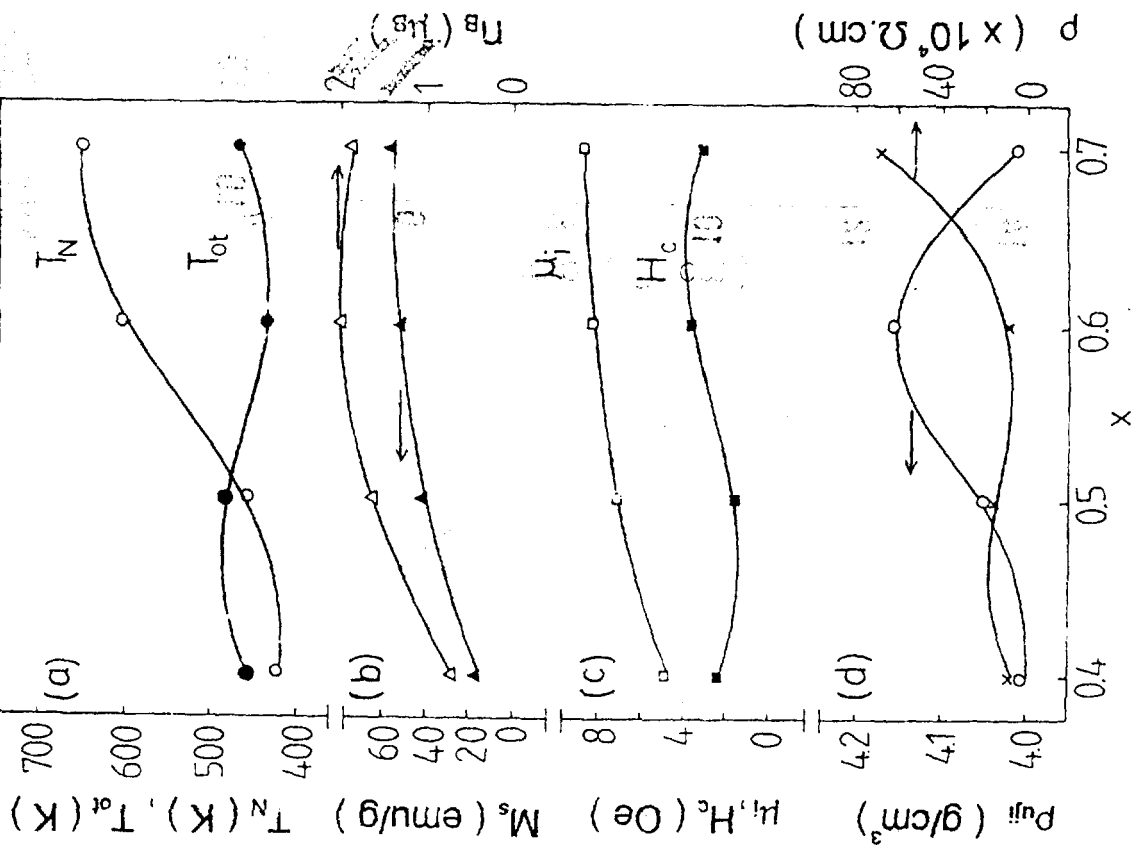
1. S. A. Mazen, A. E. Abd-el-Rahiem, J. Mater. Sci., **23**, 2917, (1988).
2. S. R. Sawant, D. S. Birajdar, S. S. Suryavanshi, A. M. Sankpal, B. L. Patil, S. A. Patil, R. N. Patil, Indian J. Pure Appl. Phys. **28**, 424, (1990).
3. S. R. Sawant, R. N. Patil, Sol. Stat. Commun. **40**, 391, (1981).
4. G. K. Joshi, A. Y. Khot, S. R. Sawant, J. Mater. Sci., **22**, 1694, (1987).
5. M. I. Abd-El-Ati, A. M. Kafafy, A. Tawfik, Act. Phys. Pol, No.9, **79**, 889, (1991).
6. B. D. Cullity, *Introduction to magnetic materials*, Addison-Wesley Publishing Company, London, ms. 189, (1972).
7. J. S. Thorp, M. E. Muhammad-Ahmad, C. Savage, J. Mat. Sci. Lett., **6**, 1341, (1987).
8. W. D. Kingery, H. K. Bowen, D. R. Uhlmann, *Introduction to ceramics*, 2nd. ed, John Wiley & Sons, New York, ms. 996, (1990).
9. S. S. Suryavanshi, R. S. Patil, S. A. Patil, S. R. Sawant, J. Less-Comm. Met., **168**, 169, (1991).
10. A. A. Gani, N. Z. Miryasov, Sov. Phys.- Solid State, No. 10, **13**, 2627, (1972).



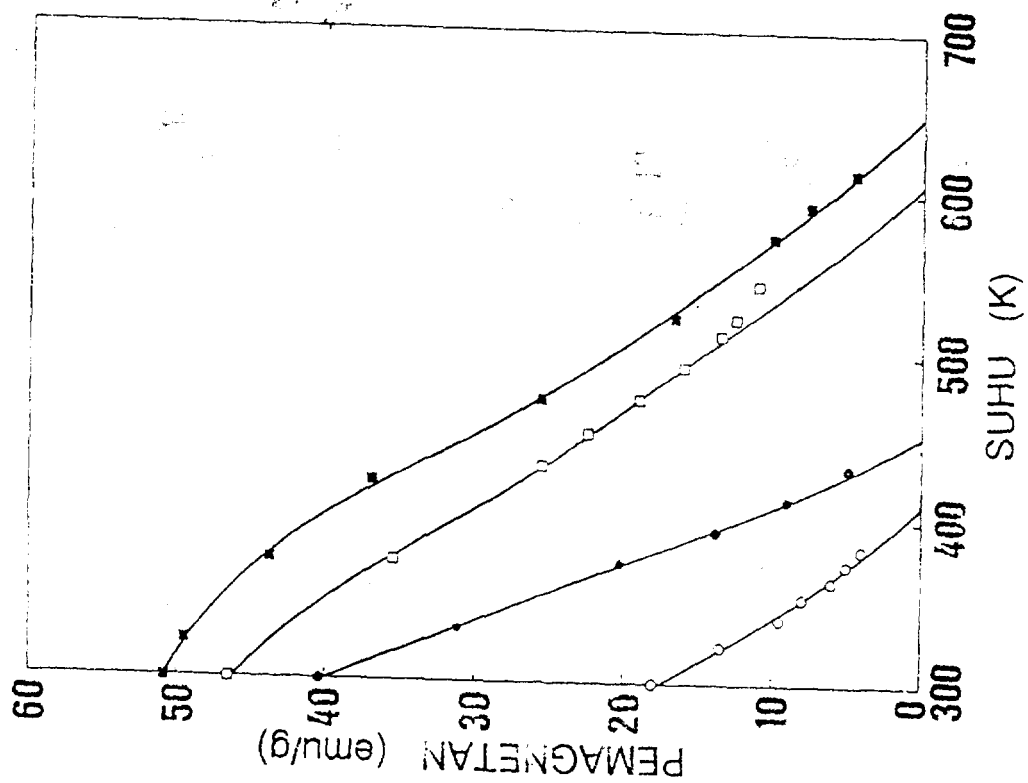
RAJAH 1. Perbandingan nilai pemalar kekisi (a) (x), ketumpatan sinar-X (ρ_{XRD}) (o) dan berat molekul (M) (•) untuk x = 0.4, 0.5, 0.6 dan 0.7.

JADUAL 1. Data-data yang diperolehi daripada pengukuran sifat magnet, sifat elektrik dan sifat struktur sampel.

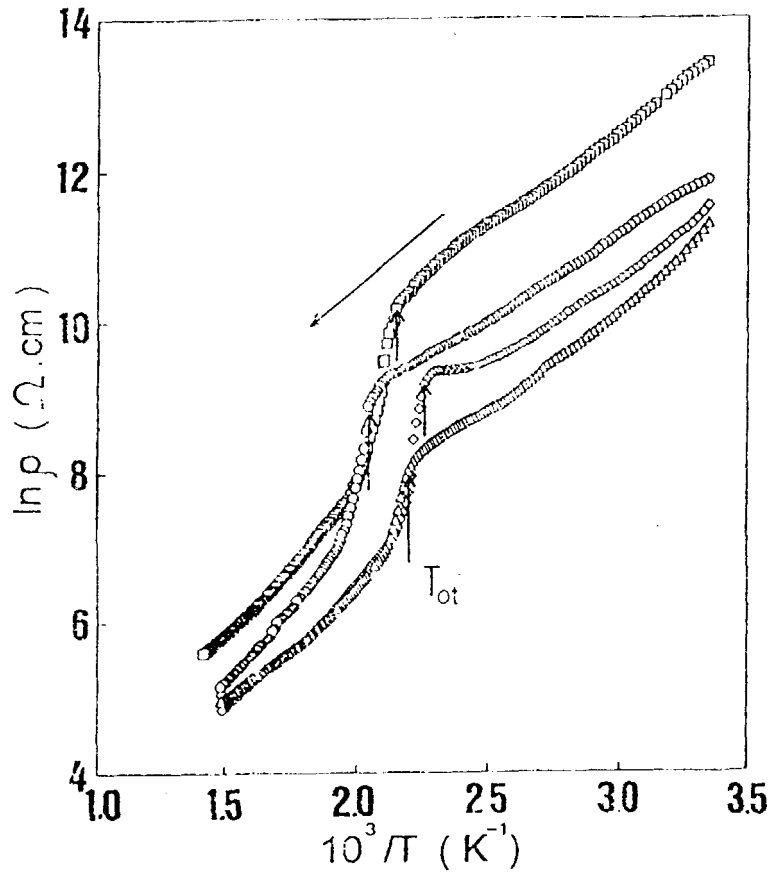
x (nominal)	0.4	0.5	0.6	0.7
Pemagnetan tepu, M_s (emu/g)	17.0	40.4	50.6	51.5
Momen magnet, n_B (μ_B)	0.68	1.60	1.96	1.95
Daya koersif, H_c (Oe)	2.4	1.5	3.5	3.1
Kebilehtelapan awal, μ_i	5	7	8	8
Suhu Neel, T_N (K)	419	456	603	650
Suhu T_{ot} (K)	454	490	445	465
E_f (eV)	0.19	0.19	0.23	0.23
E_p (eV)	0.34	0.24	0.25	0.31
Kerintangan elektrik 300 K, ρ ($\times 10^4 \Omega \cdot \text{cm}$)	8.1	14.1	10.1	66.9
Ketumpatan ujikaji, ρ_{uji} (g/cm^3)	4.01	4.04	4.15	4.01
Ketumpatan XRD, ρ_{XRD} (g/cm^3)	4.98	4.91	4.83	4.73
Keliangan (%)	19.5	17.7	14.1	15.2
Pemalar kekisi, a (\AA)	8.430	8.418	8.413	8.409
Berat molekul, M	224.64	220.53	216.43	212.32



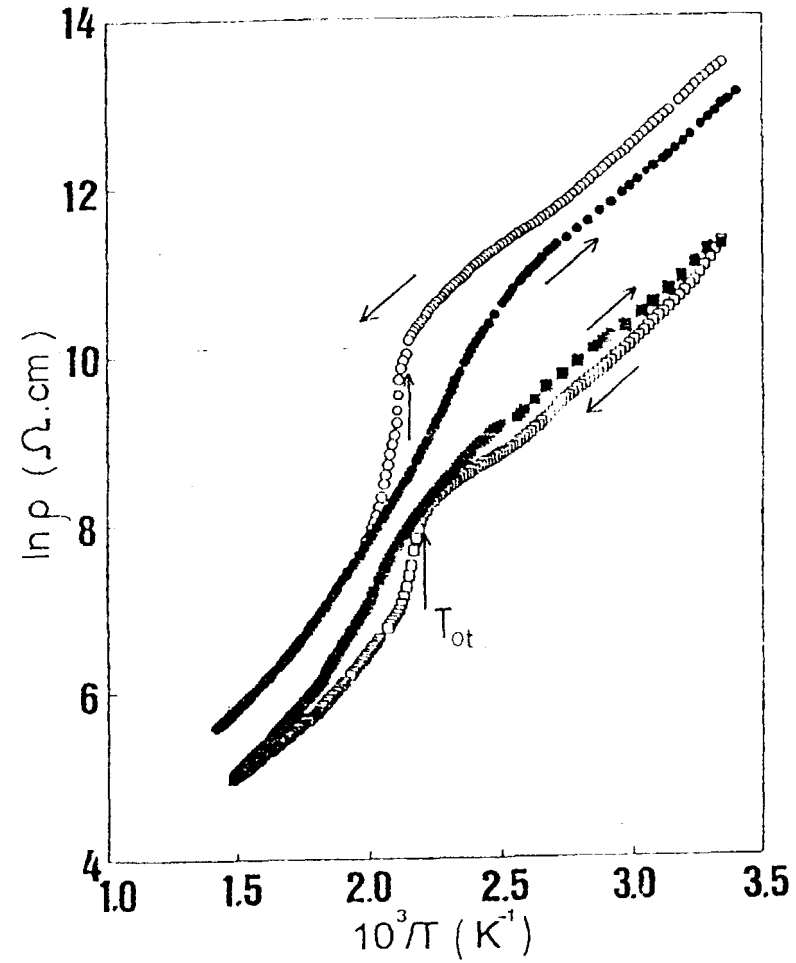
RAJAH 3. Perubahan suhu Neel, (T_N), T_{0t} , pemagnetan spontan, (M_s), momen magnet per molekul, (μ_B), pemagnetan awal, (μ_i), daya koersif, (H_c), ketumpatan ujikaji, (ρ_{0ij}) dan kerintangan elektrik a.t., (ρ) terhadap kandungan magnesium.



RAJAH 2. Lengkung pemagnetan melawan suhu untuk $x = 0.4$ (O), 0.5 (●), 0.6 (□) dan 0.7 (■).



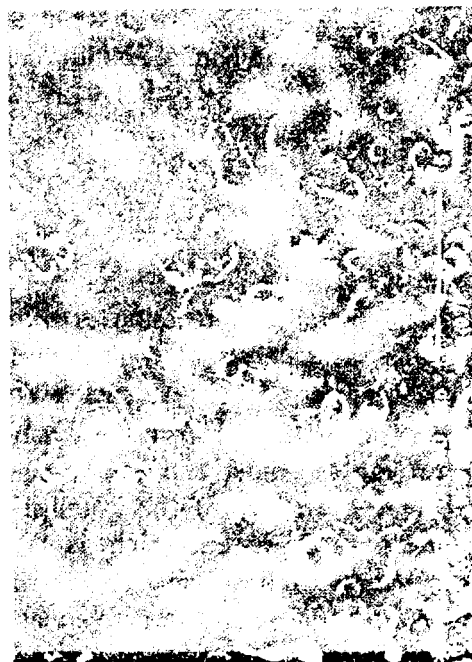
RAJAH 4 . Lengkung $\ln \rho$ melawan $10^3/T$ untuk $x = 0.4$ (Δ), 0.5 (\diamond), 0.6 (\circ) dan 0.7 (\square) menunjukkan T_{ot} untuk semua sampel. Pengukuran dibuat semasa pemanasan.



RAJAH 5 . Lengkung $\ln \rho$ melawan $10^3/T$ bagi sampel $x = 0.4$ (\circ) dan $x = 0.7$ (\square). Pengukuran semasa pemanasan dan penyejukan (dihatanikan) ditunjukkan.



x = 0.4



x = 0.7



x = 0.4



x = 0.5

RAJAH 6 . Gambarfoto SEM untuk x = 0.4, 0.5, 0.6 dan 0.7.



CATALYTIC METATHESIS OF 1-HEXENE BY Re_2O_7 IMPREGNATED ZEOLITE Y

Zainab Ramli and Halimaton Hamdan
 Jabatan Kimia, Fakulti Sains, Universiti Teknologi Malaysia,
 K.B. 791, 80990 Johor Bahru.

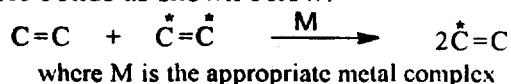
ABSTRACT

Successful metathesis reaction is promoted by the presence of homogeneous and heterogeneous catalyst of transition metals. For industrial purposes, heterogeneous catalyst is preferred because such system is convenient, economical, regenerable and can be easily separated from the reaction mixture. Re_2O_7 supported on γ -alumina has been proven the most active heterogeneous catalyst among other transition metals. However the activity of this catalyst is significant only when the concentration of rhenium is >18 wt%; which is economically unfavourable. Development of a heterogeneous catalyst using zeolite as the support for Re_2O_7 is necessary in order to study its potential as an alternative that is expected to be more superior to conventional alumina and silica-alumina supports. Zeolite Y, used in the study was modified by dealumination to form an ultrastable zeolite support of various acidity. Re_2O_7 -zeolite Y system is an active catalyst with $>90\%$ selectivity towards metathesis of 1-hexene, producing a maximum of 57.4% yield of 5-decene. Other factors such as reaction temperatures, types of solvent and wt% of rhenium loadings influence the activity of the catalytic system.

Keywords: Re_2O_7 , zeolite Y, metathesis, 1-hexene

INTRODUCTION

Metathesis of olefin is an organic reaction with many potential industrial applications; particularly in the polymer industry[1]. The term metathesis describes the interchanging of carbon atoms between a pair of double bonds as shown below:



The reaction proceeds only in the presence of a suitable transition metal compound-based catalyst and most often, in conjunction with co-catalysts as promoters.

Oxides of a number of transition elements deposited on materials with high surface areas; acting as support, have been proven to form active heterogeneous catalyst. Important examples of such catalysts are $\text{Re}_2\text{O}_7/\text{Al}_2\text{O}_3$, $\text{MoO}_3/\text{Al}_2\text{O}_3$ and $\text{WO}_3/\text{Al}_2\text{O}_3$. At room temperature and atmospheric pressure, the $\text{Re}_2\text{O}_7/\text{Al}_2\text{O}_3$ is found to be the most active and highly selective catalyst for olefin metathesis. However the high activity of such catalytic system occurs only with high concentration of Re loading. In contrast, the presence of silica in the alumina support increases the activity of the Re_2O_7 catalyst even with low loading compared to the corresponding Re_2O_7 on alumina[3,4]. Such increase in activity of Re_2O_7 supported on silica-alumina is due to the presence of Brönsted acidity of the support. Nevertheless, the selectivity for the primary product of the support is rather limited.

Zeolite or hydrated crystalline silica aluminate with framework structure, is a powerful catalyst in the cracking and hydrocracking of petrochemicals. The catalytic activity originates from the acidic properties generated within the zeolite lattice which can be modified and is expected to be a good support for Re_2O_7 [5]. Another advantage of using zeolite as the support is that the framework lattice consists of regular channels and pores of molecular dimensions which can act as sieves to the metathesis products.

Limited research on the use of zeolites as supports in metathesis reaction has been reported. A study on the metathesis of propene by using Mo supported on HNa-zeolite Y was reported by Komatsu[6]. Work reported by Hsu[7] on metathesis of propene on Re_2O_7 supported on zeolite KA, CaA and NaX showed low activity. These results demonstrated that the activity of Re_2O_7 catalyst for metathesis reaction strongly depends on the type and properties of the zeolite support used.

In this paper, we report on a study of the catalytic activity of rhenium oxide supported on modified zeolite Y towards metathesis of olefin. In our work, 1-hexene was chosen as the model reaction. The influence of other experimental parameters including temperature, wt% of rhenium loading and types of solvents on the properties of zeolite support in enhancing the catalytic activity for metathesis reaction was also studied.

MATERIAL AND METHODS

(i) Preparation of catalyst

Framework composition of the starting zeolite Y ($\text{Si}/\text{Al}=2.0$) was modified by hydrothermal dealumination. It was carried out by heating 60% NH_4^+ -exchanged Y at 500 °C in the presence of steam for 7 hours. The dealuminated zeolite Y sample was denoted as DY. The Re_2O_7 -DY catalysts loaded with 1, 3, 6 and 12 wt% Re were prepared by wet impregnation technique using calculated amount of aqueous ammonium perrhenate solution. The Re_2O_7 -DY catalysts are denoted as ReDY-1, ReDY-3, ReDY-6 and ReDY-12 in which the numbers refer to the wt% Re loading. A sample with 6 wt% Re_2O_7 loaded on γ -alumina (ReA-6) catalyst was also prepared as a comparison.

(ii) Metathesis of 1-hexene

The metathesis of 1-hexene was carried out in a Schlenck type reaction vessel, capped with silicone subaseal septum through which hypodermic syringe was inserted to permit the introduction of the reagents. The catalyst was first calcined in the stream of oxygen at 500 °C for 3 hours and was activated for another 2 hours in oxygen-free nitrogen at the same temperature. After cooling to room temperature, 0.4 g of the activated catalyst was transferred into the reaction vessel under the flow of nitrogen.

By using hypodermic syringe, about 2-3 ml of freshly distilled solvent was introduced into the vessel followed by the addition of 10 μl of tetramethyltin (TMT). The mixture was stirred for 5 minutes before introducing 1.4-2.0 ml of 1-hexene. For each reaction, the ratio of catalyst to 1-hexene (g/g) is 1:2.5 while the amount of co-catalyst and the volume of solvent were kept constant. Liquid product was periodically sampled out from the reaction mixture and analysed by gas chromatography.

The products were identified by using gas chromatography-mass spectrometers (GC-MS) detector. The calculation of the components was based on the integration of peak areas. Conversion (X) and selectivity (S) were based on the liquid phase and calculated as follows:

$$\text{Conversion (\%X)} = \frac{\sum[2(\text{olefin})]}{(1-\text{hexene}) + \sum[2(\text{olefin})]} \times 100$$

$$\text{Selectivity (\%S)} = \frac{\sum[2(5-\text{decene})]}{\sum[2(\text{olefin})]} \times 100$$

Parameters such as temperature, types of solvents, percentages of Re loading were optimised for the metathesis of 1-hexene.

RESULTS

(i) Effect of concentration of rhenium

Figure 1 shows the results of the metathesis of 1-hexene carried out at 30 °C in the presence of various percentages of rhenium loading on zeolite Y. The distribution of 5-decene increases from 1 wt% to 3 wt% Re loading and become constant when the yield approaches 50%. The reaction reached equilibrium at about 5-7 h of reaction time as shown in Figure 2. Considering that the reaction is at equilibrium, the high yield (50-60%) of 5-decene obtained from the reaction indicates that the catalyst is highly active even with 3 wt% Re loading.

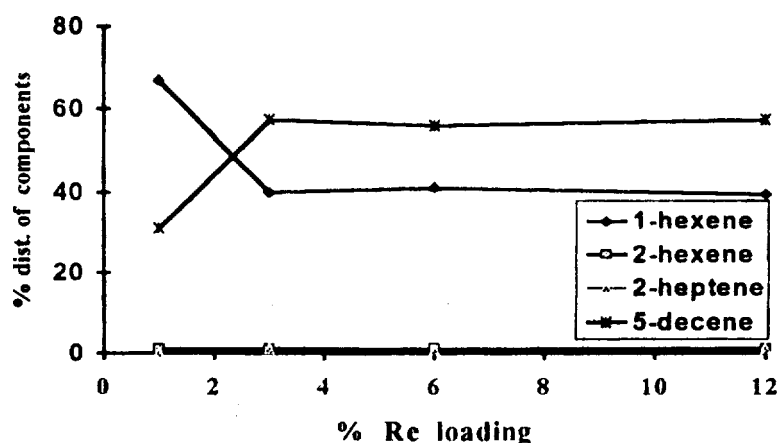


Figure 1: Distribution of components in liquid product as a function of wt% of rhenium loading on DY support.

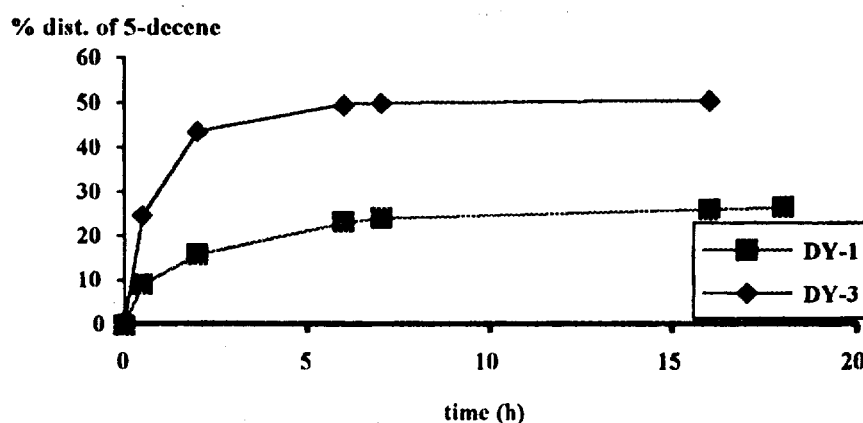


Figure 2: Percent distribution of 5-decene as a function of reaction time for the metathesis of 1-hexene on promoted ReDY-1 and ReDY-3 catalyst.

The high activity of the catalyst is evident from the high conversion of 1-hexene on ReDY-3 as shown in Figure 3. In addition, the selectivity of the catalyst is generally high with more than 90% yield of 5-decene for all percentages of Re loadings. These results are comparable to those obtained from 18 wt.% Re_2O_7 supported on γ -alumina[4].

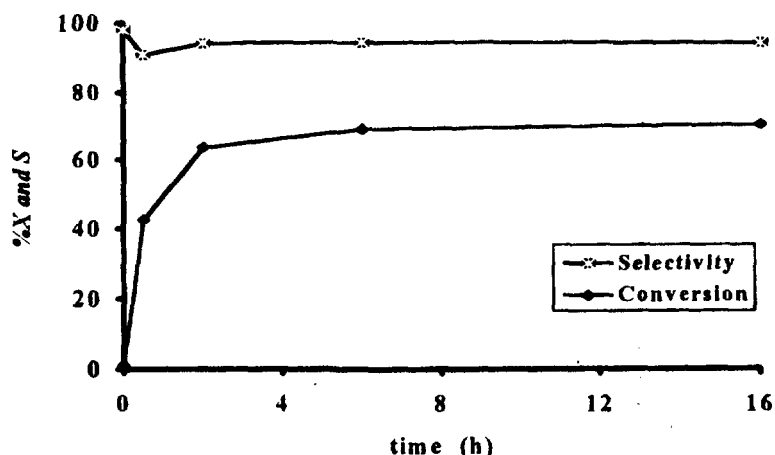


Figure 3: Conversion (X) and selectivity (S) as a function of reaction time of ReDY-3 catalyst

The effect on the type of support to the activity of the Re_2O_7 catalyst at 30 °C is given in Table 1. The results clearly show that the rhenium loaded on zeolite Y generally produces higher percentage of 5-decene. The DY support loaded with 3 wt% rhenium gives the highest product. This result clearly suggests that the high activity of the catalyst must be due to the presence of the DY support. Even with a very low rhenium loading of 1 wt%, it is evident that there is a higher production of 5-decene compared to that obtained from the 6 wt% Re loaded on γ -alumina.

Table 1: Effect of support of the activity of ReDY catalyst in metathesis of 1-hexene.

Catalyst	Support	%wt. Re	% decene
ReDY-1	DY	1	31.0
ReDY-3	DY	3	57.4
ReDY-6	DY	6	56.0
ReA-6	γ -alumina	6	23.3

(ii) Effect of temperature

The effect of temperature on the metathesis of ReDY catalyst system at the initial reaction time is shown in Figure 4. It shows that the amount of 5-decene produced increases with the increase of temperature of the reaction. However the effect of temperature is less significant after 24 h, after which time, the amount of 5-decene remains constant. Like most catalytic reactions, temperature plays a role in enhancing the initial activity of metathesis of 1-hexene until the reaction reaches equilibrium. This is in complete agreement with the Le Chatelier principle where temperature accelerates the rate of the reaction as demonstrated by the steeper gradients of the distribution curves at higher temperature.

In addition, the number of side reactions also increase with increasing temperature, as observed in the increase of dimerization products of metathesis carried out at 80 °C. More than 60% distribution of 5-decene is observed for the reaction at 80 °C after 24 h. The observed yield is more than the actual yield of the product expected because 1-hexene has a lower boiling point than 80 °C. This causes 1-hexene to exist as a gas and is not collected in the liquid phase.

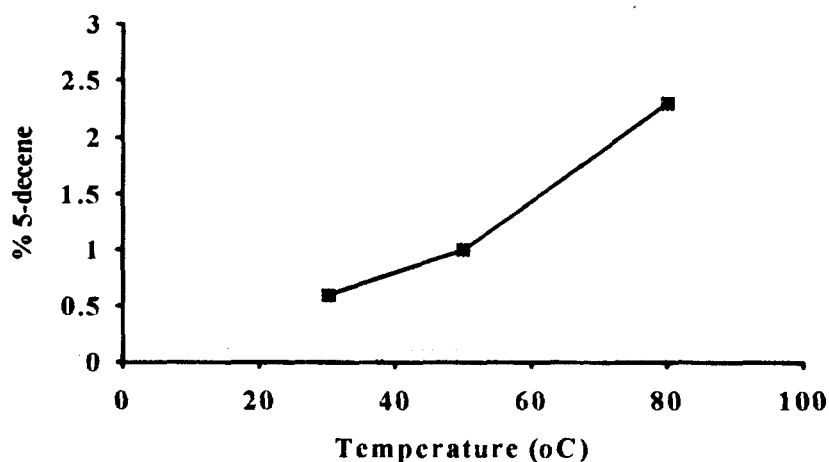


Figure 4: Percent yield of 5-decene as a function of reaction temperature at the initial reaction time for the metathesis of 1-hexene on ReDY-3

(iii) Effect of solvent

The production of 5-decene is higher when the reaction was carried out in chlorobenzene compared to in toluene as shown in Figure 5. About 60% of 1-hexene was converted to the products in chlorobenzene compared to only 30% in toluene. Furthermore, less side products (mostly dimerization product) were observed in the reaction carried out in chlorobenzene. The result clearly shows that chlorobenzene is a better solvent in suppressing the catalytic activity of side reactions.

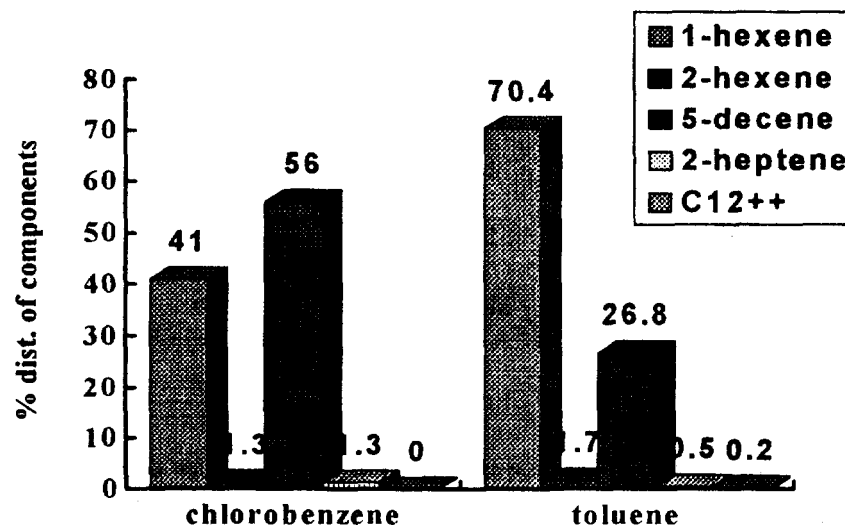


Figure 5: Percent distribution of the components in the liquid product at 24 h as a function of type of solvent in the metathesis of 1-hexene on ReDY-6.

(iv) Effect of the co-catalyst

In the absence of TMT, ReDY catalysts behave differently. Figure 6 demonstrates that instead of 5-decene, 2-hexene is the dominant product as a result of double bond shift isomerization of 1-hexene. There is also an increase in dimerization and polymerization products. This suggests that the presence of TMT in the catalytic system imposes a number of reactions other than metathesis. As a result of

competition of metathesis reaction with other reactions, less than 1% of 5-decene is produced. Since the production of 5-decene is less compared to other olefins, it is considered that normal metathesis of 1-hexene has not taken place. The result shows that TMT is important in the catalyst system in order to control the acidity of the system.

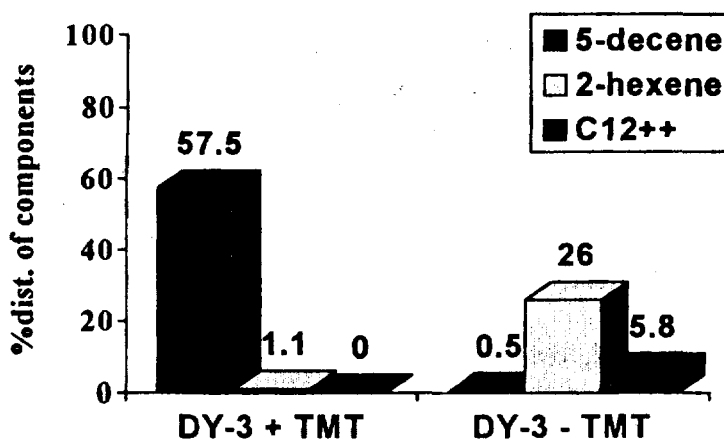
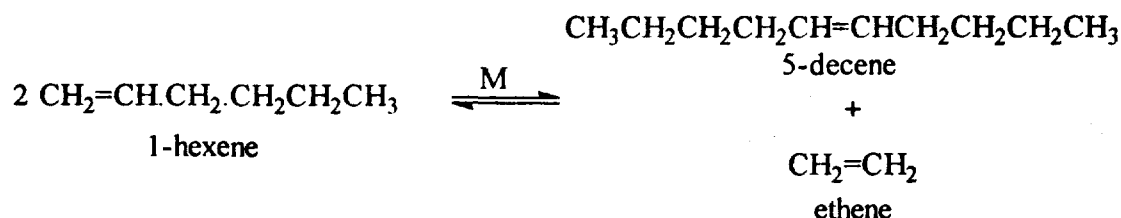


Figure 6: Percent distribution of components in the liquid product as a function of co-catalyst (TMT) on ReDY-3 catalyst after 24 h at 30 °C.

DISCUSSION

Successful metathesis of 1-hexene is expected to produce 5-decene and ethene as products according to the following reaction:



Our results have shown that with 3 wt% Re supported on dealuminated Y catalyst (ReDY-3) in the presence of TMT, 1-hexene underwent successful metathesis which produced maximum distribution of 5-decene with over 50% yield compared to only 21% produced by using 6 wt% Re on γ -alumina. In addition, the results also demonstrated that zeolite is a better support for Re_2O_7 even at very low loading, providing a catalyst of higher activity compared to that observed on γ -alumina. On the other hand, a selectivity for 5-decene of more than 90% offered by the ReDY system, is comparable to that obtained from Re on γ -alumina[9].

The higher activity shown by ReDY catalyst is related to the acidity of the zeolite Y support. Unlike alumina which contains only Lewis acidity, the Brönsted acids known to exist in the zeolite is found to greatly enhance the activity of the Re catalyst. The same was observed by Xiaoding et al[10] on rhenium supported on silica-alumina system. Since acidity in zeolite can be modified by hydrothermal dealumination[11], it is therefore possible to prepare zeolite Y consisting of Brönsted and Lewis acidity which originate from hydroxyls bonded to the framework tetrahedral Al and Al species located outside the framework respectively. Such flexibility offered by the zeolite support is an

advantage over the conventional silica-alumina system. The existence of these acidic sites in the dealuminated zeolite Y has been established in a separate study on the acid properties of rhenium supported on zeolite Y. Since γ -alumina has no Brönsted acidity, the Re supported by such system is found to be unreactive towards the metathesis reaction. Therefore the same explanation can be applied to the low activity observed in the metathesis reaction by Re_2O_7 supported on zeolite NaX and CaA catalyst [7].

The high selectivity of more than 90% yield of 5-decene in the metathesis of 1-hexene shown by the DY support is comparable to that obtained by the alumina support. In contrast, it was reported[4] that the corresponding low loading of Re_2O_7 supported on silica-alumina demonstrated a poor selectivity despite the high activity. The high selectivity of the ReDY catalysts is due to presence of the extraframework Al in DY, formed as a result of the dealumination process[12]. These extraframework Al, known to possess similar properties as the γ -alumina support, tend to suppress the active sites involved in other side reactions contributed by Brönsted acidity such as isomerization and polymerization. Consequently the selectivity of the catalyst towards the metathesis reaction is increased.

On the other hand, the catalyst behaves more like a solid acid catalyst system without a promoter such as TMT. In such case, the dominant reaction observed is isomerization. This indicates that the function of TMT is not only as metal-carbene initiator[2], but also as acidic site suppressor; interacting with the acidic surface OH groups present in the support. These results are in agreement with that obtained by other workers[4].

CONCLUSION

In conclusion, the rhenium oxide supported on zeolite Y modified by hydrothermal treatment are found to be very active and highly selective towards metathesis of 1-hexene. The activity of the catalyst increases with an increase of Re loading as shown by the increase in production of 5-decene. Maximum yield and selectivity of 5-decene was 57.4% and 90% respectively, obtained by DY loaded with 3 wt% of Re. The highly active catalyst is due to the presence of Brönsted acidity of the zeolite support while the extraframework Al created during hydrothermal dealumination of the zeolite is responsible for the high selectivity of the catalysts. The catalyst is found to be active for metathesis of 1-hexene only when it is promoted by TMT; a co-catalyst which acts as a metal-carbene initiator, as well as acidic site suppressor, preventing other side reactions to occur. The optimum conditions of the metathesis of 1-hexene by ReDY-3 catalyst were established at 30 °C in chlorobenzene as the solvent.

ACKNOWLEDGEMENTS

The authors would like to thank the Unit Penyelidikan dan Perundangan UTM and KL Rotary Research Fund for financial support, Dr. Ambar Yarmo (UKM) and Mrs. Nor Asikin Nordin (UTM) for valuable discussion.

REFERENCES

1. Y. Imamoglu, B. Zumreoglu-katan, A.J. Amass (Ed.) "Olefin Metathesis and Polymerization Catalyst; Synthesis, Mechanism and Utilization", NATO ASI Series, Kluwer, Dordrecht, 1990.
2. K.J. Ivin, 'Olefin Metathesis' Academic Press, London 1983.
3. X. Xiaoding and J.C. Mol, *J. Chem. Soc. Chem. Commun.*, 631 (1985)
4. J.C. Mol and A. Andreini, *J. Mol. Catal.*, **46**, 151 (1988)
5. J.A. Rabo and G.V. Gadja, *Catal. Rev. Sci. Eng.*, **31**, 385 (1989-90)

6. T. Komatsu, S. Wamba and T. Yashima, *Acta Physica Chemie*, **31**, 251 (1985).
7. Chun-Chin Hsu, PH.D thesis, Oklahoma University, (1980).
8. J.Klinowski, H. Hamdan, A. Corma, V. Fornes, M. Hunger and D. Freude, *Catalysis Letters*, **3**, 263 (1989).
9. A.Andreini, X. Xiaoding and J.C. Mol, *Appl. Catal.*, **27**, 31 (1986)
10. X. Xiaoding, J.C. Mol and C. Boelhouwer, *J. Chem. Soc., Faraday Trans I*, **82**, 2707 (1986)
11. V. Patzelova, E. Drahoradova, Z. Tvaruzkova and U. Lohse, *Zeolites*, **9**, 74 (1989)
12. G. Engelhardt and D. Michel, 'High Resolution Solid-State NMR of Silicates' Wiley, 1987.

COMPATIBILIZATION OF NATURAL RUBBER/POLYVINYL CHLORIDE BLENDS WITH EPOXIDISED NATURAL RUBBER

*Wan Aizan Wan Abdul Rahman , * Ibrahim Abdullah , and Abu Azam Mohd. Yassin*

*Fakulti Kejuruteraan Kimia & Sumber Asli,
Universiti Teknologi Malaysia ,
Karung Berkunci 791,
80990 Johor Bharu,
Johor Darul Takzim.*

** Jabatan Kimia,
Fakulti Sains Fisis & Gunaan,
Universiti Kebangsaan Malaysia,
Bangi,
Selangor Darul Ehsan*

ABSTRACT

Natural rubber(NR)/ polyvinyl chloride (PVC) blends show incompatibility at all composition by the presence of two distinct phases, together with poor mechanical properties. Studies were undertaken to seek suitable compatibilizing agents based on epoxidised natural rubber(ENR) to improve blends compatibility and properties. Experimental results show that the degree of epoxidation in the ENR influence the blends compatibility. Also, from the results ENR50 increases compatibility between NR/PVC blends as shown by the improvement in their mechanical properties and the limited solubility of the blends in tetrahydrofuran(THF) . Compatibility of the blends increases with the amount of compatibilizer. Investigation on the group that promote compatibility was also undertaken and it was deduced that epoxide alone unable to compatibilise the NR/PVC system but epoxide in the presence of alkene group promote compatibility. Lowering the molecular weight of the compatibilizer (ENR50) increases miscibility in the blends at molecular level only with varying mechanical properties. However, the blends undergo self-crosslinkable process in the absence of any vulcanizing agent as shown by the swelling behavior in the THF. ENR50 was found to be the best compatibilizer understudied.

INTRODUCTION

Blending of polymers have been extensively used technique in many practical applications, especially in the rubber industry. However the desired properties are often lost on mixing

because of incompatibility arises in many polymer blends. Several methods have been introduced to overcome these problem such as addition of additives generally called 'compatibilizing agents' which induce miscibility or modification of interface properties which improve adhesion between the main partners. Example of an agent used in promoting the interfacial connectivity of two-phase blend is block and graft copolymer that contain two segments identical or miscible with each phase¹ or contains an attached functional group capable of interacting with the other component².

Miscibility of the constituent polymers is generally a necessity for forming successful blends. One example of the commercially important and miscible polymer blend is that of nitrile butyl rubber and polyvinyl chloride(PVC). This blends can be conveniently milled, extruded and compression molded using traditional processing equipments for natural and synthetic rubber³. Kalfoglou et al in their earlier work have demonstrated that epoxidised polyhydrocarbons effectively produce miscible polymers example with PVC, chlorinated polyethylene, chlorinated polypropylene and proton donating polymers⁴. Work done by Varughese⁵ and Nasir et al⁶ specifically show that both PVC/ENR form compatible blends at molecular level by exhibiting a single glass transition temperature(Tg) which lies between that of PVC and ENR. Blends of NR/ENR are shown to be incompatible by the presence of 2 Tg's⁷, although ENR contains segment which is identical with NR phase. Thus it was of interest to explore the compatibilizing action of ENR on the basis of its demonstrated miscibility with PVC and having identical segment with NR.

In the present study we focus on the ability of epoxidised NR acting as a compatibiliser for the incompatible NR and PVC. Hence this report covers the investigation conducted on the level of epoxidation, the amount of compatibilizer and the effect of degrading ENR in attaining mechanically compatible blends.

MATERIALS AND METHODS

Materials

The materials used are shown in table 1.

TABLE 1: Materials Used

Materials	Description
SMR CV	Standard Malaysian Rubber of constant viscosity obtained from Rubber Research Institute (RRIM)
PVC	Powder, suspension polymerized, k value- 60 from Industrial Resin Malaysia, Johore
ENR25	Epoxidised Natural Rubber of 25% and 50% epoxidation level
ENR50	obtained from RRIM.
ENR60	ENR of 60% epoxidation level, obtained from Kumpulan Guthrie

	Bhd.
1,2 Epoxy -5-hexene.	99% pure from Aldrich was used as received.
1,2 Epoxyhexa decane	85% from Aldrich was used as received.
Tetrahydrofuran	Grade, extra pure from Merck and used as received.
Degraded ENR50	ENR 50 from RRIM was mechanically degraded on a Brabender Plasticorder PI-2000 using cam blade at ambient temperature and rotating speed of 40 rpm.
Barium/Zinc based	Irgastab BZ 552 was supplied by Ciba - Geigy South East Asia, PTE Limited ,Singapore.

Blends preparation

Blends were prepared in a laboratory internal mixer Brabender Plasticorder model PL-2000-6 using cam-blade with heated silicone oil circulation. PVC was first premixed with stabilizer Ingrastab BZ552 at 10phr. in a dry blender at high speed for 15 minutes. Then the required weight of stabilized PVC powder were charged into the mixing chamber. Preheating was allowed for three minutes. After three minutes, regular strip of the rubbery component was fed into the mixing chamber. The mix was blended for seven minutes before dumping the blend. Density of the prepared blends were measured using a density balance.

Effect of epoxidation level and compatibilizing group in ENR

For this purpose, ENR of different epoxidation level 25%,50% and 60% were examined for its role as a compatibilizing agent. The SMR/PVC ratio used was 2:3 with 16% compatibilizer under processing temperature of 150°C and speed 40 rpm for all the blends. The same ratio was used in determining the compatibilizing group of ENR.

Compatibiliser composition and chain length

SMR/PVC of 2:3 ratio was also used in studying the above effect. For the effect of composition, varying ENR50 in the blend up to 50% was examined. Whereas, studies on the chain length was done on blends containing 30% compatibiliser.

Effect of curing on blends

Blends was cured on mold press without adding any curing agent at varying temperature ranging from 30 minutes to 2 hours. These blends are examined for its swell index and the insoluble component.

Mechanical properties

All the blends were molded on hot press for three minutes and water cooled. Preparation and testing of specimens were performed in accordance to ASTM D412-87, with crosshead speed of 50mm/min at 24°C on Lloyd Instrument MTM (Model L1000R).

Average of five samples were tested for each measurement. Hardness test was conducted using Karl Frank Hardness Testing Instrument 38209 according to ASTM 1415.

Gel determination and swelling index

Solvent insoluble gel was measured by dissolving 0.39 to 0.41 gram of the prepared blend (cut into strips of 1mm x 5mm) in 40 ml tetrahydrofuran. The blends were left to stand for 20 hours at 25 °C + 2°C in the dark. The gel formed was filtered through borosilicate glass wool. Exactly 10 ml of the filtered liquid was pipetted into a dried and weighted aluminium dish. The dish was then placed on an electric hot plate at 100°C ± 10°C which alternately heated and weighted to the nearest 0.1 mg until a constant weight was achieved.

Gel content was calculated as follows:-

$$A \times 4 = B$$

$$\text{Gel \%} = \frac{(C-B)}{C} \times 100$$

where,

A = mass of the dried sol 10 cm³ volume

B = mass of the total dried sol and

C = mass of the original sample.

The filtered swollen gel was removed from traces of solvent and quickly transferred into a well-cap weighing bottle and weighed. This represent the swollen gel. Determination of the swelling index was performed as follows:-

$$\text{Swelling index} = E/D$$

where,

E = mass of the swollen gel

D = C - B

B = mass of the dried gel

Both results were obtained from the average of two determinations.

RESULTS AND DISCUSSION

a) Brabender torque and stock temperature

A sharp decrease of torque to a minimum value and gradually increase to a maximum peak was observed after the rubbery component was loaded to the preheated PVC as shown in *figure 1b* and *c*. The maximum peak indicates 'fusion' whereby polymer particles are merged into a melt. This peak was absence in blends without PVC component as indicated by the SMR/ENR50 torque profile. Thereafter the torque stabilized or drop depending on the mixing parameters used. *Figure 1a* demonstrate that prolonged shearing enhanced chain scission in SMR/ENR blends and reduced the melt viscosity which decreases the torque. The curves also showed that PVC phase provide protection from further degradation in the rubbery phase as summarized by the effect of NR/PVC ratio on torque profiles, *figure 1d*. The attainment of final steady temperature indicates a uniform exothermic mixing of the blend component and the gradual drop of temperature and torque after prolonged mixing indicate their time dependent shear degradative action.

b) Epoxidation level of the compatibilizer

Table 2 shows the mechanical properties of NR/PVC binary blends as compared to the blends with ENR type compatibilizer. The presence of ENR compatibilizer in general increases the tensile strength and hardness of the blends. The degree of epoxidation in the ENR influence blend performance. Blends at low epoxidation level shows poor mechanical properties and the increase in epoxidation level improve properties. However, comparing ENR50 with ENR60, 10% increase in epoxidation does not show much improvement in tensile and swell properties. A marked increase basically from ENR25. Therefore addition of ENR as a compatibilizer induces compatibility in NR/PVC blends either through rubber/rubber compatibility or rubber/PVC compatibility and ENR50 seems to be the optimum epoxidation level. Test on the binary blend of ENR/PVC and SMR/ENR blends also show a marked different in tensile properties exhibited by ENR25 compared to ENR50 and ENR60, but no distinct changes occurs from ENR50 to ENR60, table 3.

TABLE 2: Tensile and Swell Properties of Blends with Various Epoxidation Level

Sample	Tensile strength MPa	Elong. at brk %	In THF after 20 hours
SMR/PVC	0.5369	463	cloudy solution (2 phases)
SMR/ENR25/PVC	0.7526	957	gel-like
SMR/ENR50/PVC	2.495	224	SI =17.8
SMR/ENR60A/PVC	2.368	240	SI =16

SI -Swell Index

Ternary blend ratio 2:1:3

Binary blend ratio 2:3

TABLE 3: Tensile and Swell Properties of Binary Blends with various Epoxidation Level

Sample	Tensile strength MPa	Elong. at brk %	In THF after 20 hours
ENR25/PVC	0.2273	1195	clear solution
ENR50/PVC	16.21	933	clear solution
ENR60A/PVC	16.28	857	clear solution
SMR/ENR25	0.3302	1672	gel
SMR/ENR50	0.5892	1991	gel
SMR/ENR60A	0.7899	3204	gel

Binary blend ratio 1:1

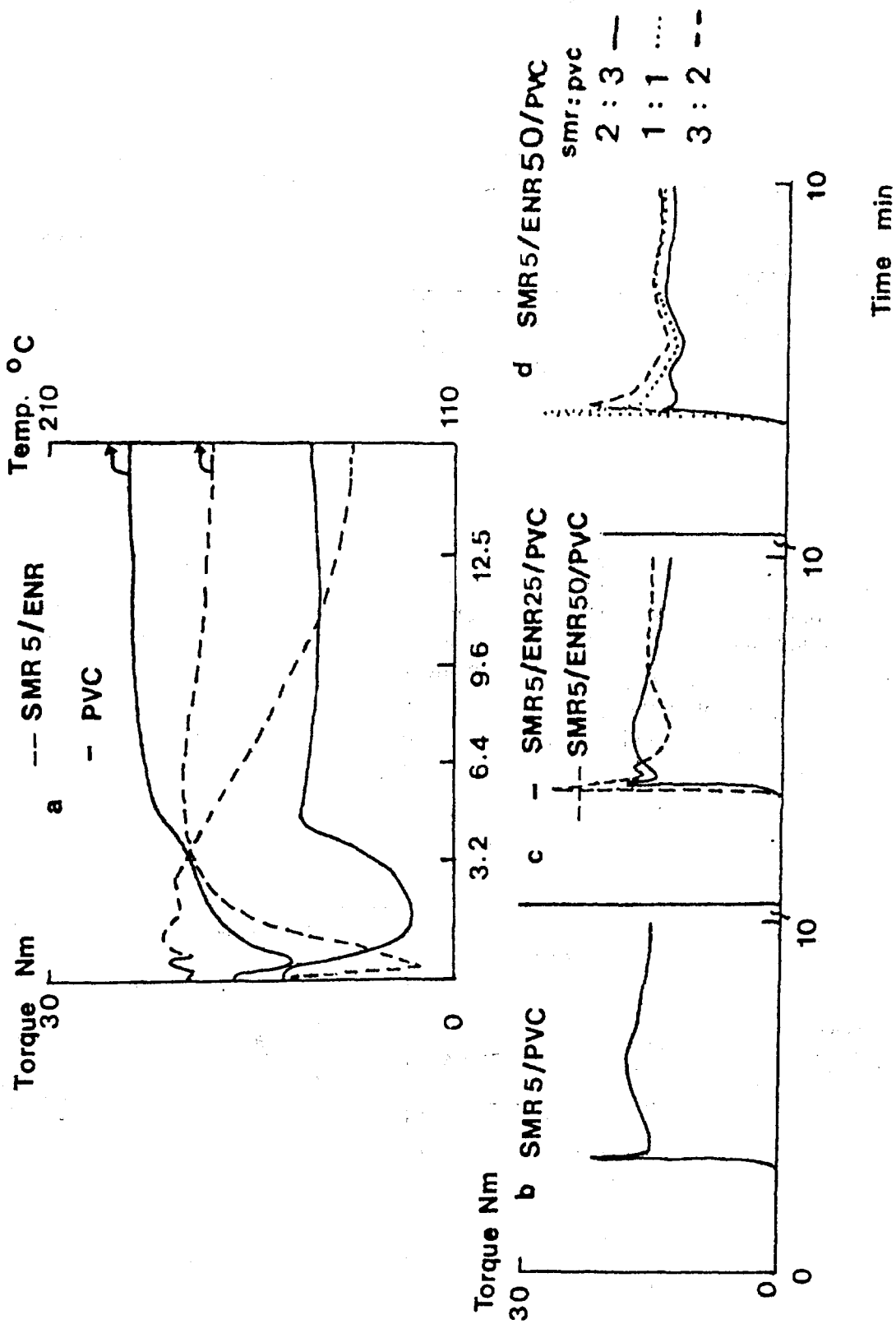


Figure 1: Torque profile of blends versus time

d) Compatibilizing factors

A study was proceeded to see factors that induces compatibility in the NR/PVC system by ENR 50. The result deduce that epoxy alone shows no interaction with epoxy nor SMR physically or chemically as shown in *table 5*, by its tensile/hardness properties and phase separated in THF. Compatibility is only observed in blends containing compatibilizer with epoxy and alkene group together from the 3-4 fold increase in properties. Therefore epoxy alone plays no part in compatibilizing the blends but epoxy with the presence of alkene group do compatibilized the blend.

TABLE 5: Groups which contribute to the Compatibilization of Blends

Sample	Tensile strength MPa	Elong. at brk %	Solubility in THF
SMR/EPOXYHEX ADECAN/PVC	0.3004	72	cloudy solution
SMR/EPOXYHEX ENE/PVC	1.262	61	gel-like solution
SMR/ENR50/PVC	0.9431	280	partially gel with swelled sample

SMR/PVC ratio 2:3

ENR50 content 5%

e) Compatibilizer chain length

The chain length of the 'epoxy-alkene' type compatibilization do play an important role in compatibilizing the NR/PVC blends. *Figure 3* shows how ENR50 chain length effect the compatibilizing ability. As the degradation time for ENR50 is increases tensile strength increases up to an optimum value. Effectiveness of ENR50 acting as a compatibilizing agent is dependent on their chain length whereby beyond the optimum chain length tensile strength is low probably because the blends are not fully compatible due to entanglements and phase size which limit homogeneous blending. Lost in tensile strength as further degradation occurs probably due to morphological changes although compatibility increases.

FIGURE 3

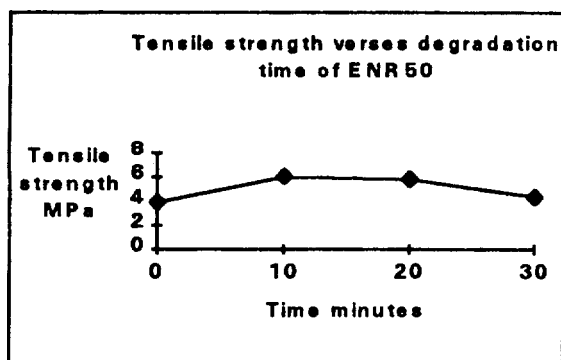
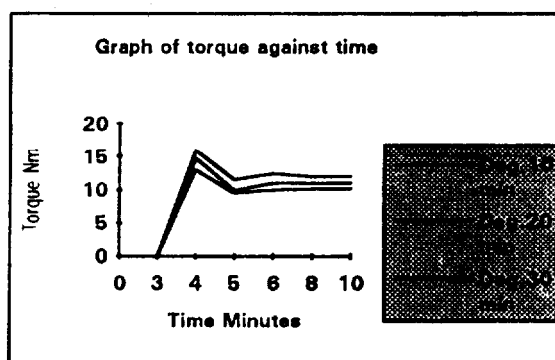


FIGURE 4



c) Composition of the compatibilizer

Generally the introduction of ENR increases the tensile strength and hardness of the blends as shown in *table 4*. Also from the table, tensile strength increases as the content of ENR50 increases to an optimum value before decreasing. Hardness value decreases as the ENR50 content increases because the total rubber content in the blend which provide the soft phase is increase. Binary blends(NR/PVC) are soluble in THF forming a two phase solution whereas ternary blends swell at low ENR50 content. However, as the ENR50 composition increases the solubility of the blends increases. This behavior is demonstrated in *figure 2* from the increase in swelling index and decrease in gel content measurement. The above result probably indicate the absence of stable physical or chemical entanglement in binary blends and ternary blend with the increase in ENR50 composition.

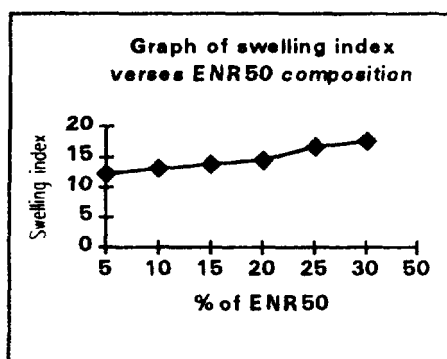
TABLE 4: Effect of ENR50 Composition on the SMR/PVC Blends

% of ENR50 SMR/ENR50/PVC	Tensile strength MPa	Elong. at brk %	Hardness ShoreA
0	0.5369	463	
5	0.9431	179	23
10	1.671	190	22
16.7	2.495	224	18.8
20	3.182	295	18.7
25	3.482	376	15.8
30	3.946	513	13.8
50	3.380	1297	9.6

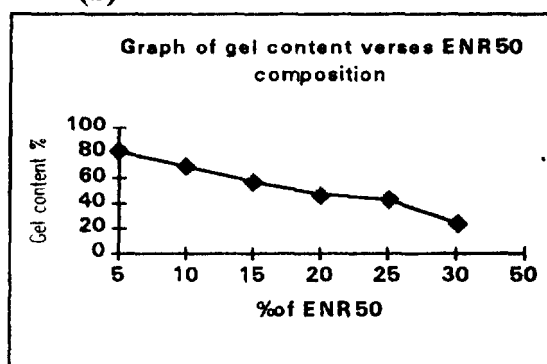
SMR/PVC ratio 2:3

Whereas ENR50 at low composition in the ternary blends induces stable entanglement to occur. Compatibility of the ternary blends however increases with ENR50 content since compatible binary blends of ENR50/PVC are fully soluble in THF forming a one phase solution. For the SMR/PVC ratio of 2:3, the blends become fully compatible physically above 30% ENR50 content. This is because stress whitening on bending (due to phase separation) was observed to disappear above 30% ENR50 content, support the above hypothesis. The compatibility observe are at molecular level only.

FIGURE 2 (a)



(b)



ACKNOWLEDGMENT

Special thanks to IRPA vot 62100 for funding the project and Faculty of Science(Chemistry Dept.) for the used of the equipments.

REFERENCES

1. D.R Paul 'Handbook of Elastomer' vol. 2, D.R Paul and S.Newman, Eds., Academic Press, New York, 1978, p213.
2. S. Ahmad and I. Abdullah, ' Mechanical and thermal behaviour of liquid natural rubber compatibilised NR-PP blends', Materials Forum ,(1992), 16,277-280.
3. George K.E, Rani Joseph and Joseph Francis D, 'Studies on NBR/PVC blends ', Journal of Applied Polymer Science,32, 2867-2873.
4. Stathis N. Koklas, Dionissia D Sotiropoulou, John K. Kallitsis and Nikos K. Kalfoglou, 'Compatibilization of chlorinated PE/PVC blend with ENR', Polymer, 1991, vol 32, no. 1 ,p66-72.
5. K.T Varughese and P.P De, 'Miscible blends from plasticised PVC and ENR', Journal of Applied Polymer Science ,(1989) ,38, p2537.
6. Z.A. Nasir and R.T Ratnam, 'Internal mixer studies of ENR/PVC blends', Journal of Applied Polymer Science ,(1989) ,38, p1219.
7. S.C.Ng and K.K Chee , 'Differential Scanning Calorimetry study of NR and ENR and their binary blends', Rubber Chemistry and Technology, (1988), vol 62, p585-591.
8. I.R. Gelling and P.E. Mente, 'Liquid Natural Rubber as co-vulcanisable process aids,' in NR Current Developments In Product Manufacture And Applications. Proceeding IRTC , June1993, Kuala Lumpur. Edited by Abdul Aziz Bin S.A. Kadir , RRIM, p193-205.
9. P. Ramesh, S.K. De, 'Self-crosslinkable plastic-rubber blend system based on PVC/ENR.' Journal of Materials Science, (1991), 26, p2846-2850.

The torque traces from the mixing study recorded in *figure 4* shows a decrease in torque as the compatibiliser chain length is shortened, results in better processing properties and promoting homogeneous blending. This trend is consistent to that reported by I.R. Gelling et al whereby effectiveness of LNR as process aids increases with decreasing molecular weight but loss of vulcanisate properties occurs below the optimized molecular weight⁸.

f) Curing effect

Figure 5 indicate that ternary and binary blends swell index decreases with curing time and the blends swell only to a limited extent. Percentage of blends undergo self cross-linking reaction with respect to time was also increased *figure 6*. This show that chemical interaction occurs within the blends during heat treatment. Since blends undergo curing without any addition of curing agent the blends are said to become self-crosslinkable. Before heat treatment binary blends are soluble in THF. The small increase in ternary blends as compared to binary blends could probably due to the small amount of ENR used as the compatibiliser. However the binary and ternary results are consistent to that observed by the Indian coworkers in ENR50/PVC blends⁹. The above effect shows that chemical interaction occurs between the epoxide group in ENR with the PVC forming c-o-c bond.

FIGURE 5

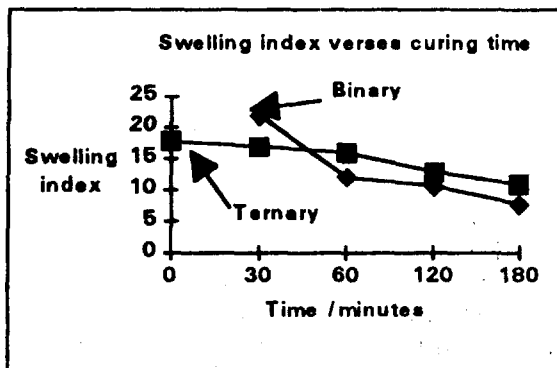
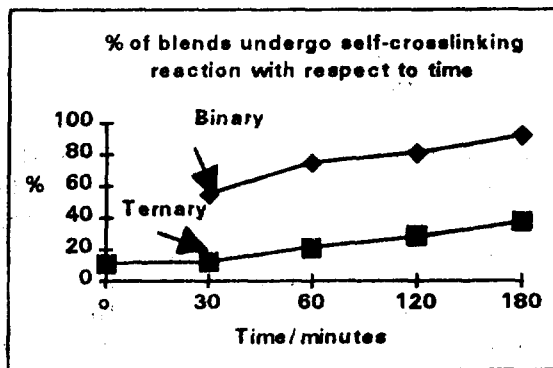


FIGURE 6



CONCLUSIONS

From the analysis, ENR improves the properties of the incompatible NR/PVC blends and ENR50 was found to be the most suitable compatibilizer compared to the other ENR system. Compatibility increases with ENR50 composition and full compatibility for NR/PVC system of ratio 2:3 is above 30 % ENR50 content. And compatibility is only observed in blends containing compatibilizer with epoxy and alkene group together. Degrading the rubber chain of the compatibilizer result in increasing the compatibility of the blends and tensile strength increases to an optimum dependent on chain length. In the absence of any crosslinking agent, NR/ENR50/PVC blends undergo self-crosslinkable reaction after heat treatment.

2.01 Plating Parameters

The plating parameters that were looked into in this study are pH, temperature and ultrasonic power. The current density determined from the Hull Cell test is kept constant during the plating process. The following were the different range of parameters selected for plating :

pH	:	3.0	4.0	5.0	6.0
Temperature	:	45 ⁰ C	55 ⁰ C	65 ⁰ C	
Ultrasonic Power	:	0w	135w	270w	

2.1 Salt Spray Test

The Salt Spray Test was conducted according to BS 5466. The specimens being plated were exposed to mist of salt spray saturated air by spraying a sodium chloride solution into an enclosed cabinet. The salt solution is made up at a concentration of 50g/l of sodium chloride in distilled water. The internal temperature is maintained at 35⁰ C \pm 2⁰ C and the test were carried out for 5 hours. The weight of specimens before and after the test were taken so that the weight of oxide can be calculated.

2.2 Adhesion Test (Bending Test)

A Mandrel Bending Tester was used for the test which is in conformity with international standard DIN 53152. The Mandrel Bending Tester is one of the most important and popular test methods for determination of the ductility and adhesion characteristic coatings under bend stress. In bending test, several mandrels with different diameter have been divided (as for the study, size of curvature is 32mm). The test sample carrying the coating is bent around the selected mandrel by turning the bending lever through 180⁰. The duration of the bend movement should be 1-2 seconds.

2.3 Microstructure and Surface Topography

Inverted Microscope was used to determine the structure of the gold coating and their surface topography. The grain size and porosity level were analysed indicating the corrosion resistivity performance.

3.0 Result and Discussion

The microstructure of the deposited gold has been observed for both with and without ultrasonic source and is shown in the Appendix (Figure 3.0(a) and 3.0(b)).

EFFECT OF ULTRASONIC AGITATION ON MECHANICAL AND CORROSION PROPERTIES OF GOLD ELECTRODEPOSITS

BY

(NOOR HISHAM AB. HAMID, TUAN HAJI JAMIL YUSOF, DR. MUSTAZA HAJI
AHMADUN & ANITA IBRAHIM
FACULTY OF MECHANICAL ENGINEERING
UNIVERSITI TEKNOLOGI MALAYSIA
SKUDAI, JOHOR)

1.0 Introduction

Electroplating is the process of depositing a coating having a desirable form by means of electrolysis. Its purpose is generally to alter the characteristic of a surface to provide improved aesthetic value, ability to withstand corrosive agents, resistant to abrasion or other desired properties. Electrolysis is carried out in a solution (bath) which may consist of dissolved fused salts or solution of various kinds. Similarly, gold electroplating is the process of depositing a gold coating on the base metal to achieve the desired characteristic of a surface under the suitable bath by means of electrolysis.

Most of industrial gold plating is carried out for electronics that requires either high purify, soft gold for semiconductor's industry or hard gold containing traces of codeposit metals used for printed circuit application, where the main requirement is wear resistance. Components such as switches, commutators, circuit breakers, slip rings and connectors, which involve contact surfaces, require gold coating to resist film formation for wear resistance and for easy solderability.

In this study, the main topic of discussion is to find out the effect of ultrasonic agitation on mechanical and corrosion properties of gold electrodeposits.

2.0 Experimental Work

Gold Potassium Cyanide¹ was used as the plating solution during this study. The mode of plating used is rack. Prior to the gold plating, the specimens were undercoat with copper for 10 minutes to ensure a good adhesion. Nevertheless, before plating with copper, the specimens were first plated with nickel for 20 minutes by using the electroless.

The platings of gold in this study were carried out in two ways. First, is plating without using any agitation and the second is with the application of ultrasonic agitation.

3.3 Adhesion

Cracking of deposits may pose a serious limitation to their usefulness. Stronger and a more ductile deposit provides a greater resistance to crack in service.

Figure 3.3(a) in Appendix, shows the specimen after the test. While Figure 3.3(b) and 3.3(c), illustrate the degree of crack under the influence of temperature, pH and ultrasonic agitation. From the Figure 3.3(b) and 3.3(c), the curve indicated that the severity of crack remains or slightly decreased as the temperature raises. These depict the temperature is not critical towards the ductility of the deposit. As for temperature, the influence of pH towards the ductility of gold deposit was also not clear, the degree of crack is still high at all cases. The final deposit is of brittle gold.

Figure 3.3(b) and 3.3(c) show that the specimens subjected to ultrasonic agitation plating exhibit severe cracked phenomena compare to the one without the influence of ultrasonic agitation for all pH and temperature under study. As for the later the peeling off effect is remarkable. The above pointed out that the ultrasonic agitation will produce a harder and stronger adhesion of gold electroplated coating.

4.0 Conclusion

The employment of ultrasonic agitation have significantly reduces the porosity level of gold coating whence providing a good property of coating corrosion resistance. The adhesion property also improved to a certain extent. The brittleness of the deposit increases which will enhance the resistance to abrasion.

REFERENCE

1. Johnson Matthey Asia Data Sheet, 1992.

3.1 Visual Inspection

The visual inspection was presented in the format degree of reflectivity (brightness) and symbolised as below :

1	=	very good
2	=	good
3	=	moderate
4	=	bad

Figure 3.1(a) and 3.1(b) in Appendix, shows the appearance of the specimens which are plated with gold coating using ultrasonic and without ultrasonic agitation. The appearance of the gold electrodeposited are varied from the influence parameters, such as agitation, pH and temperature. It can be shown in Figure 3.1(c) and 3.1(d) in Appendix.

The non-agitation specimens gave the best appearance when compare to the specimen with ultrasonic agitation. Overall, the result's appearance improves as the temperature and pH increase.

3.2 Corrosion Resistance

From the result obtained (Refer to Figure 3.2(a)-(c)) in Appendix, there is some improvement in corrosion resistance. The comparison can be make between the specimen with pH 3.0 and pH 6.0. For specimens without agitation, both give the same result where raises of temperature were concomitant increase the weight of oxide. For the specimen with ultrasonic agitation, no clear picture could be seen. But still to some extent, decreasing in weight was observed when the temperature raised.

It can also be figured out that increasing of pH value will gradually reduce the weight of oxide. Figure 3.2(b-c), clearly shows the effect of using ultrasonic agitation where the weights of oxides reduce by increasing of pH. In short, ultrasonic agitation employed during plating would upgrade the property of gold coating to better corrosion resistance. This statement can be substantiated by doing the topography analysis.

The corrosion resistance has very close relationship with the level of porosity of the plated metal that can be seen from the surface topography analysis. The higher level of porosity will give less corrosion resistant.

On the basis of on Figure 3.2(d,e,f), it clearly shows that ultrasonic agitation gives much lower porosity level compared to the one without. The void's sizes for the specimen with ultrasonic agitation are much smaller and less in number (Figure 3.2 (d, e)) compared to the specimen without agitation where the sizes are much bigger and more dense (Figure 3.2(f)).

Thus ultrasonic agitation in gold plating has a significant effect of minimizing porosity level.

APPEARANCE VS TEMPERATURE

For pH = 3.0

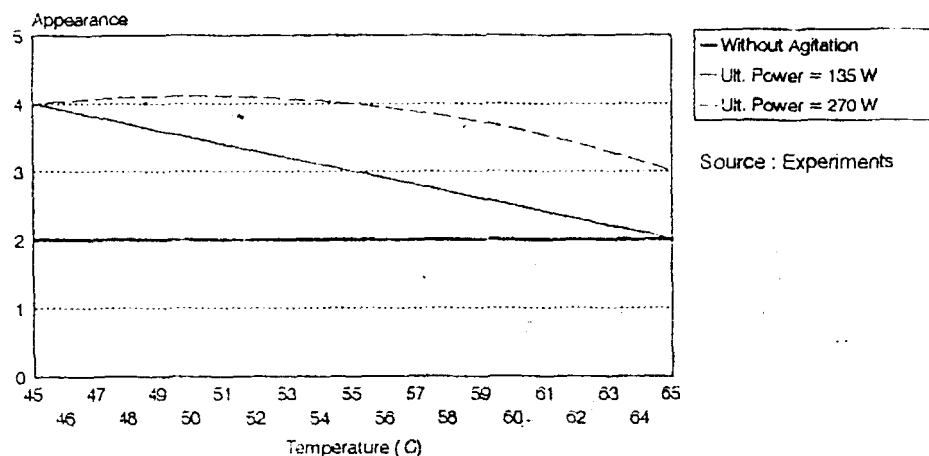


FIGURE 3.1(c)

APPEARANCE VS TEMPERATURE

For pH = 6.0

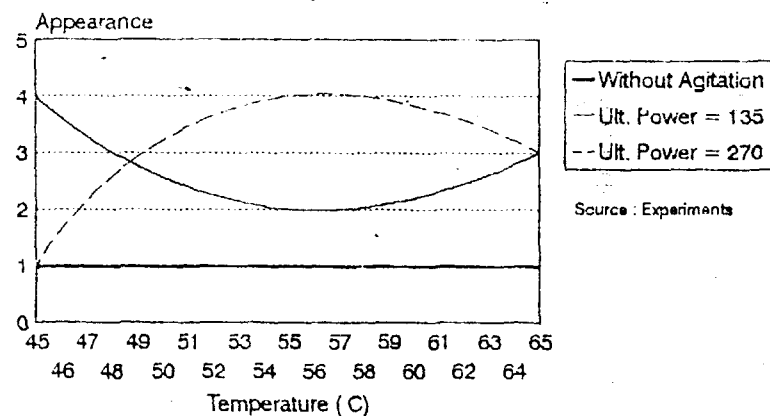


FIGURE 3.1(d)

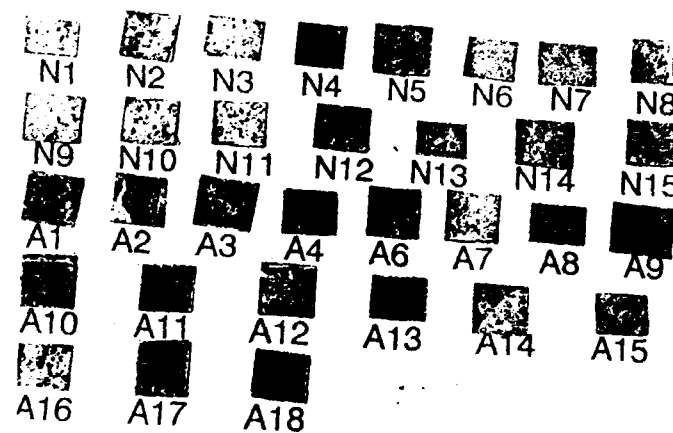


FIGURE 3.2(a) - THE CONDITION OF SPECIMENS AFTER SALT SPRAY TEST (N = NON-AGITATION, A = WITH ULTRASONIC AGITATION)

WEIGHT OF OXIDE VS TEMPERATURE

For pH = 3.0

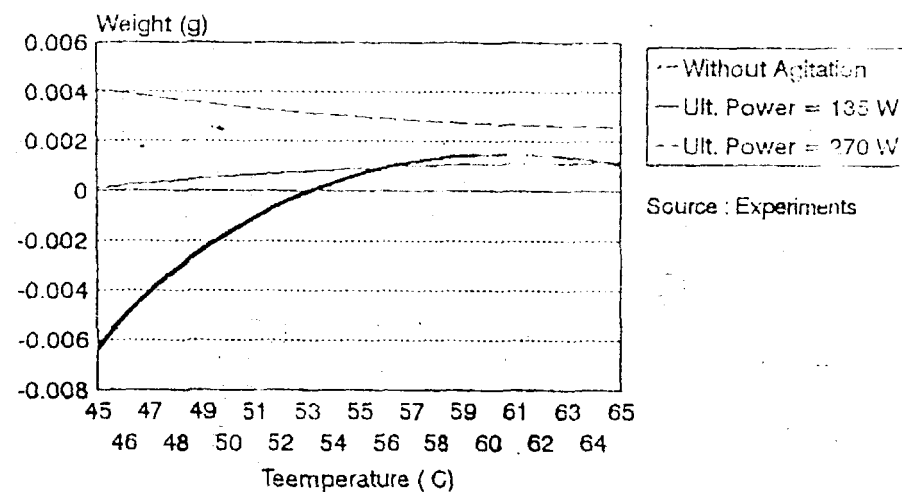


FIGURE 3.2(b)



FIGURE 3.0(a) - MICROSTRUCTURE OF GOLD ELECTRODEPOSIT WITH ULTRASONIC AGITATION(150X)



FIGURE 3.0(b) - MICROSTRUCTURE OF GOLD ELECTRODEPOSIT WITHOUT ULTRASONIC AGITATION(150X)

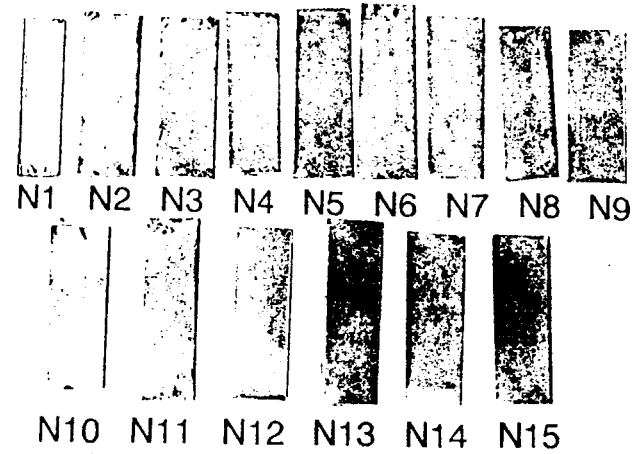


FIGURE 3.1(a) - GOLD PLATED SPECIMENS WITHOUT ULTRASONIC AGITATION

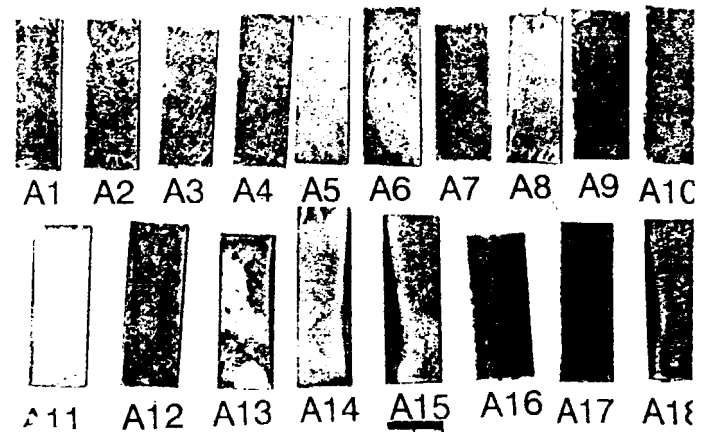


FIGURE 3.1(b) - GOLD PLATED SPECIMENS WITH ULTRASONIC AGITATION

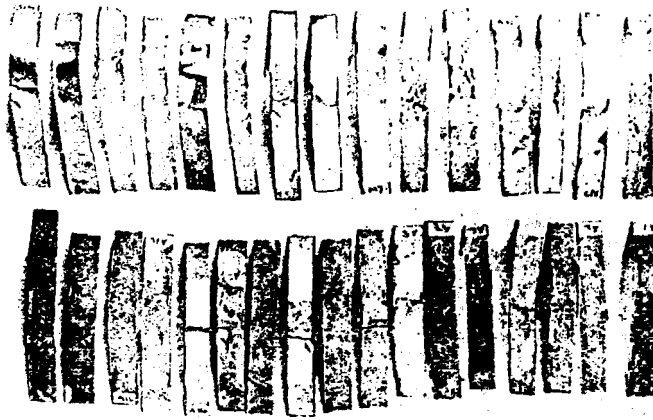


FIGURE 3.3(a) - SPECIMENS AFTER UNDERGO ADHESION TEST
(TOP = WITH ULTRASONIC ACITATION, BOTTOM = NON-AGITATION)

DEGREE OF CRACK VS TEMPERATURE For pH = 6.0

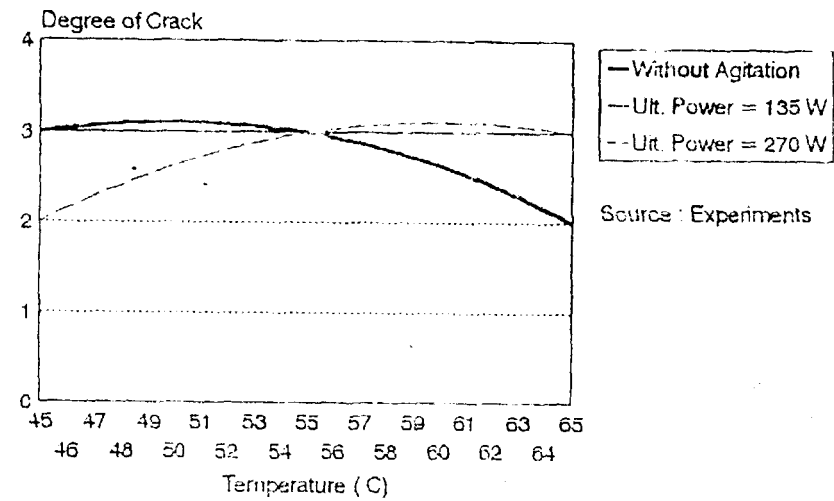


FIGURE 3.3(c)

DEGREE OF CRACK VS TEMPERATURE For pH = 3.0

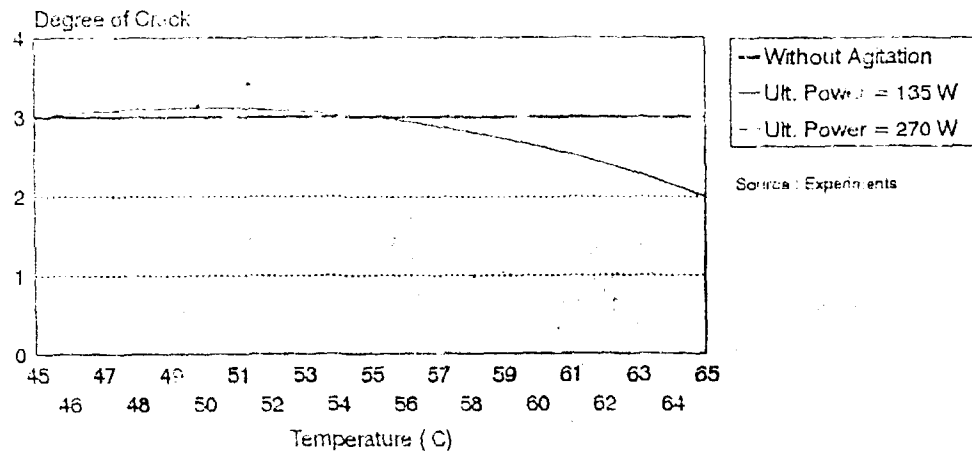


FIGURE 3.3(b)

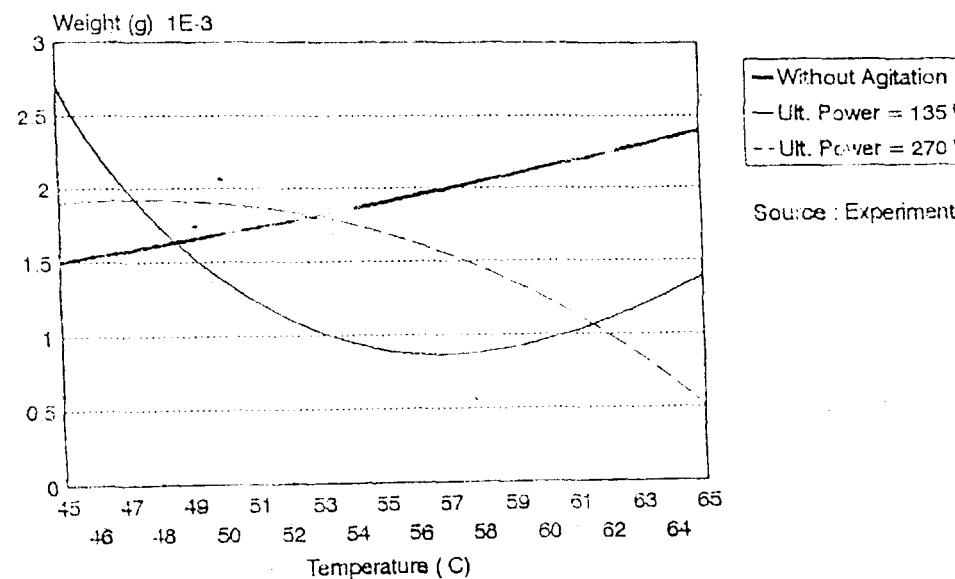


FIGURE 3.2(d) - SURFACE TOPOGRAPHY OF GOLD ELECTRODEPOSIT WITH ULTRASONIC AGITATION(150X)



FIGURE 3.2(e) - SURFACE TOPOGRAPHY OF GOLD ELECTRODEPOSIT WITH ULTRASONIC AGITATION(150X)

WEIGHT OF OXIDE VS TEMPERATURE For pH = 6.0



Source : Experiments

FIGURE 3.2(c)

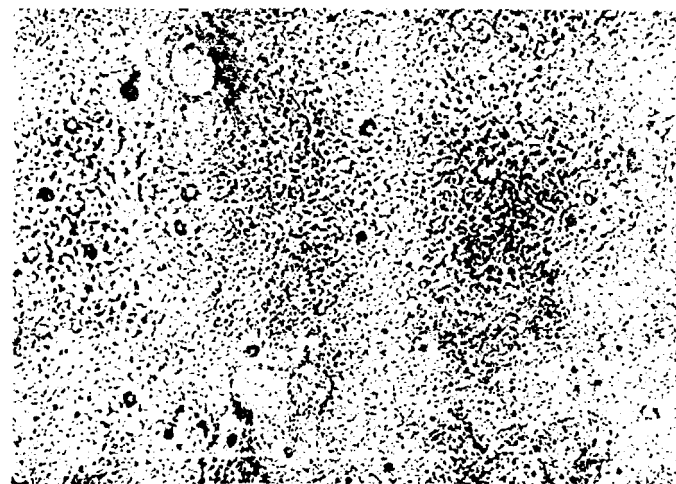


FIGURE 3.2(f) - SURFACE TOPOGRAPHY OF GOLD ELECTRODEPOSIT WITHOUT ULTRASONIC AGITATION (150X)

PENDAHULUAN

Superkonduktor adalah bahan yang boleh mengalirkan arus elektrik tanpa sebarang rintangan. Sifat ini membawa implikasi yang besar terhadap kegunaannya sebagai penjimat tenaga, peranti elektronik termaju dan lain-lain lagi. Superkonduktor suhu tinggi boleh dibahagikan kepada beberapa sistem iaitu sistem lantanum, iterium, bismuth, talium dan merkuri.

Superkonduktor suhu tinggi sistem Tl-Ba-Ca-Cu-O adalah di antara superkonduktor dengan suhu genting T_c yang tertinggi (Sheng Z. Z. et. al., 1988). Telah banyak laporan mengenai sifat-sifat fizikal superkonduktor sistem Tl ini. Meskipun begitu kajian terhadap superkonduktor sistem Bi dan Y adalah lebih meluas daripada sistem Tl. Ini adalah kerana kesulitan menyediakan bahan sistem Tl ini dengan kualiti yang tinggi. Penyediaan bahan sistem Tl dengan fasa tulen masih lagi menjadi satu cabaran (Torardi et. al., 1988 dan Junod A. et. al., 1989).

Sistem Tl boleh membentuk beberapa fasa umpamanya $Tl_2Ba_2Ca_2Cu_3O_y$ (2223) dengan $T_c = 118-125$ K, $Tl_2Ba_2CaCu_2O_y$ (2212) $T_c = 95 - 108$ K, $TlBa_2Ca_2Cu_3O_y$ (1223) $T_c = 100 - 110$ K dan beberapa lagi fasa yang lain. Beberapa kajian telah dijalankan untuk menghasilkan fasa 2223 tulen (Xin Y. et. al., 1991, Parkin S. S. P et. al., 1988, Liu, R. S. et. al., 1989 dan Narain S. et. al., 1989). Laporan ini akan membincangkan mengenai kaedah penyediaan optimum fasa 2212. Sebahagian daripada keputusan ini telah dibincangkan di dalam kertaskerja yang telah diterbitkan (Abd-Shukor, R., 1993). Sampel telah disediakan dengan kaedah tindakbalas keadaan pepejal. Keputusan pengukuran rintangan elektrik kaedah penduga empat titik dan corak pembelauan sinar-X di dalam bentuk serbuk dilaporkan. Kaedah penyediaan bahan 2212 ini dengan ketumpatan yang tinggi juga dibincangkan.

KAEDAH UJIKAJI DAN PERBINCANGAN

Sampel disediakan dengan kaedah tindakbalas keadaan pepejal. Serbuk tulen (99.99%) CaO, BaCO₃ dan CuO dengan komposisi permulaan Ba₂Ca₂Cu₃O_y dicampurkan dan dikisar supaya homogen dan dipanaskan pada suhu 900 °C selama 24 jam. Seterusnya Tl₂O₃ dicampurkan ke dalam bahan pelopor tadi untuk menghasilkan komposisi Tl₂Ba₂Ca₂Cu₃O_y dan dikisar. Bahan ini kemudiannya dimampatkan dengan penekan hidraulik menjadi pelet berdiameter 12.5 mm dan tebal 3 mm. Tekanan ~ 5,000-7,000 kg/cm² telah digunakan. Pelet ini dipanaskan pada suhu 910-925 °C di dalam relau selama 3-5 min dengan pengaliran oksigen dan kemudiannya disejukkan ke suhu bilik. Untuk

SUPERKONDUKTOR SUHU TINGGI $Tl_2Ba_2CaCu_2O_{8-\delta}$

Roslan Abd. Shukor
Jabatan Fizik,
Fakulti Sains Fisis dan Gunaan
Universiti Kebangsaan Malaysia
43600 Bangi, Selangor Darul Ehsan

ABSTRAK

Superkonduktor adalah sejenis bahan yang istimewa kerana kemampuannya membawa arus elektrik tanpa sebarang rintangan. Sifat ini membawa implikasi yang besar terhadap kegunaannya sebagai penjimat tenaga, peranti elektronik dan lain-lain kegunaan termaju. Superkonduktor suhu tinggi berasaskan $Tl_2Ba_2CaCu_2O_{8-\delta}$ yang ditemui pada tahun 1988 adalah stabil dengan suhu peralihan lebih kurang -168°C (105 K). Penyediaan bahan ini dengan ketulenan yang tinggi dan sifat-sifat yang sesuai untuk kegunaan meluas masih lagi menjadi masalah yang besar. Antara faktor penting di dalam penyediaan bahan ini ialah suhu dan masa pemanasan, komposisi permulaan dan bahan permulaan. Faktor-faktor ini telah dioptimumkan untuk menghasilkan bahan berkualiti tinggi. Satu teknik yang dipanggil pampasan talium telah digunakan untuk menghasilkan superkonduktor $Tl_2Ba_2CaCu_2O_{8-\delta}$ dengan ketumpatan yang tinggi ($> 80\%$ nilai teori) dan suhu peralihan -168°C (105 K).

Kata Kunci: ketumpatan, rintangan elektrik, pembelauan sinar-X, Mikroskop Elektron Imbasan, sintesis superkonduktor $Tl_2Ba_2CaCu_2O_{8-\delta}$

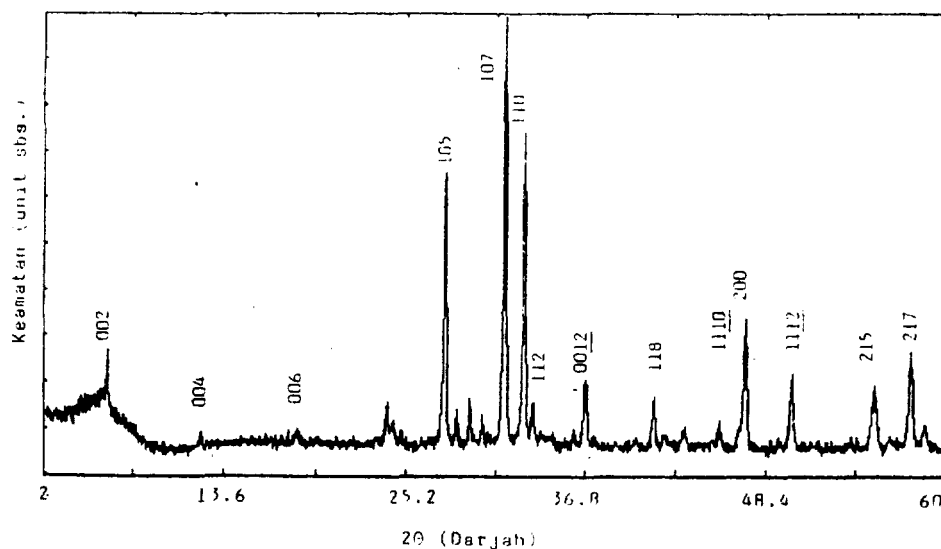
ABSTRACT

Superconductors are special materials because of their ability to conduct electricity without any measurable resistance. This property gives great implications on the application of these materials as energy saver, electronic devices and other advanced applications. The $Tl_2Ba_2CaCu_2O_{8-\delta}$ superconductor which was discovered in 1988 is a reproducible material with transition temperature of about -168°C (105 K). The preparation of this material with high purity and high density is still a major problem. Some of the important factors in preparing this material are the sintering temperature, sintering time, starting composition and starting materials. These factors have been optimized to produce high quality superconductor. The thallium compensation technique has been used to prepare high density ($>80\%$ of the theoretical value) $Tl_2Ba_2CaCu_2O_{8-\delta}$ superconductor with transition temperature of about -168°C (105 K).

Key Words: density, electrical resistance, X-ray diffraction, Scanning Electron Microscope, and synthesis of: $Tl_2Ba_2CaCu_2O_{8-\delta}$ superconductor.

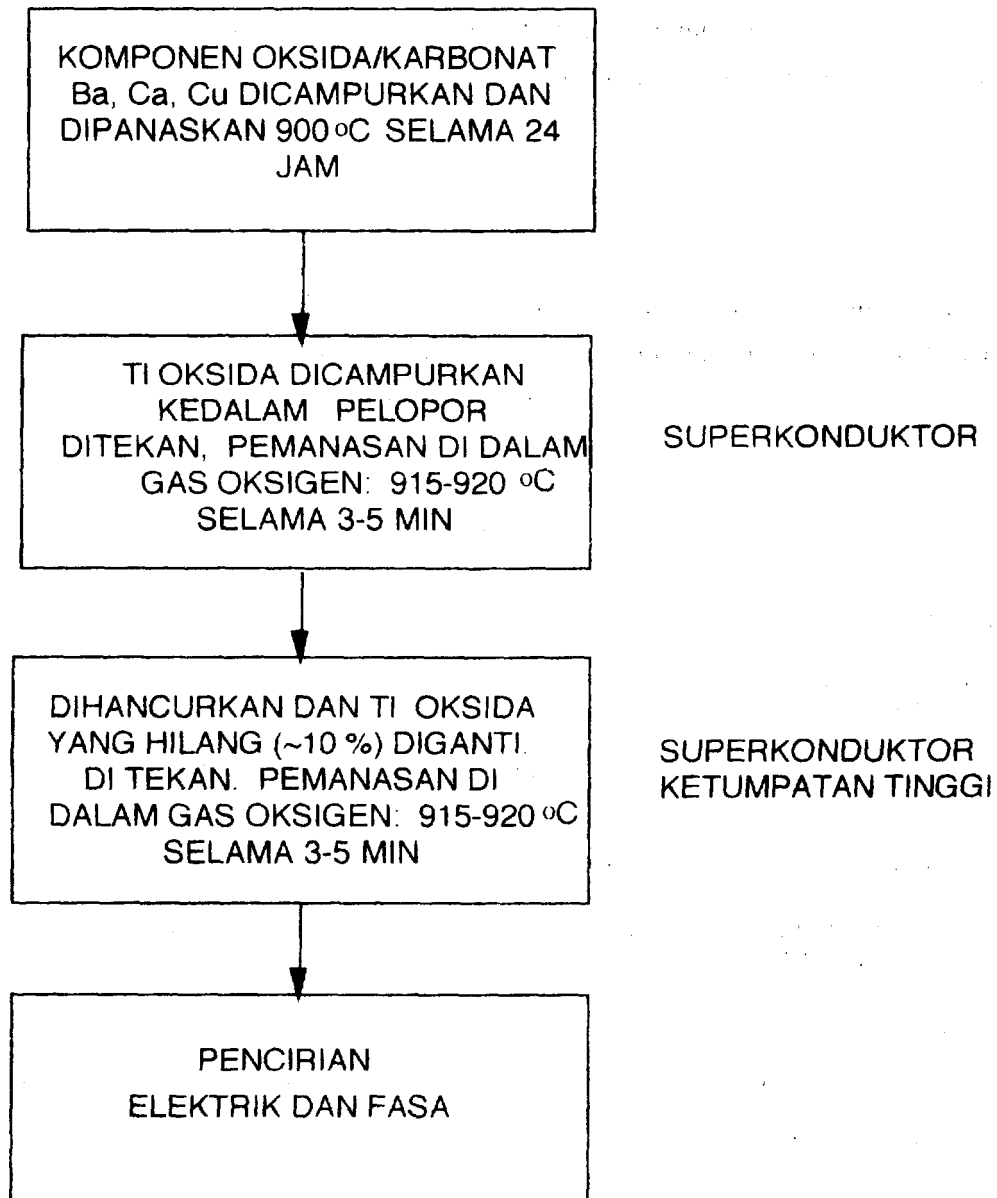
Pengukuran rintangan elektrik dijalankan dengan kaedah penduga empat titik arus terus. Cat perak telah digunakan sebagai sentuhan elektrik. Arus malar 50 mA - 100 mA telah digunakan di dalam semua pengukuran. Satu sistem kitar tertutup dari CTI Cryogenics model 22 dan pengawal suhu dari Lake Shore model 330 telah digunakan. Pembelaan sinar-X dijalankan dengan alat Siemens D 5000 menggunakan sumber Cu-K α .

Di dalam kajian ini dua puluh sampel telah disediakan. Corak pembelaan sinar-X (Rajah 2) menunjukkan hampir semua puncak pembelaan boleh diindekskan dengan unit sel tetragon (kumpulan ruang I4/mmm) dengan fasa 2212 dengan pemalar kekisi $a = 5.456 \text{ \AA}$ dan $c = 29.204 \text{ \AA}$.



Rajah 2. Corak pembelaan sinar-X serbuk bahan 2212 yang disediakan

mendapatkan bahan dengan ketumpatan yang tinggi, jumlah Ti_2O_3 yang meruap pada pemanasan awal dicampurkan semula dan bahan ini dikisar semula dan dijadikan pelet sebelum dipanaskan sekali lagi pada suhu $915 - 920^\circ C$ selama 3-5 min di dalam pengaliran oksigen. Oleh kerana talium adalah toksik, langkah-langkah keselamatan yang sewajarnya telah diambil semasa menyediakan sampel. Rajah 1 menunjukkan carta alir kaedah penyediaan bahan 2212 ini.



Rajah 1. Carta alir penyediaan bahan superkonduktor 2212

Mikrograf ini menunjukkan saiz butiran dan rongga berkurang pada bahan yang disepuhlindap dua kali dan secara langsung meningkatkan ketumpatan bahan.

Kajian ini menunjukkan bahawa superkonduktor sistem Ti-Ba-Ca-Cu-O fasa 2212 boleh disediakan dengan komposisi permulaan 2212. Suhu penyepuhlindapan 910-925 °C selama 3-5 minit di dalam pengaliran oksigen adalah sesuai untuk pembentukan dan penstabilan fasa 2212 ini. Teknik pampasan talium dapat meningkatkan ketumpatan bahan dan di dapati amaun talium yang merewap adalah sangat kecil pada pemanasan kali kedua kerana apabila talium telah berada di dalam fasa 2212 ia adalah stabil dan suhu yang tinggi tidak menunjukkan kesan yang ketara.

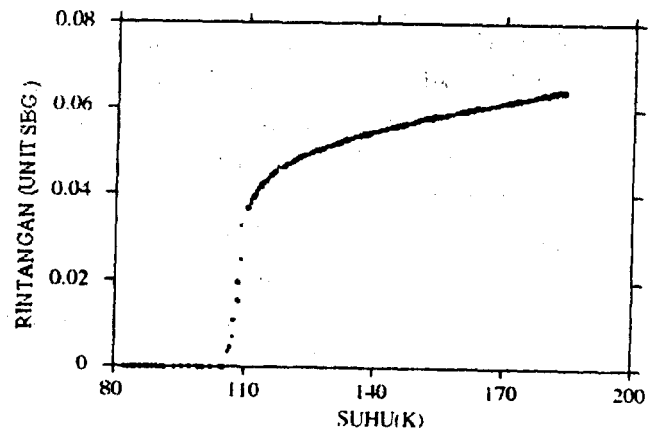
PENGHARGAAN

Penulis mengucapkan terima kasih kepada Pn. Rokiah Mohd. Yasin dan Amir Rohaizat Meor Razak yang telah membantu menjalankan kerja-kerja teknikal. Penyelidikan ini telah dibiayai oleh geran penyelidikan dari Universiti Kebangsaan Malaysia kod 101/92.

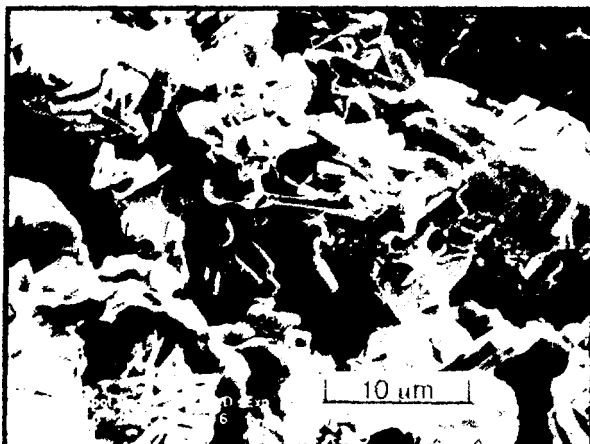
RUJUKAN

- Abd-Shukor, R. 1993. *J. Materials Sci. Lett.* **12**(18), 1428.
- Junod, A., Eckert, D., Triscone, G., Lee, V. Y. and Muller, J., 1989. *Physica C* **159**, 215.
- Liu, R.S., Wang W.N., Wu P. T., and C. T. Chang, 1989. *Physica C*, **162-164**, 113.
- Narain S. and Ruckenstein, 1989. *Supercond. Sci. Technol.*, **2**, 236.
- Parkin S.S. P., Lee V. Y., Nazzari, A. I., Savoy, R. and Beyers R., 1988. *Phys. Rev Lett.* **61**, 750.
- Sheng, Z.Z. and Hermann, A. M., 1988. *Nature* **332**, 138.
- Torardi, C.C., Subramaniam, A. M., Calabrese, J.C., Gopalakrishnan, J., Morrissey, K. J., Askew, T. R., Flippen, R. B., Chowdhry, U. and Sleight A. M., 1988. *Science* **240**, 631.
- Xin, Y., Li, Y.F., Gu, D.X., Pederson D. O., and Sheng Z. Z., 1991. *Physica C*, **184**, 185.

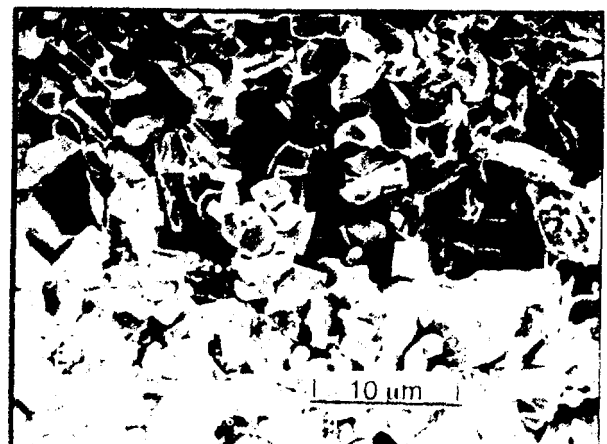
Pengukuran rintangan elektrik menunjukkan bahawa bahan ini mempunyai T_c pada suhu 105 K (Rajah 3). Pengukuran rintangan elektrik ke atas semua sampel superkonduktor yang dikaji menunjukkan bahan-bahan ini bersifat seperti logam pada keadaan biasa. Ketumpatan bahan di dapati meningkat daripada kurang dari 70 % ketumpatan teori kepada lebih daripada 80 % apabila Tl_2O_3 yang hilang diganti semula. Ketumpatan teori bahan ini ialah 7.48 g/cm^3 . Peningkatan ketumpatan ini boleh diterangkan dengan mikrograf dari Mikroskop Elektron Imbasan. Rajah 4(a) menunjukkan mikrostruktur bahan 2212 yang disepuhlindap hanya sekali dan Rajah 4.(b) menunjukkan mikrostruktur bahan yang telah digantikan Tl_2O_3 yang hilang dan disepuhlindap kali ke dua.



Rajah 3. Graf rintangan elektrik melawan suhu bahan 2212



Rajah 4(a) Mikrostruktur bahan 2212 disepuhlindap sekali.



Rajah 4(b) Mikrostruktur bahan 2212 melalui teknik pampasan talium dan disepuhlindap dua kali.

at large water content , a bilayer of oil swelled by water which gave the characteristic oily streaks texture. In this report we investigate mainly the lamellar region very near to the cubic phase and a hexagonal region with large water content along a particular water dilution line.

Experimentals

DDAB was purchased from Eastman Kodak Co. (Rochester, USA) and used without further purification. Its purity was confirmed by finding that the chain-melting point of this surfactant in the cubic phase to be around 18 deg. C. Deuterated water - 99 + % pure (purchased from Aldrich Co.) was used to provide contrast in the neutron scattering experiments which was done on the D16 spectrometer at the Institute Laue Langevin , Grenoble (contact person: Dr. P. Chieux). Octane was Gold Label from Aldrich Co. Samples with the following weight fraction of D₂O were prepared with DDAB/Octane = 3.15. C_s is the surfactant concentration given in mole and Q_{\max} is the wavevector corresponding to the first Bragg peak given in inverse Angstroms. Freeze-fracture electron microscopy was done at the Anatomy Department, Univ. of Cambridge. The samples were delivered into dimpled stubs which were slammed at high speed onto a cold (liquid nitrogen temperature) copper block at high speed (ca. 8000 K/ sec) . The samples were then kept on liquid nitrogen slush before being fractured (no etching was done) on a Balzers 300 unit and later coated with a carbon-platinum film. Observations of the films were done using a Philips EM-300 transmission electron microscope.

Samples	Weight fraction	C_s/Q_{\max}	Region
A	0.3579	8.522	Cubic
B	0.3726	9.5	
C	0.3868	9.321	
D	0.4254	9.044	
E	0.4594	11.55	Lamellar
F	0.4896	11.74	
G	0.5167	12.24	
H	0.5486	10.54	
I	0.576	12.148	
J	0.6231	11.74	
K	0.6426	11.09	

Ternary Lyotropic Liquid Crystals of Dodecyl Dimethyl Ammonium Bromide

Shahidan Radiman ¹ and Chris Toprakcioglu ²

1. Dept. of Nuclear Science, Universiti Kebangsaan Malaysia, Bangi 43600, Selangor D.E, MALAYSIA.
2. Polymer and Colloid Group, Cavendish Laboratory, Madingley Road, Cambridge CB3 0HE, U.K and
Dept. of Physics, University of Patras, GR- 26110, Patras, GREECE.

Introduction

Cubic phases of ternary liquid crystals have been intensely investigated in recent years. They are characterised by clear, ringing gel-like phase, with storage modulus as high as 10^6 Pa.s. Theoretical as well as experimental results show that this phase has very small population of defect structures. Ternary cubic phases are all bicontinuous, even though compositions containing the least amount of water can usually be considered as percolated droplets. In this way, the compositions of cubic phase containing the least amount of water are usually seen to give a single "correlation peak" (Bragg peak) in a small-angle X-ray or neutron intensity profile. Once connected (bicontinuous), this phase can be considered as consisting of constant mean curvature surfaces (CMC surfaces), and their Bragg peaks follow a certain signature depending on the levels of deuteration (contrast) as well as their symmetry. Most compositions of ternary cubic phase seems to start from about 20 up to 80 percent by weight of water. These figures cannot be explain by minimum and maximum packing of monodisperse spheres - even, knowing their bicontinuous structures and symmetries the maximum and minimum amount of solubilised water in this phase cannot be precisely predicted. Subtle interplay between entropy and curvature energies (Anderson and Gruner (1)) seem to control the symmetries of the crystallographic structures but it seems, mainly due to epitaxial relations, symmetry changes occur within a given Bonnet-related surfaces (Madafford et al (2), Anderson et al (3)), even though transitions between non-Bonnet-related surfaces cannot be rule out, like for e.g the existence of a re-entrant gyroid phase (Anderson, per. comm.). In this paper, we concentrate mainly on the off-cubic phase, namely the lamellar and the hexagonal phase. In DDAB (dodecyl dimethyl ammonium bromide) ternary systems it was found (Fontell et al (4)) that there existed two lamellar regions, one at low water content characterised by mosaic textures and another

Conclusions

We have shown that some of the off-cubic phases are quite interesting , especially the lamellar phase which showed characteristic color birefringence probably due to selective diffraction from their array of broken stacks of lamellar phases. Further experiments are underway to characterise the electric and magnetic properties of this phase with a view to possible use in display devices and sensors.

Acknowledgements

We thanked our contact person, Dr. Pierre Chieux for his help during the experiments and would like to wish him good luck on his recent retirement. Anthony Burgess at the Anatomy Dept., Univ. of Cambridge help with the freeze-fracture work and S.R would also like to thank Dr. Jeremy Skepper for useful discussions there. The Science and Engineering Research Council of U.K provide the necessary grant for the I.L.L trip.

References

1. D.M Anderson , S.M Gruner and S.Leibler, **Proc. Natl. Acad. Sci. USA. 85** , 5364 (1988)
2. P.J Madafford and C.Toprakcioglu , **Langmuir 9**, 2868 (1993)
3. D.M Anderson , H.T Davis, L.E Scriven and J.C.C Nitsche , **Adv. Chem.Phys. 77**, 337 (1990)
4. K.Fontell , A.Ceglie , B.Lindman and B.W Ninham , **Acta Chem. Scand. A40**, 247 (1986).
5. S.Radiman, C.Toprakcioglu and A.R Faruqi , **J. Phys. (France) 51**, 1501 (1990).

L	0.6604	11.55	Multiphase
M	0.6803	11.533	
N	0.698	12.28	
O	0.7384	11.82	Hexagonal
P	0.756	12.015	

Except for the cubic samples which were "tough" gels, the rest of the samples were soft gels and were delivered into a 1 mm Hellma cells using spatula and later slight warmed to get rid of air bubbles. The cubic samples were delivered at around 50 - 60 deg. C, when they were flowy. Once equilibrated to room temperature the samples were put on a 8-sample rack to run across the neutron beam. Typical samples take about 8-10 minutes, giving good counting statistics.

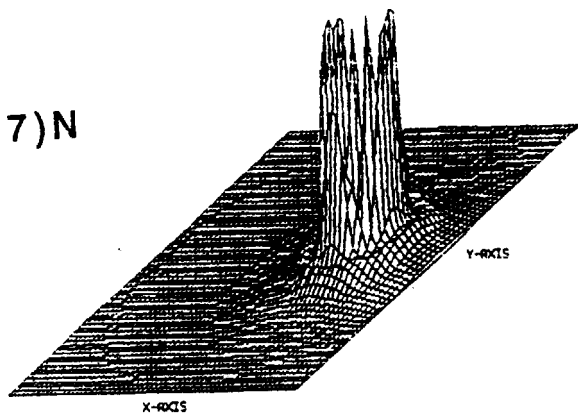
Results and discussions

Typical scattering results are given in figure 1a and b and the plot of C_s/Q_{\max} vs. water vol. fraction show that the cubic phase show a characteristic difference from the rest of the samples (fig. 2). From the scattering alone one would not be able to guess the symmetry of the phases, as most of them would give a single peak. In the case of the cubic phase they are easily characterised by spiky intensities. Other studies (Radiman et al (5)) have indicated that this is due to large crystallites formation on slow cooling. Surprisingly even then the random spikes still follow Friedel's law. To obtain good Bragg peaks cubic samples need to be quenched from high temperatures and before a powder scattering is taken. The lamellar samples were known from their optical textures as do the multiphase and hexagonal phase, which were further supported by freeze-fracture electron microscopy studies.

Figures 3a show the packed droplet structure of sample C and then broken lamellar were seen for samples E and G (fig 3b and 3c resp.) and the hexagonal phase O (fig. 3d). Optical studies also show that a range of colored birefringent phases occur starting with DDAB/Octane/D₂O = 36.84/11.69/51.47 (Bluish) through DDAB/Octane/D₂O = 31.8/10.1/58.1 (Yellowish) and various other shades in between.

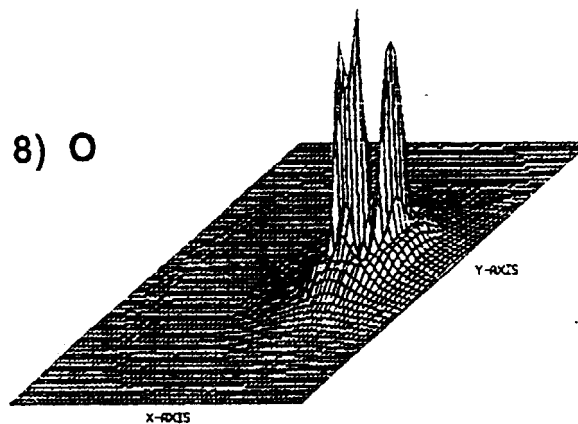
RUN NO.,EXT: 25137, 2
I(MAX) = 67248.000

7) N



RUN NO.,EXT: 25138, 2
I(MAX) = 76581.000

8) O



RUN NO.,EXT: 25139, 2
I(MAX) = 84886.000

9) P

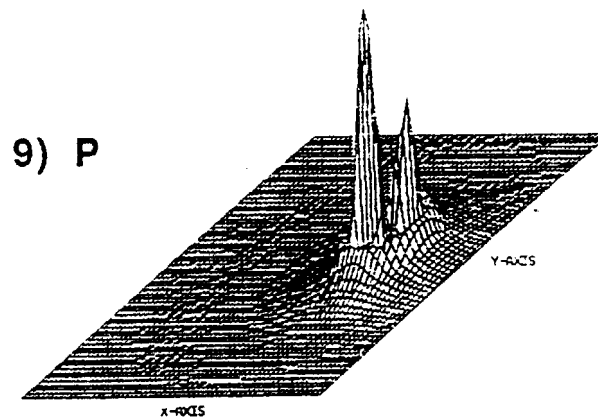
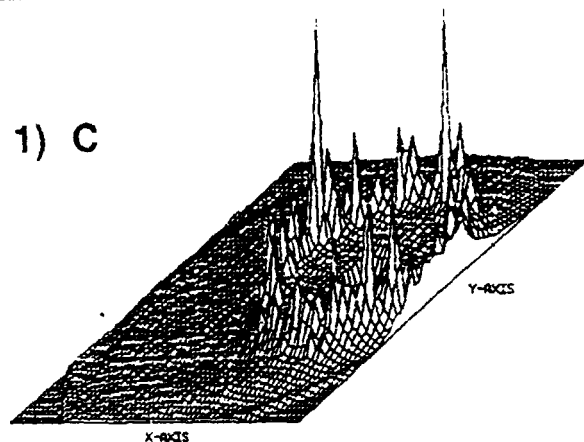


Fig. 1b.

As in fig. 1a. but for samples N, O and P.

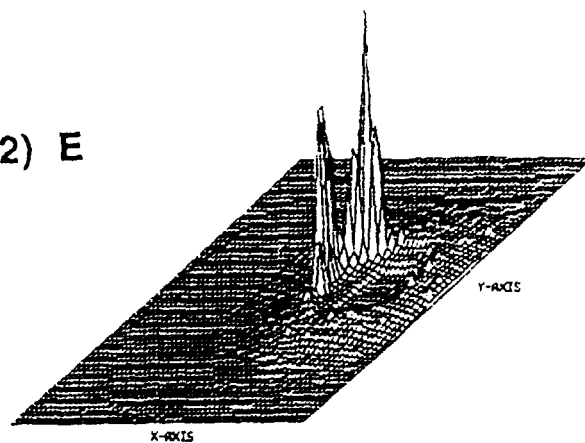
RUN NO.,EXT: 25181, 2
I(MAX) = 6335.000

1) C



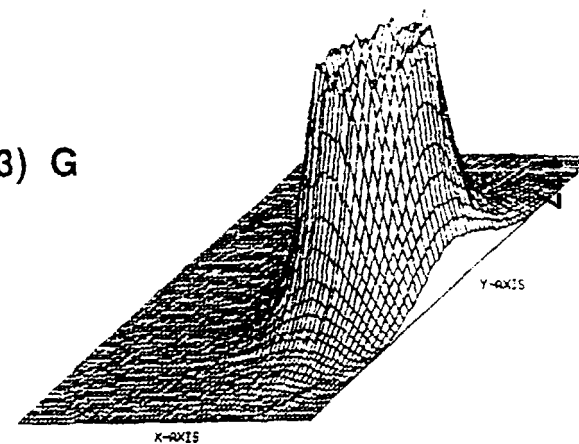
I(MAX) = 77242.000

2) E



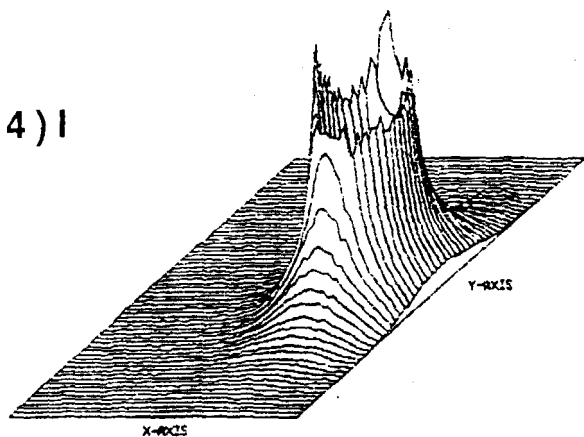
I(MAX) = 11258.000

3) G



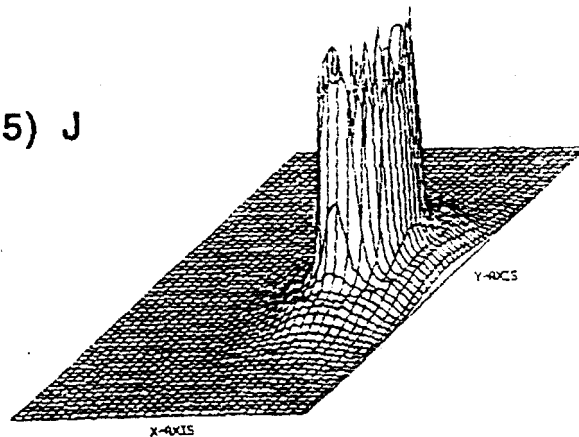
==>
-
RUN NO.,EXT: 25122, 1
I(MAX) = 23766.000

4) I



==> ==>
-
RUN NO.,EXT: 25122, 1
I(MAX) = 37226.000

5) J



RUN NO.,EXT: 25136, 2
I(MAX) = 56281.000

6) L

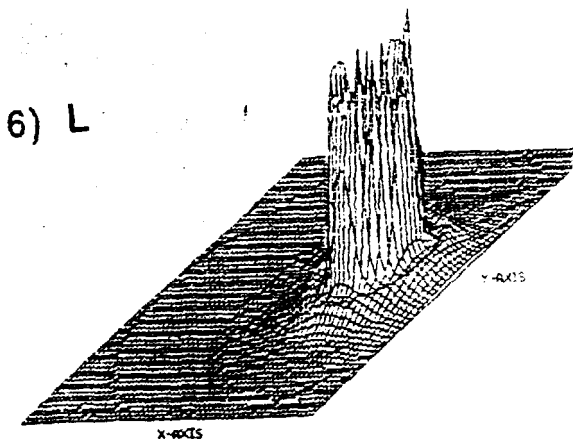


Fig.1 a.

Three-dimensional plots (Neutron intensities vertical) of the various samples C, E, G, I, J and L on the D_2O dilution along the DDAB/Octane = 3.15 wt. ratio dilution line. The x and y-axes are that of the detector.

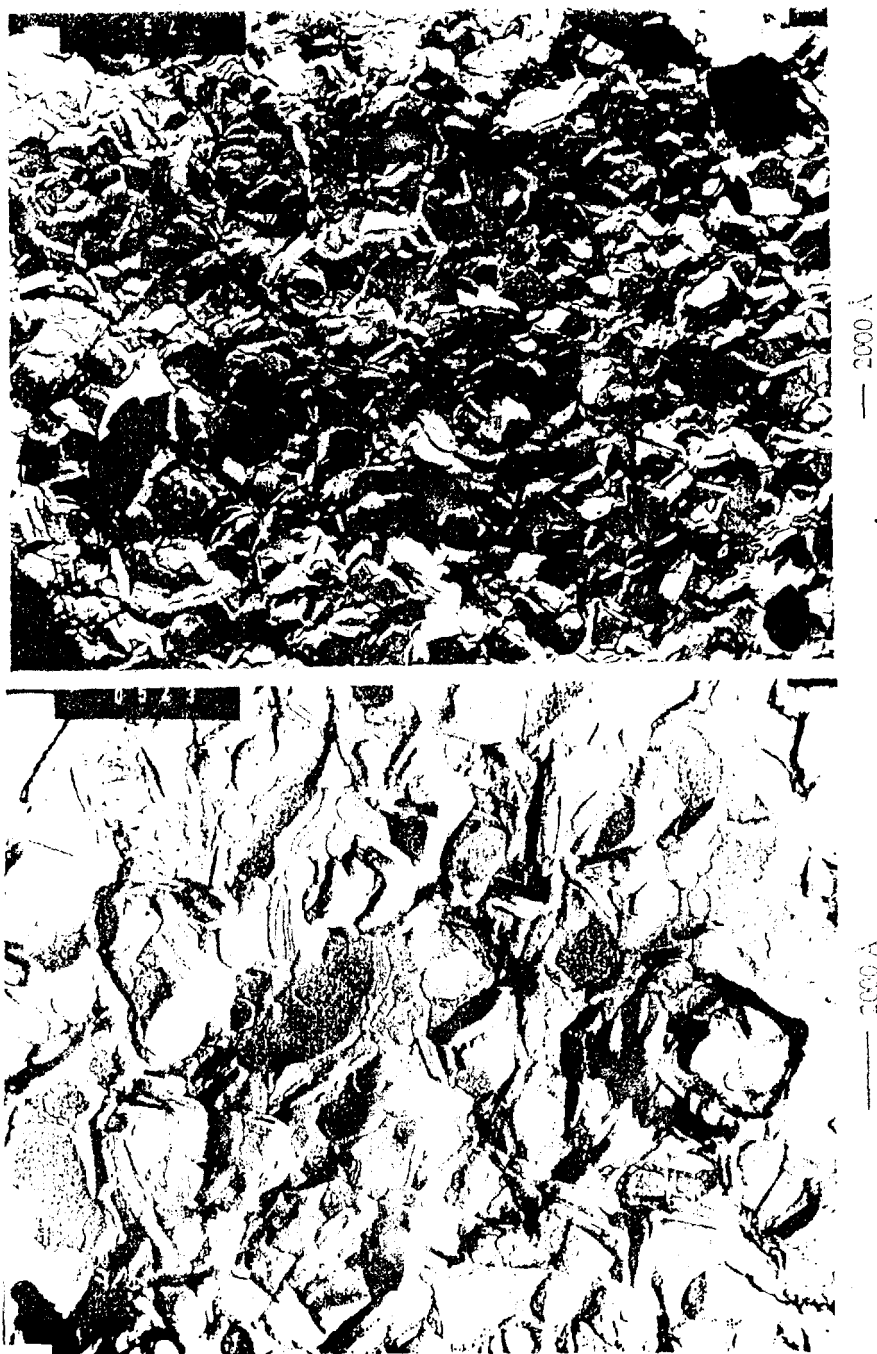


Fig. 3b (top) and 3c (bottom)

Freeze-fracture electron micrograph of sample E (top) and G (bottom) at magnifications of 28,600 and 75,000 respectively. Note the broken stacks of lamellar structures.

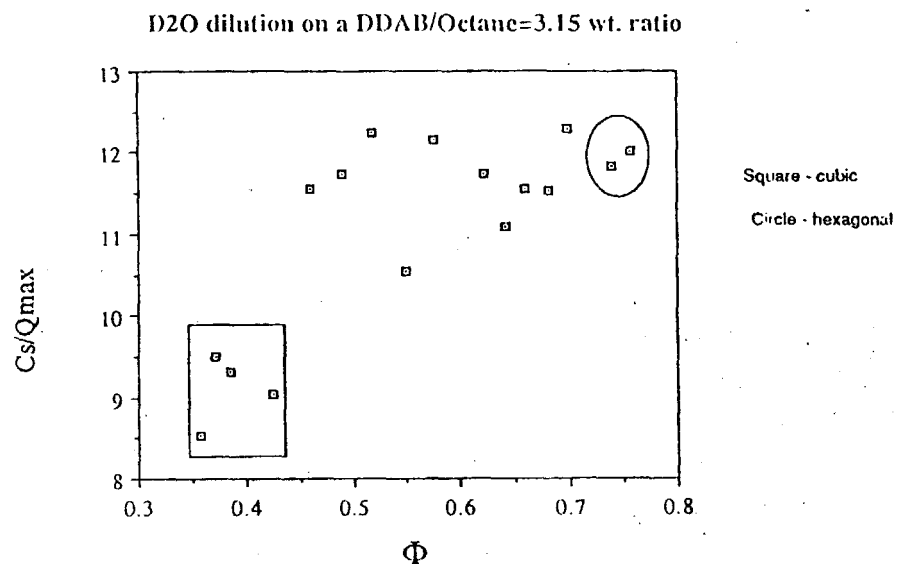


Fig. 2

C_s/Q_{max} (mol /Angs.) vs water volume fraction (Φ) plot. Note the characteristic small values for the cubic phase.



Fig.3a.

Freeze-fracture electron micrograph of sample C (in the cubic region) showing packed droplet structure. Magnification = 101,000.

PERBANDINGAN PENGHASILAN KARBON TERAKTIF DENGAN KAEDAH FIZIKAL DAN KAEDAH KIMIA

NORMAH MULOP DAN RAMLAN ABD AZIZ
Fakulti Kejuruteraan Kimia dan Kejuruteraan Sumber Asli
Universiti Teknologi Malaysia
Kuala Lumpur

ABSTRAK

Karbon teraktif daripada tempurung kelapa sawit telah dihasilkan dengan kaedah fizikal dan kaedah kimia di dalam loji pandu yang sama. Perbandingan penghasilan antara dua kaedah ini adalah dari segi kos pengoperasian, tempoh pengoperasian dan juga kualiti karbon teraktif. Kajian menunjukkan kos penghasilan karbon teraktif dengan kaedah fizikal adalah lebih rendah berbanding dengan kaedah kimia dan juga lebih rendah daripada harga pasaran karbon teraktif.

PENGENALAN

Terdapat beberapa kaedah boleh digunakan untuk menghasilkan karbon teraktif. Kaedah-kaedah utama ialah penghasilan secara fizikal, kimia dan gabungan fizikal- kimia.

Satu loji pandu untuk menghasilkan karbon teraktif dari bahan buangan pertanian seperti tempurung kelapa dan tempurung kelapa sawit telah direkabentuk dan dibina di UTM, Kuala Lumpur. Loji pandu tersebut dengan muatan maksimum 27 kg bahan mentah berkeupayaan menghasilkan karbon teraktif berbutir dengan kaedah fizikal dan juga kaedah kimia. Bahan suap yang digunakan dalam kajian ialah tempurung kelapa sawit. Kaedah fizikal melalui 2 langkah untuk menghasilkan karbon teraktif. Langkah pertama ialah proses pengkarbonan kepada arang dan diikuti dengan proses pengaktifan arang kepada karbon teraktif. Stim digunakan sebagai media pengaktifan. Kaedah kimia pula menggunakan bahan kimia seperti asid fosforik yang digaulkan dengan bahan mentah sebelum bahan mentah tersebut dikarbonkan kepada karbon teraktif. Kaedah gabungan fizikal-kimia menggunakan stim ke atas karbon teraktif yang telah dihasilkan secara kimia. Dengan itu karbon teraktif kaedah kimia mengalami proses pengaktifan lanjut.

Perbandingan dilakukan dari segi ekonomi, tempoh pengoperasian dan juga kualiti karbon teraktif yang dihasilkan.

KAEDAH

Bahan mentah yang telah digunakan ialah tempurung kelapa sawit. Dua kaedah penghasilan karbon teraktif telah dijalankan iaitu secara fizikal dan secara kimia.

a) Penghasilan karbon teraktif dengan kaedah fizikal.

Proses pengkarbonan di dalam loji pandu dijalankan selama 5 jam pada suhu 450°C bagi memastikan semua bahan mentah bertukar kepada arang. Arang yang telah sejuk seterusnya diaktifkan dengan menggunakan stim pada suhu 800°C selama 1 jam.

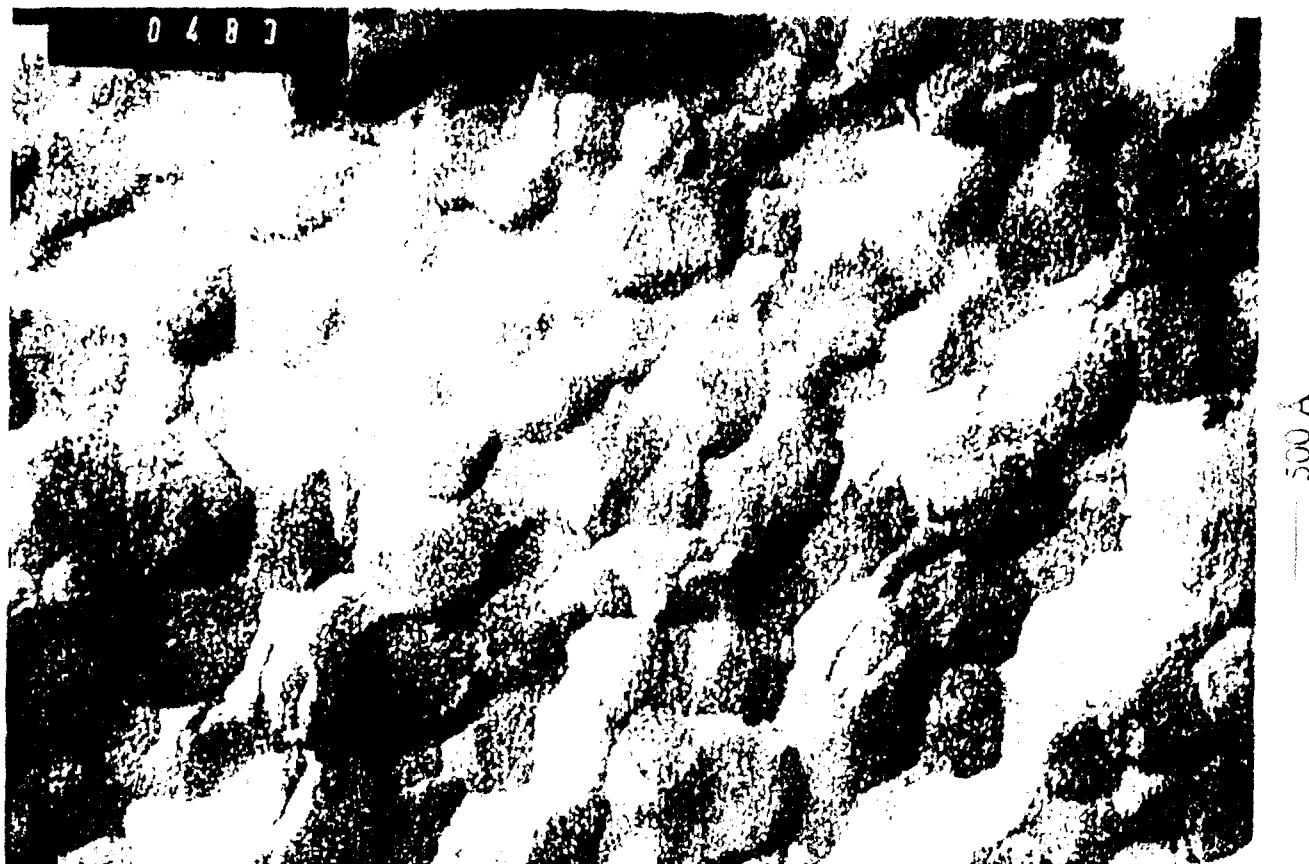


Fig. 3d

Freeze-fracture electron micrograph of sample O (hexagonal phase).
Magnification= 234,000 .

kajian menggunakan larutan bahan tersebut hanya sekali. Kos penghasilan karbon teraktif kaedah kimia boleh dikurangkan dengan menggunakan larutan asid dan larutan alkali NaOH berulang kali. Kepekatan asid dan kepekatan alkali perlu diselaraskan setiap kali proses percampuran asid dengan bahan mentah dan juga basuhan karbon teraktif dijalankan.

Kos penghasilan stim bergantung kepada ciri-ciri dandang yang digunakan seperti kecekapan dandang serta suhu dan tekanan pengoperasian dandang, suhu air suapan dandang dan kadar alir bahan api. Kajian ini menggunakan dandang John Thompson dengan muatan 15,000 lb/jam yang telah berusia 20 tahun. Muatan dandang adalah lebih besar daripada keperluan proses menyebabkan penghasilan stim dan penggunaan stim tidak ekonomi.

Terdapat kajian penyelidikan menghasilkan karbon teraktif dengan kaedah kimia menggunakan bahan kimia zink klorida sebagai bahan tambah pengaktifan. Kajian-kajian ini menggunakan nisbah bahan mentah kepada zink klorida yang berlainan. Jadual II menunjukkan hubungan nisbah bahan mentah kepada zink klorida dan kos zink klorida yang diperlukan dalam penghasilan karbon teraktif. Kos ini tidak termasuk kos bahan kimia lain, kos tenaga untuk proses pengkarbonan, kos proses peneutralan asid dan kos pengeringan karbon teraktif. Peratus pertukaran bahan mentah kepada karbon teraktif dianggap sama dengan kajian yang diperolehi daripada loji pandu iaitu 35 %. Daripada kos bahan kimia sahaja menunjukkan kos penghasilan karbon teraktif amat mahal jauh melebihi harga pasaran karbon teraktif. Dengan itu nisbah bahan mentah kepada bahan kimia yang digunakan adalah tidak praktikal.

JADUAL II: Hubungan Kos Zink Klorida dan Nisbah Baham Mentah:Zink Klorida

Nisbah bahan mentah:zink klorida	Kos zink klorida, RM
<p>1:1 (1kg:1kg) (Mohd Zubir et al, 1994)</p> <p>1:2.6 (1 kg:2.6kg) (Asiah et al, 1991)</p>	kos zink klorida (gred industri) 72.00/kg
	kos zink klorida 72.00/kg bahan mentah
	kos zink klorida 206.00/kg karbon teraktif
	kos zink klorida 187.20/kg bahan mentah
	kos zink klorida 534.80/kg karbon teraktif

Di samping kos bahan kimia yang mahal, kaedah kimia melibatkan kos penghasilan yang lebih tinggi kerana ia memerlukan aktiviti yang lebih banyak dan tempoh yang lebih lama (hampir sekali ganda) sebelum hasil karbon teraktif sedia untuk dibungkus. Jadual III menunjukkan perbandingan tempoh proses penghasilan karbon teraktif antara kaedah fizikal dan kaedah kimia. Tempoh yang lebih lama melibatkan penghasilan yang lebih rendah bagi kadar per hari pengoperasian.

Jadual IV menunjukkan perbandingan luas permukaan tentu karbon teraktif daripada kedua-dua kaedah yang dijalankan. Kaedah kimia memberi nilai luas permukaan tentu yang lebih tinggi berbanding dengan kaedah fizikal. Terdapat beberapa faktor yang mempengaruhi luas permukaan tentu karbon teraktif. Bagi kaedah fizikal, antara faktor yang terlibat ialah jangka masa pengaktifan dan kadar alir stim. Faktor yang mempengaruhi kaedah kimia pula ialah kepekatan asid yang digunakan. Rajah 1 dan Rajah 2 masing-masing menunjukkan struktur permukaan karbon teraktif daripada kaedah fizikal dan kaedah kimia. Liang-liang jelas kelihatan di permukaan kedua-dua jenis karbon teraktif tersebut.

b) Penghasilan karbon teraktif dengan kaedah kimia.

Bahan mentah tempurung sawit direndam di dalam larutan asid fosforik. Bahan mentah tersebut diasingkan daripada larutan asid dan dikeringkan dengan menggunakan matahari sebelum dikarbonkan pada suhu 450°C selama 3 jam.

Karbon teraktif terhasil disejukkan dan dibasuh dengan larutan beralkali NaOH dan kemudian dibasuh pula dengan air bagi mengurangkan abuk dan keasidan karbon teraktif. Seterusnya karbon teraktif yang telah dibasuh dikeringkan di dalam ketuhar pada suhu 105°C selama sekurang-kurangnya 4 jam untuk mengurangkan kandungan air.

Pengujian kualiti dijalankan dengan penentuan luas permukaan tentu dan juga penelitian struktur permukaan karbon teraktif tersebut.

KEPUTUSAN DAN PERBINCANGAN

Proses pengkarbonan daripada loji pandu menghasilkan antara 0.3-0.35 kg arang bagi setiap kg bahan mentah yang digunakan dan pengaktifan fizikal menghasilkan 0.9 kg karbon teraktif per kg arang yang diaktifkan (Mahadzir et al, 1991). Pengaktifan kimia pula memperolehi antara 0.3-0.35 kg karbon teraktif daripada 1 kg bahan mentah yang digunakan (Arbain et al, 1992). Perbandingan kos penghasilan merangkumi kos bahan api, kos bahan kimia dan kos tenaga proses pengeringan karbon teraktif tidak termasuk kos loji pandu serta buruh adalah seperti yang ditunjukkan dalam Jadual 1.

JADUAL I: Perbandingan Kos Penghasilan Karbon Teraktif

KAEDAH FIZIKAL		KAEDAH KIMIA	
kos bahan api 5 jam	RM 1.50/kg arang	kos bahan api 3 jam	RM 1.20/kg karbon teraktif
proses pengkarbonan		proses pengkarbonan	
kos bahan api 1 jam	RM 1.18/kg karbon teraktif	kos asid fosforik (berlainan kepekatan asid)	RM 40-70/kg karbon teraktif
proses pengaktifan		kos NaOH	RM 0.85/kg karbon teraktif
kos penghasilan stim	~ RM 0.15/kg karbon teraktif	kos air basuhan (kadar industri)	RM 0.10/kg karbon teraktif
		kos tenaga ketuhar pengeringan	~ RM 0.30/kg karbon teraktif
Jumlah	RM 2.83/kg karbon teraktif	Jumlah	~ RM 42-73/kg karbon teraktif
kos karbon teraktif serbuk dalam pasaran RM 24.00/kg (Hai-Ou Company Sdn. Bhd., 1994)			

Jadual I menunjukkan kos pengoperasian untuk menghasilkan karbon teraktif dengan kaedah fizikal dan kaedah kimia ialah RM 2.83/kg dan RM 42-73 /kg masing-masing. Kos bahan api proses pengaktifan bagi kaedah fizikal boleh dikurangkan dengan melakukan proses tersebut seurus selepas proses pengkarbonan selesai tanpa menyejukkan arang yang dihasilkan. Kos asid fosforik dan kos NaOH sangat tinggi kerana

2. Kaedah kimia memberi luas permukaan tentu yang lebih tinggi berbanding dengan kaedah fizik.
3. Penjimatan kos penghasilan boleh dilakukan dengan mengubahsuai sistem pemprosesan yang terlibat seperti menggunakan haba buangan dalam gas serombong dan penggunaan penjana stim yang sesuai dengan keperluan proses.

PENGHARGAAN

Terima kasih kepada IRPA dan Unit Penyelidikan dan Pembangunan, Universiti Teknologi Malaysia yang telah memberikan sumber kewangan bagi membolehkan projek ini dilaksanakan. Juga pengarang ingin mengucapkan terima kasih kepada juruteknik-juruteknik Fakulti Kejuruteraan Kimia dan Kejuruteraan Sumber Asli Arshad Abu Hassan, Suid Sahman dan Yahya Khalid yang telah banyak membantu dalam penyelidikan ini.

RUJUKAN

1. Mahadzir Aziz, Normah Mulop dan Ramlan Abd Aziz (1991), Penghasilan Karbon Teraktif Secara Fizik. Projek Sarjana Muda Kejuruteraan Kimia, Universiti Teknologi Malaysia.
2. Arbain Ramli, Normah Mulop dan Ramlan Abd Aziz (1992), Penghasilan Karbon Teraktif Melalui Kaedah Fizik Dan Kimia. Projek Sarjana Muda Kejuruteraan Kimia, Universiti Teknologi Malaysia.
3. Maklumat daripada HAI-OU Company Sdn. Bhd. (1994)
4. Mohd Zobir Hussein, Zulkarnain Zainal, Lau Ai Ai dan Badri Muhammad, (PORIM, 1994), Penggunaan Garam-garam Kalium sebagai Agen Pengaktifan Kimia bagi Penyediaan Karbon Teraktif daripada Serepai Batang Kelapa Sawit.
5. Asiah Hussain, Rahmalan Ahmad dan Ramlan Abd Aziz, (1991). Penjerapan Bahan Berwarna Oleh Tanah Gambut Terubahsuai dan Karbon Diaktifkan. Bul. Kim. Jil. 3, m.s. 132-146.

JADUAL III: Perbandingan Tempoh Proses Penghasilan Karbon Teraktif

KAEDAH FIZIKAL		KAEDAH KIMIA	
Pengkarbonan	5 jam	Pencampuran dengan bahan kimia	0.5 jam
Pengaktifan	1 jam	pengeringan bahan kimia (matahari)	4 jam
Penyejukan karbon teraktif	2 jam	Pengkarbonan	3 jam
		Penyejukan karbon teraktif	2 jam
		Peneutralan asid (basuhan)	0.5 jam
		Pengeringan karbon teraktif	> 4jam
Jumlah	8 jam	Jumlah	>14 jam

JADUAL IV: Perbandingan Luas Permukaan Tentu Karbon Teraktif

KAEDAH	LUAS PERMUKAAN TENTU, m ² /g
Kaedah fizikal	~ 500
Kaedah kimia	600 -750

Selain daripada kos penghasilan yang tinggi, kaedah kimia melibatkan beberapa masalah seperti:

- 1- Kakisan pada alatan disebabkan oleh bahan kimia (asid) yang digunakan.
- 2- Pencemaran udara yang lebih teruk disebabkan oleh pewapan bahan kimia semasa proses pengkarbonan.
- 3- Air basuhan karbon teraktif perlu dirawat sebelum dibuang atau digunakan semula. Ini melibatkan kos tambahan dan juga masa.

Penjimatan boleh dilakukan dengan menggunakan haba yang terdapat dalam gas serombong relau pemanasan. Gas panas tersebut terutama semasa proses pengaktifan (suhu >800°C) boleh digunakan untuk mengeringkan bahan mentah, mengeringkan karbon teraktif (kaedah kimia) dan juga memanaskan air suapan dandang (kaedah fizikal). Penjana stim yang sesuai dengan keperluan proses pengaktifan juga perlu dipertimbangkan untuk mengelakkan pembaziran stim dan kos.

KESIMPULAN

1. Kos penghasilan karbon teraktif dengan kaedah fizikal adalah lebih rendah berbanding dengan kaedah kimia dan juga harga pasaran karbon teraktif. Dengan itu kaedah fizikal boleh dimajukan ke peringkat komersial.

INTERAKSI MINERAL-REAGEN DALAM SISTEM PENGAPUNGAN STRUVERIT FOSFONIK

Hisham Bin Jabar dan Karnarudin Bin Hussin
 Pusat Pengajian Kejuruteraan Bahan dan Sumber Mineral
 Universiti Sains Malaysia
 Kampus Cawangan Perak
 31750 Tronoh
 Perak

ABSTRAK

Fenomena pengapungan mineral dalam bidang pemprosesan mineral telah diselidiki melalui sistem pengapungan Struverit-Fosfonik. Kajian ini dijalankan dengan melihat kepada maklumat-maklumat yang diperolehi daripada hasil ujikaji pengapungan tiub 'Hallimond', penentuan nilai ketumpatan penjerapan dan penentuan nilai keupayaan 'Zeta'.

Daripada hasil kajian di dapati bahawa reagen pengumpul asid fosfonik merupakan reagen pengumpul yang sesuai untuk mengapungkan mineral struverit. Kajian pengapungan menunjukkan bahawa nilai optima pengapungan mineral berlaku di sekitar nilai pH 3. Pertambahan nilai pH mengakibatkan pengurangan hasil pengapungan. Pertambahan kepekatan reagen pengumpul semasa pengapungan meningkatkan prestasi keapungan mineral.

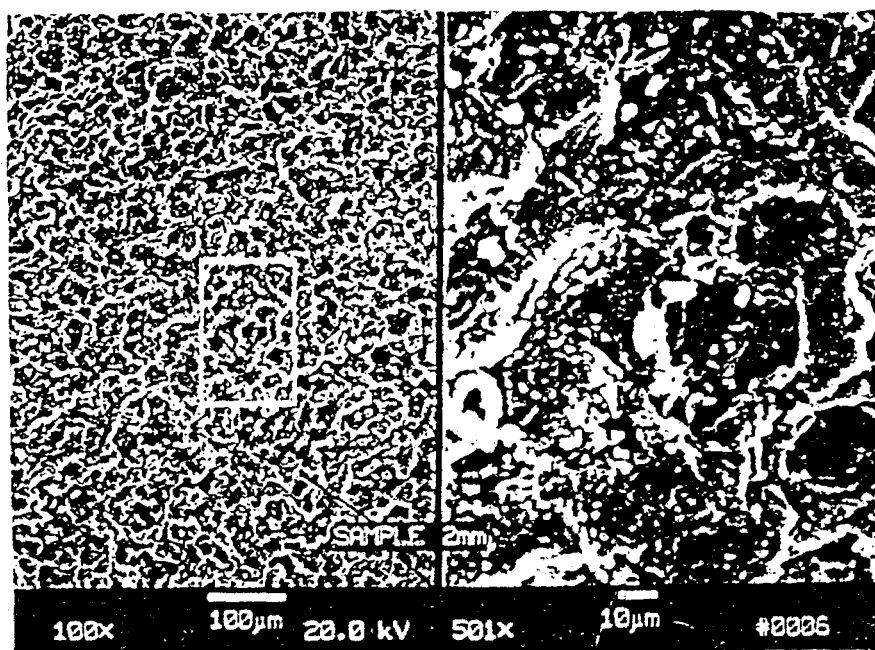
Melalui kajian penjerapan, hasil ujikaji menunjukkan bahawa titik optima penjerapan berada di sekitar pH 3. Pertambahan nilai pH mengurangkan nilai ketumpatan penjerapan pengumpul. Pertambahan dalam nilai kepekatan pengumpul dilihat meningkatkan keupayaan penjerapan pengumpul ke atas permukaan mineral.

Berdasarkan nilai keupayaan *zeta* yang diperolehi melalui kaedah elektroforesis, titik iso-elektrik dipercayai berada disekitar pH 2. Nilai *zeta* juga di dapati berkurangan dengan pertambahan nilai pH.

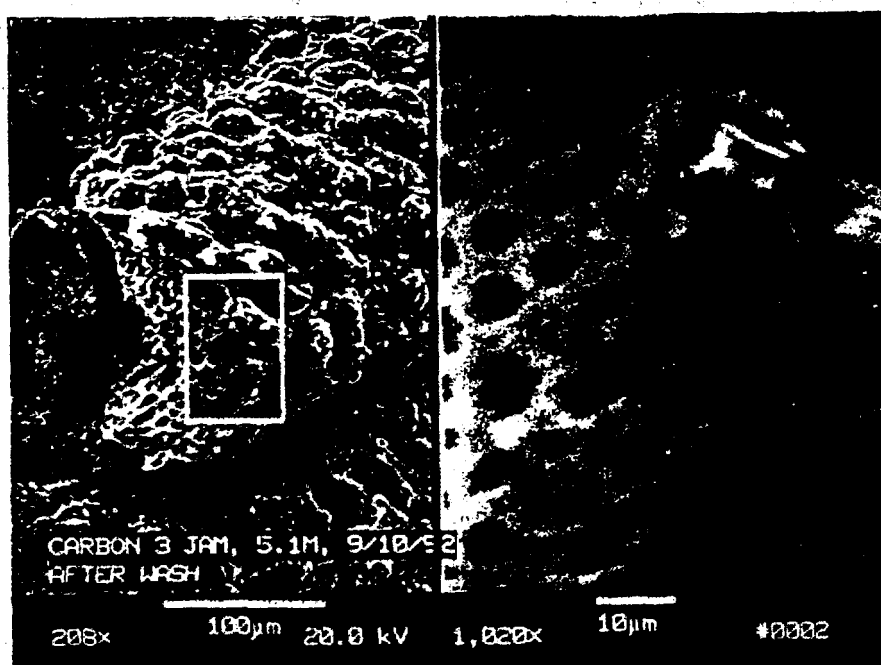
PENGENALAN

Pengapungan merupakan suatu proses pemisahan di mana partikel-partikel yang mempunyai komposisi bahan yang berlainan dipisahkan berdasarkan sifat-sifat hidrofilik dan hidrofobik permukaan partikel tersebut. Dalam proses ini, partikel-partikel yang mempunyai sifat permukaan yang hidrofobik akan bersentuhan dengan gelembong-gelembong udara. Partikel-partikel ini kemudiannya akan diangkat ke permukaan air dan meninggalkan partikel-partikel yang berpermukaan hidrofilik di dalam air.

Proses ini biasanya digunakan dalam bidang pemprosesan mineral. Kebanyakan mineral-mineral sulfida, mineral-mineral garam, mineral feldspar dan arang batu diproses menggunakan kaedah ini. Dengan menggunakan kaedah pengapungan mineral, bijih-bijih bergred rendah dapat dikonsentratkan untuk mendapatkan gred bijih yang lebih tinggi. Proses ini merupakan antara kaedah pemisahan yang penting buat masa ini kerana gred-gred bijih yang dilombong semakin rendah nilainya. Berdasarkan kepada keupayaan kaedah ini untuk menghasilkan konsentrat-konsentrat bijih yang lebih tinggi grednya daripada



RAJAH I: Struktur Permukaan Karbon Teraktif Kaedah Fizik



RAJAH II: Struktur Permukaan Karbon Teraktif Kaedah Kimia

Kajian penjerapan reagen pengumpul keatas mineral pula telah dijalankan dengan 1 gram sampel diadukkan bersama 200ml reagen pengumpul dalam masa pengadukan selama 1 jam. Sampel pengadukan kemudiannya telah dituras dengan menggunakan alat penuras milipore untuk mendapatkan larutan sampel yang tertinggal. Larutan sampel tersebut kemudiannya diuji menggunakan kaedah spektrometri ultra-lembayung untuk mendapatkan perbezaan kepekatan dan seterusnya ketumpatan penjerapan sistem struverit-fosfonik. Penjerapan untuk suhu-suhu yang berlainan telah dijalankan dalam tangki air panas dengan kaedah penjerapan yang sama.

Kajian keupayaan *zeta* telah dijalankan dengan bantuan alat mikroelektroforesis MK11 keluaran syarikat Rank Brothers dengan menggunakan kaedah sel rata (*flat cell method*).

KEPUTUSAN DAN PERBINCANGAN

Pengapungan

Rajah 1.0 menunjukkan keputusan ujikaji pengapungan mineral pada nilai pH yang berlainan. Daripada graf tersebut, proses pengapungan mineral lebih berkesan pada nilai pH yang lebih rendah. Peningkatan nilai pH menunjukkan pengurangan dalam prestasi pengapungan mineral. Nilai maksima pengapungan di dapati berada disekitar pH 3. Hasil pengapungan kemudiannya di dapati berkurangan untuk pH 5 dan seterusnya. Lengkok ini menunjukkan sedikit persamaan dengan hasil kerja Senior (1985) dan Kamarudin dan Khangoankar (1993). Senior (1985) menguji keterapungan mineral kassiterit dengan pengumpul asid fosfonik dan mendapati bahawa kesan pertambahan nilai pH mengurangkan prestasi pengapungan mineral. Kamarudin dan Khangoankar (1993) menguji keterapungan mineral struverit dengan menggunakan pengumpul sulfosuksinamat juga mendapati kesan parameter pH yang serupa.

Pertambahan kepekatan seperti yang ditunjukkan dalam rajah 2.0 menunjukkan bahawa pertambahan kepekatan pengumpul dapat meningkatkan hasil pengapungan. Keadaan ini dapat dilihat dengan pertambahan hasil pengapungan untuk nilai-nilai kepekatan 0.01mM, 0.07mM, 0.15mM dan 0.5mM. Hasil pengapungan di dapati meningkat dengan banyaknya pada julat 0.01mM hingga 0.15mM. Peningkatan hasil pengapungan juga dapat dilihat untuk kepekatan pengumpul dalam julat antara 0.15mM hingga 0.5mM tetapi ianya tidak begitu ketara seperti julat sebelumnya.

Penjerapan

Melalui Rajah 3.0, hasil ujikaji penjerapan mencadangkan kesan yang sama dengan hasil ujikaji pengapungan untuk parameter pH. Dalam rajah ini, paksi ketumpatan penjerapan telah ditukar kepada paksi logaritma untuk mendapatkan gambaran yang lebih jelas saling kait antara hasil ujikaji penjerapan dan pengapungan mineral. Ketumpatan penjerapan yang lebih tinggi diperolehi pada nilai pH yang lebih rendah dengan penurunan terhadap ketumpatan penjerapan berlaku apabila nilai pH bertambah. Ketumpatan penjerapan di dapati maksima pada nilai pH 3. Hasil ujikaji ini mempunyai persamaan dengan kajian penjerapan fosfonik asid keatas mineral kassiterit yang telah dibuat oleh Wottgen (1969).

Ketumpatan penjerapan juga di dapati bertambah dengan pertambahan nilai kepekatan reagen pengumpul yang digunakan. Seperti yang dipaparkan dalam gambarajah 4.0, nilai ketumpatan penjerapan di dapati meningkat apabila kepekatan pengumpul ditingkat daripada 0.01mM kepada 0.15mM.

Menerusi kajian perbezaan suhu seperti yang ditunjukkan dalam gambarajah 5.0, ketumpatan penjerapan di dapati berkurangan pada suhu 40°C dan meningkat semula untuk suhu 50°C. Berdasarkan keputusan ini terdapat kemungkinan bahawa proses penjerapan akan mengalami perubahan daripada proses penjerapan fizikal kepada proses penjerapan kimia. Oleh kerana ketumpatan penjerapan hanya akan meningkat apabila

bijih-bijih bergred rendah, proses pengapungan ini dijangka akan menjadi suatu proses yang utama dalam bidang pemprosesan mineral di masa-masa akan datang.

Selain daripada mineral-mineral yang semulajadi bersifat hidrofobik, mineral-mineral hidrofilik juga dapat diapungkan dengan menggunakan reagen pengumpul yang berupaya menjerap ke permukaan mineral untuk memberikan suatu lapisan hidrofobik ke permukaan mineral tersebut untuk membantu pengapungan. Hasil interaksi mineral-reagen ini akan mengubah sifat fisio-kimia permukaan mineral tersebut dan mewujudkan satu keadaan di mana dalam proses ini, reagen-reagen pengumpul yang mempunyai ciri-ciri kimia yang tertentu berupaya bersentuh dengan permukaan mineral dan dalam masa yang sama menyediakan suatu permukaan yang hidrofobik yang cukup stabil untuk membolehkan gelembong-gelembong udara bersentuhan dan membawa mineral naik ke permukaan air.

Selain daripada digunakan secara meluas dalam bidang pemprosesan mineral, kaedah ini juga telah mula mendapat perhatian daripada bidang-bidang lain seperti bidang bioteknologi dan kejuruteraan alam sekitar. Dalam bidang bioteknologi, proses pengapungan ini digunakan dengan bantuan beberapa proses lain untuk mengapungkan mikro-organisma-mikro-organisma yang dibiakkan didalam *fermentor* untuk mengekalkan kadar pertumbuhan mikro-organisma tersebut. Dalam bidang bioteknologi ini dua kaedah yang biasa digunakan adalah kaedah pengapungan udara-terlarut dan pengapungan-elektro.

Dalam bidang kejuruteraan alam sekitar, pengapungan digunakan untuk merawat air kumbahan dan air hampas. Dengan bantuan proses pengapungan, pemisahan bahan-bahan sisa seperti gentian-gentian kertas, gumpalan-gumpalan lumpur atau gumpalan-gumpalan minyak dapat dilakukan.

Selain daripada proses-proses pengapungan yang melibatkan persentuhan gelembong-gelembong udara dan permukaan partikel untuk mengapungkan bahan-bahan tersebut terdapat juga beberapa proses pengapungan lain yang menggunakan gas nitrogen dan sebagainya yang mana dalam hal ini interaksi antara partikel dan gelembong-gelembong udara tidak berlaku sebaliknya interaksi lebih kepada interaksi ion-ion dan gelembong udara.

SAMPEL, REAGEN DAN TATACARA UJIKAJI

Sampel

Sampel mineral struverit telah di dapati daripada kilang anang B.E.H. Mineral Bhd., Perak. Bahan tersebut yang merupakan hasil konsentrat beberapa siri proses pemisahan graviti, magnetik dan elektrostatik telah kemudiannya diproses dengan kaedah persampelan cone and quatering dan Jon Splitter dan seterusnya dikisar dengan bebola seramik untuk mendapatkan saiz $+63\mu\text{m}$ - $75\mu\text{m}$. Analisa mineralogi sampel dengan menggunakan kaedah XRF menunjukkan konsentrat mineral struverit sebanyak 80.1%.

Reagen

Asid fosfonik Iso-Oktil yang digunakan sebagai bahan pengumpul diperolehi dari syarikat Hoechst, Jerman dibawah nama komersial P 195. Bahan-bahan kimia untuk pengawalan pH seperti NaOH dan HCl serta bahan-bahan kimia yang lain yang digunakan untuk ujikaji merupakan reagen kimia analitikal bergred BDH.

Tatacara

Kajian keterapungan mineral telah dijalankan menggunakan tiub Hallimond dengan menggunakan 1 gram sampel yang diaduk bersama reagen pengumpul selama 5 minit. Pengapungan kemudiannya dilakukan dengan membekalkan gelembong-gelembong udara dengan kadar aliran udara 80ml/minit.

Schulze, H.J., 1984, *Physico-chemical Elementary Process in Flotation*, Elsevier Science Publishing Company, Amsterdam, Netherlands.

Senior, G.D., 1985, 'Interactions between Cassiterite Flotation Collectors and Cations Present in Flotation Pulp,' Ph. D Thesis, University of British Colombia.

Wottgen, E., 1969, 'Adsorption of Phosphonic Acids on Cassiterite,' *Trans. IMM*, Vol 78, C91-97.

bertambah julat antara 40°C hingga 50°C merupakan keadaan perubahan berlaku seperti yang dicadangkan oleh Cook dan Last (1950) dan Fuerstenau dan Rhagavan (1976).

Keupayaan Zeta

Berdasarkan nilai-nilai keupayaan yang diplotkan pada rajah 6.0, nilai pH titik iso-elektrik bagi mineral struverit berada di sekitar pH 2. Berdasarkan keputusan ini juga di dapati bahawa nilai keupayaan *zeta* ini berkurangan apabila nilai pH bertambah. Hasil kajian ini yang mendapati pengurangan nilai keupayaan *zeta* dengan peningkatan pH larutan mempunyai persamaan dengan kajian Purcell dan Sun (1963) dengan menggunakan mineral rutil dengan kehadiran pengumpul sodium oleate. Lengkok keupayaan *zeta* bagi kesan kehadiran klorida ferrik menunjukkan lengkok yang hampir serupa dengan apa yang telah ditemui oleh Senior (1985) untuk mineral kassiterit.

Berdasarkan pada lengkok rajah 7.0 dan 8.0, pengapungan dan penjerapan berlaku dengan lebih berkesan apabila nilai keupayaan *zeta* mendekati titik iso-elektrik struverit. Hubungan antara keupayaan *zeta*-pengapungan dan keupayaan *zeta*-penjerapan dapat dilihat dengan kesemua lengkok menunjukkan penurunan nilai dengan pertambahan nilai pH larutan.

KESIMPULAN

Hasil penyelidikan menunjukkan bahawa bagi sistem pengapungan fosfonik-struverit, pengapungan dan penjerapan maksima terjadi disekitar pH 3. Pertambahan nilai pH di dapati mengurangkan keberkesanan penjerapan dan juga pengapungan sistem fosfonik-struverit. Prestasi penjerapan dan pengapungan mineral juga meningkat pada kepekatan reagen pengumpul yang lebih tinggi.

Hasil kajian penjerapan pada nilai suhu yang berbeza menunjukkan bahawa terdapat kemungkinan bahawa proses penjerapan yang berlaku di bawah suhu 40°C merupakan penjerapan fizikal dan lengkok pertambahan ketumpatan penjerapan antara julat 40°C hingga 50°C mungkin menunjukkan suatu proses peralihan daripada proses penjerapan fizikal ke proses penjerapan kimia.

Hasil kajian keupayaan *zeta* mencadangkan bahawa titik iso-elektrik bagi mineral struverit berada disekitar nilai pH 2. Nilai keupayaan *zeta* juga berkurangan dengan bertambahnya nilai pH.

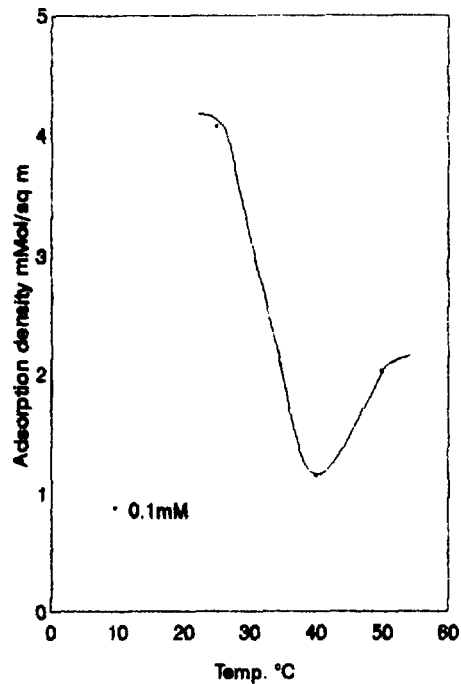
RUJUKAN

Cook, M.A. and Last, A.W., 1950, 'Flourite Flotation II', Bull. No. 47, Utah Engineering Expt. Station, Univ. Utah, 18 pp.

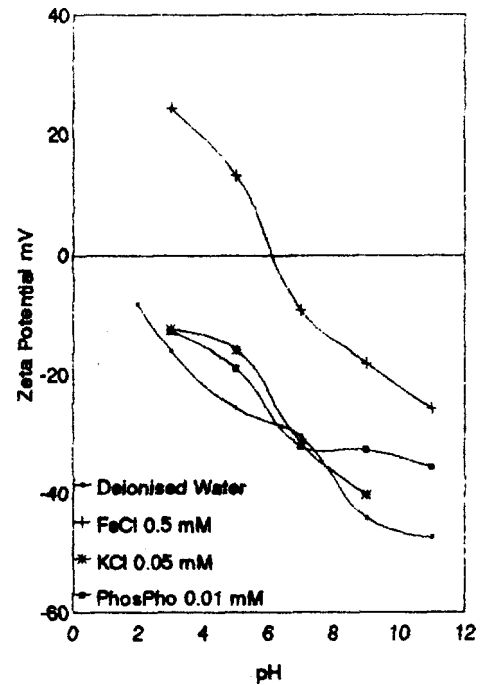
Fuerstenau, D.W. and Rhagavan, S., 1976, 'Some Aspect of Thermodynamics of Flotation,' Flotation, Fuerstenau, M.C., ed., Vol. 1, AIME, New York, pp 148-196.

Kamarudin, H. dan Khangoankar P.R., 1993, 'Studies on cassiterite-Sulphosuccinamate Flotation System,' to be published in IJMP.

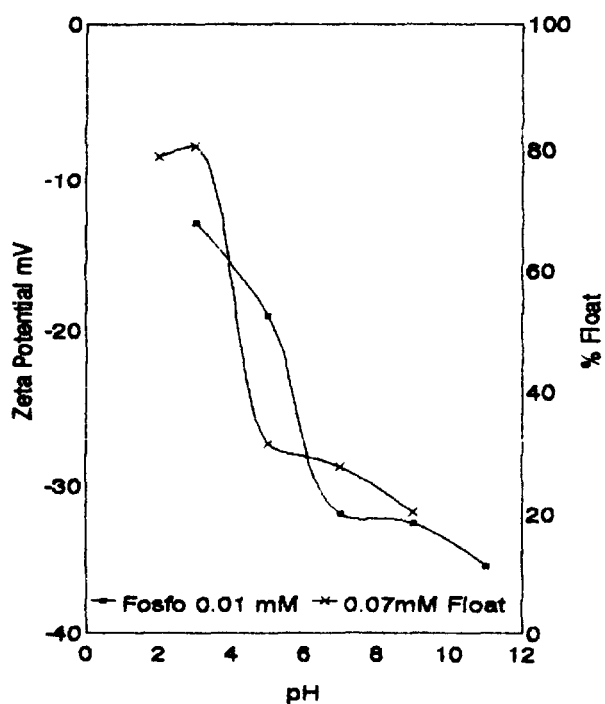
Purcell, G., and Sun, S.C. 1963, 'Significance of double bonds in fatty acid flotation', Trans American Institute of Mining and Met. Engineers.



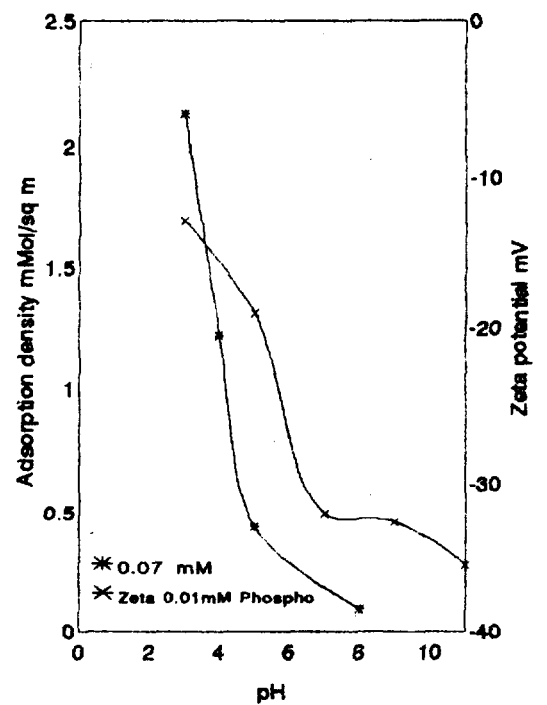
Rajah 5 - Kesan suhu terhadap penjerapan.



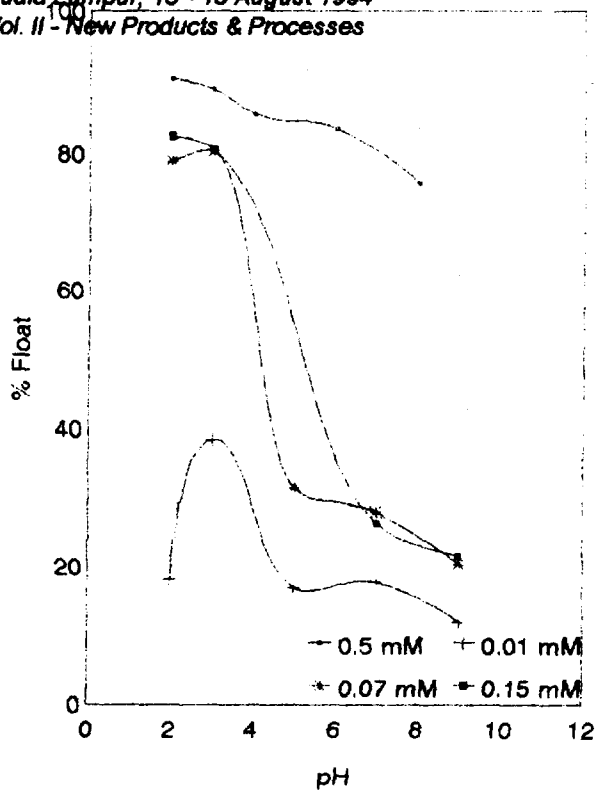
Rajah 6 - Kesan pH terhadap keupayaan zeta.



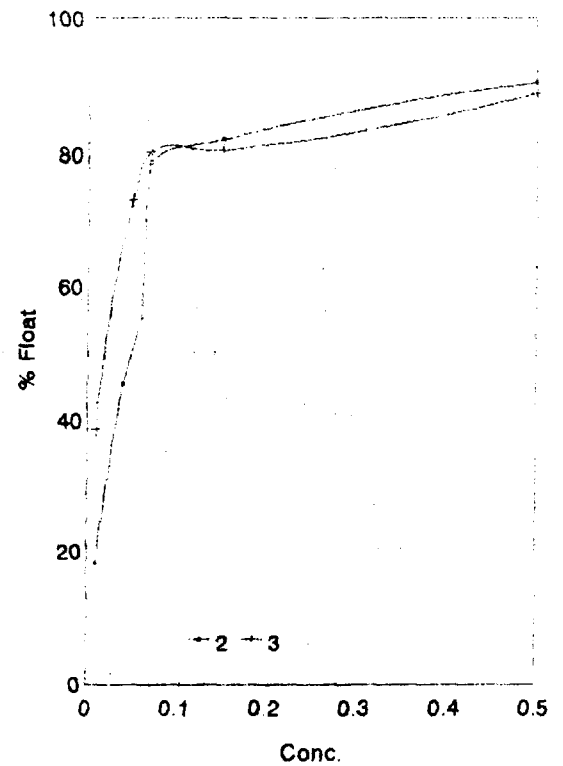
Rajah 7 - Hubungan antara pengapungan dan keupayaan zeta.



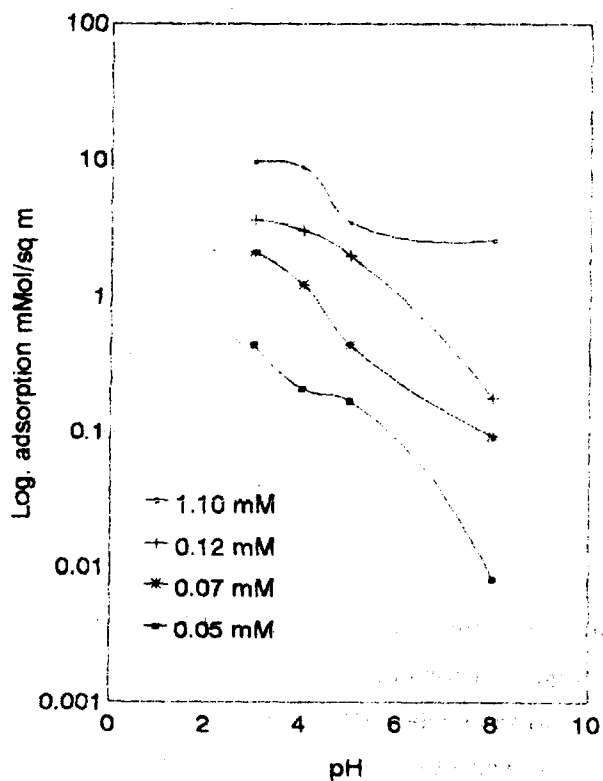
Rajah 8 - Hubungan antara penjerapan dan keupayaan zeta.



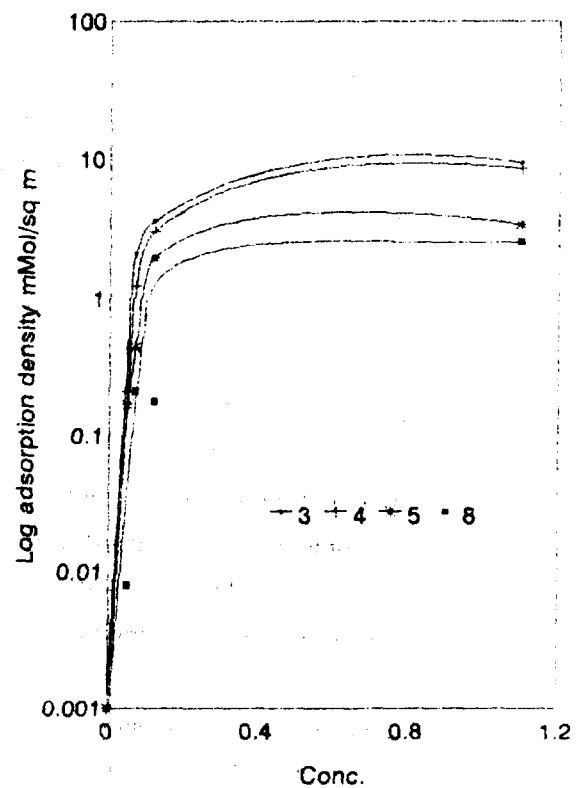
Rajah 1 - Kesan pH terhadap pengapungan.



Rajah 2 - Kesan kepekatan terhadap pengapungan.



Rajah 3 - Kesan pH terhadap penyerapan.



Rajah 4 - Kesan kepekatan terhadap penyerapan.

prediction of large scale performance. However, whenever possible plant test is required to confirm the filtration simulation from labs test data and to obtain other informations which can be obtained by bench test such as mechanical property of filter media and mechanical operation ^{2,3}.

There are four methods available for bench tests based on filtration driving force and equipment being used i.e. compression-permeability cell, capillary suction time, vacuum filtration and positive pressure filtration. The last method that is positive pressure filtration method is suitable for studying of cake filtration of low moisture content in final ⁴. Furthermore, it can be equipped with sensors and data equisation system to determine the filterability ^{2, 4, 6, 7, 8}. The parameters such as filtration rate, local hydraulic pressure, porosity, specific resistance with relation to process condition during cake formation can be investigated. These parameters are important for understanding the mechanism of filtration.

A filtration rig pressure filter (bench scale) fitted with a data equisation system was developed to study the filtration behaviour of two phase slurry (silica) and three-phase slurry (crude palm oil slurry). Result of filtration test is used to determine the suitable plant scale filter.

Apparatus

Figure 1 in Appendix shows the schematic diagram the filtration rig used in this study. It mainly consists of a mixer vessel and a filter unit which was placed in an oven.

The mixer vessel has 15 cm ID, 20.5 cm height and made from stainless steel. It include a stirrer, a sample inlet facility, a thermocouple, a sampling facility and an inlet of compressed nitrogen gas. A 1/2" globe valve is fitted between the mixer and the filter.

The filter unit was cylindrical shape 10 cm ID and 4 cm height and was made from stainless steel. Five holes at the top of filter were used to equip five pressure tubings to measure cake hydraulic and medium pressures. The head of the first tubing touched the surface of filter cloth and the second, third, fourth and fifth heads of tubing were positioned at 5 mm, 10 mm, 15 mm and 20 mm above the first tubing head. The tubings were connected to 5 - 25 mA pressure tranducers.

The temperature of slurry in the mixer was increased to desired temperature using a belt heater fitted with a on-off temperature controller. The apparatus was fitted in an oven to control the temperature to desired test temperature.

The filtrate consists of oil and water was collected in 250 ml glass measuring cylinder which was placed on the top of digital balance. The balance can measure the weight from 0 - 300 grams with 0.1 gram accuracy. It was interfaced to a computer via RS-232C. The balance can be set to zero prior weighing and also can be set to send data in desired sampling interval.

Burr-Brown Data Acquisition System was used to acquire data of weight of filtrate, medium, applied pressure, hydraulic pressures in the cake, filter temperature and stirrer speed. The system compatible to MS-DOS operating system in which it was linked to a potable computer and to a printer for recording and displaying data. The system was configured with a software, an

FILTRATION BEHAVIOUR OF DIFFERENT PHASE OF SLURRIES

BY

SA'ARI MUSTAPHA AND HAMDANI SAIDI

Department of Chemical Engineering

Universiti Teknologi Malaysia

ABSTRACT

Filtration engineers are interested to investigate hydraulic pressure distribution because they are related to filtration rate and cake dewaterability. Results of the investigation are useful for determination of suitable type of filter for filtration and dewatering processes. A filtration rig of pressure filter fitted with a data equisation system was developed to obtain a simultaneous data of operating conditions, hydraulic pressures in the cake and volume of filtrate. The rig was capable to be used for filtration of two phase slurry - silica slurry and three phase slurry - crude palm oil slurry. The hydraulic pressure distribution in the silica slurry was almost horizontal. The different in the forms can be attributed to the difference in difficulty to filter the slurries and their cake. Filtering of crude palm oil slurry and dewatering its cake was difficult than silica slurry. The paper also discussed the type of plant filter suitable for filtration of the slurries.

Introduction

The separation of solids from suspensions in a liquid by means of porous media which retains the solids and allows the liquid to pass is termed filtration ¹. It is used either for recovering of suspended solids in the suspension (or slurry) or clarification of liquid. The filtration whereby the solids forms as a cake is called cake filtration and its widely used in chemical industry such as separation and clarification of vegetable oil, dewatering mineral, peat and sludges and filtration of coal. It is a mechanical operation which demanding less energy than evaporation and drying for separating of liquid.

Knowledge of flow of liquid in open and packed beds and through filter media not sufficiently developed to enable the filtration engineer accurately predict or calculate the thickness of the cake, filtration time and property of final product ². It is therefore necessary to study the property of each slurry or suspension and to determine its filtration behaviour in order to calculate the optimum size of filter.

Study on filtration of slurry can be carried out by labs test (bench scale) and plant test (pilot and plant scale). The bench test is rapid, economic and may not require special transportation. While plant test requires takes a longer time typically many days of filtration trials, expensive and special transportation (ship or trailer). The labs test can be used to determine the cake resistance, suitable of filter cloth, clarity of filtrate, liquid content in the cake, cake compressibility and cake handling. The result of the test is useful for preliminary evaluation and

from $\pm 0.1^{\circ}\text{C}$ to $\pm 0.9^{\circ}\text{C}$ for filtration at 25°C and 90°C respectively. The reduction of precision of the temperature data probably due to the electrical noise from the oven heater and oven's fan. It also could be due the unhomogenised of the slurry temperature.

Slurry and Cake Compositions

Compositions of slurry and cake of silica and crude palm oil slurries are presented in Figure 2. Slurry and cake of silica consist of two-phase that is water and solid. The solids in the cake of silica increased three fold, whilst water reduced to four fold. The solids content in the cake of crude palm oil increased 100% but liquids (water and oil) in the cake reduced only slightly (5%) of their original content in the slurry. The difference in cake composition probably due to the property of the slurry and particle characteristics in the cake as discussed by several researchers¹⁰.

Two-phase Flow of Filtrate

In term of composition of filtrate (% oil or water per volume), the changes of composition with time is plotted in Figure 3. The percentage of water is at maximum for beginning of filtration and reduced linearly as filtration proceed. Whilst the changes of oil percentage is reversed i.e. at a minimum for early filtration and then increased linearly until filtration is stopped. The oil and water percentages in the filtrate after filtration were similar to their percentages in the slurry. The result shows that no separation occurs through out filtration process. The flowrate of oil (dispersed phase) slower than flowrate of water (continuous phase) because the dispersed phase needs to coalesce to certain size before it can flow out¹¹.

Cake Characteristic

Cake resistance is one design parameter for industrial filter. Therefore it is important to determine that the data fit the standard model as given in equation (14) Appendix. If the filtration data does not fit the standard model a appropriate cake resistance value must be assigned or an adjustment to the testing procedure must be made to produce data that fit the standard model for calculation of cake resistance⁷.

Figure 4 and Figure 5 show plots of t/V versus V from filtration of silica and crude palm oil slurries. The Figures show that the plots are linear which indicate the data fit the standard model. The values of cake resistance of silica and crude palm oil slurries at 1 bar are 3.63×10^{11} m/kg and 3.87×10^{13} m/kg respectively.

analog input board, a termination panel and a number of analog signal cables. Number of channel for this study were 10 i.e. 7 analog channels (6 pressure channels and 1 temperature channel), 1 parse and 1 time. The maximum period of data aquisition is 3600 seconds for 60 seconds sampling rate between the sampling data. The data was displayed in numeric form on computer monitor for easiness monitoring of filtration process.

Material and Method

Material

The slurry was filtered using polyester multifilament twill weaves with air permeability of $20 \text{ cm}^3/\text{cm}^2/\text{sec}$.

Method

Initially the filtration rig was heated up to desired temperature for 4 hours (except for filtration of silica slurry where it was filtered at room temperature). The temperature of apparatus inside the oven was kept constant by oven's temperature controller. An amount of 600 ml of homogenised crude palm oil slurry at 60°C was placed into the mixer of filtration rig through the sample inlet facility. The slurry was continuously homogenised by stirring at 1200 rpm by mixer's stirrer. The temperature of the slurries was increased to 90°C using a controlled belt heater which blanketing around the mixer. At the beginning, the readings of applied pressure (P1) and medium pressure (P2) were set to zero. Then the pressure valve was opened slowly until P1 (displayed on the monitor) had reached to the desired pressure. An amount of 50 ml sample was taken through the sampling facility to check its composition.

The valve V1 (refer to Figure 1) was slowly opened to start filtration and the data acquisition was activated simultaneously. Filtration tests were carried out at temperature 90°C (except for filtration silica slurry) and pressures of 1 bar. The composition of wet and dry cakes was determined.

Result and Discussion

Accuracy and Reliability of Filtration Rig

The accuracy and reliability of filtration rig depend on the instruments used in measuring pressures, temperatures and weight of filtrate. Two types of signals i.e. analog and pulse signals were employed to send signals to data equisation system. Pressure and temperature were sent by analog signals while weight of the filtrate was sent by pulse signal. Analog signals particularly more influenced by relatively low level of noise compared to pulse signal which is discrete in nature⁹. The effect of noise was significantly reduced by using screen cables and earthling the screens wire which coats the internal wires. Precision of pressure data was good where the highest precision can be obtained from filtration of silica slurry i.e. ± 0.0 psi and the lowest was from the filtration of crude palm oil slurry ± 0.4 psi. The precision of temperature data was low i.e.

effective concentration c^* at beginning of the cake formation. The changing of c^* is related to the rapid changed of moisture content near the filter medium ¹⁷.

The value of R_m calculated using equation (18) by measuring the medium pressure were positive. This result seems more realistic (positive values) compared to R_m value obtained by graphical method where the R_m value was negative. Most the values of R_m obtained by equation (18) were higher than the values of R_m obtained by graphical method. Willis et al. ⁵ . also found that R_m values obtained by determination of medium pressure were higher than R_m values calculated by graphical method on the filtration of silica, cupric oxide, talc and geon slurries. The values of R_m calculated by equation (18) are determined by medium pressure and viscosity of filtrate. The medium pressure is influenced by permeability of filter cloth.

A typical profile of increasing medium resistance (R_m) of diluted crude palm slurry versus time is depicted in the Figure 10. The increase of medium resistance from the filtration of the diluted crude palm oil slurry similar to the increasing of medium resistance of silica slurry (Figure 11). Both figures show that the medium resistance are not constant as assumed in conventional filtration equation but increased a form of parabolic curve.

Conclusion

1. The measurement of cake and medium resistances using filtration rig pressure filter fitted with data equisation has several advantages over other methods. Among the advantages such as reproducible slurry preparation (either at room temperature or elevated temperatures), good precision of measurement parameters, less attention to data collection, give realistic result of medium resistance and convenient to manipulation data.
2. Parabolic data was obtained from filtration 2-phase slurry (silica slurry) and 3-phase slurry (crude palm oil slurry) . Therefore cake resistance can be determined using standard model.
3. The pressure drop in various depths of cake of crude palm oil slurry is almost zero. For low concentration of solids in the slurry such that the concentration of non-oily solids in the crude palm oil slurry, the thin cake filtration is recommended to maintain high filtration rate.
4. The crude palm oil slurry is difficult to filter because it has wide range particle distribution, irregular shape of non-oily solids particles and oil emulsion in the slurry.
5. The medium resistance from filtration of silica and crude palm oil slurries increased in parabolic form.

References

1. Coulson, J.M., Richrdson, J.F. (1978). Chemical Engineering. Vol. 2. Pergamon Press. 321.
2. Capey, M., Hooton, J.A. (1970). "Plant Testing For The Assesment of Filter Presses". Filtration and Separation. 333 - 343.
3. Fluch, H.W., Perchthaler, H. (1982). " Separation of Oil and Water From Oil Refinery Sludge ". Filtration and Separation. Sept. /Oct. 420 - 423.

Cake Hydraulic Pressures

For the compressible cakes the hydraulic pressures of the cake change linearly with the cake thickness while in the incompressible cakes the changes of the hydraulic pressure gradient was not linear i.e. in the forms of a curve near the filter medium ¹².

However the hydraulic pressures distribution in the cake for the filtration of crude palm oil slurry is significantly different compared to the hydraulic pressure distribution in the incompressible and compressible cakes. The distribution of hydraulic pressure of various depths of the palm oil slurry cake (Figure 6) is almost constant or almost independent of time. However, the medium and hydraulic pressures distribution in the cake of silica slurry (Figure 7) is similar as reported by Leu (1981); where they are constant at early filtration but reduce in parabolic form as filtration proceed. The same finding was early reported by Shirato ⁶ in which he used manometer-type probes to find the hydraulic pressure distribution in the cake of ignition plug slurry. Pressure drop in the cake from the filtration of the diluted crude palm slurry is too small compared to the pressure drop across the silica slurry, where the pressure drop across the cake from filtration crude palm oil slurry is 0.4 psi whilst pressure drop from filtration of silica slurry cake is 3.2 psi. The lowest of pressure drop across the cake of crude palm oil slurry because most of the applied pressure was used to overcome medium resistance.

The shape and size of particles determine the arrangement in the cake. Figure 8 shows that the non-oily solids particles has a wide range particle-size distribution (from sub-micron to 600 microns and consisting of different shape of particles) compared to silica particles whose size from microns to 200 microns (Figure 9). Under electron microscope a cell debris contains a number of voids. The cake formed from these particles behaved like a sponge i.e. highly compressible. The wider the size distribution and shape irregularity reduced the pore size and resulted in slow filtration rate¹⁴. In addition to that factors, the oil particles or oil emulsion which are trapped in the cake structure gave sealing properties and thus affected the porosity and filtration rate ¹⁵.

Since the pressure drop across the cake of crude palm oil slurry is almost zero, it is suggested to use thin cake filtration method to maintain high filtration rate. While for filtration and dewatering of silica slurry where its pressure drop across the cake is high, either filter press or belt filter could be suitable for the purposes.

Medium Resistance

The medium resistance (R_m) obtained by graphical method from filtration of crude palm oil slurry i.e. equation (17) is negative. The negative sign (error) has no physical meaning ¹⁶. The erroneous occurred due to the R_m obtained by extrapolation of graph to the ordinate ($t/V = 0$). At early stage of plot t/V versus V , the relation is not linear possibly due a changing of

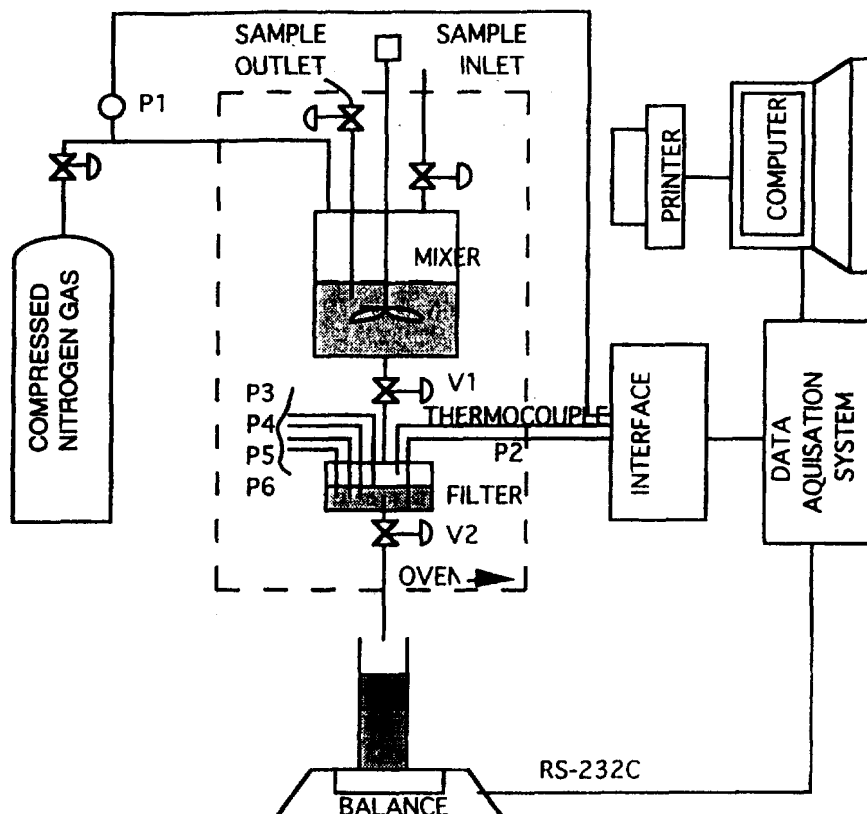


FIGURE 1: SCHEMATIC DIAGRAM OF FILTRATION RIG

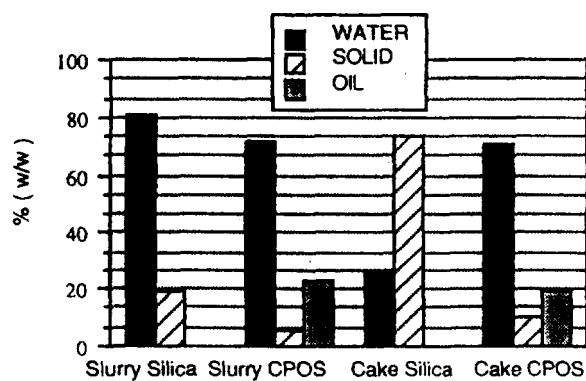


Figure 2: Composition of Slurry and Cake
(Silica and Crude Palm Oil Slurries)

4. Wilhem, J. H. (1978). " The Use of Specific Resistance Data in Sizing Batch-Type Pressure Filter ". Water Pollution Control Federation Journal. Jan. / Mar. 471 - 483.
5. Willis, M.S., Shen, M., Gray, K.R.(1974). " Investigation of The Fundamental Assumption Relating Compression-Permeability Data Filtration". J. Chem. Eng. (Canada). 52, 331 - 337.
6. Shirato M. , Sambuchi M., Murase T., Aragaki T., Kabayashi K., Iritani E. (1987). " Theoretical and Experimental Studies in Cake Filtration ". Memoirs of the Faculty of Engineering Nagoya University. 37 (1); 38 - 92.
7. Christensen, L., Vick, R.I. (1985). "Specific Resistance Measurements: Nonparabolic Data". Jour. of Enviromental Engineering. 111 (3); 243 - 247.
8. Harvey, M.A., Bridger, K. (1988). " Apparatus for Studying Incompressible and Moderately Compressible Cake Filtration ". Filtration and Separation. Jan. / Feb. 1988, 21 - 29.
9. Burr-Brown (1990). The Handbook of Personal Computer Instrument, Data Aquisition, Test, Measurement and Control. 5th Ed.; 4-15 - 4-19.
10. Puttoc, S.J., Wainwright, M.S.(1984). " Role of Surfactant and Particles Characteristics in Dewatering of Minerals". Chem. Eng. In Australia. 4, 31 - 34.
11. Dahliquist, E. and Steterwal, F (1985). Filtech Conference 1987. Uni. Tech. of Loughbrough. 37 (1), 49; 36 - 43.
12. McCabe, W.L. and Smith, W.C.(1993). Unit Operation of Chemical Engineering. Mc Graw - Hill, New York; 5th. Ed. 1018 - 1019.
13. Leu, W. F. Cake Filtration . Phd Dissertation University of Houston,. 1981.
14. Kakwani, R.M., Gala, H.B., Chiang S.H., Klinsing, G.E. and Tierney, J.W. (1985) " Dewatering of Fine Coal - Micrographic Analaysis of Filter Cake Structure" . Powder Technology. 41; 239 - 250.
15. Roger, W.F.(1963). "Composition and Properties of Oil Well Drilling Fluids" . Gulf Publishing Company. 3td. Ed. ; 562.
16. Wronski, S.K. and Laskowski, L.K. (1976)." Anamalous Behaviour During The Initial Stage of Constant Pressure Filtration". The Chemical Engineering Journal.12; 143 - 147.
17. Rushton, A.(1978). "Basic Flow Equations, Cake and Medium Resistance Calculation", A Filtration Course, U.T.M., Kuala Lumpur.
18. Gale, R.S.(1967). " Filtration Theory With Special Reference to Sewage Sludges". Water Pollution Control ; 622 - 631.

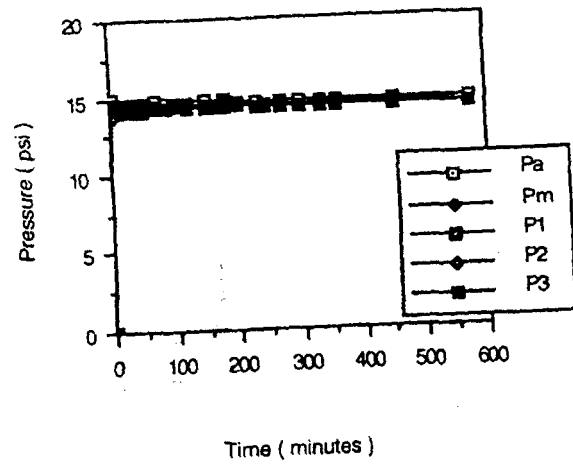


Figure 7: Hydraulic Pressure in Cake of Crude Palm Oil Slurry

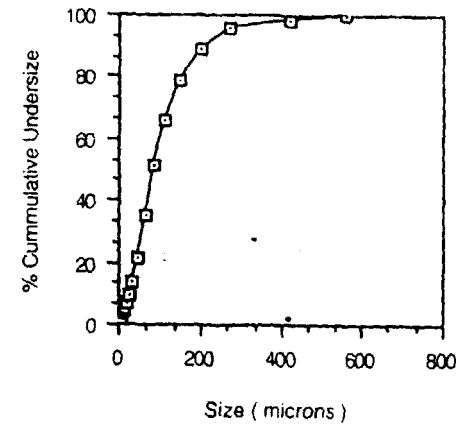


Figure 8: Particle Size Distribution of Non-Oily Solid Particles

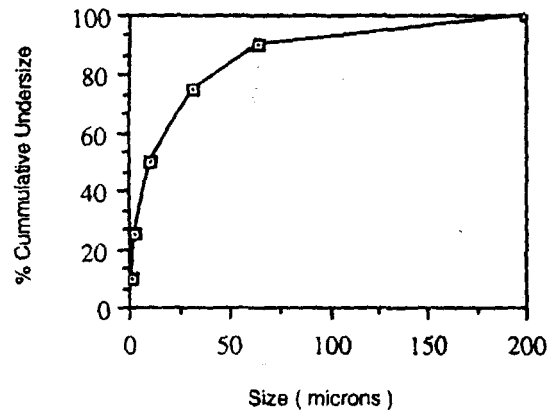


Figure 9: Particle Size Distribution of Silica Particles

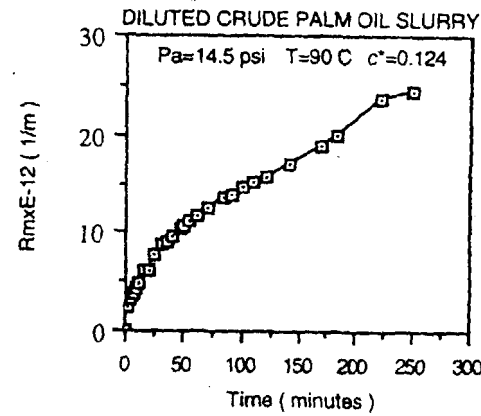


Figure 10: Plot Rintangan Medium Versus Time
(Crude Palm Oil Slurry)

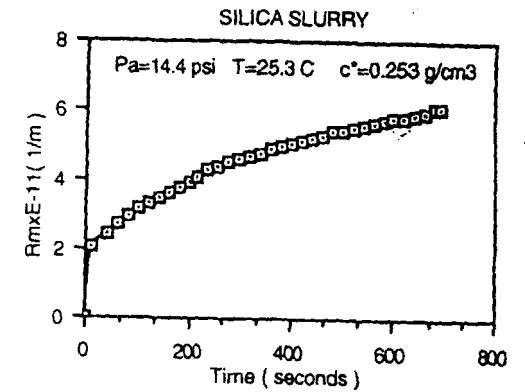


Figure 11: Plot Medium Resistance Versus Time
(Silica Slurry)

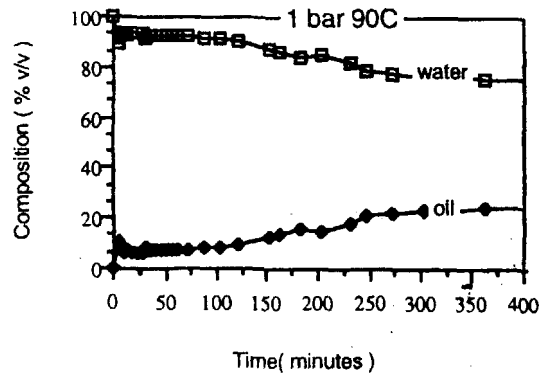


Figure 3 : Plot Composition Versus Time
(Crude Palm Oil Slurry)

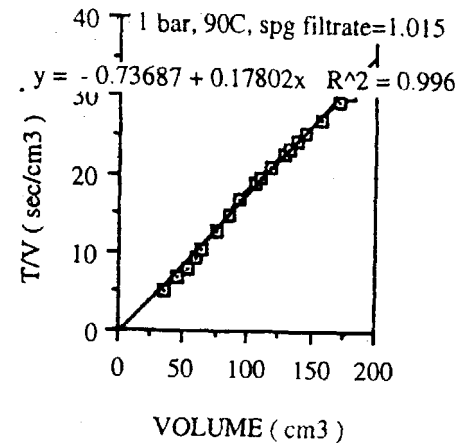


Figure 4: Plot T/V versus V of Filtration. Diluted Crude Palm Oil Slurry

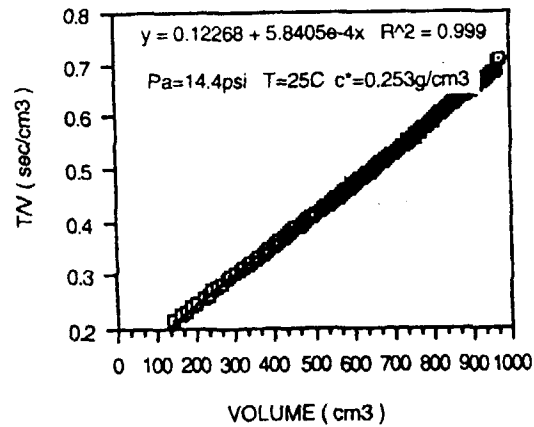


Figure 5: Plot t/V versus V from Filtration Silica Slurry

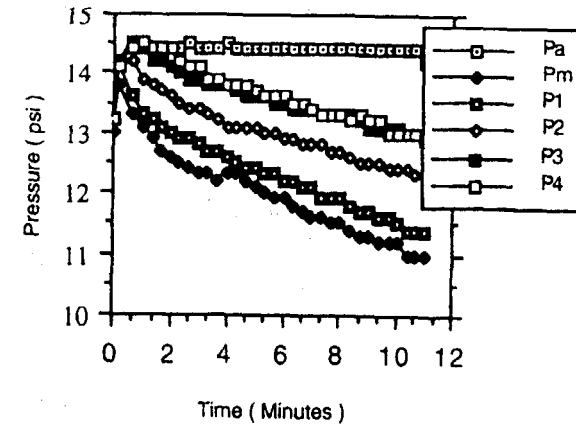


Figure 6: Hydraulic Pressure in Cake of Silica Slurry

PRODUCTION OF ACTIVATED CARBON FROM PALM KERNEL SHELLS BY STEAM ACTIVATION

by

**HOI WHY KONG AND PUAD ELHAM
FOREST RESEARCH INSTITUTE MALAYSIA
KEPONG, 52100, KUALA LUMPUR,
MALAYSIA**

ABSTRACT

Palm kernel shells were carbonised in an indirect pyrolysis reactor at 750°C. The charcoal were then crushed, grind and sieved. The granulated shell charcoal was then activated at 800°C in an atmosphere of superheated steam. It was found that good palm kernel shells activated carbon with an average CTC and I₂ value of 50% and 900 were obtained respectively. Based on a production capacity of 1250 tonne per annum and the current market price of raw material, direct labour cost, factory overhead, the net profit return of the plant was found to be 34.6%-37.8%

1.0 Introduction

Ordinary commercial charcoal has a specific surface area of only 1-2 m²/g and has very limited ability to absorb substances in the liquid and gaseous phase. To increase its absorption capacity, it must first be activated by removing the tarry material which blocks the surface of the carbon skeleton of the charcoal. With activation, the surface area of the porous skeleton is increased to 300-2000 m²/g. With such a large surface area, molecules of other substances can be held or adsorbed and thus removed from gases or liquids in which the treated charcoal is placed. Charcoal processed in this way is called activated charcoal.

The use of charcoal in producing activated carbon is relatively new when compared to its use in the steel and chemical industries. The market of activated charcoal only started to develop in Europe around the beginning of this century. Today more than seventy types of activated carbon are marketed for various applications in the food and chemical industries.

There are two main manufacturing process for activated carbon, namely by zinc chloride activation and by steam activation. In zinc chloride activation, zinc chloride is cooked at a temperature of 500°C-900°C (Goos and Reither 1946; Randtke and Jepsen 1981; Hoi et al 1991). The charcoal is cooked and washed to remove the tars and volatiles. The activating chemicals is recovered.

In steam activation, charcoal is heated to a temperature of about 800°C in an atmosphere of superheated steam in order to permit the breakdown and removal of tars blocking the microfine structure of charcoal (Crittenden 1987). The charcoal is then allowed to cool until it reach ambient temperature.

2.0 Manufacturing process

The main processes under which activated carbon are manufactured from palm kernel shells in the plant is illustrated in the flowchart. Briefly, palm kernel shells

were converted into charcoal, which are then crushed, grinded and sieved. The granular charcoal is then sent into the rotary kiln (Hassler 1983). The granulated shell charcoal was then activated at 800°C in an atmosphere of superheated steam. Under intense heat and steam, the charcoal gradually turn into highly micro porous activated carbon (Zichermann and Williamson 1982). It was found that good palm kernel shells activated carbon with an average CTC and I₂ value of 50% and 900 were obtained respectively. The bulk density of the material was found to be 420-540 g/cc and its hardness index was found to be 95-98%.

3.0 Plant and machinery

The factory that is equipped with plant and machinery which has a maximum capacity of approximately 1250 tonnes (M/T) of activated carbon (palm kernel shell based) per annum. The principal machinery which determines the production yield and efficiency is the rotary kiln (heating furnace).

The cost of the plant is estimated to be as follows:-

Cost of Machinery (Activation plant* & main laboratory testing equipment**)	RM3500000
Cost of Granulation Plant	RM300000
Cost of Land and Factory	RM700000
Working Capital requirement	RM500000
Total	RM5000000

*List of activated carbon machinery

Variable speed Feeding System with Bucket Conveyor and Silo c/w platform.
 Rotary Kiln Shell c/w Bearings and Rollers.
 Insulation and Firebricks.
 Hydraulic Motor Drive System s/w Pillar Chain.
 50 KVA stand-by Generator.
 Cooling Spiral.
 Heat chamber with Chimney.
 2,000 lbs Boiler (One unit) c/w Chimney and Steam piping with PRV.
 Low gravity Diesel Burner (One unit).
 Air Wash System (One unit).
 Vibro Sieves (Two units).
 Jumo Thermocouples (Four units).

**Laboratory testing equipment

Required to carry out 6 major test (i.e.. Bulk Density, CTC Adsorption, Moisture Content, Ash Content Hardness and Particle Size Distribution).

Memmert Oven (One unit).
 Triple Beam Balance (One unit).
 Mettler Balance (One unit).
 CTC Test Equipment (One set).
 Bulk Density Test Vibrator (One unit).
 Ro-Tap Sieve Shakers c/w Test Sieves.

The plant will require a land space of not less than 0.6 hectares. The built up area of the factory should be approximately 2050 m². The portal frame factory will house a double storey office with a total area of approximately 230 m². The overall factory is a plate frame structure with 2.5 m to 3 m walls on the sides and back portion. The flooring must be cement rendered of minimum 15 cm (1:2:4 concrete mix). Two reinforced concrete Rotary Kiln stand must be built with piling, to withstand 80 to 100 tonne weight each. The factory must have normal public water supply and electric supply requirement should be approximately 200A.

4.0 Raw material requirement

The main direct raw material is cheap palm kernel shell charcoals which are available locally through local supplier, while the main indirect raw material consist of packing materials (PP woven bags or kraft reinforced paper bags and inner plastic bags).

These direct and indirect raw materials are purchased directly from local manufacturers of palm kernel products and plastic bags manufacturers. Palm kernel shell charcoals is estimated to cost approximately RM420 per tonne while that of indirect packing materials cost about RM2.50 per 25 kg export pack of activated carbon. Palm kernel shells are generally 30% cheaper.

It takes about ten (10) tonne of palm kernel shell charcoals to convert into four (4) tonne of activated carbon (yield : 40%) when the shells were carbonised in an indirect pyrolysis reactor at 750°C. The charcoal were then crushed, grind and sieved. At an average cost, the above direct and indirect raw materials cost works out to be approximately RM1050 and RM100 respectively per tonne of finished granular activated carbon (or RM1150 per tonne). It is important to maintain the following stock level of raw materials based on the following year production requirements :-

Palm kernel or palm kernel shell Charcoals	:	One (1) month stock
Packing Materials	:	One (1) month stock

5.0 Management and labor force requirement

The following will be the management and labor force required :-

Management & Office staff

- 1 Managing Director
- 1 General Manager
- 1 Marketing Manager
- 1 Accountant
- 3 Clerical
- 1 Purchaser

Total management and office staff = 8 persons

Factory Personnel (3 shifts)

- 1 Production Manager
- 2 Supervisors (Kiln operators)
- 2 Maintenance
- 1 Engineers
- 2 Laboratory Technicians (Q.C.)
- 10 Production workers
- 2 Granulation workers (1 shift)
- 1 Store clerk

Total factory personnel for 3 shifts = 21 persons

However direct labor requirement for a 8 hourly shifts of operation per day is about 21 persons.

6.0 Direct and indirect cost

6.1 Direct labor cost

Direct labor requirement is in the region of twenty one (21) workers for eight (8) hourly shifts of operation a day.

The direct labor cost is approximately RM8400 per month or RM100800 per annum. This cost is assumed to increase by 5% annually.

6.2 Factory overhead

Indirect labor cost is approximately RM10300 per month or RM123600 per annum. This cost is assumed to increase by 5% annually. Bonus is assumed to be one month of the direct and indirect labor costs.

EPF and SOCSO contributions are estimated to be 12 1/4% of the total direct and indirect labor costs. Depreciation of factory's plant and machinery are computed on a straight line basis. The rates are as follows :-

Plant and Machinery	:	10% p.a.
Motor vehicle	:	20% p.a.
Tools and Equipment	:	10% p.a.
Office Equipment	:	10% p.a.

Repairs and maintenance are estimated to be about 1 1/2% on the cost of the plant and machinery in the first year and thereafter a 10% increase over the cost in the first year is provided for the years following.

Factory insurance is estimated to be at 1% of all insurable assets at the factory. General factory expenses are estimated based on informed judgment and assumed to increase by 5% annually.

Transport expenses are estimated to be at RM40 per tonne of finished products transported to the nearest port of loading.

7.0 Product and pricing

Activated Carbon has very diverse usage, as it offers itself as a raw material that can be conditioned into myriad form of applications for purification of air, gas, liquids and in recovery of precious metals (i.e., gold) from ores (Anon 1987, Culp et. al 1981). It is specially processed to have immense capacity for adsorption. The quality ranges from mainly iodine 900 to iodine 1300 with the price quoted as USD1000 to USD1500 per tonne respectively.

The main market areas are from the developed countries (i.e. USA, France, UK., Australia, Taiwan, Japan etc.). The activated carbon are of a high quality and the export prices are very competitive with those of other countries. There are only a few manufactures in Malaysia producing activated carbon using palm kernel shells and various types of sawdust, but they are generally foreign owned.

Although the local size is rather small, the level of competition cannot be disregarded because of the potential market growth. Foreign manufactures can be found mostly in countries which have abundant palm kernel shells, i.e. Sri Lanka, Philippines, Indonesia etc.

In 1993, the world market demand for Activated Carbon are already very substantial (about 600000 tonne annually). However, these markets are still growing at very high rate since the product relates directly to promoting environmental preservation in an era where environmental awareness are very much supported worldwide.

8.0 Profitability studies

The profitability of a typical company's operations is reflected as follows.

	Year 1	Year 2	Year 3	Year 4	Year 5
Gross Profit Rate	44.3%	43.8%	43.1%	42.6%	41.9%
Net Profit Rate	37.8%	37.3%	36.3%	35.4%	34.6%
Return of Capital Employed	34.8%	35.7%	34.7%	33.9%	33.1%

9.0 Conclusion

In conclusion, it was found that palm kernel shells carbonised in an indirect pyrolysis reactor at 750°C and activated at 800°C in an atmosphere of superheated steam can produce good quality activated carbon. The activated carbon was found to have an average CTC and I₂ value of 50% and 900. Based on a production capacity of 1250 tonne per annum and the current market price of raw material, direct labour cost, factory overhead, the net profit return of producing activated carbon from palm kernel shells was found to be 34.6%-37.8%.

References

Anon, 1987 "Products demand" Petroleum Gazette 25(7): 3-6

Crittenden JC, 1987 "Design of rapid fixed bed adsorption tests for non constant diffusivities." Journal of Environmental engineering division ASCE 113 (2) : 243-259

Culp R, Faisst J and Smith C, 1981 "Granular activated carbon installation." US EPA Report 600/2-81-177

Goos AW and Reither AA, 1946 "Industrial and engineering chemistry" pp 38

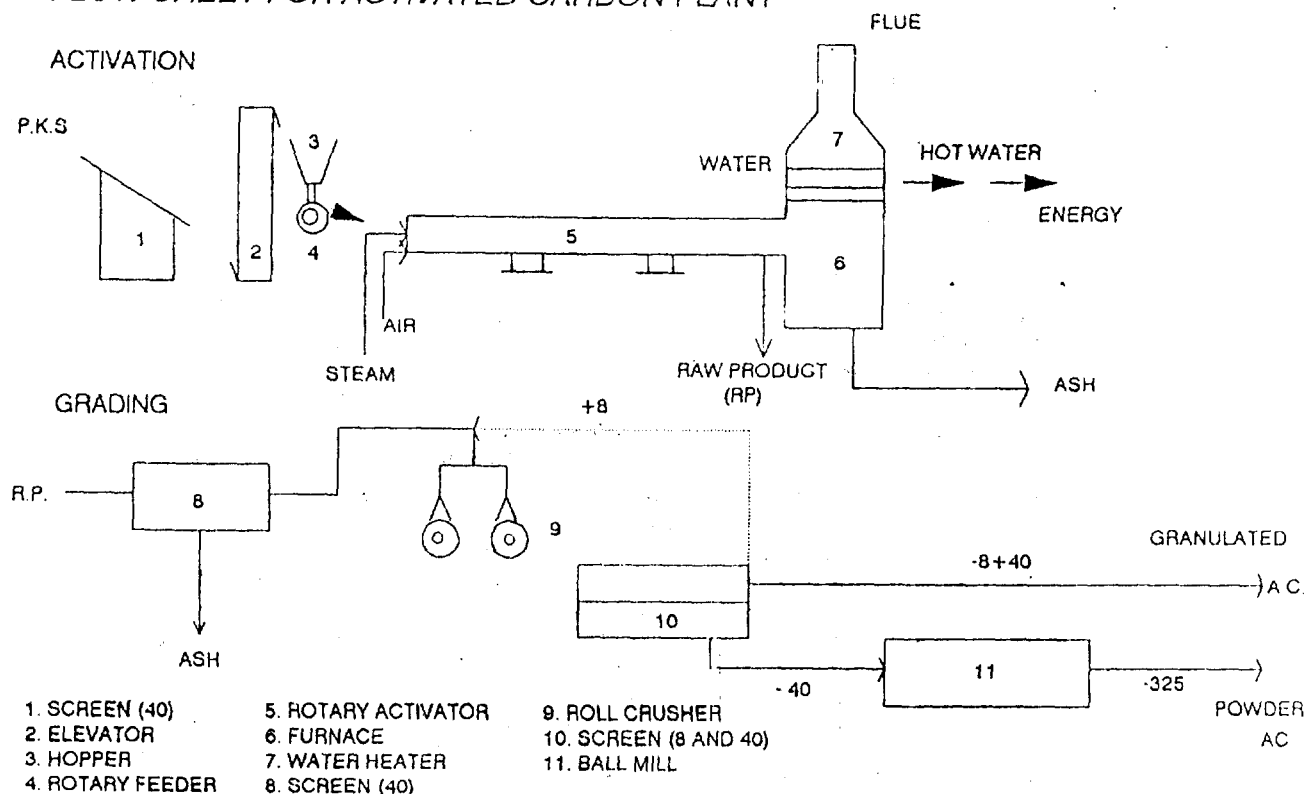
Hassler, JH 1983, "Activated carbon". New York, Chemical Publication Company. 620 pp.

Hoi WK, Razak MA and Gan LT, (1991), "Biomass potential and opportunities in ASEAN. Paper presented at 6th European Conference on Biomass for Energy, Industry and Environment, 22-26 April, Athens, Greece, 11 pp.

Randtke SJ and Jepsen CP, 1981 "Chemical pretreatment for activated carbon adsorption." Journal of American Water Works Association, 73 (8) : 411-419

Zichermann, JB and Williamson RB 1982, "Microstructure of wood charcoal Part 1- Fire Retardant Treated Wood, Wood Science and Technology, 16, pp 19-34

FLOW SHEET FOR ACTIVATED CARBON PLANT



PROCESS DESIGN & MODELLING OF PHYSICAL REFINING : PROBLEMS AND OPPORTUNITIES IN PHYSICAL REFINING DEODORISER COLUMN

Mustafa Kamal Abdul Aziz, Prof. Dr. Abu Azam Mohd Yassin, Harun Sani,
Rusli Jaafar, Mohd Halim Shah Ismail .

LIPIDS APPLIED SCIENCES AND ENGINEERING RESEARCH (L.A.S.E.R.).
Department of Chemical Eng., Faculty of Chemical and Natural Resources Eng.,
University Teknologi of Malaysia, Jalan Semarak, 54100 Kuala Lumpur, Malaysia.

ABSTRACT

This paper is a review of the physical refining deodoriser design, modelling and operations in the plate, packings and falling film columns to identify the current trend of the process and implements to its progress. Finally it will recommendations future areas of investigation in the design, modelling and scale-up of this process.

The trend toward process intensification using thin liquid film phenomena of falling film, and packed column to enhance separation performances in deodorisation have revealed problems in the liquid film stability of palm oil. The problems in crude physical refining are due to the:-

1. The dearth of critical engineering properties of palm oils required in thin liquid film phenomena regime.
2. The inability to select the correct process models and to simulate the complex and simultaneous processes of deacidification, deodorisation and decolourisation of palm oil occurring in the physical refining column.
3. The scale-up factors in adapting laboratory-scale results and process models for commercial production.

Further investigations are thus necessary in the above critical areas. The critical questions and choices faced by researcher in these studies are best summarised as:-

1. Determination of engineering properties of thin liquid film; surface tension, vapor liquid equilibria and diffusion.
2. Effect of palm oil components structure, chemistry and reactions on the properties, process model and scale-up design of process.
3. The choice between the conservative equilibrium stage method and the mass transfer rate method in modelling structured packing physical refining.
4. The choice of mass transfer theories, between two film theory, penetration theory and surface renewal theory for palm oil steam vacuum distillation.
5. The choice of structured packing performance correlations of other researchers and confidential manufacturer correlations and their limitations.
6. The choice of structured packing scale-up methods between HETP, $HTU \times NTU$ and pilot plant scale-up study.

In conclusion, the proposed areas of investigation are; Molecular structural chemistry of palm oil components and its effect on engineering properties, Saturated and Unsaturated Lipids Reactions and its effect on process modelling and simulation and Surface Phenomena of thin liquid film of Palm oils and its effect on scale-up design and pilot plant studies.

AIM

This paper discussed the problems of modelling the deodoriser and to identify the critical gaps in the deodoriser design and modelling. Finally, it proposed future areas of investigation and on future deodoriser design and modelling.

INTRODUCTION

The recent trend in the palm oil deodoriser design has been the application of **Thin Liquid Film Phenomena**, Sjoberg¹. Thin liquid film phenomena are exploited in the falling film, structured packed column and molecular distillation equipment to enhance separation performance in deodorisation. This regime enhanced the mass transfer rate and enlarged the surface area respectively. Due to inherently small liquid thickness, liquid film stability is vital and relies on the film physio-chemical properties, packing material surface in contact, column operating conditions, column liquid - vapour capacity and distillation system design. Usually, it is a trade-off between these factors to achieve optimum performance.

Basis of Investigation.

Recent investigation by Mustafa Kamal^{2,3} on palm oil surface phenomena influence on vapour pressure and surface tension have raised question on the palm oil liquid film stability in the deodoriser. The basis of this surface phenomena were previously reported by Szabo Sarkadi⁴, Pryde⁵ and Fristad⁶ whom attributed these effects to molecular association reactivity between high molecular weight unsaturated lipids. Indeed, Szabo Sarkadi⁴ went further by hypothesing the molecular association of fatty acids with oil molecules which he deduced from a vapour pressure experiment.

Complex Lipids Mixture.

For the purpose of this investigation, natural edible oils are defined as 'Complex Mixture' meaning possession of a combination of saturated and unsaturated lipids and a combination of low and high molecular weight lipids.

The **Complex PFAD - RBDL test mixture** model for vacuum distillation was proposed by Mustafa Kamal^{2,3} to extend the existing models of Szabo Sarkadi⁴ and Stage⁷. This model, unlike the previous models, emphasised the role of **unsaturated and high molecular weights fatty acids** in molecular association reactions. It predicted that the **unsaturated and high molecular weight fatty acids** chemical reactions are mainly responsible for physio-chemical properties of the mixture. Thus, these variations reduced the ability of the mixture to be separated in vacuum distillation.

Surface Tension.

Mustafa Kamal² found that in the PFAD - palm oil mixtures had very low surface tension varying between 20 to 30 mN/m in the deodoriser operating regime. In addition, the surface tension of unrefined palm oils are linearly inversely proportional to temperature.

More importantly, it is non-linearly inversely proportional to the concentration of PFAD in the oils. PFAD - palm oil mixtures behaves as a surfactant solution; at a critical low concentration of PFAD of 1 %, the surface tension increases rapidly. It was calculated that a 0.5 % drop in free fatty acid concentration at 1 % causes a 10 % increase in surface tension in this regime.

Vapour Pressure.

Similarly, Mustafa Kamal³ also found PFAD and PFAD - palm oil mixtures vapour pressure in the deodoriser operating regime. PFAD vapour pressure curve was about 40 percent lower than the calculated ideal mixture vapour pressure. PFAD vapour pressure curve lies between stearic acid and oleic vapour pressure between 1 torr to 0.1 torr.

This experiment was to account for the reported molecular association between fatty acids. These associated fatty acids, such the conjugated fatty acids acids, have long been suspected as the cause of decreasing separation efficiency, at lower PFAD concentration as reported by Stage⁶ in the falling film deodoriser experiments.

Nevertheless, even after compensating for PFAD fatty acids association effects, the PFAD - palm oil vapour pressure curve was still lower than estimated with an average about 20 - 40 percent lower than the calculated ideal mixture vapour pressure from 5 to 1 %. Below 1 %, vapour pressure dropped rapidly.

Molecular Association.

This series of investigation by Mustafa Kamal^{2,3} has obtained circumstantial evidence of Szabo Sarkadi hypothesis of associated fatty acids - oil molecules formation, Szabo Sarkaidi⁴. It further advocated that the molecular association reaction is a possible dominant mechanism driven by unsaturated high molecular weight compounds in the mixtures as observed by Fristad⁶. It has showed the affect of this reaction on palm oil thin liquid film surface tension, vapour pressure and relative volatility.

Structured Packings.

Mustafa Kamal^{2,3} then studied the impact of these findings on structured packing deodoriser column. It was found that the current stainless steel packings, e.g. the Mellapak, wettability were only been measured for materials with surface tension of 40 mN/m. Thus, it was

concluded that the performance of these packings for palm oils surface tension below 40 mN/m as reported by Flingoh⁹ and then by Mustafa Kamal², have not been measured. However, it was universally assumed the packings was completely wetted in this regime in Kister¹⁰.

Furthermore, the structured packings were reported by Fair & Bravo¹¹ and Bolles & Fair¹² as being very sensitive to the surface tension variation affecting wetting and in need of further investigation. In this case, Mustafa Kamal³ estimated from the surface tension data that there is a rate of 20 % increase in surface tension below 1 % PFAD concentration. This qualified as a substantial surface tension variation.

Mustafa Kamal³ then used the vapour pressure data to calculate the 'Apparent Relative Volatilities' of the 5 to 0.5 percent mixture of PFAD - palm oil. It was estimated that it decreased sharply from 40,000 to 200 indicating a rapid loss of separation capability as the amount of PFAD decreased in unrefined palm oil. This sudden and rapid fall will caused a dramatic increase in packing height to attain the original separation efficiency. The options open to design to overcome this effect are:-

1. Increase packing height thus increasing pressure drop and incur higher capital cost.
2. Decrease vacuum pressure or increase refining temperature which will be costly and degrade the oil respectively.
3. Finally and frequently, the stripping steam consumption is increase incurring a higher operating cost.

Relative volatility is vital for the determination of the Theoretical Number of Plates (N.T.P.) and for the overall mass transfer coefficients of the process. Fair & Bravo¹¹ stated that the neglect of the liquid phase mass transfer coefficients especially in vacuum distillation operations could undermine structure packing mass transfer capability.

In private communications, the H.E.T.P. of structured packings for palm oil deodorisation has yet to be determined. Primarily, the dearth of physio-chemical data is the outstanding obstacle. Secondly, the precision experiments to measure structured packing performance in the palm oil deodorisation have been difficult and tedious to design, control and run. Only recently, with the availability of laboratory scale structured packings by SULZER have work on test distillation mixture been undertaken, Hufton¹³.

In Malaysia, for the last four years, L.A.S.E.R. have designed, built and measuring structured packings performance in palm oil deodorisation from the 1 inches diameter laboratory scale to the 9 inches diameter pilot plant. The former extends the work by Hufton¹³ on laboratory scale structured packings whilst the latter is in progress, Mustafa Kamal¹⁴.

This work was augmented by earlier work and still on-going work on the rigorous modelling and simulation of the palm oil deodorisation using Tridiagonal Matrices computation by the author.

Nor Azian¹⁵ is also investigating the vapour - liquid surface interactions of the high molecular weight palm oils components in high temperature and very low vacuum pressure. This work will be extended to a variety of structured packing material and surfaces.

Underwetting.

In these light of the evidence of large relative volatility, surface tension variations and vapour - liquid surface interactions reported by Mustafa Kamal²³, Nor Azian¹⁵ and based on Kister¹⁰ reports of 'Underwetting' of acetone - water mixture with similar characteristics, Mustafa Kamal³ then proposed the probable thinning and instability of the palm oil liquid film in thin liquid film mass transfer equipments. This proposed underwetting phenomena usually causes a sharp decline in separation efficiency of thin liquid film mass transfer at below 1 % PFAD concentration.

Mustafa Kamal³ proposed that Stage⁸ had observed underwetting but had not reported as an underwetting phenomena. Stage noted the decline of separation efficiency below 1 % in the falling film deodoriser. This have been extensively observed and attributed to associated fatty acids, such the conjugated fatty acids acids. Presently, deodoriser designers have compensated for this effect by introducing a 15 % overdesign in the height of packings for vacuum distillation operations as reported by Kister¹⁰. This is a standard practice at SULZER and possibly TETRA LAVAL columns.

Impedements.

Undeniably, there was now an increasing gap in the understanding and estimation of packing efficiency of structured packed column deodoriser dealing with the low surface tension, large surface tension variation and rapid reduction of relative volatility of PFAD - palm oils thin liquid film mixtures between 5 to 0.005 % PFAD.

At this juncture, it is concluded that the current constraints in deodoriser design, particularly the recent structured packed column and the falling film column are due to the:-

1. Palm oil chemistry and reactions influence on mass transfer and thermodynamics of palm oil thin liquid film phenomena.
2. Accuracy and reliability of current palm oil liquid film properties estimation methods at the deodoriser operating regime.
3. Modelling and simulating palm oil thin liquid film behaviour in the structured packing pre-stripper, scrubber and the deodoriser design.
4. The lack of information to select the correct process models to simulate the complex and simultaneous processes of deacidification, deodorisation and decolourisation of palm oil occurring in the physical refining column.
5. The lack of experimental pilot plants measurement of the performance parameters of structured packings in palm oil deodorisation and scale-up to production scale process design and model.

Rationale for Future Research.

Therefore, future investigation are necessary in the palm oil surface phenomena to overcome its instability in order to exploit the process intensification strategy. The critical questions and choices faced by researcher in these studies are best summarised as:-

1. The determination of further engineering properties of thin liquid film surface properties; Liquid Diffusion Constant, Molecular Association Reaction Rate Constant and Thermal Diffusivity properties.
2. The influence of PFAD minor palm oil components and their molecular chemistry on the physio-chemical properties.
3. The choice between the conservative albeit safe equilibrium stage method with the complex but more accurate the mass transfer rate method in the modelling and simulation of structured packing physical refining deodorisation.
4. The choice of mass transfer theories between the traditional two film theory, the popular penetration theory and the tedious surface renewal theory.
5. The choice of structured packing separation efficiency parameters between HETP, HTU x NTU and other pilot plant empirical values.
6. The choice of structured packing performance correlations between Bravo et. al., Messner et al and confidential manufacturer correlations and understanding its limitations.

Future Research and Development.

These fundamental technologies will be critical toward establishing Product - Quality - Process - Utilities relationships in the deodoriser design and modelling.

1. Molecular Chemistry, Reactions & Design of High Molecular Weight Unsaturated Lipids.
2. Unsaturated Lipids Reactions Kinetics.
3. Surface Phenomena of Thin Liquid Film.
4. Film & Surface Mass Transfer Theory.
5. Advanced Mass Transfer Materials (Ceramics, Non Ferrous Metals & Surface Coated Catalyt).
6. Complex, Batch & Reactive Distillation Processes.
7. Novel Zeolite Catalyst.

Future Paradigm of the Palm Oil Industry.

Inevitably, global markets will demand future palm oil and oleochemicals products which are environmental friendly, high quality specification, wide variety and most important, high value.

This will required a flexible equipment configuration, adaptable to low and high production volume, control of high quality speciality products, highly automated and rapid turnaround processes. Furthermore, it must be efficient and environmental friendly.

CONCLUSION

Finally this paper has proposed the linkage between the palm oil thin liquid film physio-chemical properties and the separation efficiency and utilities requirements of thin liquid film mass transfer processes. The impact of these findings will be most profound in the design and modelling of packed column, thin falling film column and molecular distillation column processes. For the equipment manufacturers, it will affect the separation efficiency and capital costs of these equipment. On the other hand, Malaysian palm oil refiners will be more concerned with the impact on utilities costs of stripping steam, vacuum pressure and refining temperature of these processes.

It is our frevent hope that the understanding and eventual mastery of this phenomena will give birth to a new generation of deodoriser design which should possessed a wider range of product flexibility, a higher process efficiency and a much larger production capacity. It is our eternal wish that this technology will make Malaysian refiners more competitive, more productive and even more environmental friendly.

BIBLIOGRPAHY

1. Sjoberg P. (1987), New Development in the Deodorization Process, 1987 International Oil Palm / Palm Oil Conferences : Progress & Prospects, 29th June - 1st July 1987, Kuala Lumpur, Malaysia.
2. Mustafa Kamal Abdul Aziz (1993), Surface Tension Of Palm Fatty Acids Distillate (PFAD) - Palm Oils Mixture., Malaysian Science & Technology Congress '93 : R& D Progress and Achievements, Ming Court Hotel Kuala Lumpur, Malaysia
3. Mustafa Kamal Abdul Aziz (1994), Process Modelling & Design of Physical Refining : Influence of Fatty Acids - Palm Oils Equilibria ., 1994 PORIM National Palm Oil Milling and Refining Technology Conference, Kuala Lumpur Hilton, Malaysia.
4. Sarkadi D.S(1958), Laboratory Deodorizer with a Vaporization Efficiency of Unity, *JAOCS*, 35 : 472 - 475.
5. Pryde E.H (1979), Fatty Acids, *JAOCS*.

6. Fristad W.E (1992), Oligomerization of Saturated and Unsaturated Fatty Compounds, *Henkel - Referate 28*, Henkel - Referate International Edition, p39 - 42.
7. Stage H.(1985), The Physical Refining Process, *JAOCS*, 62(2) :299 - 308.
8. Stage H.(1984), New Energy Saving Multi-Stage Counter Current Film Process for Physical Refining of Vegetable Oils with Extreme Low Environmental Load. *ATT Chem. Eng. Prog.*, Serie O, no. 17.
9. Flingoh and Let C.C (1992), Surface Tension of Palm Oil, Palm Olein and Palm Stearin, *ELAEIS*, PORIM, 4(1) 6 : 27 - 31.
10. Kister H.Z and Gill D.R (1992), Distillation and Absorption, Institution of Chem. Engrs., U.K, Birmingham.
11. Fair J.R and Bravo J.L (1990), Distillation Columns Containing Structured Packing, *Chem. Eng. Prog.*, 86(1) : 19 - 29.
12. Bolles W.L and Fair J.R (1982), Improved Mass-Transfer Model Enhances Packed-Column Design, *Chem. Eng.*, 7 : 109 - 116.
13. Hufton J.R (1983), Performance and Scale-up of Laboratory Scale Distillation Columns Containing Structured Packing, M.S Thesis The University of Texas, Austin.
14. Mustafa Kamal Abdul Aziz (1993), Design and Scale-up of Vacuum Distillation Process for the Deacidification of Crude Palm Oil. Malaysian Science & Technology Congress '93 : R& D Progress and Achievements, Ming Court Hotel Kuala Lumpur, Malaysia
15. Nor Azian Morad (1994), Measurement of Vapor Pressure of Palm Oil Constituents Under Vacuum, 1994 PORIM National Palm Oil Milling and Refining Technology Conference, Kuala Lumpur Hilton, Malaysia.

KAJIAN KEMUNGKINAN PENGUBAHSUAIAN KOMPOSISI GAS PETROLEUM CECAIR DI MALAYSIA

Zainal Zakaria**, Mohd Norani Abd. Rahman, Abd. Aziz Abd. Kadir
G. Raju, Abu Samah Nasir & Mohd Redhuan Ramlee

**Jabatan Kejuruteraan Polimer & Gas
Fak. Kej. Kimia & Kej. Sumber Asli
Universiti Teknologi Malaysia**

ABSTRAK

Penggunaan secara meluas gas petroleum cecair di Malaysia bermula pada tahun 1985 dengan purata jualan sebanyak 250 matrik tan sebulan. Kebanyakan pembekalan gas dibuat melalui selinder mudahalih kepada pengguna-pengguna domestik, komersial dan industri. Komposisi campuran yang dibekalkan adalah secara 30% propana dan 70% butana. Penggunaan komposisi berkenaan telah mewujudkan fenomena ketidakhabisan gas. Purata kuantiti baki dalam selinder berkapasiti 50 kg sebanyak 5.78 kg dengan komposisi 2.17/97.82 antara propana dan butana. Kajian yang dilakukan melalui pengubahsuaian kandungan propana ke dalam campuran gas petroleum cecair. Kajian melibatkan satu fabrikasi rig mudah. Keputusan yang diperolehi menunjukkan semua komposisi termasuk propana komersial gagal mengosongkan selinder. Walau bagaimanapun, berdasarkan faktor-faktor kejatuhan suhu, tekanan dan pengeluaran jisim maka propana yang melebihi 60% perlu dipertimbangkan sebagai satu rekabentuk komposisi baru bagi meminimumkan baki.

PENGENALAN

Perkembangan penggunaan gas petroleum cecair di Malaysia masih di peringkat permulaan dan hanyalah terhad kepada kawasan-kawasan yang tidak dilalui oleh talian paip gas asli. Penghantaran gas tersebut dilakukan melalui sistem selinder pukal dan sebahagian secara selinder pukal¹. Objektif muktamad negara adalah untuk mempelbagaikan penggunaan tenaga dan mengurangkan pergantungan terhadap minyak sebagai sumber tenaga utama².

Memandangkan sektor ini masih terlalu baru maka masalah ketidakhabisan gas dalam selinder mudahalih telah dikenalpasti. Malah ini terjadi apabila gas petroleum cecair dikeluarkan secara peruwapan kelompok di mana suhu dan tekanan jatuh sehingga takat di mana tekanan tidak cukup untuk membekalkan daya tolakan yang diperlukan³. Akhir-akhir ini banyak rungutan daripada pengguna telah diterima oleh pihak yang terlibat tentang masalah di atas. Terdapat juga segelintir pihak pembekal yang tidak bertanggungjawab telah mengambil kesempatan ini di mana mereka telah mengumpul baki-baki tersebut. Laporan yang diterima oleh pengkaji bahawa total baki daripada 13 selinder akan menghasilkan 1 selinder pada kuantiti jualan.

Kajian mengenai gas petroleum cecair secara terperinci tidak banyak dilakukan sehingga kini terutamanya mengenai penganalisan baki. Hanya satu pada tahun 1970 oleh syarikat ESSO united Kingdom⁴. Lain-lain kajian hanya tertumpu kepada aspek pembakaran.

Objektif dan Skop

Objektif kajian adalah untuk mempertingkatkan pemahaman terhadap kelakuan proses peruwapan gas petroleum cecair dalam selinder mudahalih berdasarkan kepada keadaan persekitaran Malaysia.

Skop kajian ditumpukan kepada komposisi gas petroleum cecair yang berbeza-beza pada selinder mudahalih berkapasiti 50 kg, suhu persekitaran 30°C dan 35°C dan kadar alir mengikut beban penggunaan sektor komersial. Parameter-parameter yang diselidiki adalah profile suhu, profile tekanan dan profile pengeluaran jism.

METODOLOGI

Percubaan dijalankan dalam makmal melalui satu fabrikasi rig mudah tetapi lengkap seperti ditunjukkan dalam Rajah 1.

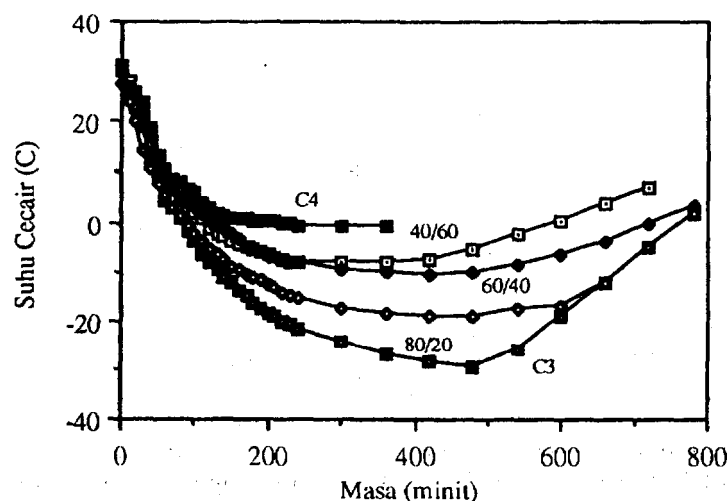
Pembacaan data-data yang diselidiki dibuat pada julat masa 10 minit dan selepas tempoh empat jam julat ditukar kepada satu jam. Nilai kadar alir ditetapkan pada permulaan percubaan mengikut beban penggunaan sektor komersial iaitu 10 m³/jam, 15 m³/jam dan 20 m³/jam. Suhu persekitaran dikawal menggunakan kotak kawalan suhu antara 30°C dan 35°C. Tatacara kajian diulas dalam bentuk carta alir seperti ditunjukkan dalam Rajah 2.

KEPUTUSAN DAN PERBINCANGAN

Keputusan dan perbincangan dikemukakan melalui pengambilan contoh tertentu daripada percubaan yang dilakukan.

Profile Suhu

Suhu mempunyai corak yang sama untuk semua komposisi di mana pengkonding suhu yang paling bawah mencatatkan bacaan yang paling rendah. Ini kerana semasa proses peruwapan, haba di ambil daripada sekitar dan cecair itu sendiri. Oleh yang demikian semakin jauh titik daripada permukaan maka suhunya menjadi semakin rendah kerana pengambilan haba berlaku secara terus menerus.



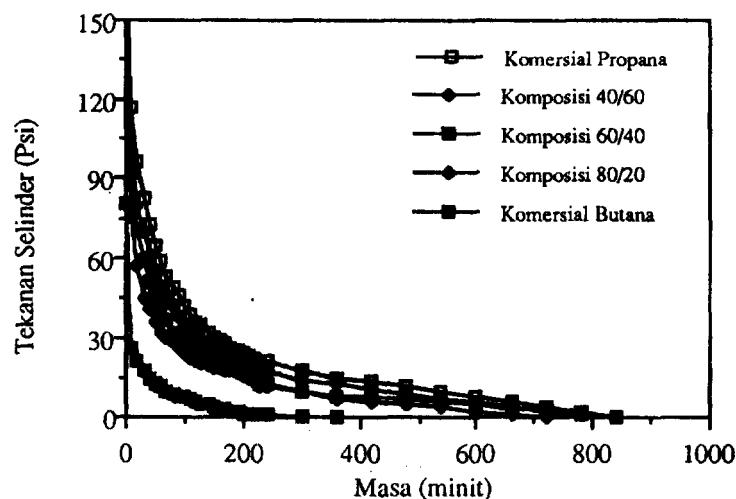
RAJAH 3: Kesan Kejatuhan Suhu Melalui Penambahan Kandungan Propana ke Dalam Butana Pada Kadar alir 10 m³/jam dan Suhu 35°C

Apabila lebih banyak propana dicampurkan maka lebih rendah suhu dicatatkan.

Walau bagaimanapun, propana masih mampu melakukan proses peruwapan kerana propana mempunyai suhu takat didih jauh lebih rendah daripada butana. Oleh yang demikian, kuantiti haba yang diperlukan untuk meruwap lebih sedikit diperlukan oleh propana berbanding butana⁵. Dalam merumuskan peranan suhu terhadap rekabentuk komposisi gas petroleum cecair maka faktor cepat atau lambatnya mencapai takat embun adalah dipertimbangkan. Ini kerana apabila takat embun dicapai maka peruwapan akan terhenti⁶.

Profile Tekanan

Gambarajah 4 adalah contoh kejatuhan tekanan yang terjadi pada pelbagai komposisi dengan kadar alir $10 \text{ m}^3/\text{jam}$ dan suhu persekitaran 35°C . Berdasarkan kepada rajah tersebut, maka 3 rumusan yang boleh dibuat.



RAJAH 4: Kesan Pertambahan Kandungan Propana Terhadap Kejatuhan Tekanan Pada $10 \text{ m}^3/\text{jam}$ dan Suhu 35°C

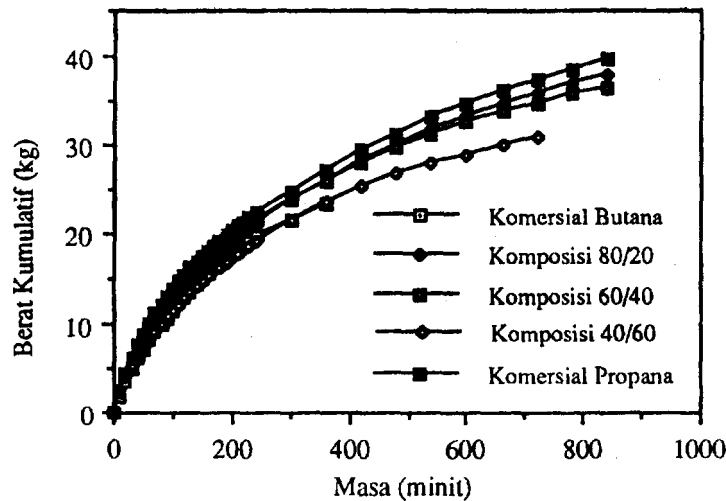
Pertama, semua komposisi melakukan corak kejatuhan tekanan yang sama iaitu kejatuhan paling cepat berlaku pada permulaan percubaan dan lama kelamaan menjadi semakin perlahan dan mengahala ke nilai kosong. Keadaan ini terjadi disebabkan pada permulaan percubaan haba bekalan datangnya daripada kedua-dua punca tetapi pada satu ketika pembekalan hanya datang daripada cecair sahaja⁷.

Kedua, Semakin tinggi kandungan propana menghasilkan kejatuhan yang agak sukar. Ini disebabkan propana mempunyai tekanan wap yang tinggi.

Ketiga, komposisi 60/40 dan 40/60 melakukan kejatuhan yang hampir sama sehingga ke suatu ketika tetapi berbeza apabila semakin lama percubaan dilakukan. Ini bermakna molekul-molekul propana melakukan kelakuan yang sama di antara kedua-dua komposisi iaitu membantu molekul butana yang wujud bersama-sama dalam selinder.

Profile Pengeluaran Jisim

Corak pengeluaran jisim dalam selinder sama seperti corak kejatuhan tekanan iaitu akan menghampiri nilai kosong walaupun pada hakikatnya angka kosong tidak akan dicapai⁷. Walau bagaimanapun keputusan pengeluaran berat dipersembahkan secara pengeluaran kumulatif. Rajah 5 merupakan contoh pengeluaran jisim secara kumulatif pelbagai komposisi pada kadar alir $10 \text{ m}^3/\text{jam}$ dan suhu persekitaran 35°C .

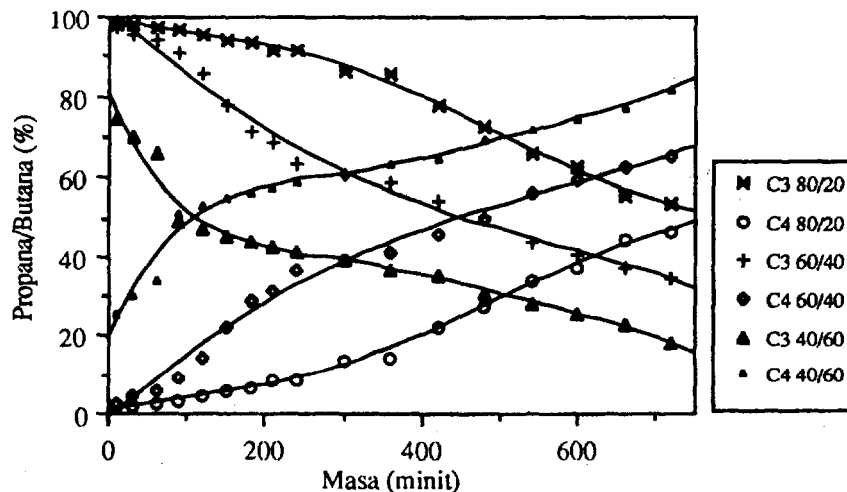


RAJAH 5: Contoh Pengeluaran Berat Kumulatif Berbagai Komposisi Pada Kadar alir $10\text{m}^3/\text{jam}$ dan Sekeliling 35°C

Berdasarkan kepada rajah tersebut menunjukkan corak pengeluaran jisim kumulatif merupakan suatu garis lengkung dan akan mendatar pada suatu ketika. Semakin lambat pendataran terjadi maka semakin minimum baki yang terhasil. Oleh yang demikian, kandungan propana yang berkualiti 60% dan lebih mempunyai kecenderungan yang agak lambat berbanding komposisi 40/60 dan butana komersial.

Komposisi Wap Terkeluar

Rajah 6 menunjukkan corak komposisi wap terkeluar pelbagai komposisi campuran pada kadar alir $10\text{ m}^3/\text{jam}$ dan suhu persekitaran 35°C .



RAJAH 6 : Perbezaan Komposisi Wap Terkeluar Pelbagai Komposisi Pada Kadar alir $10\text{ m}^3/\text{jam}$ dan Suhu Persekitaran 35°C

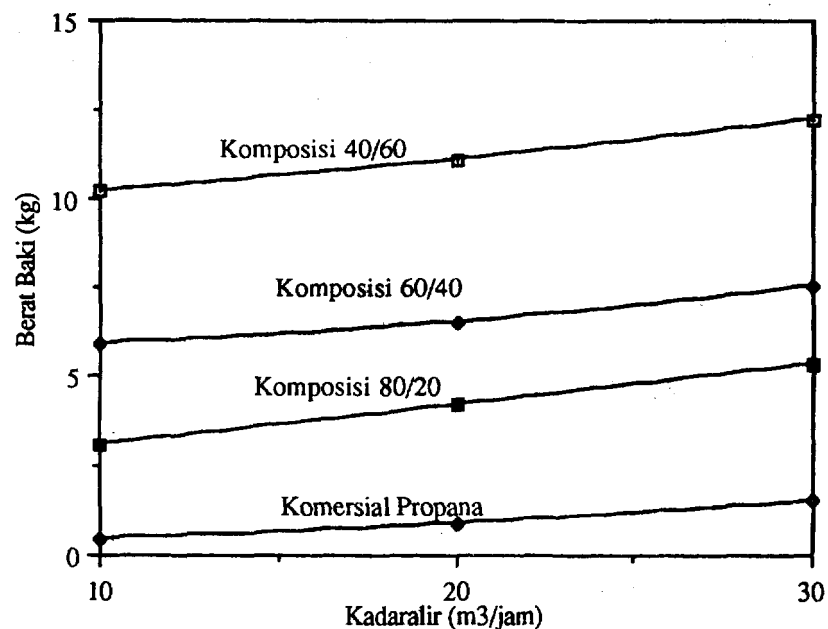
Daripada rajah tersebut menunjukkan propana semakin berkurang sementara butana semakin bertambah terhadap masa. Ini disebabkan propana mempunyai tenaga

kinetik yang lebih tinggi maka lebih cepat dan senang terlepas ke dalam fasa wap seterusnya keluar daripada selinder. Walau bagaimanapun, garisan yang diperolehi tidak menunjukkan garisan yang licin. Keadaan ini disebabkan semasa proses peruwapan, wujudnya proses perolakan kerana haba yang dibekalkan lebih banyak diperolehi daripada lokasi yang berdekatan dengan dinding selinder dan yang terbanyak di bahagian dasar selinder⁸. Justeru itu, molekul-molekul yang terlepas hanya berlaku jika tiada halangan terhadap pergerakannya.

Komposisi campuran 80/20 menghasilkan garisan berbentuk cembung dan kecembungannya semakin berkurang pada komposisi campuran 60/40. Walau bagaimanapun, garis berbentuk cekung terjadi pada komposisi campuran 40/60. Ini bermakna molekul propana dalam komposisi campuran 40/60 lebih cepat keluar dan akan menghadapi masalah dalam pengagihan tenaga kepada molekul butana pada masa berikutnya.

Baki Gas Petroleum Cecair

Semua komposisi gas petroleum cecair dalam selinder tidak dapat mengosongkan selinder. Tetapi apabila lebih banyak propana dicampurkan akan menghasilkan baki yang lebih minimum. Rajah 7 menunjukkan hubungan kuantiti baki pelbagai komposisi campuran dan kadar alir pada suhu persekitaran 30°C.



RAJAH 7 : Hubungan Kuantiti Baki Pelbagai Komposisi Terhadap Kadar alir dan Suhu Persekitaran 30°C

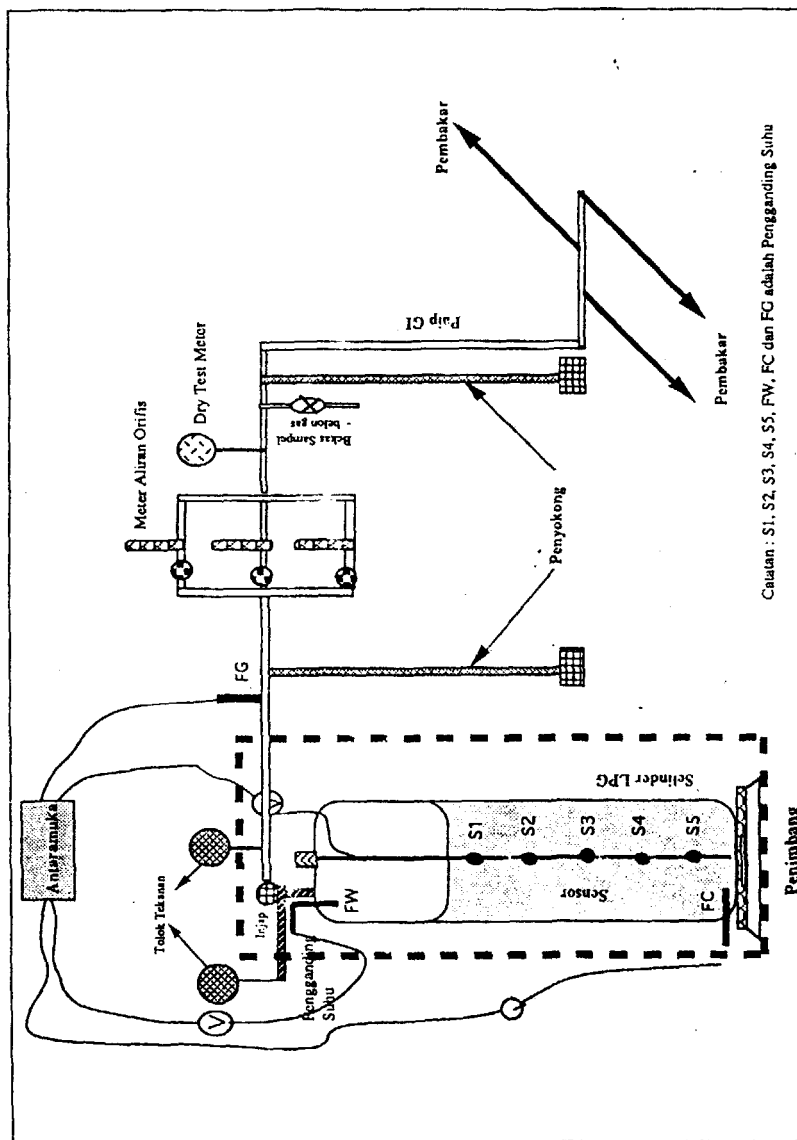
Berdasarkan kepada rajah tersebut, hubungan kuantiti baki dan kadar alir merupakan suatu garis eksponen. Perbezaan antara komposisi campuran 80/20 dan 60/40 akan semakin kecil dengan peningkatan kadar alir. Ini memberi petanda bahawa komposisi campuran 60% propana atau lebih perlu dicampurkan dalam campuran gas petroleum cecair. Walau bagaimanapun pada kadar alir melebihi 20 m³/jam, hanya propana komersial sesuai digunakan.

KESIMPULAN

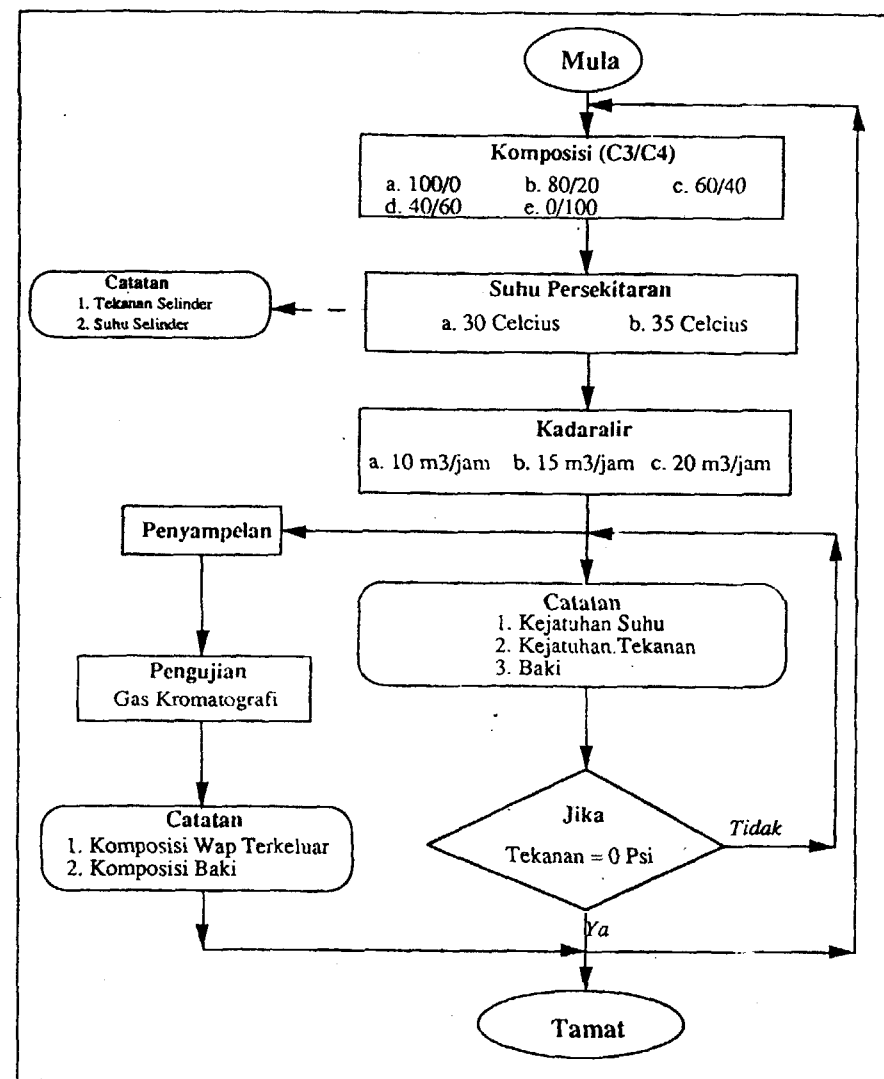
Semua komposisi gas petroleum cecair yang dicampurkan dalam selinder berkapasiti 50 kg yang diwapkan secara peruwapan asli gagal mengosongkan selinder. Pengurangan baki boleh dikurangkan apabila peratus propana adalah sebanyak 60% atau lebih. Ini disokong dengan penggunaan gas petroleum cecair di Thailand yang menggunakan peratus berat secara 70% propana dan 30% butana⁹. Malaysia boleh menambahkan kepada kuantiti tersebut memandangkan berlakunya pertambahan pengeluaran propana secara berlebihan¹⁰.

RUJUKAN

1. Surani Abd. Rahim (1991). Sistem Pengagihan Gas - Kajian Terhadap Faktor Keserentakan. Tesis Sarjana Muda. Fakulti Kejuruteraan Kimia & Kejuruteraan Sumber Asli. Universiti Teknologi Malaysia.
2. Azizan Zainal Abidin (1993). The Petroleum Industry in Malaysia. Its Currents Goals and Future Challanges. Oil & Gas News. 6.
3. Zainal Zakaria (1993). Fenomena Peruwapan Gas Petroleum Cecair Dalam Persekitaran Malaysia. Prosiding. Simposium Sumber Alam Tropika. Universiti Malaysia Sarawak. Sarawak.
4. Dick, M.N. & Timns (1970). The Prediction of Vapour Offtake Rates from LPG Cyclinder. Journal of The Institute of Fuel. Vol. XIII, 407.
5. Clark, W.W. (1983). Physical and Chemical Properties. Handbook Butane-Propane Gases. Second Edition. William Publisher. New York.
6. KOSAN (1986). Liquefied Petroleum Gas. KOSAN. Tokyo, Japan.
7. Turner, C.C. (1955). The LP-Gas Man's Encyclopedia of Method and Equipments. First Edition. A Moore Gas Publication. New York.
8. Zainal Zakaria (1994). Penganalisaan Baki Gas Petroleum Cecair Dalam Selinder Mudahalih. Buletin. Fakulti Kejuruteraan Kimia & Kejuruteraan Sumber Asli. Universiti Teknologi Malaysia.
9. Suphochana, S. (1981). Substitution of LPG for Diesel Engine in Farm Machinery. Preliminery Report on Testing. Petroleum Authority of Thailand.
10. Petronas Dagangan Sdn. Bhd. (1992). Effect of Change Composition on Flame Characteristics. Preliminery Report on Testing. Tidak Terbit.



RAJAH 1 : Diagram Skematik Rig Kajian



RAJAH 2 : Carta Alir Percubaan Kadar alir Berterusan

SPECIFIC HEAT CAPACITY OF VEGETABLE OILS USING THE HEAT-FLUX DIFFERENTIAL SCANNING CALORIMETER

Noor Azian Morad, Mohammad Idrees and Siva Kumar Supramaniam
Lipids Applied Science and Engineering Research (L.A.S.E.R.), Department of
Chemical Engineering, Universiti Teknologi Malaysia, Jalan Semarak, 54100
Kuala Lumpur, MALAYSIA.

ABSTRACT

The lack of data on physical properties has been the main reason as to the inability to improve, optimise and design the various unit operations in the palm oil refinery. There had been some advances in the energy conservation and equipment modifications. However, a comprehensive approach to this aspect must rely on a sound database. One of the physical properties which is of considerable importance in the energy optimization calculations is the specific heat capacity, C_p of palm oil.

This work relates to the determination of specific heat capacity of some of the common vegetable oils. The specific heat capacity of palm oil together with other vegetable oils; soyabean, corn, coconut and peanut oils are determined using a heat flux differential scanning calorimeter. The specific heat values of palm oil are compared and correlated to its binary triglyceride mixture of the two major components, namely 1,2-dipalmitoyl-3-oleoyl, PPO and 1,2-dioleoyl-3-palmitoyl, OOP.

The specific heat capacity values obtained using this method are demonstrated to be reliable based on rigorous statistical analysis. The data generated through this work is expected to be of significant use both to the palm oil industries and to the researchers in this area.

Keywords: specific heat capacity, differential scanning calorimeter (DSC), vegetable oil, palm oil, triglycerides, binary mixture.

INTRODUCTION

The need for the reliable specific heat capacity data in the design of unit operations cannot be overemphasised. The heat duty during transfer operations which is required throughout chemical industries depends largely on the specific heat capacity of the materials. Although heat capacity can be defined in many ways and all are in common use, the specific heat capacity at constant pressure, C_p is of greatest interest in heat transfer work. Specific heat data are of fundamental importance in the heat exchanger calculations in process equipment design. The importance of energy conservation in reducing manufacturing costs in the processing of palm oil has long been recognised and some of the means of achieving this in palm oil refining have been outlined Wong¹ and Musitah and Wood². Nevertheless, proper and considerable energy conservation can only be realised if reliable C_p data are available in the whole range of industrial operating conditions.

Some data in the past have been reported on specific heats of oils and fats, but so far only one refers specifically to palm oil or palm kernel oil³. Timms³ has specified that for practical purposes the specific heats of liquids oils and fats can be estimated using a simple linear relationship. According to Timms³, the relationship is probably satisfactory for palm kernel and coconut oils since the variation of specific heat with molecular weight is small. The temperature range in which this correlation is applicable however, is not specified.

Similar correlations have been published for other oils in both solid and liquid phases at specified temperature ranges as reported in Bailey's⁴. However, most of the published data on the specific heat of oils at high temperatures have been of a low order of accuracy (Bailey's⁴). Specific heat capacity data for palm oil is not available at high temperatures even though some processes such as deodorisation in palm oil refining is carried out at temperatures of 250°C at 1mmHg (under vacuum).

A survey of literature published on the estimation of liquid heat capacity revealed two types of methods with general application (Reid, Prausnitz and Poling⁵). A set of methods which can be

classified as group contribution methods and the other methods based on the principle of the corresponding state methods.

Empirical methods for estimating the specific heat capacity of liquid triglycerides have been reviewed and compared with experimental values in a previous paper by the authors⁶. It has been shown that the estimation methods developed by *Phillips and Mattamal*⁷ (a group contribution method) gave the best approximation of within 6% deviation from the experimental specific heat capacity values. The correlations however, are only applicable to saturated triglycerides. Other estimation methods reviewed in the above article were found to be quite unsatisfactory.

For liquid mixtures, *Teja*⁸ has examined the extension of the multiple reference fluid method to the liquid heat capacity prediction. This method does not use the assumption that the mixture molar heat capacity is a mole fraction average of the pure component values, an assumption which neglects any contribution due to the effect of temperature on heats of mixing. *Vittal Prassad et al.*⁹ combine the concept of both group contribution and corresponding state to produce a correlation similar to the Antoine equation in predicting vapor pressure. The method has been extended to liquid mixtures with the same constants and incorporating some correlations for estimating mixture properties.

Both the estimation methods for liquid mixtures *Teja*⁸ and *Vittal Prassad et al.*⁹ require critical properties of the pure components. Critical properties of palm oil and triglycerides are not available, and therefore, none of these estimation methods could be applied to palm oil. In this work, a relationship between C_p values of refined bleached and deodorised palm oil, RBDO to its binary triglyceride mixture of the major components namely 1,2-dipalmitoyl-3-oleoyl, PPO and 1,2-dioleoyl-3-palmitoyl, OOP is sought.

Specific heat capacity of some other common edible oils have also been determined and presented in this work and the results have been compared with some of the earlier reported values.

MATERIALS AND METHODS

Samples

The binary triglyceride mixture samples were made from a mixture of pure triglyceride samples 1,2-dipalmitoyl-3-oleoyl, PPO and 1,2-dioleoyl-3-palmitoyl, OOP obtained from Sigma Chemical Co, England, with a purity of higher than 99%. Refined bleached, deodorised palm oil, (RBDO) were obtained from Pandamaran Oil Product, Felda Refinery Corporation in Port Klang, Selangor, West Malaysia. The soyabean, corn, coconut and peanut oils were obtained from the market shelf with labels claiming that these oils contained 100% of the pure oils. All the vegetable oil samples were sent to PORIM for their triglyceride composition (by carbon number) analysis.

Apparatus

A Seiko DSC 220 heat-flux type DSC instrument connected to a Seiko SSC 5200 thermal analysis system was used in these experiments.

Procedure

The method known as the round robin test, RRT was used in specific heat capacity measurements (*Morad et al.*¹¹). The procedure requires two empty aluminium, open containers with approximately the same weight. The experiment was run from 50 °C to 250 °C with nitrogen flow in the furnace. The operating conditions i.e. the sample weight, the scan rate and the nitrogen flow for the various sample types of sample binary triglyceride mixture, RBDO and vegetable oils were different and the best operating conditions were determined through rigorous experimentation and using a statistical analysis described in a previous paper by the authors¹¹.

RESULTS AND DISCUSSION

The study of the specific heat capacity of pure triglycerides, binary triglyceride mixture as well as the refined, bleached and deodorised palm oil, RBDO is necessary in establishing correlations between pure triglycerides, binary triglycerides mixture and palm oil mixture.

The chemical composition of the palm oil varies between species and also within the same species depending on geographical location and harvesting and processing practice. A typical analysis of palm oil from tenera species (the major species in Malaysia) is reported by *Abdul Kifli*¹⁰ and is reproduced here, *Table 1*. It can be observed from the above analysis that the two major triglyceride

components of the palm oil are 1,2-dipalmitoyl-3-oleoyl, PPO (C50) and 1-palmitoyl-2,3-dioleoyl, POO (C52) in the ratio of 27.5 mole% to 22.6 mole % respectively. If we consider the palm oil consisting of binary mixture PPO and POO, then the ratio is 55% : 45% mole. 1-palmitoyl-2,3-dioleoyl, POO is not available commercially, therefore 1,2-dioleoyl-3-palmitoyl, OOP which has the same molecular weight and the atomic composition (but different in molecular structure) was used as a substitute for POO. It was assumed here, that for similar structures such as 1-palmitoyl-2,3-dioleoyl, (POO) and 1,2-dioleoyl-3-palmitoyl, (OOP), the difference in acid group positions should not influence the physical property. On this basis, the binary triglyceride mixture was made from 55 mole % 1,2-dipalmitoyl-3-oleoyl, PPO and 45 mole % 1,2-dioleoyl-3-palmitoyl, OOP.

The improved operating conditions for the specific heat capacity of triglycerides with our DSC and under the range of operating conditions (*Morad et.al.*¹¹) were used with the binary triglyceride mixture. The optimum operating conditions for RBDO were determined by the same procedure and were found to be scan rate 17°C/min, sample weight of 21mg and nitrogen flow of 25ml/min. Both the results for binary triglyceride mixture and RBDO are reported at a confidence level of 95%. In another study the specific heat capacity of some of the more common vegetable oils were determined by *Supramaniam*¹², the optimum operating conditions of the DSC for these set of oils were found to be 15° C/min., 21mg and nitrogen flow of 100ml/min respectively. Coconut oil was used as a basis to determine the best operating conditions in this study and the confidence level of 90% was used on the results. The specific heat capacity of all the samples studied can be represented by a straight line relationship given by:

$$C_p \text{ (J/g } ^\circ\text{C)} = A (T ^\circ\text{C}) + B.$$

This is summarised in *Table 2* for all the vegetable oils.

The specific heat capacity of the binary triglyceride mixture (OOP - PPO) and the pure triglycerides (OOP and PPO) are plotted in *Figure 1*. Had the binary triglyceride mixture followed the mixture rule:

$$C_{p(\text{mix})} = \sum x_i C_{p_i} \quad (2)$$

where, $C_{p(\text{mix})}$ - specific heat capacity of liquid mixture,

x_i - mole fraction of the pure component, and

C_{p_i} - specific heat capacity of pure component liquid,

the specific heat capacity of the binary mixture would have fallen approximately between the two curves for the pure components. However, it was observed that the specific heat capacity of the binary triglyceride mixture was close to one of its components, 1, 2-dioleoyl-3-palmitoyl, OOP (C52) which is the dominant (major) component in the mixture (55 mole % in the binary mixture and 27mole % in the palm oil). This major component also happens to be the poly(di) unsaturated triglyceride. This also indicates that there is a possible association between the two triglycerides when mixed.

Further, it was observed that the specific heat capacity of RBDO are similar to those of its binary triglyceride mixture as illustrated in *figure 2*. Therefore, if one can provide a satisfactory relationship between the binary triglyceride mixture and its pure component triglycerides, it should be possible that the specific heat capacity of vegetable oils can be approximated to its binary triglyceride mixture.

For practical purposes *Timms*³ has proposed a generalised equation for vegetable oils and fats including palm oil. *Figure 3* shows that the specific heat capacity calculated by the correlation proposed by *Timms*³ are higher than those found experimentally for palm oil. The values estimated by the correlation are higher by about 3% at lower temperatures and increase up to 6% at higher temperatures (>200°C). However, *Timms*³ has not specified for which type of palm oil the correlation applied (since palm oil may refer anything from its crude form right up to the fully processed oil) nor the temperature range in which the correlation may be applied. This suggests that the correlation proposed is a crude approximation for the specific heat capacity for all oils and fats and therefore has failed to indicate any distinct variation between the specific heat capacity of palm oil from the other oils.

The specific heat capacity of all the vegetable oils tested, coconut, corn, peanut soyaoil and RBDO (palm oil) are compared in *figure 4*. RBDO (palm oil) was found to have a similar slope to that

for soya oil. The specific heat capacity values of palm oil are however higher than soya oil. The specific heat capacity of all the three other oils, coconut, corn and peanut have a much more gradual slope, thus the specific heat of these oils are lower than those of palm oil at higher temperatures. A comparison with reported experimental values are also made for the case of peanut and soya oil as shown. Comparison is difficult since the specific heat capacity values are dependent on the triglycerides present. The oils may be the same but the triglyceride composition may vary according to species. Table 3 gives the GC analysis on all the vegetable oil samples in terms of the triglycerides present in the oil (Tang¹³). The analysis indicated that the major triglycerides found in soya oil, corn oil and peanut oil are the C52 and C54 which made up 80 - 90% of all the triglycerides whilst RBDO (palm oil) has the major triglyceride components as C50 and C52. Coconut oil has the widest range of the lower carbon number triglycerides, the majority of which fall within C32 and C40. Comparing the specific heat capacity values of the vegetable oils with the triglyceride composition, it can be concluded that the specific heat capacity values are not only influenced by the triglyceride carbon number but also on the degree of unsaturation present in the triglycerides.

CONCLUSIONS

1. The specific heat capacity of the binary triglyceride mixture is similar to one of its pure component triglyceride, 1,2-dioleoyl-3-palmitoyl, OOP (C52), suggesting that the specific heat of the mixture is controlled by the major polyunsaturated triglyceride component and that there is a possible association between the molecules. The mixture rule is not appropriate to be used to estimate the specific heat capacity of the binary mixture.
2. Specific heat capacity of the RBDO (palm oil) was found to be similar to its binary triglyceride mixture of the major component triglycerides.
3. The specific heat capacity correlation for all the vegetable oils tested; coconut, corn, peanut, soya oil and RBDO (palm oil) can be correlated by a linear relationship.
4. The specific heat capacity of vegetable oils are not only influenced by the triglyceride carbon number but also the degree of unsaturation present in the triglycerides.
5. It is postulated that the specific heat capacity of vegetable oils can be estimated from its pure component triglyceride properties if the major triglyceride composition is known. However, more data may be required to confirm this.

ACKNOWLEDGEMENTS

The authors wish to express appreciation to MIMOS for the DSC equipment, Government of Malaysia for research grant and members of the LASER group for their support and co-operation.

NOMENCLATURE

- | | |
|----------------------------|---|
| C | - carbon number - e.g. C36 indicates a carbon number 36 |
| C _p | - specific heat capacity at constant pressure in J/g K |
| C _{p_i} | - specific heat capacity of pure component liquid. |
| C _{p(mix)} | - specific heat capacity of liquid mixture |
| DSC | - differential scanning calorimeter |
| GC | - gas chromatography |
| OOP | - 1,2-dioleoyl-3-palmitoyl, a triglyceride |
| PPO | - 1,2-dipalmitoyl-3-oleoyl, a triglyceride |
| T | - temperature, C |
| x _i | - mole fraction of the pure component i |

REFERENCES

1. Wong MH (1985). Steam Energy Conservation In Palm Oil Physical Refining Plants, *paper presented at Chem. Asia, Singapore.*
2. Masitah Hasan and R. M. Wood (1987), The Application Of Pinch Technology For Energy Conservation In A Palm Oil Refinery, *paper presented at 4th. APCChE, Asian Pacific Confederation Of Chemical Engineering.*
3. Timms RE (1985). Physical Properties of Oils and Mixtures of Oils, *JAOC'S*, **62**(2): 241- 248.
4. *Bailey's Industrial Oil and Fat Products*, Swern (1979), Editor, Vol. 1, 4th Ed., John Wiley and Sons, New York.
5. Reid RC, Prausnitz JM and Poling B E (1988). The Properties of Gases and Liquids, 4th Ed., Mc Graw Hill, New York.
6. Morad NA, Idrees M and Hasan AA (1994). Specific Heat Capacity of Pure Triglycerides By Heat-Flux Differential Scanning Calorimeter, to be published in the *J. Thermal Analysis.*
7. Phillips JG and Mattamal MM (1976). Correlation Of Liquid Heat Capacities For Carboxylic Esters, *J. Chem. Eng. Data*, **21**: 228.
8. Teja AS (1983). Simple Method for the Calculation Of Heat Capacities of Liquid Mixtures, *J. Chem. Eng. Data*, **28**: 83-85.
9. Vittal Prasad TE, Rajiah A and Prasad DHL(1993). On the dependence of liquid heat capacity on temperature and molecular structure, *The Chemical Engineering Journal*, **52**: 31-35, .
10. Abdul Kifli H (1981). *Study Of Palm Oil With Special Reference To Interesterification*, M.Sc. Thesis , University of St. Andrews, United Kingdom.
11. Morad N A, Idrees M and Hasan AA(1994). Improved Conditions for the Measurement of Specific Heat Capacity, C_p of Pure Triglycerides By Differential Scanning Calorimeter, to be published in *J. Thermal Analysis.*
12. Supramaniam SK(1993). *Penentuan Haba Spesifik Minyak Sayuran Menggunakan Alat Heat-Flux DSC*, B.Sc. Project Thesis , FKKKSA, UTM, Kuala Lumpur, Malaysia.
13. Tang TS (1993). Palm Oil Research Institute Of Malaysia (PORIM), *Private Communication*, April.

TABLE 1. MAJOR TRIGLYCERIDE COMPONENTS IN THE MALAYSIAN OIL PALM SPECIES

Carbon Number	Major Triglycerides	Dura	Tenera	Pisifera	Melanococca
46 ¹		0.5 (0.7) ²	0.4 (0.6)	0.1 (tr)	
	PMP	0.2	0.2	0.1	
48		6.7 (7.2)	6.7 (8.4)	3.4 (4.1)	0.4 (0.8)
	PPP	4.5	5.0	2.6	0.2
50		41.1 (44.6)	37.8 (40.6)	31.4 (35.5)	8.6 (9.3)
	PPO	31.7	27.5	21.2	4.8
	PPL	7.8	7.9	8.6	2.1
52		40.8 (39.4)	42.1 (39.5)	46.4 (44.7)	40.1 (40.7)
	POO	22.7	22.6	21.4	20.4
	POL	9.3	11.2	14.5	13.7
	SPO	6.2	4.7	5.7	0.5
	PLL	0.9	1.3	5.3	1.8
54		10.9 (8.1)	13.0 (10.9)	18.7 (15.7)	50.4 (49.2)
	OOO	4.3	5.0	5.7	21.7
	OOL	2.4	3.5	5.3	19.6
	OOS	2.4	2.1	3.0	0.9
		100	100	100	100

The composition are given in mole %.

¹ The % mole of triglycerides for the respective carbon number are given in the first row, only the % mole of the major components are displayed in the consecutive rows.

² Values in brackets refer to GLC analysis of the whole oil.

TABLE 2. SPECIFIC HEAT CAPACITY CORRELATIONS FOR SOME VEGETABLE OILS

Sample	Temperature Range (°C)	A	B
Soya Oil	40 - 250	0.002619	1.8102
Coconut oil	40 - 250	0.001689	2.0854
Corn oil	40 - 250	0.001298	2.1659
Peanut oil	40 - 250	0.001082	2.1502

The specific heat capacity of all vegetable oils can be correlated by the linear equations ;

$$C_p (\text{J/g } ^\circ\text{C}) = A T (^\circ\text{C}) + B$$

TABLE 3. TRIGLYCERIDE COMPOSITION OF SOME VEGETABLE OILS DETERMINED THROUGH GAS CHROMATOGRAPHY

Sample	Triglycerides Composition								
	C28	C30	C32	C34	C36	C38	C40	C42	C44
Soya oil	-	-	-	-	-	-	-	-	-
Corn oil	-	-	-	-	-	-	-	-	-
RBDO	-	-	-	-	-	-	-	-	0.1
Peanut oil	-	-	-	-	-	-	-	-	-
Coconut oil	0.7	3.3	12.5	16.1	18.6	17.2	11.0	7.8	4.7

Sample	Triglycerides Composition								
	C46	C48	C50	C52	C54	C56	C58	C60	C62
Soya oil	-	0.4	4.6	30.0	61.4	2.0	0.6	0.1	-
Corn oil	-	1.9	5.1	35.5	53.7	2.4	0.4	0.2	-
RBDO	0.5	4.3	40.7	42.6	9.9	0.5	0.1	-	-
Peanut oil	-	0.3	3.2	35.4	44.8	13.3	0.8	0.3	0.1
Coconut oil	2.7	2.1	1.4	1.0	0.7	-	-	-	-

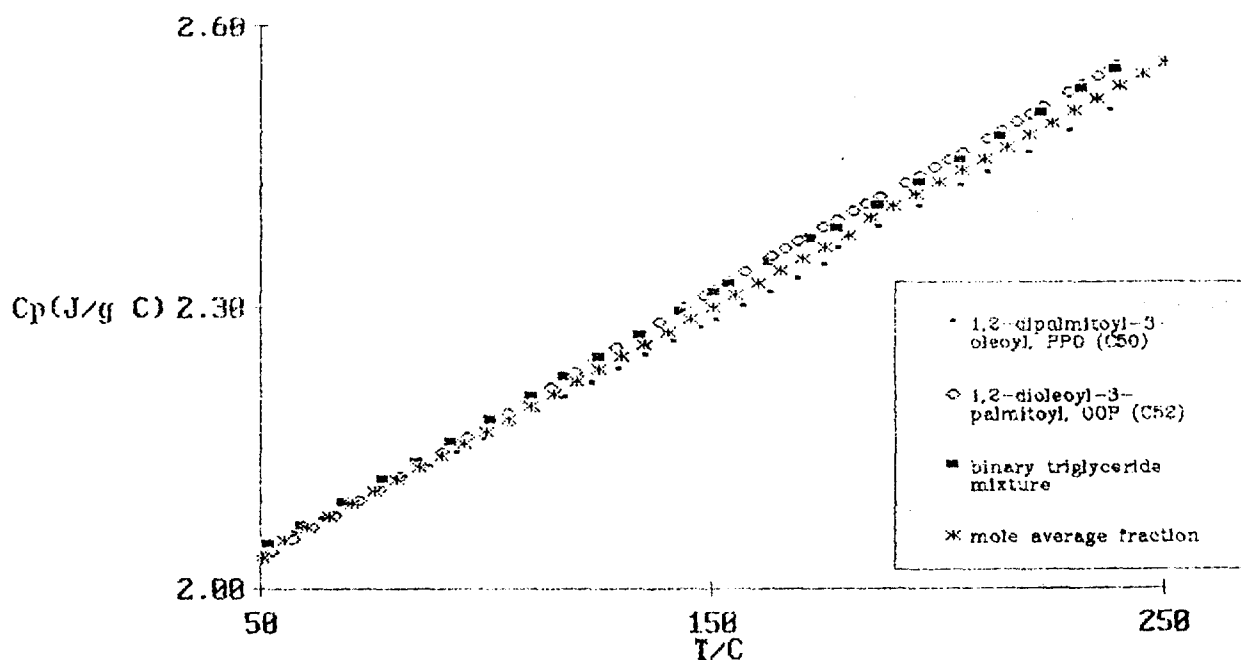


FIGURE 1. SPECIFIC HEAT CAPACITY OF BINARY TRIGLYCERIDE MIXTURE IN RELATION TO ITS PURE COMPONENT PROPERTIES AS A FUNCTION OF TEMPERATURE.

— the specific heat capacity values of the binary triglyceride mixture were found to be similar to those of 1,2-dioleoyl-3-palmitoyl, OOP.

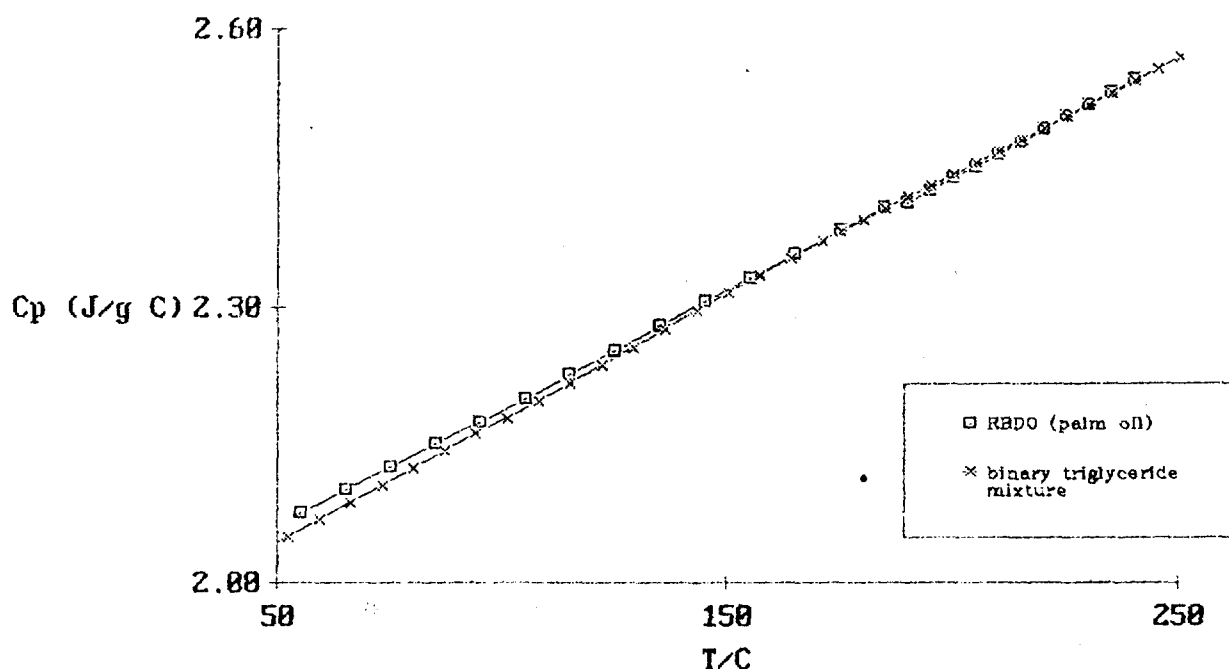


FIGURE 2. SPECIFIC HEAT CAPACITY OF RBDO (PALM OIL) IS ALMOST SIMILAR TO THE BINARY TRIGLYCERIDE MIXTURE OF THE MAJOR COMPONENTS PRESENT IN THE PALM OIL.

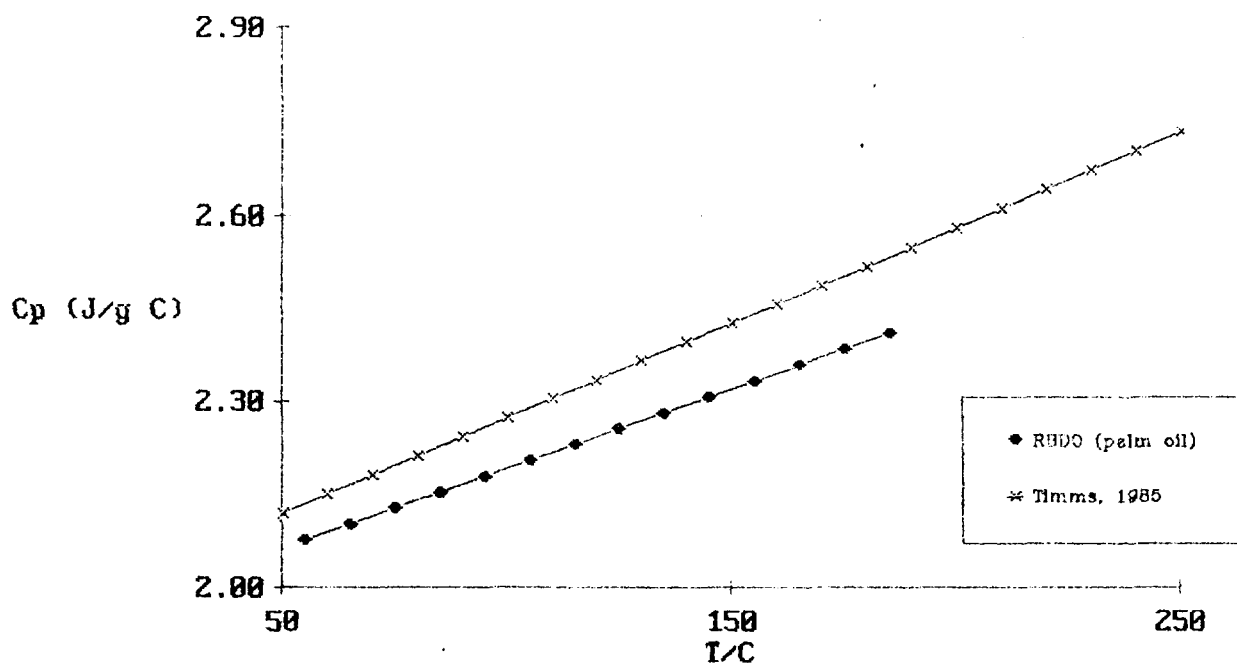


FIGURE 3. SPECIFIC HEAT CAPACITY OF RBDO (PALM OIL) AS A FUNCTION OF TEMPERATURE.

— the specific heat values using the correlation suggested by Timms, 1985 are much higher than the experimental values.

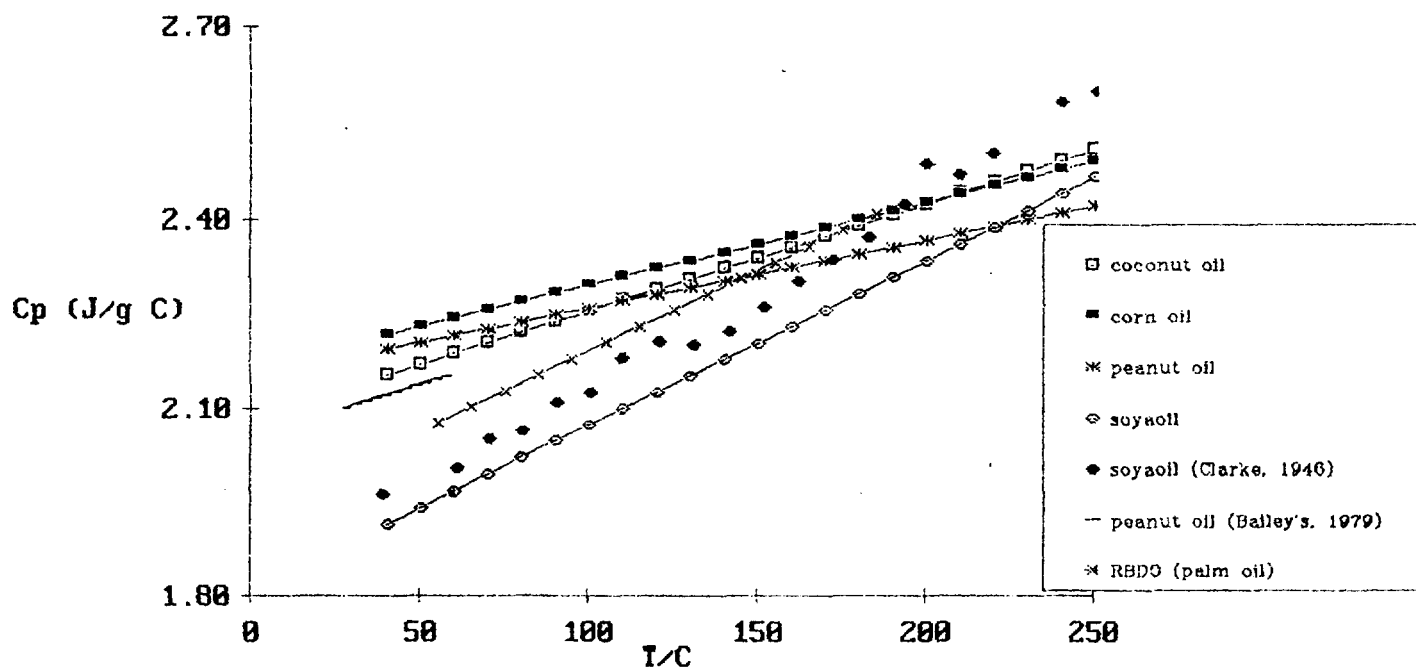


FIGURE 4. SPECIFIC HEAT CAPACITY OF OTHER VEGETABLE OILS AS A FUNCTION OF TEMPERATURE.

— the values for soya oil and peanut oil are compared with reported values.

PEMROSESAN PASIR HAMPAS DARI KAWASAN PERLOMBONGAN UNTUK KEGUNAAN INDUSTRI TEMPATAN

HASHIM HUSSIN, MOHD SUHAILI ISMAIL, KHAIRUN AZIZI MOHD AZIZLI DAN ABDUL KADIR MASROM.

**PUSAT PENGAJIAN KEJURUTERAAN BAHAN DAN SUMBER MINERAL
UNIVERSITI SAINS MALAYSIA
KAMPUS CAWANGAN PERAK
31750 TRONOH PERAK**

ABSTRAK

Sejak harga bijih timah jatuh di pasaran antarabangsa akibat pengeluaran bijih timah yang berlebihan, hampir semua lombong bijih timah di Malaysia memberhentikan operasi perlombongan mereka. Kesan daripada penutupan operasi perlombongan tersebut negara telah kehilangan punca pendapatan hasil dari jualan komoditi ini.

Sebagai alternatif, beberapa kajian telah dijalankan ke atas sumber lain, misalnya pasir hampas yang banyak di dapati di kawasan lombong hasil daripada operasi perlombongan bijih timah. Pasir hampas ini berpotensi untuk menjadi sumber bahan mentah utama di dalam industri pembuatan kaca, seramik, industri pembuatan keluli dan lain-lain industri yang berkaitan jika grednya dapat ditingkatkan mengikut spesifikasi yang diperlukan. Mineral lain yang menjadikan gred pasir hampas ini rendah ialah besi oksida, ilmenit, tourmalin, kasiterit, zirkon, mika dan tanah liat.

Kajian yang telah dijalankan menunjukkan gred pasir hampas ini boleh ditingkatkan dengan melalui beberapa kaedah pemprosesan. Kertas kerja ini akan membincangkan beberapa kaedah pemprosesan yang boleh digunakan untuk meningkatkan gred pasir hampas supaya dapat digunakan di dalam industri tempatan. Hasil daripada kajian ini diharapkan dapat membantu pengusaha lombong supaya mengalih pandangan kepada aktiviti pemprosesan pasir hampas dan seterusnya membantu di dalam mempelbagaikan sumber komoditi negara.

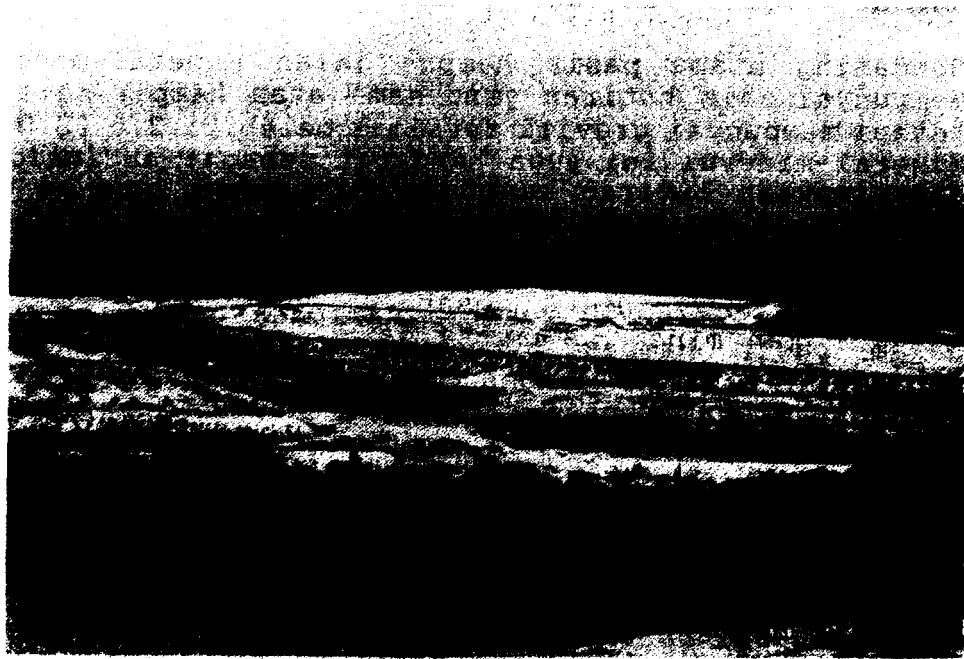
Pengenalan

Penyediaan pasir hampas sebagai bahan mentah kepada industri, terutamanya di dalam pembuatan kaca dan seramik perlulah menitik beratkan beberapa kriteria yang penting iaitu sifat-sifat kimia, fizik dan mineralogi bahan tersebut. Misalnya di dalam pembuatan kaca, komposisi kimia pasir mestilah konsisten supaya kaca yang dihasilkan akan mempunyai sifat-sifat yang sama. Manakala saiz partikel pasir juga mestilah di dalam julat yang kecil dan seragam supaya kadar peleburan adalah sekata. Jika julat saiz terlalu besar, partikel kasar tidak akan melebur dengan sempurna dan akan menjadi *stone* di dalam kaca yang dihasilkan. Begitulah sebaliknya jika partikel pasir terlalu halus maka kebanyakan partikel akan dihembus keluar oleh udara panas di dalam relau.

Mineralogi

Dari sudut mineralogi, pasir hampas mengandungi lebih daripada 90% kuartza. Kebanyakan butiran kuartza adalah terdiri daripada kuartza yang bersih dan berwarna putih cerah. Walau bagaimanapun terdapat butiran kuartza yang diselaputi oleh selaput tanah liat dan juga besi oksida. Sejumlah kecil juga mengandungi mineral-mineral gelap halus sebagai *inclusion* atau terlekat dipermukaan. Bendasing utama di dalam pasir hampas ini ialah mineral-mineral berat seperti tourmalin, zirkon, magnetit, ilmenit, rutil, dan sebagainya. Sedikit fragmen batuan mungkin terdapat di dalam bahagian yang bersaiz kasar. Jadual 1.0 menunjukkan komposisi kimia yang tipikal bagi pasir hampas dari empat lokasi di sekitar Lembah Kinta. Gambar 1.0 menunjukkan salah satu kawasan bukit pasir di Lembah Kinta.

Taburan saiz butiran pasir hampas adalah berbeza dari satu lokasi ke lokasi yang lain seperti yang ditunjukkan oleh jadual 2.0. Saiz butiran adalah berjulat dari saiz kelodak hingga saiz pebel. Walau bagaimanapun julat saiz yang boleh digunakan di dalam industri kaca adalah hampir sama di setiap lokasi. Bentuk butiran lazimnya adalah angular, sub angular, irregular dan kadangkala memanjang iaitu berbentuk jarum (rujuk gambar 2.0).



Gambar 1.0: Menunjukkan salah satu kawasan bukit pasir di Lembah Kinta.



Gambar 2.0: Bentuk partikel pasir yang dilihat di bawah mikroskop elektron imbasan (S.E.M).

Kaedah Pemprosesan Pasir Hampas

Bendasing utama pasir hampas ialah mineral-mineral berat yang mempunyai saiz butiran yang sama atau hampir sama dengan kuartza tetapi mempunyai graviti spesifik melebihi 2.6 (S.G Kuartza = 2.6). Mineral-mineral ini juga terdapat sebagai *inclusion* di dalam atau di permukaan butiran kuartza. Kontaminan yang ke dua ialah dalam bentuk selaput tanah liat atau oksida besi di permukaan butiran kuartza. Selain itu terdapat juga mineral seperti mika dan bahan-bahan berkarbon. Pemprosesan yang betul perlu dilakukan bagi mengasingkan mineral kuartza daripada bendasing yang terdapat di dalam pasir hampas tersebut. Kaedah-kaedah pemprosesan yang digunakan dipilih dengan merujuk kepada jenis bendasing yang terdapat di dalam pasir.

a) Basuhan dan Pensaizan

Pasir hampas biasanya ditapis secara basah (*wet screening*). ~~Sewaktu~~ proses penapisan ini dijalankan partikel halus tanah liat atau kelodak akan dapat disingkirkan. Tujuan utama melakukan proses penapisan ialah untuk mengelaskan partikel yang bersaiz halus daripada partikel yang bersaiz kasar. Alat yang biasa digunakan ialah *trommel* (alat penapis berputar) atau *grizzly bar*. Untuk mengelaskan kepada saiz yang lebih halus, *wire mesh screen* boleh digunakan. Biasanya pasir komersil yang digunakan di dalam industri adalah bersaiz di antara 0.1mm hingga 1.0mm.

b) Attrition Scrubbing

Tujuan utama proses ini ialah untuk mengeluarkan sebanyak mungkin kotoran yang terdiri daripada tanah liat ataupun besi oksida yang menyelaputi permukaan partikel. Proses ini juga boleh dilakukan samada di dalam keadaan berasid dan beralkali. Daripada kajian yang telah di jalankan di dapati keadaan yang sesuai bagi proses ini ialah di bawah pH 3 untuk keadaan berasid dan di atas pH 10 untuk keadaan yang beralkali. Bagi proses yang memerlukan keadaan berasid, asid sulfurik boleh digunakan. Manakala untuk keadaan beralkali soda kostik perlu ditambah. Proses ini dijalankan di dalam mesin *attrition* yang tertutup dan mempunyai *impellers* yang besar dan kuat juga mempunyai dayatahan terhadap kakisan. Untuk memastikan proses ini berlaku dengan sempurna pasir mestilah dalam bentuk buburan (*slurry*) iaitu sekurang-kurangnya 70% pepejal.

c) Pengasingan Pilin

Alat ini amat sesuai digunakan untuk mengasingkan mineral-mineral berat daripada kuartza. Pengasingan berlaku disebabkan oleh daya

emparan yang bertindak ke atas suatu sistem aliran buburan yang dipamkan dari bahagian atas dan dialirkan ke bawah melalui pilin yang melingkar. Partikel mineral berat akan bertumpu di bahagian tengah pilin dan kuartza dan mineral yang lebih ringan akan terempar ke bahagian tepi. Manakala bahagian tengah adalah campuran diantara mineral berat dan kuartza (*midling*). *Midling* biasanya akan diproses semula samada dengan menggunakan pilin yang lain ataupun diulang semula dengan menggunakan pilin yang sama. Peratusan pepejal yang biasa digunakan di dalam buburan ialah sekitar 20%-30%. Jadual 3.0 menunjukkan keputusan analisis kimia yang tipikal bagi pasir hampas sebelum dan selepas proses pemisahan pilin.

d) Pengasingan Magnetik

Pengasingan magnetik adalah proses yang biasanya digunakan dan berkesan untuk mengasingkan mineral yang mempunyai tarikan terhadap daya tarikan magnet. Contoh mineral yang dapat diasingkan oleh alat ini ialah magnetit, ilmenit, mika dan besi oksida. Penggunaan alat ini di dapati banyak membantu di dalam meningkatkan gred pasir silika kerana ia adalah lebih *selective* jika dibandingkan dengan alat pemprosesan yang lain. Jadual 4.0 menunjukkan komposisi kimia yang tipikal bagi pasir hampas sebelum dan selepas proses pengasingan magnetik.

e). Pengapungan Buih

Kaedah ini didapati sangat berkesan jika gred pasir yang sangat tinggi diperlukan. Proses pengapungan buih dilakukan secara terbalik (*revers flotation*) di mana bendasing akan timbul dan pasir silika yang diperlukan akan tinggal di dalam sel pengapungan. Untuk melakukan proses pengasingan dengan kaedah ini bahan pengumpul dan pembuih perlu ditambah di dalam sel. Bahan pengumpul yang biasa digunakan ialah dari jenis anionik dan *fatty acid* (pada pH neutral). Jika kandungan feldspar dan mika tinggi, pengumpul amine sering digunakan. Ini bermakna dua siri pengapungan diperlukan. Pembuih yang kuat dan stabil perlu digunakan jika mineral berat yang hendak ditimbulkan adalah kasar. Asid sulfurik biasanya digunakan sebagai pengawal pH jika proses dilakukan di dalam keadaan berasid. Tetapi perlu diingatkan bahawa kaedah ini adalah agak mahal di dalam pengendaliannya. Ia boleh dijalankan jika harga produk tersebut adalah tinggi. Ini kerana kos bahan kimia adalah sangat mahal. Jadual 5.0 menunjukkan komposisi kimia yang tipikal bagi pasir hampas sebelum dan selepas proses pengapungan buih.

Kesimpulan

Pasir hampas adalah sumber yang boleh dieksploitasikan sebagai bahan mentah kepada beberapa industri yang menguntungkan jika

teknik pemprosesan yang murah dan cekap digunakan. Kajian yang telah dijalankan membuktikan bahawa pasir hampas daripada kawasan lombong adalah berkualiti dan mempunyai nilai komersil jika diproses dengan kaedah yang betul.

Menggunakan pasir hampas sebagai bahan tambakan sebelum kualitinya dinilai adalah suatu langkah yang kurang bijak kerana kebanyakan bukit pasir yang terdapat di kawasan perlombongan adalah berpotensi dijadikan sebagai sumber pasir silika di dalam industri yang lebih menguntungkan misalnya industri pembuatan kaca.

Rujukan

1. Brown, C.J. & Redeker, I.H. (1980): Processing glass grade sand from dune sand. - Proc. 4th. Industrial Minerals Internat. Congr. Atlanta, p.1 - 8, London.
2. Friedrich, M. N. (1984): Quality of quartz sand - glass technological aspects. -5th Conf. on Mineral Engineering, p. 70 - 78.
3. Khairun Azizi et ell. : Processing of Mine Taling Sand, A source for Silica (SiO_2) by Spiral Control.- Paper presented at Seminar dan Kongres Sains & Teknologi Sempena Minggu Sains Kebangsaan Ke 6. 7 - 13 ogos 1992. Malaysia.
4. Lynch A.J. & Davis J.J (1993): Silica: Properties, Production and Markets. - Short Course on Industrial Processing of Kaolin, Quartz/Silica Sand and Feldspar. 20th - 22nd April. Presented at Universiti Sains Malaysia, Perak Branch Campus, Seri Iskandar 31750 Tronoh, Perak. Malaysia.

Jadual 1.0 : Komposisi kimia pasir hampas yang tipikal dari empat lokasi di sekitar Lembah Kinta.

Komposisi	A%		B%		C%		D%	
SiO ₂	97.90	- 99.30	94.10	- 98.10	94.70	- 98.50	97.50	- 98.40
Al ₂ O ₃	0.25	- 0.93	0.44	- 1.67	0.54	- 1.36	0.65	- 1.53
Fe ₂ O ₃	0.09	- 0.40	0.11	- 1.77	0.19	- 1.20	0.11	- 0.44
TiO ₂	0.07	- 0.40	0.09	- 2.02	0.38	- 2.91	0.07	- 0.13
CaO	0.01	- 0.42	0.03	- 0.71	0.02	- 0.04	0.02	- 0.50
MgO	0.02	- 0.26	0.07	- 0.57	0.02	- 0.04	0.05	- 0.11
Na ₂ O	0.01	- 0.03	0.02	- 0.11	0.02	- 0.06	0.04	- 0.06
K ₂ O	0.04	- 0.24	0.03	- 0.17	0.01	- 0.09	0.04	- 0.22
L.O.I	0.18	- 0.57	0.17	- 0.97	0.24	- 0.63	0.26	- 0.72

Jadual 2.0: Taburan saiz partikel yang tipikal bagi pasir hampas dari empat lokasi di sekitar Lembah Kinta.

Saiz (Mikron)	A %	B %	C %	D %
> 4000	5.7	2.9	3.5	0.5
-4000 +3350	1.9	0.8	1.3	0.1
-3350 +2000	9.7	5.9	11.2	3.4
-2000 +1000	22.5	19.4	19.1	15.1
-1000 +710	12.3	13.6	12.3	12.3
-710 +500	13.6	16.1	14.4	17.7
-500 +355	11.6	14.1	11.9	17.0
-355 +250	10.8	13.5	12.6	18.0
-250 +180	6.2	7.7	8.0	9.4
-180 +125	3.7	4.2	4.1	4.5
-125 +90	1.0	1.1	0.8	1.1
-90 +63	0.2	0.3	0.2	0.3
-63	0.8	0.4	0.6	0.6

Jadual 3.0 : Komposisi kimia pasir yang tipikal (a) sebelum dan (b) selepas operasi pemisahan pilin.

Komposisi	(a) %	(b) %
SiO ₂	96.50	98.90
Al ₂ O ₃	1.52	0.32
Fe ₂ O ₃	0.72	0.12
TiO ₂	0.46	0.19
CaO	0.12	0.09
MgO	0.14	0.02
Na ₂ O	0.08	0.05
K ₂ O	0.08	0.06
LOI	0.40	0.23

Jadual 4.0 : Komposisi kimia pasir yang tipikal (a) sebelum dan (b) selepas proses pengasingan magnetik.

Komposisi	(a) %	(b) %
SiO ₂	95.70	96.80
Al ₂ O ₃	1.68	1.22
Fe ₂ O ₃	0.39	0.10
TiO ₂	0.06	0.02
CaO	0.02	0.02
MgO	0.05	0.02
Na ₂ O	0.06	0.05
K ₂ O	0.85	0.68
LOI	0.43	0.32

Jadual 5.0: Komposisi kimia pasir yang tipikal (a) sebelum dan (b) selepas proses pengapungan.

Komposisi	(a) %	(b) %
SiO ₂	97.19	99.04
TiO ₂	0.85	0.07
Al ₂ O ₃	0.81	0.63
Fe ₂ O ₃	0.35	0.03
MnO	0.02	0.00
MgO	0.03	0.05
CaO	0.01	0.00
Na ₂ O	0.03	0.03
K ₂ O	0.01	0.00
P ₂ O ₅	0.02	0.01
Total	99.98	99.81
L.O.I	0.15	0.18

COMPARATIVE ANALYSIS OF ACID ZINC CHLORIDE ELECTROPLATING SYSTEM

(BY NOOR HISHAM AB. HAMID & NOR ARBA'AYAH BT RAMLI*.
FACULTY OF MECHANICAL ENGINEERING,
UNIVERSITI TEKNOLOGI MALAYSIA,
SKUDAI, JOHOR)

ABSTRACT

The world current trend indicates that the acid baths are replacing the cyanide bath due to predicament incurred by cyanide on the environment and Malaysia is of no exception. Three different acid chloride baths have been studied - the ammonium chloride base, potassium chloride base and mixed bath of ammonium and sodium chloride base. All the three baths produce different results in electroplating system.

The mixed bath of ammonium and sodium chloride base shows a better result compared to the other two baths especially in their corrosion properties. Although all the three baths exhibit a fine grain deposits in their microstructure and a smooth surface of their topography, mixed base can be graded as the best, followed by ammonium and potassium.

Currently, the experimental activity on the mixed bath have been carried out involving various parameter such as pH, temperature and composition. The result obtained was as the temperature and pH increases the effective working current density decreases. This is the characteristic features of the mixed bath.

* Research Assistant

COMPARATIVE ANALYSIS OF ACID ZINC CHLORIDE ELECTROPLATING SYSTEM

(BY NOOR HISHAM AB. HAMID & NOR ARBA'AYAH BT RAMLI*,
FACULTY OF MECHANICAL ENGINEERING,
UNIVERSITI TEKNOLOGI MALAYSIA,
SKUDAI, JOHOR)

1.0 INTRODUCTION

The trend of replacing cyanide with non-cyanide in zinc electroplating has been steady for the past 15 years. However, it has accelerated greatly in the eighties. Currently, non-cyanide counter parts by more than 2 to 1. Figure 1.0 segments the 1985 bright zinc plating industry by bath type.

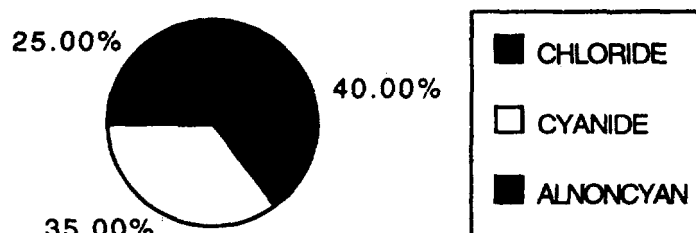


FIGURE 1.0 - BRIGHT ZINC ELECTROPLATING BY BATH TYPE IN 1985

The accelerated growth of non-cyanide zinc is due to changes happen in industry. One is the stringent enforcement of EPA guide lines for the metal finishing industry and Malaysia is of no exception. Another factor is that our awareness of the hazards toxic materials has heightened following the tragic deaths of some 2000 people and injury of 200,000 more in Bhopal, India caused by a leak of methyl isocyanite gas.

Finally, the process themselves must be considered. Since the first commercial installations of non-cyanide bright zinc (alkaline and acid) in United States during the mid 1960's and early 70's, technological milestones have been achieved, making these baths not only a viable but often an advantageous alternative to the cyanide variety.

Acid chloride zinc, one of non-cyanide bath has captured the major share of the worldwide market for both decorative and functional applications. The bath now constitutes 40% to 50% of all zinc bath in throughout the world. This is due to its cathode efficiency where acid zinc baths operate at current efficiencies of 95% to 98%, normally much higher than cyanide or alkaline processes, especially at higher current densities as shown in Appendix 1.0¹. Because of their high cathode efficiency, acid chloride baths produce minimal hydrogen embrittlement when compared to other zinc baths. Acid zinc baths also have much higher conductivity in comparison to cyanide and alkaline baths, producing substantial energy savings.

2.0 EXPERIMENTAL WORK

A study was undertaken to determine the differences of three different acid chloride bath which are Ammonium base, Potassium base and Mixed bath of ammonium and sodium base, on their corrosion resistance using the salt spray test conducted according to BS 5466. Meanwhile, Inverted Microscope is used in determining their microstructure and surface topography. Different bath constitutes of different concentration and Table 2.0 below shows the solution make-up for all the three baths.

	AMMONIUM BASE ²	POTASSIUM BASE ³	MIXED BASE
Zinc Chloride (g/l)	42	90	30 - 40
Ammonium Chloride(g/l)	210	-	25 - 35
Potassium Chloride (g/l)	-	190	-
Sodium Chloride (g/	-	-	100-140
Boric Acid (g/l)	-	25	-

Table 2.0 - Acid zinc chloride solution make-up

The plating process was carried out with different parameter of pH and plating time.

The actual plating concentrate to the Mixed Bath is as below :

Zinc Chloride	34g/l
Ammonium Chloride	30g/l
Sodium Chloride	120g/l

The activity is by looking into the effect of varying composition and its operating parameters which have been found from previous work. Table 2.1 below shows the varying composition of Mixed Bath.

	(1)	(2)	(3)	(4)	(5)	(6)	(7)	(8)
Zinc Chloride (g/l)	34	34	35	35	35	30	40	35
Ammonium Cl. (g/l)	30	30	25	30	35	30	30	30
Sodium Cl. (g/l)	120	120	120	120	120	120	120	100

Table 2.1. Composition of Mixed Bath

3.0 RESULTS AND DISCUSSION

All the three baths show a wide range of current density and a bright deposits out of bath. Ammonium base operates quite steadily from 0.5 to 5 Amp/dm² whilst potassium base from 2 to 6 Amp/dm² and mixed base from 2 to 7 Amp/dm².

The plating process was carried out with various temperature and pH. Different temperature and pH produces different range of effective working current density as shown in table 2.2.

Temperature	pH	CD (Amp/dm ²)
25	5	4 - 6
25	5.5	1 - 6
28	5.5	1 - 4
28	6.0	0.5 - 3
31	5.5	2 - 5
31	6.0	1 - 2

Table 2.2 The Range of Working Current Density At Varying Temp. and pH.

3.1 Corrosion Resistance

After six hours of salt spray test, the weight of oxide gained by the samples plated with different solution are as listed in Table 3.0. On average, mixed base shows the best corrosion resistance compared to the other two baths.

SAMPLE	AMMONIUM BASE	POTASSIUM BASE	MIXED BASE
a	0.0011	0.0014	0.0014
b	0.0004	0.0018	0.0006
c	0.0008	0.0053	0.0015
d	0.0001	0.0007	0.0001
e	0.0023	0.0006	0.0003
f	0.0007	0.0044	0.0013
g	0.0020	0.0016	0.0006
h	0.0015	0.0025	0.0001

Table 3.0 - Weight of Oxide after Salt Spray Test

The corrosion resistance has a very close relationship with the level of porosity of the plated metal that can be seen from the surface topography analysis. The higher level of porosity will reduce the corrosion resistance ability of plated metal. All three baths show a smooth surface but different level of porosity. Potassium base shows the highest level of porosity amongst the three baths and this explain its least corrosion resistance. Ammonium base also exhibits porosity but not as high as potassium, and the mixed base posses the least. Appendix 2.0 shows the microstructure and the surface topography of the zinc coatings.

In reference to Figure 3.2 in Appendix 3.0, it shows that in corrosion resistance ability, mixed-base perform quite steadily throughout the range between 20 to 50 minutes but ammonium is best only between 30 to 40 minutes. Potassium-base exhibit the least corrosion resistance. However, usually the thickness applied for a component is around 10um to 15um and this proves further that the mixed system is more superior and suitable.

3.2 Effect of pH

pH also gives much effect on corrosion resistance of zinc coating. Figure 3.3 in Appendix 3.0, clearly exhibits that all three baths show a better resistance at pH 4.5 and pH 5.5. Amongst the three bath, ammonium base is less affected by pH variation.

3.3 Strength and Ductility

All three baths do not show major differences in ductility and their strength. Ammonium base and mixed base exhibit quite similar result where both baths give better strength and ductility compared to potassium base.

3.4 Adhesion

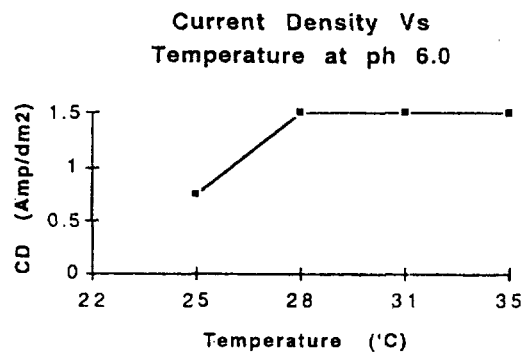
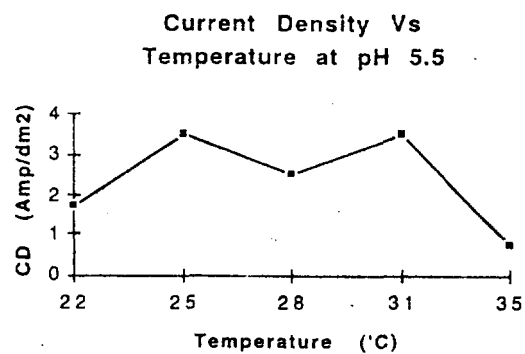
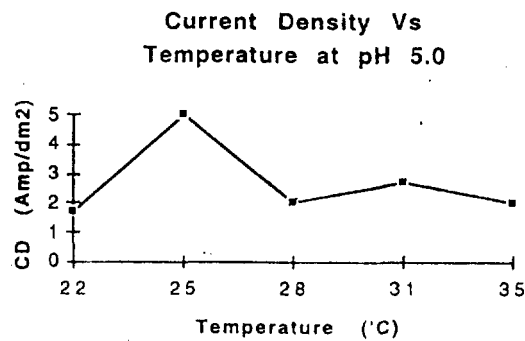
All three deposits show a superb adhesion where even after the tensile test they show no peeling off phenomena.

4.0 CONCLUSION

From the above results and discussions, it points out that for best performance with reference to corrosion resistance is the mixed bath Ammonium-Sodium Chloride system whilst maintaining its deformability factor strength and one of the characteristic which have been found is that as the temperature and pH increases the effective working current density decreases.

REFERENCES.

1. H.H Geduld, Board Chairman Columbia Chemical Corp. and ASM Comm. on Zinc Plating (Juan Hadju, Vincent Pineccasio, Roger Marce), Metal Handbook, American Society For Metals, p244 (1982).
2. Dipsol Chemical Ltd. , 1991.
3. Rica Marketing Sdn. Bhd , 1989.

CHARACTERISTIC OF MIXED ZINC CHLORIDE BATH AT VARYING PARAMETER

PERFORMANCE OF MIXED ZINC CHLORIDE BATH AT VARYING TEMPERATURE

NO	Temp. (C)	pH	CD (Amp/dm ²)	Smoothness	Porosity	Aesthetic
1	22	5	0.5-3	3	2	3
2		5.5	0.5-2	5	5	3
3		6	None	4	1	1
4	25	5	4.0-5.0	3	4	2
5		5.5	0.5-6	4	3	4
6		6	0.5-1.0	5	5	2
7	28	5	1.0-3.0	5	4	3
8		5.5	1.0-3.0	2	3	5
9		6	0.5-3.0	1	1	4
10	31	5	0.5-4.0	5	4	5
11		5.5	0-7.0	4	3	5
12		6	0.5-3.0	3	3	4
13	35	5	1.0-3.0	5	5	4
14		5.5	0.5-1.0	5	4	4
15		6	1.0-2.0	5	4	5

Key: 5-Very good
4-Good
3-Moderate
2-Bad
1-Worse

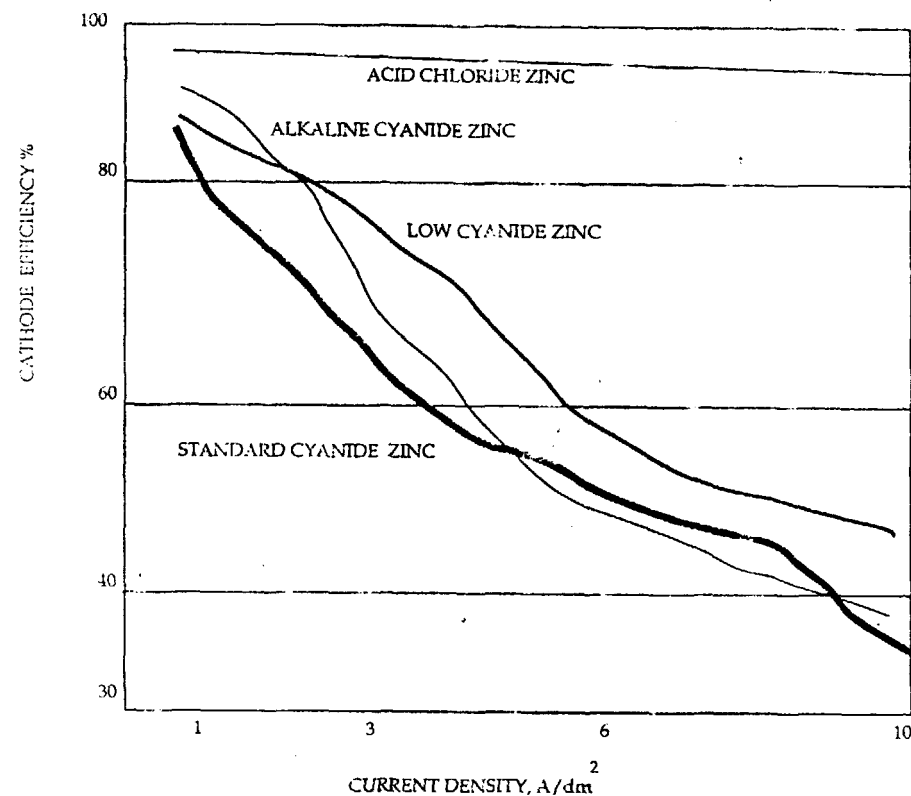


FIG. 1.1 - COMPARISON OF CATHODE CURRENT EFFICIENCIES OF BRIGHT ZINC PLATING ELECTROLYTE



FIGURE 2.1 (a) - MICROSTRUCTURE OF POTASSIUM BASE (x 200)



FIGURE 2.1 (c) - MICROSTRUCTURE OF MIXED BASE (x 200)



FIGURE 2.1 (b) - MICROSTRUCTURE OF AMMONIUM BASE (x 200)

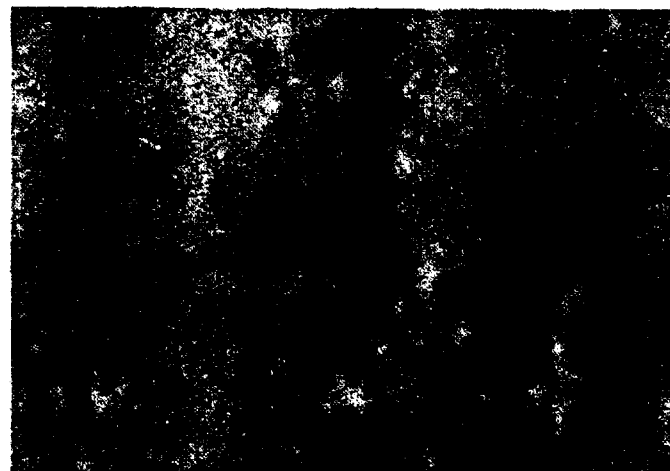


FIGURE 2.1 (d) - SURFACE TOPOGRAPHY OF POTASSIUM BASE (x 200)

POOR QUALITY
ORIGINAL

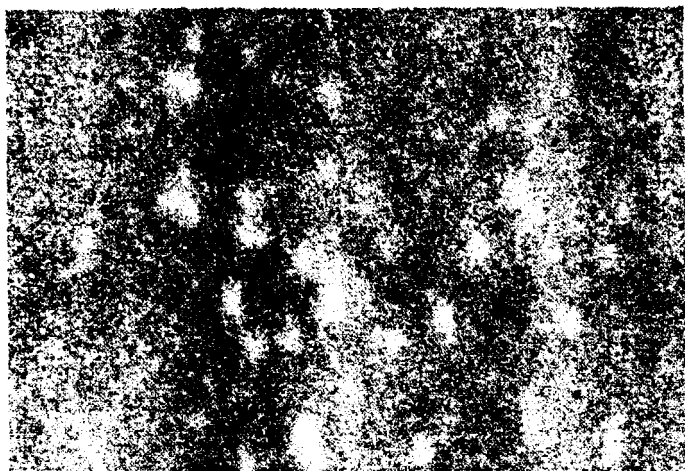


FIGURE 2.1 (c) - SURFACE TOPOGRAPHY OF AMMONIUM BASE (x 200)



FIGURE 2.1 (f) - SURFACE TOPOGRAPHY OF MIXED BASE (x 200)

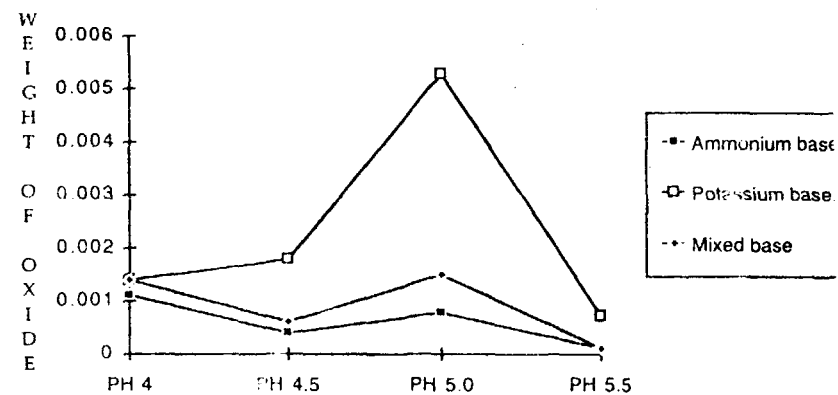


FIGURE 3.1 - WEIGHT OF OXIDE (g) Vs pH

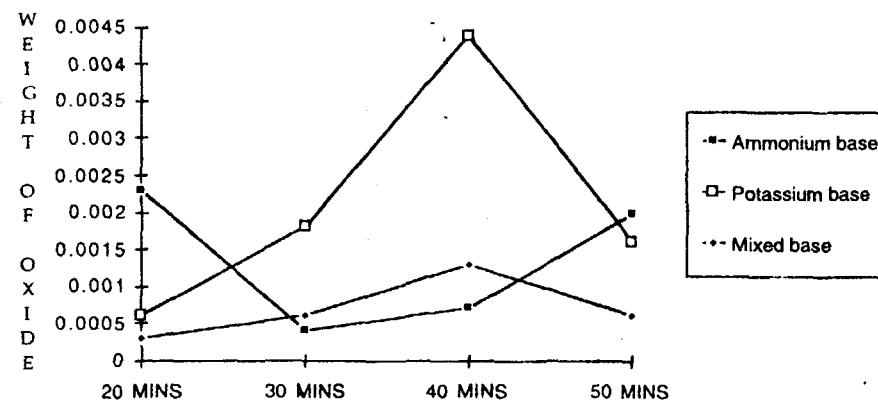


FIGURE 3.2 - WEIGHT OF OXIDE (g) Vs TIME

STUDY ON THE DESIGN AND OPERATION OF FINE/SPECIALTY CHEMICAL BATCH PLANT

Badhrulhisham Abdul Aziz and Khairiyah Mohd. Yusof

Process System Engineering Group
Department of Chemical Engineering
FKKKSA, Universiti Teknologi Malaysia,
Jalan Semarak, 54100 Kuala Lumpur.

ABSTRACT

Recently, the increased demand for fine/specialty chemicals worldwide has led to renewal interest of batch processes or plants. Consequently, studies on how to design and operate batch plant optimally, are becoming important. This particular paper present an overview of technology applicable for batch plant. In addition, an example of research done in the designing batch plant is presented by taking batch distillation design as a case study. Finally, possible applications of the technology mentioned to Malaysian fine/specialty chemicals industry are highlighted and future works on these are listed.

Keywords : Batch process/plant, multipurpose/multiproduct plant, scheduling, CIM.

INTRODUCTION

In response to the first oil shock in 1973, there was a trend in chemical industries to shift the target of production from commodity chemicals which is high volume, low profit margin to fine/specialty chemicals which are low volume and high price. The specialty chemical represents approximately 15% of worldwide chemical's production with the value of US\$150 billion per year. Consequently, the high demand for specialty or fine chemicals has raised the importance of batch plant (at which these chemicals are being produced) recently and in the future. Parakrama (1985) revealed that from the results of a survey of 74 companies in the United Kingdom operating 99 batch processes, 50% of the companies totally depend on the batch processes. In addition, only 6% of those batch processes have the possibility to be replaced in the future by continuous processes. The same trend was also reported by Hasebe and Hashimoto (1991) where in a survey of 34 companies which operated 60 batch plants in Japan, only 18% are being considered to be replaced by continuous plant in the future. In Malaysia, fine/specialty chemicals batch plants are gaining attention since there are many type of these chemicals can be produced from local-based industries such as palm oil, rubber and others in those plants.

The processes involve in a batch plant have distinct characteristics. The differences of the processes compared to those in continuous plant can be seen in Table 1.

TABLE 1

Batch Processes	
Specialty chemical	Commodity chemical
Low volume, high price	High volume, low profit margin
Market driven quality considerations	Need for high yield
Small equipment	Large Equipment
Low energy operating cost	High energy user, high throughput
Unusual analytical instruments	Standard instruments
company-specific technology	Commercial technology

Therefore, due to the importance of the batch plant and its special characteristics, systematic studies on how to design and operate batch plant are very important and should be explored. This particular paper present an overview of technology applicable for batch plant. In addition, an example of research done in the designing batch plant is presented by taking batch distillation design as a case study. Finally, probable applications of the technology mentioned to Malaysian fine/specialty chemicals industry are highlighted and future works on these are listed.

CURRENT AND FUTURE TECHNOLOGY OF BATCH PLANT

Research on batch processes/plants have been concentrated in developing effective methodologies in designing and scheduling. Among those are the application of scheduling techniques to multiproduct and multipurpose plant, application of Computer Integrated Manufacturing (CIM). Among the latest innovation in CIM is designing the 'pipeless' batch plant, which was designed and developed by several Japanese companies.

Scheduling of Multiproduct and Multipurpose Plant.

Generally, batch chemical plants can be divided into two categories; multiproduct and multipurpose. In multiproduct plant, all products follow the same sequence of processing steps or procedures. For the multipurpose plant, the products follow different paths through the plant. Figure 1 shows the difference of these two plants. For both of these plants, the plant production schedule will determine the overall productivity and economic effectiveness. Several algorithms have been proposed by researchers in production planning and most of them involve short-term and medium-term scheduling. In solving most of the problems, they employed three general approaches i.e. MILP (Mixed Integer Linear Program), BAB (Branch and Bound) and Heuristics. Descriptions on all of these approaches can be found in literature (Ku et. al, 1987).

CIM : Pipeless Batch Plant

CIM is being promoted actively in many batch plant recently due to the situation of rapid changes in production demand. The main purpose of introducing CIM is to produce more kind of products with a short lead time without increasing inventory. This led to the studies of automation of batch plant. In Japan for example, the automation of batch plant is extensively being carried out especially in JIT (Just in Time) production system.

One of the interesting and potential outcome of this study is the 'pipeless' batch plant. This kind of plant consists of movable vessels, stations where feeding, processing, discharging and cleaning operations are carried out. The reactants are carried in vessels (AGV; automated guided vehicles). This plant is very flexible, and eliminates the need for pipe cleaning. Figure 2 shows the difference between conventional batch plant and the 'pipeless' batch plant.

EXAMPLE : RESEARCH ON THE DESIGN AND OPERATION OF BATCH DISTILLATION

One of the most frequently utilised unit operation in batch plant is batch distillation. As an example to one of the research in batch plant which is being carried out in UTM is the design and operation of batch distillation. In the operation of batch distillation, we will look at four different procedures in the start-up operation and also the reflux-operation. Two design studies will be

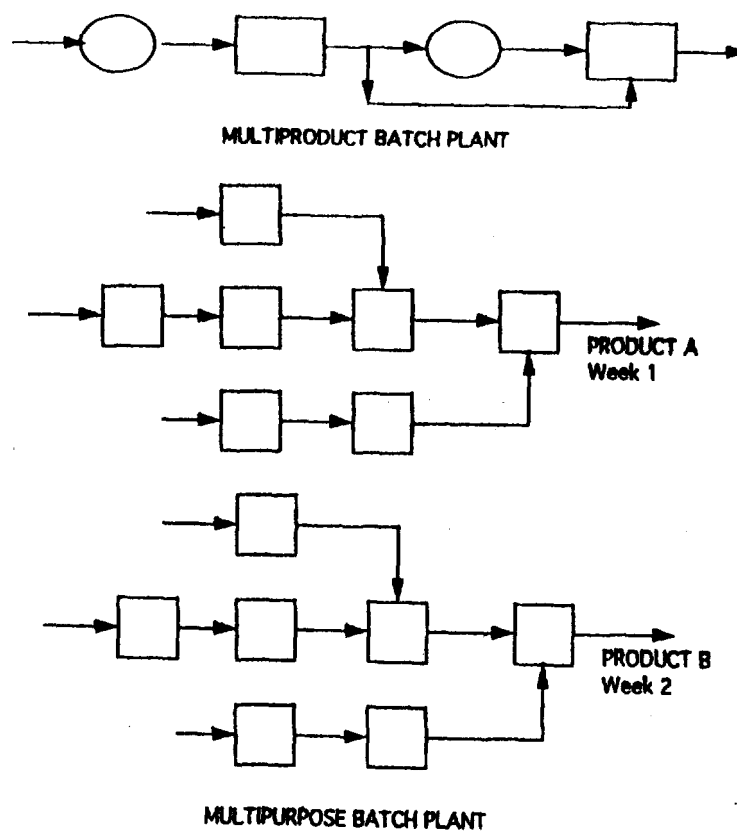


FIGURE 1 TWO DIFFERENT CONFIGURATION OF BATCH PLANT

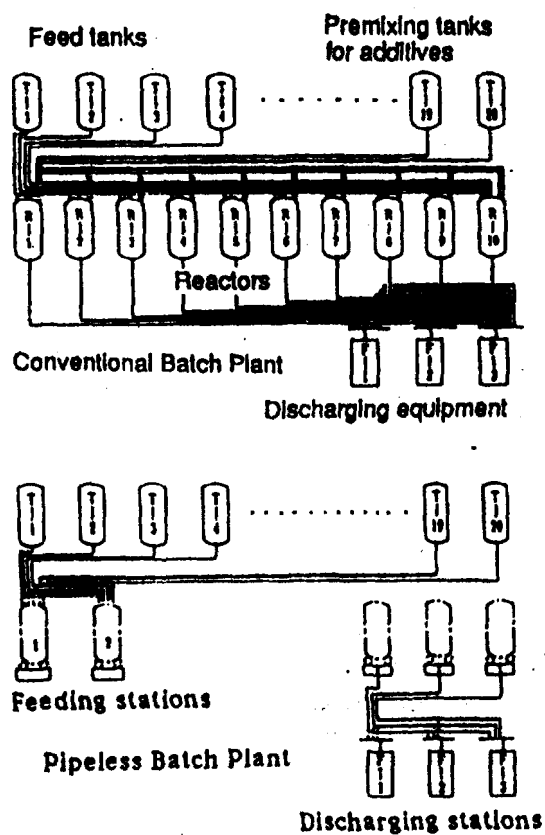


Fig. 2. Configuration of Conventional and Pipeless Plants

discussed i.e. the effect of holdup and new design of batch distillation configuration replacing the conventional batch distillation.

Operation : Startup Operation

In batch distillation processes, the startup operation is one of the important operations which affect the overall separation performance. There are different startup models which were utilized when analyzing batch distillation operation. In our work, four different models (Models A, B, C, and D) representing the dynamic behavior of startup operation for binary and ternary batch distillation have been simulated and investigated. The effect of operation and design parameters such as the tray and reflux drum holdups, amount of feed, product specification, number of trays, and relative volatility on startup time were studied and analyzed for all the above models. The effect of the startup time on the overall separation performance was also analyzed. For most of the cases, it was found that startup time and the composition profile through the column at the end of startup for simple Model A and complicated Models C and D are quite the same. The results from this study is very valuable in the early stage of design and in developing a guidance system for operators in the later stage.

Design : (a) Effect of Holdup

In this study, the effect of column holdup on the separation performance was analyzed in detail for easy, moderate and difficult separation problems. By executing simulations for many conditions, it was clarified that the tray holdup and the reflux drum holdup have different effect to the separation performance. Figure 3 and Figure 4 shows the effect of tray and drum holdup, respectively, for different degree of separation difficulty.

As for the effect of tray holdup, in the case of easy and moderate separation, increasing the tray holdup created a beneficial effect. The large tray holdup will cause the accumulation of the light component at the upper part of the column during the startup period, and it made the product withdrawal period longer. This is the dominant reason why the large tray holdup contributes to the increase of the separation performance. For difficult separation, the increase of the tray holdup significantly lengthens the startup and slopcut withdrawal periods. Therefore, the beneficial effect is decreased when the separation becomes difficult. The reflux drum holdup strongly affects the startup time, and this increase in startup time outweighs the beneficial effect of holdup. By this reason, the increase of the reflux drum holdup decreased the separation performance in every case.

Design : (b) Alternative Design : Complex Batch Column

In this part of research, a new configuration of batch distillation is proposed. Figure 5 shows the different between conventional and the new complex column. From our simulation studies for four different set of conditions, it was found three out of four shows advantage of complex column over the conventional one. Table 2 shows the comparison of the performance.

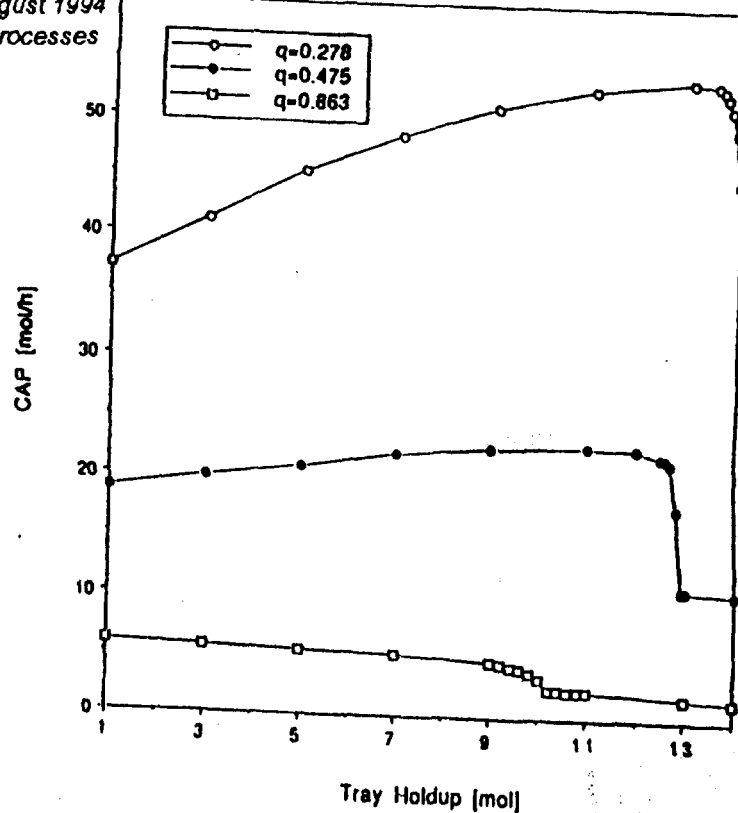


Figure 3 Effect of tray holdup on the separation performance, CAP at various degree of difficulty

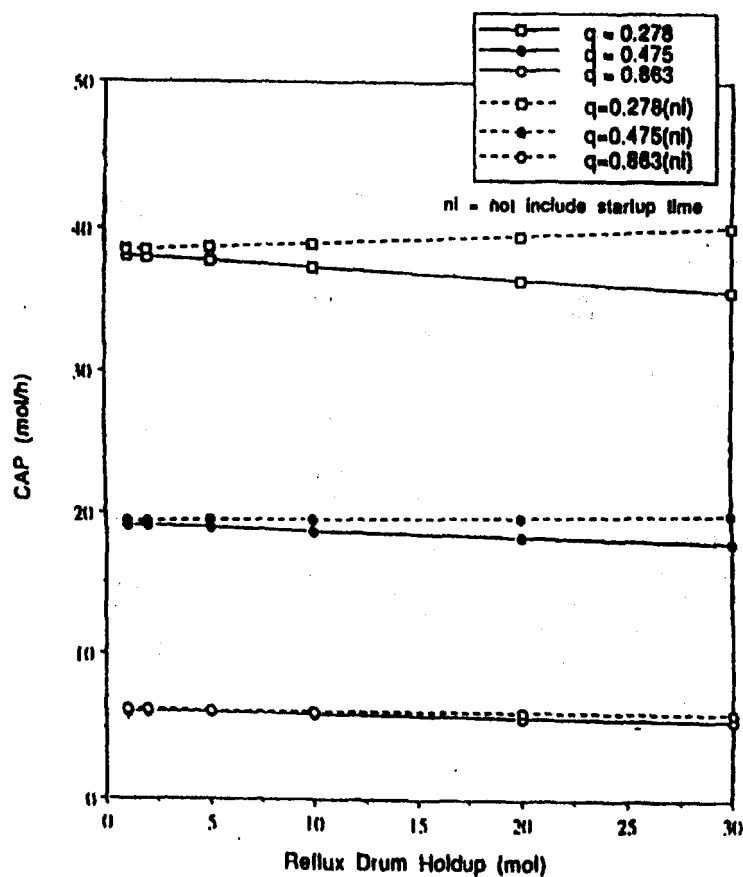
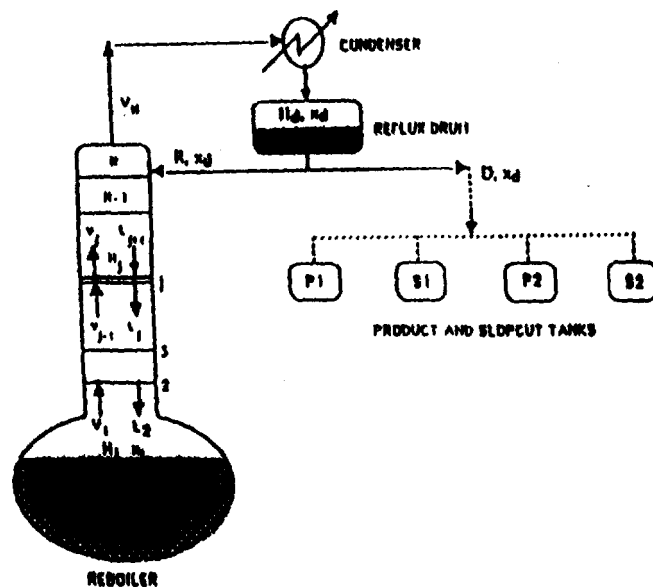
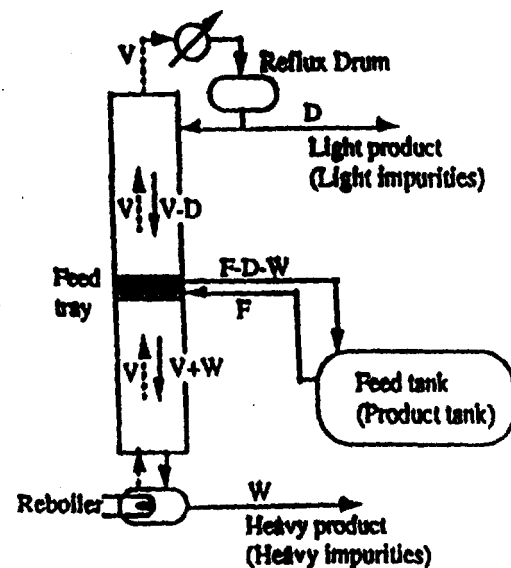


Figure 4 Effect of reflux drum holdup on the separation performance, CAP at various degree of difficulty.



A typical configuration of batch distillation column



Complex Batch Distillation Column

Figure 5 Two Different Column Configurations of Batch Distillation

Table 2. Simulation Results

	CAP	Time* (hr)	optimal values of the variables				P.I.**
			x _{R0}	x _{B0}	Rf1	Rf2(Rb1)	
Case 0)							
Ordinary column	1636	25.1	0.99		4.0	0.47	0.77
Complex column	1266	36.9	0.50	0.20	91	81	
Case 1)							
Ordinary column	1103	37.7	0.44		8.6	0.44	1.27
Complex column	1399	33.1	0.34	0.14	79	93	
Case 2)							
Ordinary column	1229	32.0	0.99		6.9	0.40	1.35
Complex column	1660	28.1	0.55	0.10	75	80	
Case 3)							
Ordinary column	1536	25.7	0.99		6.0	0.10	1.61
Complex column	2460	17.8	0.10	---	14	---	

* Time : Total batch time including startup

** P.I. = (CAP of complex column) / (CAP of ordinary column)

*** : Heavy Impurity is not withdrawn from the bottom.

FUTURE WORKS

There are few projects in the design and operation of batch plant are going on and in planning. Most of these projects are and will be related to applying recent technology in designing and operating batch plant to Malaysian industries. In the end, a flexible multipurpose and multiproduct batch pilot plant will be design and constructed.

First of all, research on optimal design and operation of batch distillation will be continued. This is due to the fact that, batch distillation constituted about 85% of the unit operation in batch plant. Research on this will comprises of the design and operation of reactive batch distillation for non-ideal mixtures (include azeotropic and non-homogeneous system).

There is also an on-going project on studying the application of scheduling techniques to a small batch plant consisted of reactors and mixing tanks. A prototype of this small batch plant is being constructed equipped with PLC (Programmable Logic Controllers) and computer. It is intended for studying the control aspects as well as scheduling operation of batch plant in the future.

Finally, all the results from research projects will be integrated and utilized for developing a 'pipeless batch plant' that handle the production of several specialty chemicals taking into account the flexibility and efficiency aspects. This kind of plant, which has been described in the earlier part of this paper, is very promising in the future and can be developed locally at a competitive cost.

CONCLUSION

The demand in fine/specialty chemicals has led to the importance of batch plant. In order to exploit full potential of this phenomena, systematic study on the design and operation of batch plant should be carried out. The results from these research can greatly help the local chemical industries in manufacturing fine/specialty chemicals optimally and efficiently through employing advanced technology.

ACKNOWLEDGMENT

We would like to thanks all the personnel involved in this work especially the members of PSE group. Thanks also due to UTM and IRPA for providing the financial support.

REFERENCES

Abdul Aziz, B. "Study on the Optimal Design and Operation of Batch Distillation", Ph.D. Thesis, Kyoto University, 1994.

Hasebe, S. and I. Hashimoto, "Present Status of Batch Process Systems Engineering in Japan", presented at NATO Advanced Study Institute in Batch Processing System Eng., Turkey, 1992.

Ku, H., et. al., "Scheduling in Batch Process", Chemical Engineering Progress, August 1987.

Parakrama, R. "Improving Batch Chemical Processes", The Chem. Engineer, Sept. 1985.

DYNAMIC MECHANICAL TESTING OF BITUMENS

Hasanan bin Md. Nor
Faculty of Civil Engineering
Universiti Teknologi Malaysia
Locked Bag 791
80990 Johor Bahru

ABSTRACT

Bitumen, a viscoelastic material, exhibits both viscous and elastic behaviours and displays a time dependent relationship between an applied stress and the resultant strain. Within the linear viscoelastic region of bitumen, the interrelation of stress and strain is influenced by time alone, and not by magnitude of the stress. Traditionally, the most commonly used measurements for characterising bitumen have been the penetration and softening point tests. These tests are empirical in nature, and do not provide rational information in engineering terms. Dynamic mechanical test, on the other hand, provides complete information on the linear viscoelastic response of bitumens at all temperatures of interest to the bitumen technologists. The aim of this paper is to demonstrate that the rheological behaviour of bitumens can be characterised with good accuracy using dynamic mechanical test. This system of characterisation would allow reasonably accurate characterisations to be made on a variety of bitumens with much less testing than is normally required. Results on high quality, low quality and recycled bitumens are discussed.

INTRODUCTION

The classical theory of elasticity deals with mechanical properties of perfectly elastic solids for which stress is always directly proportional to strain but independent of rate of strain. The theory of hydrodynamics deals with properties of perfectly viscous liquids for which stress is always directly proportional to rate of strain but independent of the strain itself. These categories of behaviour are idealisations and real materials show deviations from both of them.

There are two important types of deviation. In the first, the strain (in a solid) or the rate of strain (in a liquid) may not be directly proportional to the stress. This is described as non-linear behaviour. In the second, the stress may depend on both the strain and the rate of strain together, as well as higher time derivatives of the strain. Such time anomalies reflect a behaviour which combines liquidlike and solidlike characteristics and is described as viscoelastic.

If only time anomalies exist and stress anomalies are absent, the behaviour is described as linear viscoelastic. The description thermoplastic implies that the viscoelastic behaviour is also importantly affected by temperature.

The parameters used to characterise the linear elastic behaviour of a solid are the Young's modulus (E), the shear modulus (G), the bulk (or volume) modulus (K) and the Poisson's ratio (ν). These have their counterparts in the characterisation of a linear visco-elastic material but, because of the dependence of deformation response on time, they are complex parameters with real (elastic) and imaginary (viscous) vector components. The complex shear modulus, for example, of a viscoelastic material G^* is $G' + iG''$ where G' is the elastic component and G'' is the viscous component.

When a viscoelastic material is stress sinusoidally, there is a phase difference between the maximum displacement and the maximum force (the time anomaly). If the stressing is in simple shear, the ratio of the maximum force to the maximum displacement is directly proportional to the absolute value of the complex shear modulus (at the frequency of stressing) $|G^*|$. The two components of the complex shear modulus G^* are given by $G' = |G^*| \cos \phi$ (elastic) and $G'' = |G^*| \sin \phi$ (viscous), where ϕ is the angular phase difference between the force and the displacement.

DYNAMIC MECHANICAL TEST

Deformation Under Sinusoidal Loading

This form of mechanical testing is very important for characterising the viscoelastic behaviour of bituminous binders.

The sinusoidal patterns of the displacement and force (at the driving frequency) are as shown in Figure 1. In general, there is a phase difference between the displacement and the force which is on the diagram by phase angle ϕ . The ratio of the maximum force to the maximum displacement multiplied by a (form) factor which is dependent only on the geometry of the test assembly gives the absolute value of the complex (shear) modulus of the material $|G^*|$ (ratio of maximum stress to maximum strain).

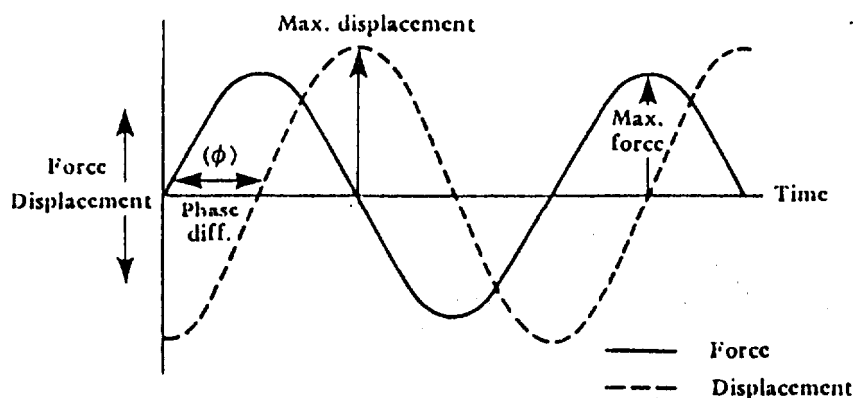


FIGURE 1 : Deformation Response of Bitumen to Repeated Sinusoidal Loading

The instrument used for the purpose of this research was Carrimed Controlled Stress Rheometer. This method rotates bituminous samples sinusoidally clockwise and anti-clockwise in a horizontal plane.

The phase angle can be any value between 0 and 90 degrees. If it is 0 degree then the deformation response is purely elastic and, if it is 90 degrees, the response is that of a purely viscous liquid.

Complex modulus and phase angles are measured over a range of driving frequencies and the variation of $|G^*|$ and ϕ with a range of frequencies. Both $|G^*|$ and the frequency are plotted on logarithmic scales and the angular frequency ω (2π times the Hertzian frequency) is used.

As the frequency increases the response becomes more elastic with the modulus increasing and the phase angle decreasing.

Construction of Master Curves

In constructing a master curve using time-temperature superposition, dynamic data are first collected over a range of temperature and frequencies. A standard reference temperature must then be selected. The reference used in analysing data in this research was 25°C. The data at all other temperatures is then shifted with respect to time, until the curves merge into a single, smooth function. The shifting may be done based on any of the viscoelastic functions; if time-temperature superposition is valid, the other viscoelastic functions will all form continuous functions after shifting. In this research, the shifting was done on complex modulus and phase angle.

This horizontal shifting process to give a master curve is known as superposition and theoretically a small vertical shift should be done at the same time. For the condition of bitumen testing, however, this vertical shifting process can be neglected (Dickinson, 1984).

The construction of master curve of complex modulus for Penetration Grade Bitumen 80/100 bitumen conducted in this study is shown in Figure 2. A master curve for phase angle can be constructed by similar method.

Carrimed Controlled Stress Rheometer

Carrimed was designed to be a universal instrument applicable to a wide range of materials, from simple oils to complex foodstuffs. Many testing geometrics are available to accommodate this wide range of applications. The Carrimed was established to work as a practical instrument for bituminous material using a 2 cm plate and platen assembly. In the test, the Carrimed (Figure 3) shears a sample between two parallel plates through the action of an electronically controlled induction motor supported by a low friction air bearing. Both the angular displacement and applied torque are measured by the data acquisition system.

All operations of the instrument are under program control and once set can be repeated on each new sample. Frequency, temperature, peak strain and torque are all controllable by the program. Treadea and Witt² have discussed the working of the system in detail.

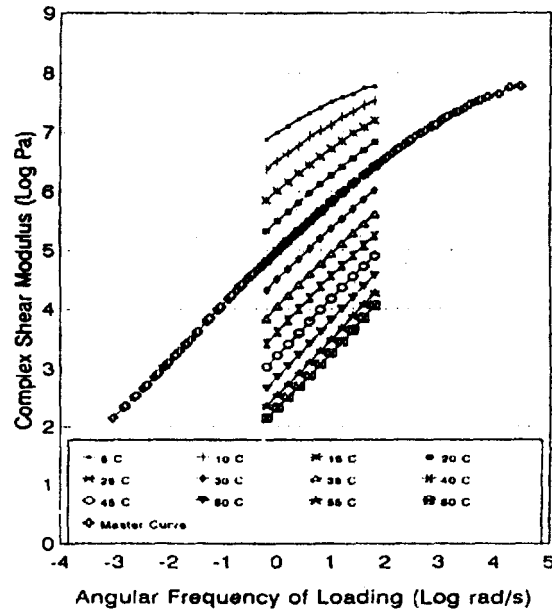


FIGURE 2 : Construction of Complex Shear Modulus Curve for Grade 80/100 Bitumen

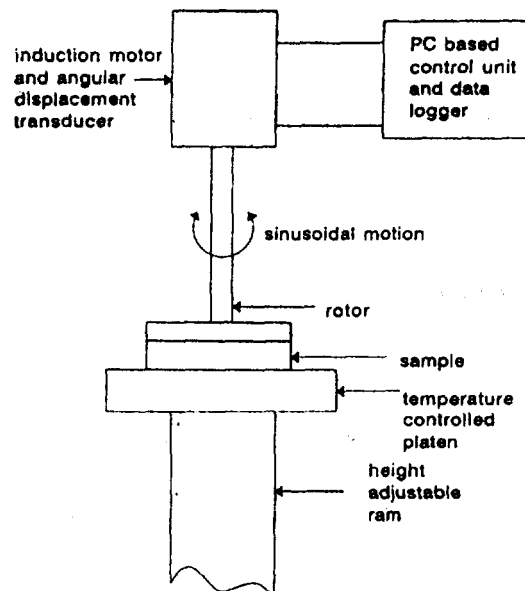


FIGURE 3 : Carrimed Controlled Stress Rheometer

Carrimed Operation

On completion of testing at each test temperature a data file is stored to disc along with various sample details and instrument settings (11 tests from 60°C to 5°C in 5°C steps). An example of raw Carrimed Output is shown in Table 1.

```
49999,0.1000,5.0,69.42,6440000,4.9418E-3,45.33,45.33
49999,0.1585,4.9,145.2,8118000,3.9201E-3,41.17,41.17
49999,0.2512,4.9,199.4,9913000,3.2105E-3,37.77,37.77
49999,0.3981,5.0,240.0,1.228E7,2.5923E-3,33.92,33.92
49999,0.6310,5.0,272.7,1.444E7,2.2046E-3,30.27,30.27
49999,1.000,5.0,299.6,1.659E7,1.9184E-3,26.62,26.63
49999,1.585,5.0,326.8,1.911E7,1.6649E-3,20.96,20.96
49999,2.512,5.0,353.8,2.120E7,1.5013E-3,18.48,18.48
49999,3.981,5.0,380.1,2.240E7,1.4206E-3,19.19,19.19
49999,6.310,5.0,405.0,2.535E7,1.2557E-3,14.87,14.87
49999,10.00,5.1,430.1,2.592E7,1.2287E-3,15.17,15.18
"torq.", "freq.", "temp.", "time", "G*", "strain", "delta", "phase"
"micro N.m", "Hz", "Deg C", "sec", "N/m^2", "", "degrees", "deg"
```

TABLE 1 : Raw Carrimed Output for Grade 80/100 Bitumen at 5°C.

A typical primary output of data analysis with SHIFTT software for Grade 80/100 bitumen is as shown in Table 2. The master curve plot of complex modulus and phase angle of that data is shown in Figure 4. Samples of binders for both before and after Rolling Thin Film Oven (RTFO) treatment were tested with the rheometer. The RTFO was used to measure the durability of the bitumens. Vallerga² defined bitumen durability as resistance to change in original properties during construction and in service ageing.

	-0.702	-0.002	0.190	0.390	0.590	0.790	0.990	1.190	1.390	1.590	1.790	
5.0	45.32	41.17	37.77	33.92	30.27	26.62	20.96	18.48	19.19	14.87	15.17	-0.9922
	6.975	6.999	1.102	7.225	1.324	7.016	7.518	1.597	7.643	1.755	7.777	0.9931
10.0	57.80	54.71	51.64	47.89	42.70	41.83	38.76	32.37	29.92	24.44	21.39	-0.9977
	6.972	6.506	1.641	6.773	6.824	7.029	7.120	7.358	7.361	7.456	7.523	0.9972
15.0	67.37	64.92	62.69	59.87	57.46	53.32	50.59	46.36	43.72	38.82	34.40	-0.9939
	5.451	6.004	1.156	6.206	6.404	6.578	6.719	6.848	6.942	7.004	7.199	0.9907
20.0	73.64	72.19	70.62	68.71	66.00	64.09	61.20	58.30	55.56	50.82	46.03	-0.9903
	5.320	5.492	1.649	5.809	5.960	6.122	6.274	6.412	6.506	6.591	6.836	0.9905
25.0	77.99	76.89	75.73	74.30	72.71	71.15	69.28	67.10	64.29	61.27	57.49	-0.9921
	6.047	6.880	1.151	5.722	5.492	5.853	5.813	5.859	6.125	6.277	6.421	0.9906
30.0	80.79	80.56	79.41	78.23	77.02	76.94	76.49	72.79	70.00	68.16	63.72	-0.9907
	6.314	6.495	6.474	6.852	5.920	5.201	5.267	5.522	5.495	5.657	6.010	0.9907
35.0	84.12	83.37	82.16	81.44	80.55	79.24	78.15	76.84	75.21	73.41	70.90	-0.9951
	7.051	9.041	6.720	6.405	6.505	6.703	6.820	6.112	7.282	5.447	5.412	0.9900
40.0	85.89	85.21	84.57	83.60	82.91	81.95	80.94	79.74	78.12	76.44	74.51	-0.9912
	1.425	1.624	1.815	2.009	2.184	2.371	2.552	2.720	2.905	3.071	3.245	0.9900
45.0	87.87	86.49	85.18	83.49	81.74	80.59	82.04	82.04	80.75	79.13	77.19	-0.9161
	1.517	3.224	3.470	3.613	3.802	3.980	4.174	4.360	4.540	4.721	4.900	0.9900
50.0	87.44	87.57	87.20	86.87	86.72	85.91	84.00	82.72	82.34	81.04	79.10	-0.9579
	2.449	2.862	3.051	3.217	3.436	3.629	3.821	4.007	4.194	4.382	4.568	1.0000
55.0	86.16	87.10	87.50	87.46	87.10	86.72	85.90	85.27	84.13	82.61	80.82	-0.9745
	2.265	2.561	2.730	2.921	3.114	3.301	3.494	3.680	3.860	4.041	4.270	1.0000
60.0	88.33	89.04	87.95	87.90	87.81	87.49	86.00	85.94	84.84	83.52	81.54	0.9900
	2.149	2.729	2.912	3.101	3.288	3.470	3.655	3.843	4.035	4.265	4.561	0.9900

Temp	SHIFT
4.99	2.663
9.99	1.929
14.96	1.236
19.90	0.594
24.82	0.000
29.87	-0.587
34.93	-1.055
39.99	-1.493
45.00	-1.901
49.99	-2.278
55.01	-2.614
59.97	-2.844

BEST VALUE OF TS	= 49.4
SUM OF SQUARES	= 0.0101

Description of the top table

1st Row - Test frequencies (Log rad/s)

2nd Row - Temperature (°C) followed by measured phase angle at each frequency

3rd Row - Measured complex modulus

Log (G*) at each frequency

Last Column - Correlation Coefficient

Description of the top table

- 1st Row - Test frequencies (Log rad/s)
- 2nd Row - Temperature (°C) followed by measured phase angle at each frequency
- 3rd Row - Measured complex modulus Log (G*) at each frequency
- Last Column - Correlation Coefficient

TABLE 2 : Primary Outputs from SHIFTT for Grade 80/100 Bitumen

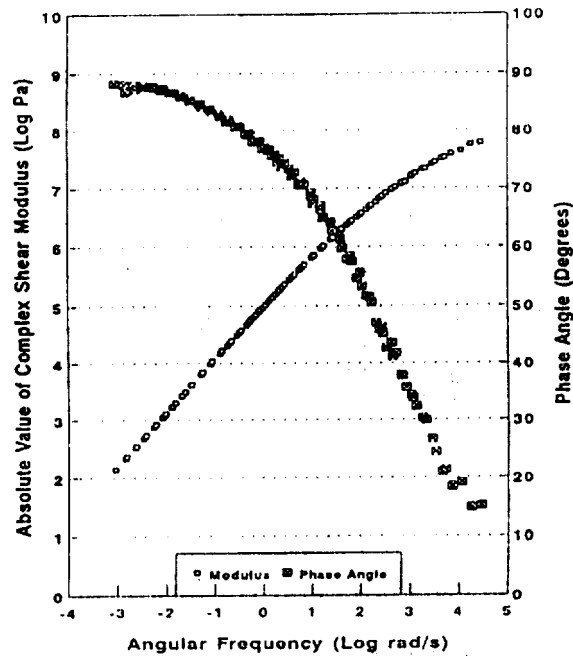


FIGURE 4 : Master Curves for Grade 80/100 Bitumen

The SHIFTT programs also calculate the Characteristic Temperature (TS) of the binders. Characteristic temperature is a measure of the material's tendency to change its flow and deformation properties with changes in temperature. The TS has some physical meaning because it is approximately 50°C above the glass transition temperature. Table 3 summarises the characteristic and transition temperatures of the bitumens tested in this study.

Binder Type	Characteristic Temperature (°C)	Glass Transition Temperature (°C)
A	40.4	-9.6
B	45.3	-4.7
C	41.2	-8.8
A(RTFO)	44.0	-6.0
B(RTFO)	46.8	-3.2
C(RTFO)	43.0	-7.0

Note : A - Penetration Grade 80/100 Bitumen
 B - Propane Precipitated Asphalt
 C - Recovered Bitumen from Milling Waste
 (RTFO) - After Rolling Thin Film Oven Treatment

TABLE 3 : Characteristic Temperature and Glass Transition Temperature of Binders

DISCUSSIONS

Characteristic Temperature (TS)

The characteristic temperature (TS) of a bituminous binder is a measure of the material's tendency to change its flow and deformation properties with changes in temperature. The range of values recorded for various binders extends from 45°C for tar like binders (high temperature susceptibility) through to 35°C for high penetration index (low temperature susceptibility) binders.

The values of the characteristic temperature for the binders were obtained from SHIFTT Program data. The temperature for Grade 80/100 is the lowest whereas that for propane precipitated asphalt is the highest.

Glass Transitions In Paving Binders

A change in the physical state of amorphous viscoelastic materials such as paving binders takes place when their temperature is reduced. The change observed is the so called glass transition and, under load, the mechanical response changes from that of a visco-elastic liquid to that of a glass. Unlike the crystallisation of a chemical compound from its melt, the transition to the glassy state is a gradual process, and an ordered structure is not obtained. In the glassy state, brittle fracture readily takes place under load.

The glass transition is best described in terms of a discontinuity in the coefficient of expansion which is also accompanied by discontinuities in heat capacity and compressibility.

Many of the properties of liquids demonstrate the presence of a substantial proportion of free volume, and the thermal expansion coefficient represents primarily the creation of additional free volume with rising temperature. In a material such as bitumen at a temperature high enough so that local Brownian motion is rapid, adjustment of molecular configurations takes place quickly when a stress is applied. As the temperature is reduced, however, there is a reduction in free volume and a state is finally reached where the adjustment of molecular configurations is very slow (negligible within the loading time span). When this stage is reached, the only residual volume contraction is of a solid-like character and any remaining free volume is presumed to remain constant.

Dickinson³ mentioned that, glass transition temperature is approximately 50°C below the characteristic temperature (TS).

The Grade 80/100 bitumen has the lowest glass transition temperature whereas the PPA has the highest. High quality bitumen has lower glass transition temperature than low quality bitumen.

CONCLUSIONS

Dynamic mechanical test is used as a way to measure the rheology of binders. It provides rational information in engineering terms which cannot be provided by the traditional method of characterising bitumen i.e., penetration and softening point tests.

Dynamic mechanical test allows one to fingerprint the viscous and elastic nature of bitumens over a wide range of temperatures and loading rates. It provides complete information on the linear viscoelastic response of bitumens at all temperatures of interest to the industry of road and highway constructions. The test enable bitumens to be compared in term of their qualities.

ACKNOWLEDGEMENTS

The author would like to thank the Highway and Transportation Research Group (HTRG) of the Faculty of Civil Engineering, UTM and the Australian Road Research Board (ARRB) for the contributions toward this research.

REFERENCES

- [1] Treadrea, P., and Witt, H.P. (1983). Towards a Method for Determining the Flow and Deformation Properties of Bituminous Binders and Their Relationship with Pavement Performance. Discussion Note. Australian Road Research Board.
- [2] Vallergera, B.A. (1981). Pavement Deficiencies Related to Asphalt Durability. Proceedings of the Association of Asphalt Paving Technologists, Vol. 50.
- [3] Dickinson, E.J. (1984). Bituminous Roads in Australia. Australian Road Research Board.

A NEW COMPRESSION TESTING FACILITY

Hamidon Musa, S. Rajesham and Jamaliah Idris
Faculty of Mechanical engineering
Universiti Teknologi Malaysia
Locked Bag 791, 80990 Johor Bahru

ABSTRACT

The development of a new compression testing facility that can be used with a press is described. The compression testing tool is light in construction and allows true stress and true strain calculations to be inferred from both the height and diameter measurement of the test specimen.

An experimental set up for conducting tests involving the developed facility is described. The set up consists of displacement and force transducers for data recording, frequency amplifiers for signal conditioning and a micro computer to operate data acquisition hardware and software as well as software for data processing.

1. INTRODUCTION

Compression testing is an important experimental tool to researchers and product manufacturers dealing in areas such as material testing and metal working. In metal working, for example, compression testing finds wide application in flow curve determination, strain limit determination and tribology studies. Compression testing will also be employed by press makers and operators who want to determine the accuracy of a particular metal forming machine tool.

A compression testing facility essentially requires a pair of platens to compress a specimen and some means of holding various transducers needed to measure the test parameters. Different compression testing facilities have been developed. Some are designed for application with a standard laboratory testing equipment such as a universal testing machine, and others with an actual production press. They can be designed for room temperature [1] or elevated temperature [1, 2] application. Some are of a closed construction type in which alignment of the top and bottom sub-assemblies are achieved by a guidance system built into the facility while others are of an open construction type which relies on guidance provided by the testing equipment or by the press.

2. PARAMETER MEASUREMENT

In compression testing the two most important parameters to be determined are usually the nominal or engineering stress, σ_E and the engineering strain, ϵ_E values or the true stress, σ and true or natural strain, ϵ .

The normal method of experimentally determining the stress and strain values is by measuring the reduction in height, s , of the specimen being compressed, besides the deformation force, F . The instantaneous height reduction at a force F is given by:

$$s(F) = h_0 - h(F) \quad (1)$$

where h_0 is the initial specimen height and $h(F)$ the instantaneous specimen height at the force F .

True or logarithmic strain, ϵ can be obtained from this approximation:

$$\epsilon(F) \approx \ln \left[\frac{h(F)}{h_0} \right] \quad (2)$$

Hence, the true strain can be calculated as:

$$\epsilon(F) \approx \ln \left[1 - \frac{s(F)}{h_0} \right] \quad (3)$$

True stress is given by:

$$\sigma(F) \approx \frac{F}{\pi r^2(F)} \quad (4)$$

where $r(F)$ is the instantaneous specimen radius at the force F . Making use of the law of constant volume,

$$\sigma(F) \approx \frac{F h}{\pi r_0^2 h_0} \quad (5)$$

where r_0 is the initial radius of the specimen.

Hence, true stress can be calculated from:

$$\sigma(F) \approx \frac{F[h_0 - s(F)]}{\pi r_0^2 h_0} \quad (6)$$

Some methods of after-test corrections require measurement of such parameters as a (radius of the mid-section of a bulging specimen), R (contour or radius of the bulge) and μ (coefficient of friction) in the bulge correction factor method by Reicherter [3]:

$$\sigma = \frac{F}{\pi a^2 \left[1 - \frac{a}{4R} - \frac{\mu (2a - h)}{3h} \right]} \quad (7)$$

or simply a and R as in the correction method by Saluja [4]:

$$\sigma = \frac{F}{2\pi a R \left[1 - \frac{a}{4R} \right] \ln \left[1 - \frac{a}{2R} \right]} \quad (8)$$

3. ERRORS IN MEASUREMENT

The following discussion will consider the case where bulge corrections are not required.

Looking at equations 3 and 6, it can be seen that the error in the measurement of F will propagate into the calculated stress value while error in s will propagate into both the stress and strain values. With a load cell of a high accuracy, the error in F is small. However, with growing equivalent strain, the error in measurement of height propagates more and more into the calculated stress. Poehlandt [5] analysed the effect of systematic errors of measurement on the inferred values of stress and strain in tension, compression and torsion tests and concluded that the compression test using height measurement is the most inaccurate method.

The other disadvantage of inferring stress and strain from height measurement is due to the error contributed by the elastic deformation of the upsetting device. With increasing strain the cross section of the specimen grows and gives rise to increasing error due to elastic deformation. Poehlandt and Lange [1] recommended that in order to reduce this effect, the dies should be made of hardened steel and the reduction of height of the specimen should be measured directly between the dies close to the specimen.

The method of measuring the diameter of the specimen provides a possibility of overcoming the errors associated with the measurement of height. In this case instead of equation 3, the true strain will be calculated using:

$$\epsilon(F) = \ln \frac{A_0}{A(F)} = 2 \ln \frac{d_0}{d(F)} \quad (9)$$

and instead of equation 6, the true stress will be calculated using:

$$\sigma(F) = \frac{4F}{\pi d^2(F)} \quad (10)$$

This possibility has not been utilised fully due to the increased difficulty in developing a test facility that will allow a convenient way of holding displacement transducers to record the diameter. The first attempt was made by Rasmussen [6] who made use of an upsetting tool with a transducer ring to hold six transducers in a horizontal plane using compression springs and guide pins. The construction is rather heavy since guide posts and ball bearing guide bushings are used for alignment purpose. The top platen is provided with holes to accommodate the guide pins during the downward stroke of the press slide.

Poehlandt remarked that the method of diameter measurement such as the one developed by Rasmussen is at a disadvantage due to the lack of commercially available testing facility [5]. Instead, another testing facility was proposed [2]. This is also of a closed construction type with guide posts and guide pins for alignment. The load cell, unlike in other designs, is housed inside the construction hence restricting the specimen size that can be tested. The main disadvantage of the facility is that it allows stress and strain calculation to be based on height measurement only.

4. DESIGN AND PERFORMANCE REQUIREMENT

When developing or selecting a compression facility, several factors should be considered. They are briefly outlined below:

4.1 Purpose of Compression Test

The purpose of the test and the type of assessment intended to be carried out will influence the type of parameters that need to be recorded. Decision is also made on the method of parameter measurement. For example force can be measured using a commercial load cell or by means of strain gauges on a press element that transmits force such as the connecting rod. The choice of measuring specimen height or diameter has been highlighted in section 3.

4.2 Size Consideration

The overall height of the compression facility is an important factor especially if the test is to be conducted using a press. The shut height of the press should be considered. This may affect selection of the load cell and specimen sizes.

4.3 Strength Consideration

The platens will be subjected to high forces and shocks during use. The thickness of the platens should be adequate to allow it last longer. A good option is to prestress the platen in a ring. Design requirement for radii and hold sizes must also be satisfied.

4.4 Material Selection

The platen material must be of adequate hardness to be able to upset the specimens and to maintain smoothness of the polished platen surfaces. Tool steels, hardened and tempered to 60 HRC can be used for specimens of low and medium hardness range. However for very hard materials, tungsten carbide is recommended.

Since high impact is involved the material should have good toughness and impact resistance qualities.

4.5 Platen Finishing

During compression testing, friction will develop between the platen-specimen interfaces. Different approaches of suppressing the effect of friction exist. In the sticking friction method, the platen will be machined with circular grooves. The other approach is by reducing friction. The platens should be polished to a roughness value of $R_t \leq 1 \mu\text{m}$ [7].

5. NEW COMPRESSION FACILITY

A new design is put forward here (Figure 1). The design attempts to retain the advantage of the ability to measure specimen diameter as in Rasmussen's construction while simplifying the design by adopting an open construction concept. Thus, the upper platen assembly can be fastened to the press slide and the bottom assembly is positioned on a load cell. The open construction option allows a simpler and lighter testing facility, since guide posts, guide bushings and other additional components are no longer required.

Two displacement transducers are held in the horizontal position on each side of the specimen by a transducer ring. As in Rasmussen's design the ring can slide in the vertical direction through four guide pins. The horizontal position of the ring and hence those of the transducers are regulated by means of eight compression springs, four below and four above the ring. By selecting guide pins of suitable lengths, it is not necessary to provide holes on the upper platen. Two additional displacement transducers for measuring the specimen height are attached to the lower platen.

The platens are made of AISI D2 tool steel (1.55% C, 12.0% Cr), hardened and tempered to 60 HRC. The surfaces of the platens to be in contact with the specimen are lapped to roughness value, $R_t < 0.2 \mu\text{m}$.

Figure 2 shows a schematic drawing of an example how the compression facility can be used in a compression test to determine the flow curve of a material. The force and displacement transducers are connected to a six-channel measuring amplifier system. The conditioned signals are passed on to a micro computer equipped with data acquisition hardware and software. Data processing softwares will then allow treatment and processing of the recorded data. Finally the desired output can be reproduced by means of a plotter or printer.

6. CONCLUSION

A new compression testing facility is presented. The advantage of the facility is its much lighter and simpler construction. It allows stress and strain to be inferred based on both the height and diameter method.

REFERENCES

1. K. Poehlandt and K. Lange, Recommendations for an Unified Upsetting Test for Determining Flow Curves, CIRP Annals, Vol. 38/1 (1989).
2. J. F. Alder and V. A. Phillips, J. Inst. Metals, Vol. 38 (1954), 80.
3. K. Reicherter, Investigations on the Plastic Behaviour of Cylindrical Specimens, Thesis, TH Stuttgart, 1950.
4. S. S. Saluja et al, A Simple Method for Flow Stress Determination under Metal Working Conditions, Proc. NARMC-IX, University Park, PA (1981), 153.
5. K. Poehlandt, Materials Testing for the Metal Forming Industry, Springer-Verlag, Berlin, 1989.
6. S.N. Rasmussen et al, Further Development of the Rastegaev Upsetting Test for Recording Flow Curves, Wt. -2. Ind. Fertig. 74 (1984), 667.
7. Billigmann and Feldmann, Upsetting and Pressing, Carl Hauser Verlag, Munich, 1973.

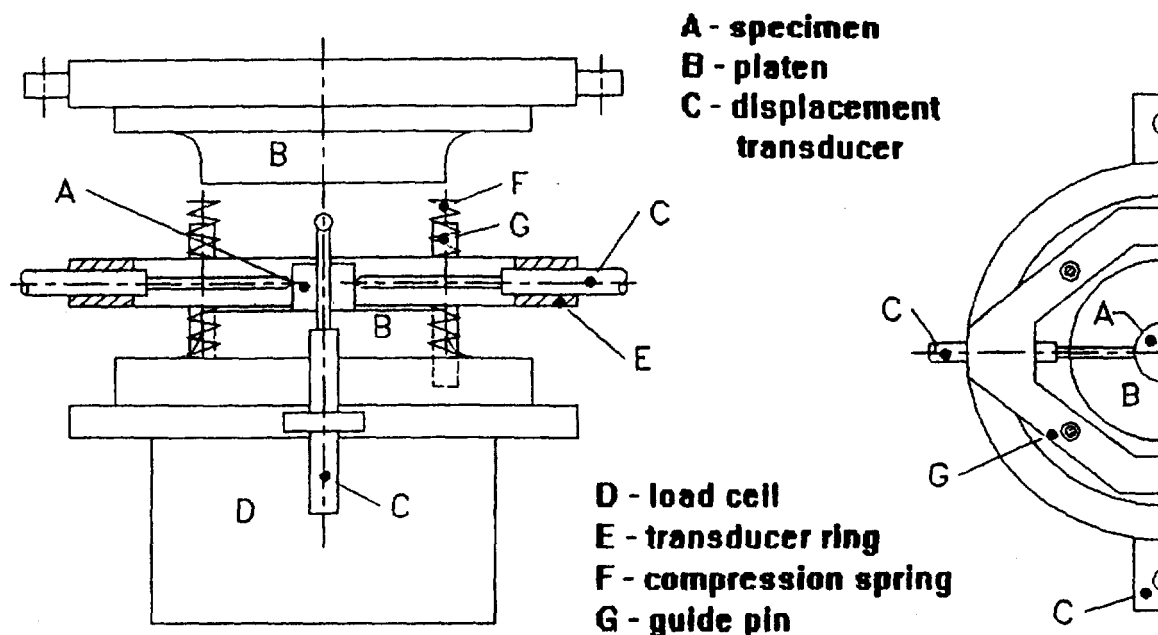


FIGURE 1: Compression Facility For Height And Diameter Measurement

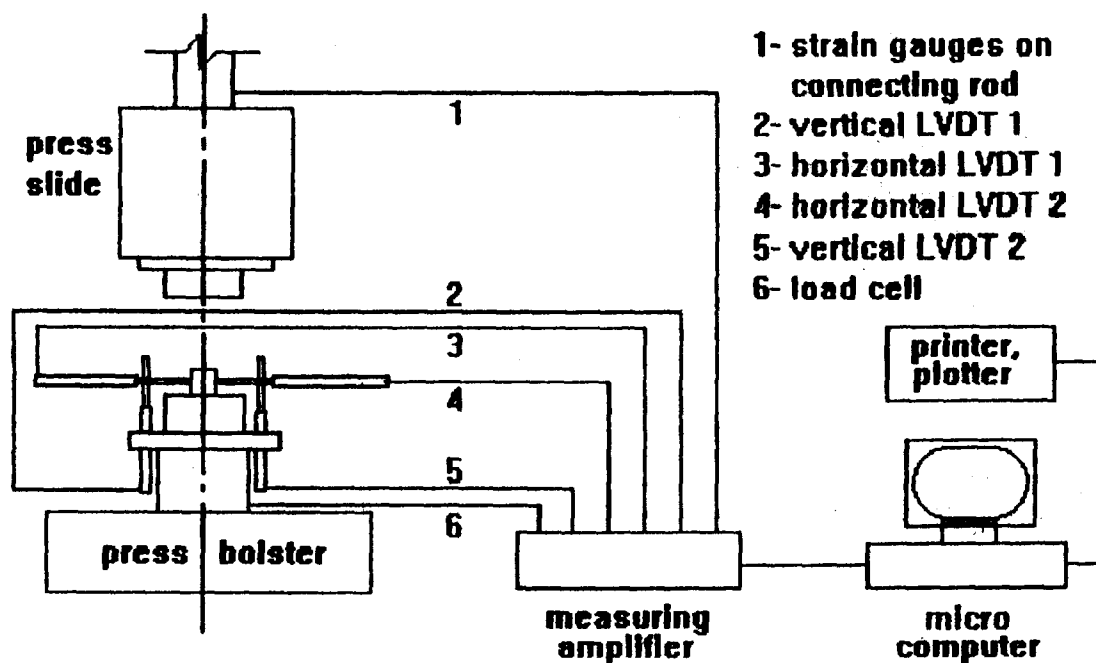


FIGURE 2: Experimental Set Up For Compression Testing

THE USE OF MULTIPLEXER-DEMULPLEXER CIRCUIT FOR CENTRALISED MONITORING OF FIRE ALARM PANEL

Ahmad Maliki Omar, Mohd Fadzil Saldon and Habibah Hashim

Department of Electrical Engineering

Institut Teknologi MARA

40450 Shah Alam

ABSTRACT

This paper is concerned with the development of a centralised monitoring alarm system employing the use of a number of multiplexer circuits in conjunction with demultiplexers designed to provide links between various existing alarm panels to a central controller. The developed system can be used to retrofit existing fire-alarm panel as part of an automation work.

Keywords : *Alarm System, Automation, Digital Techniques*

1. INTRODUCTION

The implementation of Industrial Master Plan (IMP) in Malaysia has resulted in transformation of its economies from the traditional agricultural based to that of the industrial based. These has inevitably resulted in shortages of human resources due to the wide availability of job as well as increases in labour cost.

To overcome related problems it is anticipated that the country requires more automation system with high technological content to replace the traditional use manual operation.

One of the current activities traditionally available in any organisation is the work of security personnels in monitoring fire alarm panels located at each building constructed. For a high rise building problems are negligible due to centrally located alarm panel. This is not so in the case of scattered buildings for a medium organisations with a number of buildings. Problems with these situation are related with the system of building monitoring panels peculiar to each building with non-availability of central links. With the availability of a number of panels scattered throughout the entire area, monitoring becomes almost impossible; especially when manpower are hard to come-by.

In this project it is proposed that a central monitoring alarm system employing the use of a number of multiplexer circuits in conjunction with

demultiplexers is designed to provide links between various existing alarm panels to a central controller. Other attractive features for the designed system could include minimum number of cable used for the link since the transmission of data is done in serial form; where 256 different alarm units can be easily monitored in matter of milliseconds. Furthermore, the system can also be interfaced to a personal computer for displays of the current status of the alarm panels being monitored. There is also a possibility of providing link-up with modem through telephone lines. The developed system can be used to retrofit existing fire-alarm panel as part of an automation work.

2. PROPOSED SYSTEM

The proposed system for the central monitoring alarm unit can be illustrated by the block diagram of figure 1. A number of alarm panels designated Block A to F are linked to a multiplexer. This multiplexer in turn will transmit signals to a demultiplexer that will enable a transfer of data from the sensors. Signals received by the demultiplexer will then be sent to the display panel for visualisation or alarm triggering.

2.1 Zone Controller

The purpose of the zone controller is to interface with existing alarm panel; thus providing a base to

collect information from the transducers in the form of switches as will be described.

From figure 2 it can be observed that the unit comprise four main components; i.e decoder, clock generator, counter and multiplexing chips. A total of 16 multiplexer(MUX) chips are used to provide an input of 256 alarm signals.

2.2 Monitoring Station

This is to enable for a supervisory monitoring of the status of each alarm panel with the respective conditions that could arise. It could normally be located at a place where security personnels are manned so as to provide 24 hours monitoring.

It can be observed that the unit comprise four main components; i.e decoder, counter, display unit and demultiplexer(DEMUX) chip. At the monitoring station a total of 16 DEMUX chips are used to receive sequential input signals and reproduce 256 parallel output signals; identified through demultiplexing process.

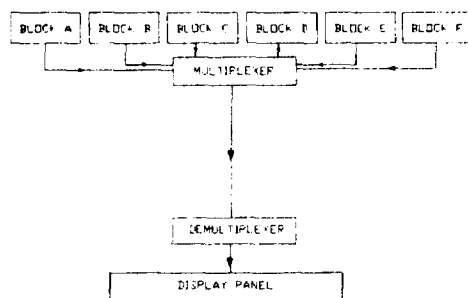


Figure 1 : Proposed System

3. DESIGN DESCRIPTION

The system consists of five main parts namely sensors, multiplexing, demultiplexing, display unit and a control unit. The sensors monitor the status of the fire-alarm panel through existing switches. The multiplexing unit then monitors signals from sensors and convert signals from 16 parallel input into 1 sequential output at the zone controller as in figure 2. This signal is then transmitted through a transmission line to the monitoring station which will then demultiplex the signals to ascertain the status of the alarm through initiation of display unit. The various operation and units available in the system are as described in the followings.

3.1 Multiplexing/Demultiplexing Unit

Signals from sensors are read in the form of digital input. The process of multiplexing/demultiplexing is based on a time division method. The same chip could equally be used for multiplexing as well as demultiplexing purpose based on CD4067.

3.2 Control Unit

Communication between the sending and receiving stations are carried out through the control unit which keeps the scanning process of the multiplexer and demultiplexer synchronised. The control unit comprise of three control lines namely reset, clock pulse and ground lines, two decoders and counters complete with a clock generator. The detailed circuit showing connections common to each multiplexer unit is as shown in figure 3; comprising decoders, counters and clock generator.

3.3 Clock Generator

The function of the clock generator is to produce suitable clock pulses for the counters such that the transmitted data are synchronised between the sending and receiving ends.

3.4 Decoder

The function of the Decoder is to select the MUX or DEMUX sequentially. If one multiplexer/demultiplexer is activated the other 15 multiplexers/demultiplexers are inhibited. The same process is repeated until all 16 units of the multiplexer/demultiplexer have been attended to. When the 16th step is completed(i.e. bit 1111 has reached) the counters will reset its count back to 00000000 and the process of scanning of the input data will repeat as long as the clock pulses are available at the counters.

3.5 Counter

The 12-Mod counter serves the purpose of providing the select bit (i.e. from 0000 to 1111) for the decoder to sequentially select all of the multiplexers/demultiplexers.

The other 4 bit of the counter are used to scan the status of 16 alarm switches connected to each multiplexer/demultiplexer unit sequentially through all of the possible states 0000 to 1111. At each state of the bit, the switch status for the corresponding alarm will be selected by the multiplexer and passed over to the demultiplexer unit through the transmission link. The corresponding LED and alarm will then be activated to alert the operator on duty.

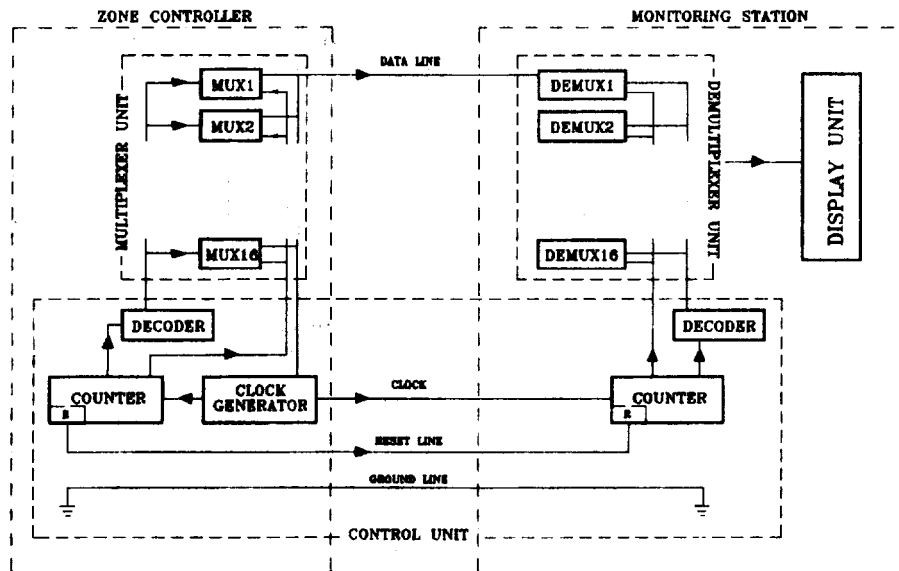


Figure 2 : Block Diagram of Proposed System

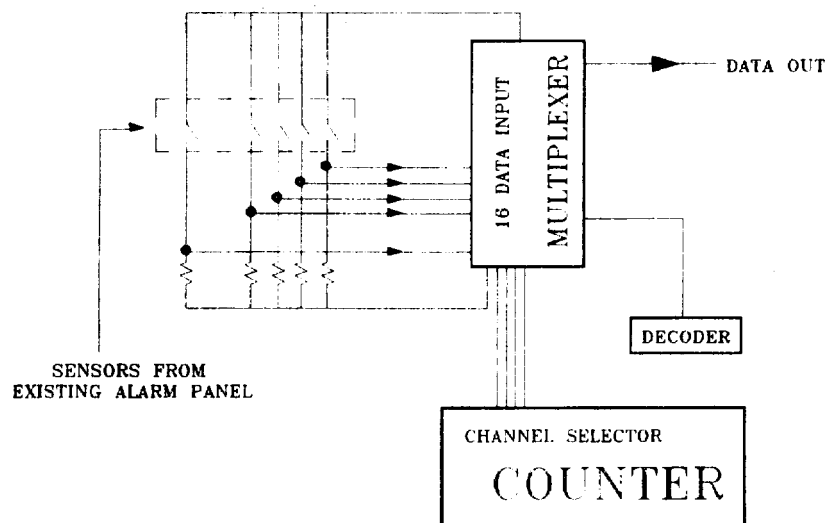


Figure 3 : Detailed Multiplexer Circuit

3.6 Display Unit

Signals from the DEMUX which represents each of the 256 sensor channels at the zone controller are used to identify respective problems and translated in the form of switching of light indicators or the turning-on of alarm signal making use of switches. Thus a mimic panel could be constructed to indicate the zone or problem; whilst the alarm signal will provide the alert warning.

4. SEQUENCE OF OPERATION

The sequence of operation can be easily comprehend by referring to figure 4. Each alarm is assigned an address code when initially installed. As can be seen, 16 possible address codes are available through addr-1 to addr-4 during which one multiplexer unit is enabled and the other 15 units are inhibited.

The multiplexer unit is enabled when receiving a bit 0 or 'low' from the decoder for a determined duration until all 16 addresses assigned to each multiplexer unit has been scanned. Then the next multiplexer unit in line will be enabled and the previous multiplexer is given a bit '1' or 'high' to inhibit it. The procedure repeats until all 16 number of multiplexer units or 256 addresses have been processed after which the counter resets its count. The process of selecting, scanning and transmitting input data to the monitoring centre continues throughout the normal working hours and also during non-occupancy periods provided that the clock and other parts of the system are still servicing.

5. TESTS

Tests were carried out to determine the performance of the transmission line using square data transmission on a line with a loop resistance of 284 ohm. This has resulted in a frequency of 6.8kHz and 1.37 kHz being achieved for a distance 12 metres and 100 metres respectively. In the case of voltage drop; it was discovered that the value is 0V and 0.3V respectively.

Operational tests were also being carried out to determine satisfactory operation of the system by putting a dummy circuit. Results have shown the system to be capable of operation within its specified requirements subject to previously described constraints.

6. CONCLUSION

A simple technique employing the use of a number of multiplexer circuits in conjunction with demultiplexer units in providing links between various scattered existing alarm panels to a central controller has been presented. Through further developments, the system can then be used to retrofit existing panels in operation for monitoring purposes; providing monitoring interface that could relay informations to a central controller/monitor to signal problems.

This technique has certain limitation for long distance location, which results with slower rate of transmission. Furthermore, system becomes less efficient due various factors such as voltage drop, propagation delay time, power dissipation and noise margin. These problems could be minimised by using CMOS logic family in the system as well as a unit of RS232 device at both sides of the link point.

7. ACKNOWLEDGEMENT

The authors wish to express their deepest gratitude to Mustafar Kamal Hamzah from Electrical Department, Institut Teknologi Mara for his encouragement, editorial and constructive comments; invaluable to the preparation of this paper.

REFERENCES

- [1] Trevor Housely, 'Data Communications and Teleprocessing Systems', Second Edition, Prentice-Hall International Inc.
- [2] Ronald J. Tocci, 'Digital Systems - Principle and Applications', Fifth Edition, Prentice Hall Inc.
- [3] M. Moris Mano, 'Digital Logic and Computer Design, Prentice Hall Inc.
- [4] Muhamad Zainon, 'Central Monitoring Alarm System At Station MARDI Serdang, Selangor

Figure 4 : Multiplexing Sequence of Operation

